

HUI YAO

# Butyrate Production from Methanol and CO<sub>2</sub> in Microbial Electrosynthesis



HUI YAO

**Butyrate Production from Methanol  
and CO<sub>2</sub> in Microbial Electrosynthesis**

**ACADEMIC DISSERTATION**

To be presented, with the permission of  
the Faculty of Engineering and Natural Sciences  
of Tampere University,  
for public discussion in the Auditorium Pieni Sali 1  
of the Festia building, Korkeakoulunkatu 8, Tampere,  
on 24 October 2025, at 13 o'clock.

ACADEMIC DISSERTATION

Tampere University, Faculty of Engineering and Natural Sciences  
Finland

*Responsible  
supervisor  
and Custos*

Professor Marika Kokko  
Tampere University  
Finland

*Supervisors*

Academy Research Fellow  
Antti Rissanen  
Tampere University  
Finland

Doctor Igor Vassilev  
Eppendorf  
Germany

*Pre-examiners*

Associate Professor  
Ludovic Jourdin  
Delft University of Technology  
The Netherlands

Associate Professor  
Sunil A. Patil  
Indian Institute of Science  
Education and Research, Mohali  
India

*Opponent*

Professor Eileen Yu  
University of Southampton  
The United Kingdom

The originality of this thesis has been checked using the Turnitin Originality service.

Copyright ©2025 Hui Yao

Cover design: Roihu Inc.

ISBN 978-952-03-4155-8 (print)

ISBN 978-952-03-4156-5 (pdf)

ISSN 2489-9860 (print)

ISSN 2490-0028 (pdf)

<http://urn.fi/URN:ISBN:978-952-03-4156-5>



Carbon dioxide emissions from printing Tampere University  
dissertations have been compensated.

PunaMusta Oy – Yliopistopaino  
Joensuu 2025

# ACKNOWLEDGEMENTS

This thesis was carried out at the Faculty of Engineering and Natural Sciences, Tampere University. I am extremely grateful for the generous financial support provided by the Academy of Finland, the Finnish Cultural Foundation, and the Business Finland

I owe my deepest gratitude to my responsible supervisor, Prof. Marika Kokko, who has guided me with care, encouragement, and patience throughout these past years. I feel blessed to join her group and it has been an incredible journey from the very first beginning to the last bit of my doctoral work. Her support and insightful feedback have been instrumental in shaping both this thesis work and my growth as a researcher. I am also sincerely thankful to my co-supervisor, Dr. Igor Vassilev, for his countless pieces of advice and hands-on guidance in the laboratory, which laid the foundation for much of this work. My gratitude also goes to Dr. Antti Rissanen, whose invaluable expertise in bioinformatics greatly enriched this research.

I am immensely grateful to all collaborators for their fruitful discussions and innovative contributions. In particular, I wish to thank Dr. Johanna Rinta-Kanto from Tampere University and Prof. Ulla Lassi, Dr. Anne Heponiemi, and Dr. Davide Bergna from the University of Oulu for their significant input and guidance. I also warmly thank Associate Prof. Sebastià Puig, Dr. Meritxell Roman-Casas, and Associate Prof. Paolo Dessim for their expertise in joint publications and for their kind hospitality in Girona. My sincere thanks extend to the laboratory teams at Tampere University and the University of Girona for their technical assistance and support.

I would also extend my heartfelt thanks to my pre-examiners, Associate Prof. Ludovic Jourdin from the Delft University of Technology, and Associate Prof. Sunil A. Patil from Indian Institute of Science Education and Research, Mohali, for their thorough evaluation of this dissertation, and to my opponent, Prof. Eileen Yu from

University of Southampton, for kindly participating in my defense and offering valuable discussions.

Beyond academia, I am grateful to my friends who have been part of my life. Special thanks to Yakui, for a friendship that has lasted since middle school, and to Roy, for sharing the same lab since our days in Wageningen.

Living abroad has not always been easy, and I would not have come so far without being supported and loved by my family. I have cherished every moment shared with my parents and sister and thank you for always being there whenever I need it. Finally, my deepest love and gratitude to MY for being an inseparable part of my life and soul.

Tampere, September 2025

Hui Yao

*In loving memory of my grandparents*

# ABSTRACT

Microbial electrosynthesis (MES) is a promising technology for producing value-added chemicals from carbon dioxide ( $\text{CO}_2$ ). In MES, microorganisms serve as the biocatalyst and are cultivated in a cathode chamber of an electrochemical cell and use the electrons or  $\text{H}_2$  derived from cathode for the reduction of  $\text{CO}_2$  to short chain fatty acids. Acetate has been a common product in MES. Various studies have indicated that adding extra electron donors is an effective strategy to shift the product spectrum towards butyrate, which has a higher economic value compared to acetate. Methanol is a promising electron donor. Methanol can be produced from organic waste or synthesized directly from  $\text{CO}_2$ . In fermentation process, methanol has been used both with pure and mixed cultures as the electron donor for chain elongation, which elongates  $\text{CO}_2$  and acetate to other carboxylates like butyrate. However, the utilization of methanol in MES has never been reported.

This doctoral dissertation investigated the feasibility of methanol addition in MES for butyrate production. First, a mixed culture microbial community was enriched in MES reactors fed with methanol and  $\text{CO}_2$ . Butyrate was the predominant product with methanol acting both as carbon and electron donor. Subsequently, operational parameters were optimized, including the cathode pH, temperature, methanol/ $\text{CO}_2$  ratio, pressure, and  $\text{CO}_2$  feeding mode. With optimized conditions, butyrate production was obtained with 87% selectivity (carbon basis) and production rate of  $0.6 \text{ g L}^{-1} \text{ d}^{-1}$  ( $107.4 \text{ g m}^{-2} \text{ d}^{-1}$ ). Additionally, 16S ribosomal RNA gene sequencing and shotgun metagenomic sequencing revealed that *Eubacterium callanderi* was the responsible genus for methanol and  $\text{CO}_2$  assimilation via the Wood-Ljungdahl pathway as well as the butyrate production via the reverse  $\beta$ -oxidation pathway in methanol assisted MES. These findings highlight the potential of methanol assisted MES for efficient carbon utilization and contribute to the development of bioprocesses for platform chemical production.



# CONTENTS

1	Introduction .....	17
1.1	Context and knowledge gaps .....	17
1.2	Research goal and research questions .....	19
1.3	Structure of the dissertation.....	20
2	Theoretical background.....	21
2.1	Biological CO <sub>2</sub> fixation .....	21
2.2	CO <sub>2</sub> valorization in microbial electrosynthesis.....	23
2.2.1	Fundamental principles of MES.....	23
2.2.2	Reactor types and electrode materials in MES.....	25
2.2.3	Operational parameters affecting MES performance .....	27
2.2.4	Product spectrum in MES.....	32
2.3	Butyrate production in MES.....	36
2.3.1	Usage of electron donors for butyrate production.....	36
2.3.2	Butyrate producing microbial communities in MES.....	40
3	Research methodology .....	42
3.1	Culture and cultivation media.....	42
3.2	Experimental set-up and operation .....	42
3.2.1	MES with graphite granules as the cathode.....	43
3.2.2	MES with graphite felt as the cathode.....	44
3.2.3	Experimental operation.....	47
3.3	Analytical methods .....	48
3.3.1	Chemical analysis.....	48
3.3.2	Microbiome characterization.....	49
3.4	Calculations and statistical analysis .....	50
4	Results and discussion.....	52
4.1	Microbial community enrichment and taxonomic characterization.....	52
4.1.1	Enrichment of the microbiome utilizing methanol and CO <sub>2</sub> .....	52
4.1.2	Taxonomic profiling of the enrichment culture .....	53
4.2	Methanol assisted MES: proof of concept and optimization.....	55
4.2.1	Revealing the potential roles of methanol in MES.....	55
4.2.2	Improving the butyrate selectivity by optimizing cathodic pH .....	57

4.2.3	Continuous CO <sub>2</sub> feeding resulted in mainly acetate production (unpublished results).....	61
4.2.4	Investigating the effects of temperature, methanol/CO <sub>2</sub> ratio and pressure on butyrate production during fermentation.....	61
4.2.5	The optimized operation conditions for butyrate production in methanol assisted MES.....	64
4.3	Potential biochemical pathways in methanol assisted MES .....	67
4.3.1	Methanol and CO <sub>2</sub> assimilation pathways.....	67
4.3.2	Butyrate production pathways.....	70
5	Conclusions and outlook.....	71
6	References.....	74

## List of Figures

<b>Figure 1.</b>	Schematic representation of a MES of CO <sub>2</sub> to acetate with H <sub>2</sub> as the electron shuttle. The number of molecules depicted does not reflect stoichiometric ratios and is intended for illustrative purposes only. The blue circles on the surface of the cathode represent the microorganism (Created with BioRender).....	24
<b>Figure 2.</b>	Reactor used in publication I-II, with a) photo of the granular bed reactor, and b) schematic of the reactor. ....	44
<b>Figure 3.</b>	Reactor used in publication I, with a) photo of the granular bed reactor, and b) schematic of the reactor. ....	44
<b>Figure 4.</b>	Reactor used in publication III, with a) photo of the compact reactor, and b) schematic of the reactor (reproduced from Morais et al., 2024, Chemical Engineering Journal, licensed under CC BY 4.0). ....	46
<b>Figure 5.</b>	Reactor used in publication III, with a) photo of the graphite felt cathode, and b) photo of the reactor.....	46
<b>Figure 6.</b>	Microbial composition at the end of different enrichment batches with ten most abundant genera. Specifically, the <i>f_Ruminococcaceae</i> stands for family level as the genus remains unidentified. The error bars indicate the standard deviations between duplicates (Adapted from publication I, licensed under CC BY 4.0). ....	54
<b>Figure 7.</b>	VFAs profile obtained with different feeding regimes (a), carbon source consumption and production in ME-CD (b), electron recoveries in ME-CD (c) and total 16S rRNA gene copies measures with different feeding regimes (d). The error bars present duplicate reactors (Adapted from publication I, licensed under CC BY 4.0). ....	56
<b>Figure 8.</b>	Acetate (a, b) and butyrate (c, d) concentrations at cathodic pH of 5.5, 6 and 7. The dashed lines represent the results with semi-batch CO <sub>2</sub> feeding obtained from triplicated reactors with error bars showing the standard deviations, and solid lines represent the results with continuous CO <sub>2</sub> feeding. The results at pH 5.5 were shown in orange, those at pH 6 in green, and those at pH 7 in blue.....	59
<b>Figure 9.</b>	Acetate (a) and butyrate titers (b) at different temperatures, and butyrate titer (c) and butyrate yield (d) at different pressures. Significance of the results between different conditions was tested by one way ANOVA test, with Tukey HSD post-hoc analysis. The symbol * represents p < 0.05, symbol ** represents p < 0.005,	

symbol n.s. represents not significant (Reproduced from publication III).....63

**Figure 10.** VFAs and methanol concentrations throughout the MES experiments at 35°C. Error bars show the duplicate results (Reproduced from publication III). .....65

**Figure 11.** Putative metabolic pathway for butyrate production from methanol and CO<sub>2</sub>. Abbreviations: CODH, carbon-monoxide dehydrogenase; FDH, formate dehydrogenase; FTHFS, Formate-tetrahydrofolate ligase; MTHFC, methenyltetrahydrofolate cyclohydrolase; MTHFD, methylenetetrahydrofolate dehydrogenase; MTHFR, methylenetetrahydrofolate reductase; MeTr, 5-methyltetrahydrofolate---corrinoid/iron-sulfur protein Co-methyltransferase; ACS, CO-methylating acetyl-CoA synthase; ACAT, acetyl-CoA C-acetyltransferase; HAD, 3-hydroxyacyl-CoA dehydrogenase; ECH, enoyl-CoA hydratase; SCAD, short-chain acyl-CoA dehydrogenase BCoAT, butyryl-CoA,acetate CoA transferase; BUK, butyrate kinase; PTB, phosphate butyryltransferase; ACC, acetyl-CoA carboxylase; MAT, malonyl transferase; KAS, ketoacyl-ACP synthase; KAR, ketoacyl-ACP reductase; FAB, hydroxyacyl-ACP dehydratase; ENR, enoyl-ACP reductase; TE, thioesterase; MethI, methionine synthase; mtaA, [methyl-Co(III) methanol-specific corrinoid protein]---coenzyme M methyltransferase; mtaB, methanol---corrinoid protein Co-methyltransferase. \* and \*\* represents that *E. callanderi* contribute to over 50% and 90% of the abundances, respectively. (Adapted from publication II (Yao et al., 2025), licensed under CC BY-NC 4.0.). .....69

## *List of Tables*

<b>Table 1.</b>	Selected of MES studies with different operational conditions and their corresponding observations.....	28
<b>Table 2.</b>	Products reported in MES or MES integrated processes.....	34
<b>Table 3.</b>	Comparison of butyrate production in mixed culture MES studies fed with CO <sub>2</sub> and with different electron donors. For each electron donor, the first reported studies and studies with the highest butyrate production rates/titers are included in the table. (Adapted from publication II (Yao et al., 2025), licensed under CC BY-NC 4.0.).....	39
<b>Table 4.</b>	Tested operational conditions in this dissertation.....	48
<b>Table 5.</b>	List of analytic methods/instruments used in the study.....	49

# ABBREVIATIONS

16S rRNA	16S ribosomal RNA
3D	Three-dimensional
ACAT	Acetyl-CoA C-acetyltransferase
Acetyl-CoA	Acetyl coenzyme A
AEM	Anion exchange membrane
ANOVA	One way analysis of variance
Atm	Atmospheric pressure
ATP	Adenosine triphosphate
BCoAT	Butyryl-CoA:acetate CoA-transferase
BES	Bioelectrochemical system
BPM	Bipolar membrane
BUK	Butyrate kinase
CEM	Cation exchange membrane
CoP	Cobamide-binding corrinoid protein
CR	Carbon recovery
DoR	Degree of reduction
ER	Electron recovery
FAB	Fatty acid biosynthesis
FDH	Formate dehydrogenase
FID	Flame ionization detector
FTHFS	Formate-tetrahydrofolate ligase
GC	Gas chromatography
GHG	Greenhouse gas
HSD	Honest significant difference
IEM	Ion exchange membrane
MES	Microbial electrosynthesis
MetH	Methionine synthases
MTI	Methanol—corrinoid protein Co-methyltransferase
MTII	Methyl-Co(III) methanol-specific corrinoid protein—coenzyme M methyltransferase

MTHFC	Formate-tetrahydrofolate ligase
MTHFD	Methylenetetrahydrofolate dehydrogenase
MTHFR	Methylenetetrahydrofolate reductase
N <sub>2</sub>	Nitrogen
N <sub>2</sub> O	Nitrous oxide
NADH	Nicotinamide adenine dinucleotide
P <sub>CO2</sub>	Partial pressure of carbon dioxide gas
PCoA	Principal coordinate analysis
PERMANOVA	Permutational analysis of variance
PHB	Polyhydroxy butyrate
P <sub>H2</sub>	Partial pressure of hydrogen gas
PTB	Butyryltransferase
qPCR	Quantitative polymerase chain reaction
RBO	Reverse β-oxidation
SHE	Standard hydrogen electrode
SEM	Scanning electron microscopy
TCD	Thermal conductivity detector
THF	Tetrahydrofolate
TIC	Total inorganic carbon
VFA	Volatile fatty acid
WLP	Wood–Ljungdahl pathway

# ORIGINAL PUBLICATIONS

- Publication I Yao, H., Rinta-Kanto, J. M., Vassilev, I., & Kokko, M. (2024). Methanol as a co-substrate with CO<sub>2</sub> enhances butyrate production in microbial electrosynthesis. *Applied Microbiology and Biotechnology*, 108(1), 372.
- Publication II Yao, H., Romans-Casas, M., Vassilev, I., Rinta-Kanto, J. M., Puig, S., Rissanen, A. J., & Kokko, M. (2025). Selective butyrate production from CO<sub>2</sub> and methanol in microbial electrosynthesis—Influence of pH. *Bioelectrochemistry*, 109000.
- Publication III Yao, H., Dessi, P., Romans-Casas, M., Puig, S., Kokko, M. (2025). Optimizing butyrate production from methanol and CO<sub>2</sub> in microbial electrosynthesis. *Bioresource Technology* 437, 133150.

# AUTHOR'S CONTRIBUTIONS

- Publication I The author and I. Vassilev designed experimental work. The author executed the experimental work and interpreted the results. The author wrote the original draft and revised it based on comments and suggestions from all co-authors.
- Publication II The author designed experimental work. The author executed most of the experimental work and interpreted the results. M. Romans-Casas executed part of the experimental work and interpreted results related to the thermodynamical model. The author wrote the original draft and revised it based on comments and suggestions from all co-authors.
- Publication III The author designed and executed the experimental work and interpreted the results. The author wrote the original draft and revised it based on comments and suggestions from all co-authors.



# 1 INTRODUCTION

## 1.1 Context and knowledge gaps

Greenhouse gas (GHG) emissions have been associated with anthropogenic activities since the industrial revolution. With the growing population, the past decade (2010-2019) has obtained the highest annual GHG emissions so far (Calvin et al., 2023). GHGs are mainly composed of carbon dioxide (CO<sub>2</sub>), methane (CH<sub>4</sub>) and nitrous oxide (N<sub>2</sub>O). The accumulated GHG emissions in the atmosphere absorb solar energy, and thus are the major contributors to the global warming—the global surface temperature rising since 1850 (Calvin et al., 2023). In 2024, the annual average near-surface temperature was the warmest since 1850 (NOAA, 2025). Consequently, human-caused climate change has resulted in extreme weather events such as the killer heat waves, receding glaciers, heavy precipitation and increases the risk of extinction for species (Calvin et al., 2023; Kerr, 2007). Large amounts of CO<sub>2</sub> have been emitted accompanied by the usage of fossil fuels for more than a century. Currently, about two-thirds of the anthropogenic CO<sub>2</sub> emissions derive from combusting coal, oil, and gas to generate energy (IEA, 2023). Additionally, the majority of chemicals are derived from fossil fuel-based processes. To mitigate the climate change caused by GHG emissions, an intergovernmental action has been proposed since 2015 aiming for achieving net zero GHG emissions by 2050. Reaching this target not only requires the development of alternative energy sources but also carbon-neutral pathways for chemical production to support the transition toward a bio-based economy.

CO<sub>2</sub> is an abundant and inexpensive carbon source that could be recovered from various waste streams. CO<sub>2</sub> can originate from both concentrated point sources, such as industrial gaseous waste streams, and from the atmosphere. A wide range of CO<sub>2</sub> utilization technologies has been explored, including chemical catalysis, electrochemical reduction, and photochemical conversion (Leonzio & Shah, 2024). Additionally, microbial conversion of CO<sub>2</sub> has shown potential to produce fuels and chemicals in biotechnological processes with advantage of operating under mild conditions. Several biotechnologies are currently under development for microbial CO<sub>2</sub> utilization, including gas fermentation with acetogens and microalgal cultivation

(Thakur et al., 2018). As the carbon atom in CO<sub>2</sub> is at the highest oxidation state, the reduction of CO<sub>2</sub> into organics requires energy input. In nature, biological carbon fixation is widely present, in which autotrophic microorganisms utilizes energy from light and/or inorganic compounds, such as hydrogen. In addition, microbial electrosynthesis (MES) is a process in which electrode serves as an energy source to support microorganism growth and the production of biochemicals, including acetate, ethanol, butyrate and caproate (Jourdin & Burdyny, 2021; Nevin et al., 2010; Rabaey & Rozendal, 2010). In MES, CO<sub>2</sub> is reduced biologically in the cathode of an electrochemical cell, which can be powered by renewable electricity. The global availability of renewable electricity has increased significantly during the past years. For example, the electricity generation from renewable energy sources in EU countries (including hydro, solar, wind energy etc.) has increased from 407 TWh in 2000 to 1 080 TWh in 2022, surpassing the electricity from fossil fuels (1078 TWh) as the major contributor to electricity in the EU (Eurostat, 2022). Despite the potential in renewable electricity development, renewable sources can be affected by changes such as the variable solar irradiance and wind conditions, and thus the power generation has the risk of being intermediate. Through MES, intermittently available electricity can be stored as liquid and gaseous chemicals, which can serve as energy carriers, fuels, and feedstocks for industry (Deutzmann et al., 2022).

The first MES study was carried out in 2010 by Nevin et al., (2010) and employed *Sporomusa ovata* for the bioreduction of CO<sub>2</sub> to acetate. Ever since, efforts have been applied to improve the performance of MES. Acetate has been the most common product in MES studies (Jourdin & Burdyny, 2021). However, acetate has a market value of ca. 500 euro t<sup>-1</sup> (Statista, 2025), limiting the competitiveness of MES over other biotechnology processes. In 2015, a study carried out by Ganigué et al., (2015) reported a butyrate production from CO<sub>2</sub> in MES. Butyrate is a short-chain volatile fatty acid with a market value of ca. 1500 euro t<sup>-1</sup> (IMARC Group. 2024) and having applications in various fields, such as animal feed, fragrances, pharmaceuticals, food, and chemical industries (Câmara-Salim et al., 2021). Butyrate is currently produced from petroleum derivatives propylene or butyraldehyde. In addition, sugar-based fermentation processes have been developed for butyrate production (Câmara-Salim et al., 2021). With growing interest in bio-based organic acids in food and pharmaceutical applications, MES is an optional platform for butyrate production without the rely on fossil fuels or biomass.

Although several studies in MES have claimed butyrate production with only the electrode as the electron source, it has been suggested that the electric current does not provide sufficient energy for butyrate production and other electron donors are

required. Such electron donors can either be produced *in situ* in the cathode compartment from CO<sub>2</sub> (e.g., formate, ethanol) or added externally to provide reducing power. Ethanol, lactate and formate are the known examples of electron donors used to promote the production of butyrate in MES, out of which ethanol has obtained the most selective butyrate production in MES with 78% selectivity on a carbon basis (Romans-Casas et al., 2024). Currently, ethanol production is not fossil fuel based with the major feedstocks being sugarcane and corn (Hoang & Nghiem, 2021). However, current ethanol production relies on agricultural lands creating potential competition with food production.

Methanol can be a promising alternative electron donor in MES, as it has the same degree of reduction of 6 per carbon as ethanol. Methanol is considered a bulk chemical, with an annual production of approximately 110 million metric tonnes (“The Methanol Industry,” n.d.). While conventionally synthesized from syngas, renewable methanol production has gained attraction in the past decade. Commercial-scale methanol synthesis processes utilizing CO<sub>2</sub> from industrial waste and H<sub>2</sub> from water electrolysis powered by renewable sources, such as hydropower, have been implemented globally (Wagner et al., 2023). In addition, methanol can be recovered from industrial wastewaters, such as pulp and paper industry condensates (T. Pio et al., 2022). Similar to ethanol, microbial utilization of methanol has been reported since 1980s (Genthner et al., 1981; Litty, 2021), with butyrate being the main product. Ethanol, however, often promotes further conversion of butyrate into other products such as caproate or butanol (Jiang et al., 2020; Romans-Casas et al., 2024). Despite methanol’s potential for selective butyrate production, its application as an electron donor in MES has not yet been reported, which requires further investigation of methanol assisted MES systems.

## 1.2 Research goal and research questions

The goal of this research was to investigate the utilization of methanol in MES and optimization of the operational parameters for selective butyrate production. The research questions (RQs) include:

1. Can methanol addition facilitate butyrate production in MES?
2. What are the microbial community compositions and responsible biochemical pathways for utilizing methanol and for producing butyrate in MES?

3. How do operational parameters (cathodic pH, pressure, methanol/CO<sub>2</sub> ratio, and temperature) affect methanol utilization and butyrate production in MES?

RQ1 was answered by comparing the butyrate production in MES reactors with combined methanol and CO<sub>2</sub> feeding to only CO<sub>2</sub> or only methanol feeding (Publication I). RQ2 was answered by 16S rRNA gene and shot gun metagenomic sequencing of both biofilm and planktonic microbial communities in methanol assisted MES (Publications I and II). RQ3 was answered by comparing the performance of methanol assisted MES with different cathodic pH values (Publication II), pressures, methanol/CO<sub>2</sub> ratios, and temperatures (Publication III).

### 1.3 Structure of the dissertation

The structure of the dissertation is organized into five chapters. Chapter 2 provides background information and identifies the knowledge gaps of this research. It discusses the fundamental principle of MES, reviews the state of art studies of utilizing electron donors in MES, and discusses current butyrate producing microbial communities in MES. Chapter 3 outlines the methodological approach and summarizes the analytical methods applied in each publication. Chapter 4 presents the main research findings and addresses the research questions through detailed results and discussion. Chapter 5 concludes this dissertation and offers perspectives for future research. The original publications referred to in this dissertation are attached to the end of this document.

## 2 THEORETICAL BACKGROUND

### 2.1 Biological CO<sub>2</sub> fixation

In nature, autotrophic organisms fix inorganic CO<sub>2</sub> through various carbon fixation pathways, thereby sustaining the carbon cycle and forming the basis of primary energy and carbon flow in ecosystems. Seven natural carbon fixation pathways have been discovered, including the Calvin-Benson-Bassham cycle (Calvin & Benson, 1948), the reductive tricarboxylic acid cycle (Evans et al., 1966), the Wood–Ljungdahl Pathway (WLP) (Schulman et al., 1972), the 3-hydroxypropionate bicycle (Strauss & Fuchs, 1993), the dicarboxylate/4-hydroxybutyrate cycle (Berg et al., 2007), the 3-hydroxypropionate-4-hydroxybutyrate cycle (Huber et al., 2008), and the reductive glycine pathway (Sánchez-Andrea et al., 2020). Through these pathways, CO<sub>2</sub> is converted to organic intermediate compounds including pyruvate, acetyl-CoA, or glyceraldehyde-3-phosphate, which support cell growth and biosynthesis (Zhao et al., 2021).

As the carbon atom in CO<sub>2</sub> molecules is in the highest positive valence state, the fixation of CO<sub>2</sub> requires energy input. Light, hydrogen and reduced sulfur compounds are the commonly known energy sources, supplying energy in the form of adenosine triphosphate (ATP) (Gong et al., 2018). Among the seven carbon fixation pathways, the WLP requires the least amount of ATP (0.5 molecules) to fix one molecule of CO<sub>2</sub>, making it energy efficient (Zhao et al., 2021). Although the reductive glycine pathway is also proposed to consume 0.5-1 molecules of ATP for one molecule of CO<sub>2</sub> fixation, such pathway is only found to support natural autotrophic growth in *Desulfovibrio desulfuricans* (Sánchez-Andrea et al., 2020) up to date. In the WLP, four molecules of H<sub>2</sub> are the primary electron donors, driving the reduction of two molecules of CO<sub>2</sub>: one to a methyl group, and the other to carbon monoxide (CO), which are subsequently condensed to form acetyl-CoA (Ragsdale & Pierce, 2008). Acetyl-CoA is an important intermediate to produce valuable biochemicals, which makes the WLP a promising pathway for biotechnological CO<sub>2</sub> utilization.

Gas fermentation is the biological conversion of gaseous carbon compounds (CO and CO<sub>2</sub>), that can be derived from exhaust gases or syngas (mixture of CO, CO<sub>2</sub>

and H<sub>2</sub>), into biochemicals. These gases can originate from various waste streams, such as agricultural or industrial waste. Globally, steel manufacturing alone releases approximately 1400 million tons of waste gases per year (De Tissera et al., 2019), which have the potential to be used as carbon feedstocks. Gas fermentation is employed by chemolithoautotrophic bacteria via the WLP (Dürre, 2016). Most commonly, acetogenic bacteria are responsible for gas fermentation (Liew et al., 2016). Gas fermentation possesses several advantages compared to other processes using syngas as the feedstock. Unlike chemical processes, gas fermentation operates under mild conditions and can tolerate a wider range of contaminants present in industrial gas streams (Dürre, 2016). For instance, ammonia, carbonyl sulfide, and hydrogen sulfide, which are known to poison chemical catalysts, can instead serve as nutrient sources for microbial growth in gas fermentation (Phillips et al., 2017). Additionally, microbial platforms can be easily re-engineered or substituted to diversify products, making gas fermentation a flexible and potentially lower-cost solution, compared to chemical processes (Köpke & Simpson, 2020). Significant progress has been made in the scale-up of gas fermentation over the past decade. For example, ethanol production in gas fermentation has reached 369 g L<sup>-1</sup> d<sup>-1</sup> in pressurized systems and over 192 g L<sup>-1</sup> d<sup>-1</sup> at atmospheric pressure (Molitor et al., 2016).

Despite its promising prospects, gas fermentation still faces several key bottlenecks which need to be addressed. Among them, the most prominent bottleneck is the energy limitation in the production of ATP during CO<sub>2</sub> reduction, which poses a fundamental constraint on microbial metabolism (Dürre, 2016). While CO and H<sub>2</sub> in syngas can provide reducing power, CO<sub>2</sub> is thermodynamically inert and requires an external energy source for biological activation. The energy shortage results in slow cell growth, low product yields, and limited productivity, especially when CO<sub>2</sub> is the only carbon source. To overcome these challenges, bioelectrochemical systems (BES) have emerged as a promising solution, where biological processes are coupled with electrochemical reactions. Up to date, BES have been explored for diverse applications, including generating electricity (Liu et al., 2004), resource recovery (Ul et al., 2024), bioremediation (Ceballos-Escalera et al., 2021) and biosynthesis (Rabaey & Rozendal, 2010). By integrating an electrochemical system, external electrons can be supplied as an additional reducing power source, potentially enhancing microbial metabolism, preventing the use of additives for balancing redox states and addressing limitations of conventional gas fermentation (Barbosa et al., 2021).

## 2.2 CO<sub>2</sub> valorization in microbial electrosynthesis

### 2.2.1 Fundamental principles of MES

Microbial electrosynthesis (MES) is a technology which employs microorganisms as the biocatalyst for CO<sub>2</sub> reduction in an electrochemical cell (Figure 1). In principle, microorganisms are cultivated on the surface of cathode or in the catholyte and utilize electrons supplied by the external power source to catalyze enzymatic reactions, typically, the CO<sub>2</sub> reduction to organics (Nevin et al., 2010; Rabaey & Rozendal, 2010). The exogenous electrons are used to supply energy to drive the CO<sub>2</sub> reduction and regenerate the reduced form of the co-factors (reduced form of nicotinamide adenine dinucleotide (NADH) or reduced form of nicotinamide adenine dinucleotide phosphate (NADPH)) (Lee et al., 2021; Schlager et al., 2017). The most common anodic reaction is the abiotic oxygen evolution reaction (OER), in which protons and electrons, together with oxygen, are released through water splitting. The other alternative anodic reactions include microbial oxidation of wastewater (Xiang et al., 2017), oxidation of ferrocyanide (Yang et al., 2021), oxidation of sulfur (Dinh et al., 2022), using sacrificial carbon electrodes (Rohbohm et al., 2023), etc. However, each of these alternatives have limitations. For example, ferrocyanide is costly and unsustainably produced, while the use of a bioanode requires tight control of anodic potential, adding operational complexity and diverting attention from optimizing cathodic performance. Therefore, OER is still the dominant anodic reaction in MES studies. The technical and economic limitations of these alternative anodic reactions have been further discussed by Abdollahi et al., (2022).

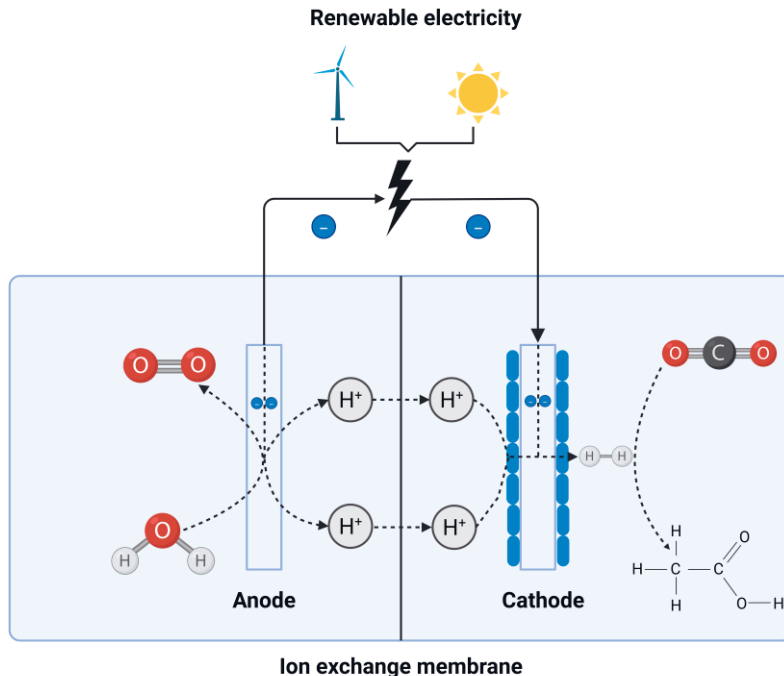


**Figure 1.** Schematic representation of a MES of  $\text{CO}_2$  to acetate with  $\text{H}_2$  as the electron shuttle. The number of molecules depicted does not reflect stoichiometric ratios and is intended for illustrative purposes only. The blue circles on the surface of the cathode represent the microorganism (Created with BioRender).

Although membrane-less reactor designs exist, the growth of the microorganisms in the cathode of the MES are sensitive to the produced oxygen. Therefore, most of the MES reactors include an ion exchange membrane (IEM) to separate the anodic and cathodic chambers. The most used IEM is cation exchange membrane (CEM), which is permeable to cations (e.g. protons). The usage of anion exchange membrane (AEM) and bipolar membrane (BPM) has also been reported (Xiang et al., 2017). With the IEM, the oxygen diffusion is restricted, and the electric circuit is completed by the ion flux between chambers.

In BES, electron transfer between electrode surface and microorganisms can be categorized as direct or indirect electron transfer. Direct electron transfer is facilitated by specific outer-membrane structures. Cytochromes associated with the surface of cell membranes are the most common proteins responsible for the electron transportation in microorganisms, such as *Geobacter sulfurreducens* and

*Shewanella oneidensis* (Hartshorne et al., 2007; Leang et al., 2003). A more unique transmembrane structure is nanowire, which could reduce the electron transfer resistance and enable a more rapid interfacial electron transfer (Creasey et al., 2018). Although direct electron transfer is widely present in the natural biogeochemical cycles (Lovley, 2017), its mechanism has most been studied in anodes of BES, where electrons flow from microbial cells to the electrode. However, direct electron transfer has not been fully elucidated in cathodes of MES. In fact, the cytochromes used for the extracellular electron transfer by *Geobacter* and *Shewanella* possess a redox potential of ca. -0.05 V (vs. standard hydrogen electrode (SHE)), which is more positive than the CO<sub>2</sub> bio-reduction in MES (i.e., from ca. -0.4 V to ca. -0.2 V vs. SHE) (Xu et al., 2022), suggesting that further investigation on direct electron transfer is needed in cathodic MES.

In indirect electron transfer, electron shuttles or mediators are used to facilitate either the transfer between electrode surface and the microbial cells or the interspecies electron transfer within a mixed microbial community. The electron shuttles can be endogenous, which are excreted naturally by microorganisms, such as riboflavin, methylviologen (Zhang et al., 2023), and neutral red (Song et al., 2022), or compounds added to the electrolyte (Zhang et al., 2020). Specifically in MES, the most important electron shuttle is H<sub>2</sub>, which is obtained by operating the MES at a more negative potential than the standard redox potential for H<sub>2</sub> evolution (theoretically -0.41 V vs. SHE). Thus, the cathodic H<sub>2</sub> evolution can occur either electrochemically or biologically.

## 2.2.2 Reactor types and electrode materials in MES

The performance of MES is highly dependent on the design of the reactor. The typical MES reactors include H-type, bottle-type, and flat cell type. A typical H-type reactor comprises two glass chambers separated by an IEM. Liquid mixing in H-type reactor is typically achieved by continuous stirring using a magnetic stirrer. The H-type reactor is commercially available, autoclavable and easy to assemble. Thus, the H-type reactors are widely used in preliminary laboratory scale experiments focusing on pure culture cultivations, studying microbial metabolism and developing electrode materials (Kim et al., 2024; Li et al., 2023; Nevin et al., 2010; Boto et al., 2023). However, H-type reactors are not ideal for improving productivity in MES, due to limited mass transfer and high internal resistance (Krieg et al., 2019). Another suitable reactor type for fundamental research in MES is bottle-type reactor, in which

both anode and cathode are placed in one vessel. The IEM is attached to one end of a tube, which is filled with anolyte and placed in the bottle that serves as a cathode. The bottle-type reactor is also easy to set up, yet the performance is greatly affected by the position of cathode which has raised uncertainties about the reproducibility in these reactor types (Liu et al., 2023).

The flat cell type reactors are adapted from conventional fuel cell designs, in which two or more flat chambers are separated by IEM. Compared to H-type reactors, the flat cell type reactors increase the membrane to volume ratio and decrease the distance between electrodes, thus reducing the internal resistance of the reactor. The mixing and substrate availability is ensured by recirculating the electrolyte through recirculation bottles. With recirculation bottles, the gas to liquid ratio can also be increased. Therefore, the flat cell type reactors are suitable for scaling up and improving the performance of MES, although they are more complicated to assemble compared to H-type reactors (Krieg et al., 2019). In fact, the highest acetate and butyrate production rates have been obtained with the flat cell type reactors (Flexer & Jourdin, 2020; Jourdin et al., 2019).

In addition to the reactor type, cathode material affects MES performance. The cathode material for MES not only should be electrochemically stable for hydrogen evolution, but also biocompatible and have a high surface area-to-volume ratio for microorganism growth. To meet these criteria, carbon-based materials have been the most commonly used cathode materials in MES (Xie et al., 2025). The non-carbon alternatives (e.g., stainless steel, titanium, copper) have been tested but are typically less effective or unsustainable (Bajracharya et al., 2024; Soussan et al., 2013). Specifically, graphite has emerged as one of the most widely used commercial carbon materials in MES. Graphite possesses a planar sheet structure and offers several advantages in aqueous cultures, including a wide electrochemical window, chemical stability, electrical conductivity, easy surface modification, reusability, and high compatibility with microbial systems (Hui et al., 2023). The usage of graphite can be in the form of single blocks, sheet, felt or rod, but can also be in a packed structure, in which the chamber is filled with electrode material (Bajracharya et al., 2022). The high porosity and expanded surface area of granular graphite cathode enhanced microbe-electrode interactions, enabled sustained biofilm activity and improved MES performance (Marshall et al., 2013). However, the contact between the current collector and the graphite granules is limited by the irregular shape of the granules and thus increases the electrical resistance of the cell (Dong et al., 2018).

Additionally, recent developments have focused on true three-dimensional (3D) electrodes. These materials are characterized by having similar dimensions in all

spatial directions, allowing microorganisms to grow on the interior volume of the electrode rather than just the surface. Examples include highly porous plane structures like reticulated vitreous carbon, foams, and carbon sponges (Flexer & Jourdin, 2020; Huang et al., 2021). These 3D materials typically contain macropores in tens of micrometers range, and these multidirectional pores facilitate fluid flow throughout the structure, increasing the accessible surface area for microbial attachment and maximizing electrochemical performance (Flexer & Jourdin, 2020).

### 2.2.3 Operational parameters affecting MES performance

Operational parameters, including temperature, pH, pressure, feeding mode and cathode potential have been reported to affect the MES performance (Table 1). In principle, increasing temperature can enhance the ion mobility and thus increase the conductivity of the electrolytes. MES typically operates between 15–45°C as the acetogenic bacteria are mostly mesophilic (e.g. *Sporomusa ovata*, *Clostridium ljungdahlii*, and *Acetobacterium woodii*). By using the thermophilic *Moorella thermoautotrophica* in MES, a 2.8-fold enhancement on acetate production rate was obtained at 55 °C compared to 25 °C (Yu et al., 2017). Similar results were obtained by Faraghiparapari & Zengler (2017) who compared *S. ovata* and *M. thermoautotrophica* in MES across a temperature range of 25 to 70 °C. Each strain performed the best at its optimal growth temperature: 25 °C for *S. ovata* and 60 °C for *M. thermoautotrophica*. Although *M. thermoautotrophica* showed enhanced production at higher temperatures, the highest acetate titer achieved with *S. ovata* was more than two-fold higher than that of *M. thermoautotrophica*. Moreover, a mixed culture study evaluated MES performance across a temperature range of 10 °C to 70 °C, and the highest acetate production rate was obtained under mesophilic conditions (both 25 °C and 35 °C) (Yang et al. 2021). The enhanced performance was likely associated with the highest relative abundance of acetogenic genera observed at these temperatures.

**Table 1.** Selected MES studies with different operational conditions and their corresponding observations.

Operational parameters	Main effects on MES	Microbial culture	Observations	References
Temperature	Mainly affects through changing the microbial metabolism and community composition	<i>Moorella thermoautotrophica</i>	A 2.8-fold increase in acetate production rate was observed at 55 °C compared to 25 °C	(Yu et al., 2017))
		<i>Sporomusa ovata</i>	The highest acetate production was observed at 37 °C within the tested temperature range between 25 °C and 70 °C	(Faraghiparapari & Zengler, 2017)
		Mixed culture	The highest acetate production was obtained at 25 °C and 35 °C within the tested temperature between 10 °C to 70 °C, which corresponded with the highest relative abundances of acetogenic bacteria at these temperatures.	(Yang et al., 2021)
Cathodic pH	CO <sub>2</sub> availability, microbial community and composition	<i>Knallgas</i> dominated mixed culture	Isolated a thermoacidophilic bacteria: <i>Knallgas</i> for MES operated at pH 3.5	(Reiner et al., 2020)
		Mixed culture	pH 5.8 improved the proton and CO <sub>2</sub> availability, and thus promoted the acetate production	(Baille-Villanova et al., 2016)
		Mixed culture dominated by <i>Clostridium</i>	pH 4.9 promoted solventogenesis	(Vassilev et al., 2019)
		Mixed culture dominated by <i>Acetobacterium</i>	pH 5 promoted hydrogen production, pH 6.5 promoted acetate production	(LaBelle et al., 2014)
Pressure	H <sub>2</sub> and CO <sub>2</sub> availability, microbial metabolism	Mixed culture dominated by <i>Clostridium</i>	pCO <sub>2</sub> (<0.3 atm) and pH <sub>2</sub> (>3 atm) promoted ethanol production	(Romans-Casas et al., 2023)

	Mixed culture dominated by <i>Megasphaera</i>	pH <sub>2</sub> (1.7–1.8 atm), and limiting CO <sub>2</sub> supply promoted the butanol production	(Romans-Casas et al., 2024)
Feeding mode	Nutrient availability, microbial growth, product washout, pH control, removing the product inhibition	Mixed culture dominated by <i>Acetobacterium</i>	Highest acetate production rate was obtained with hydraulic retention time of 3 days compared to 7 days (Izadi et al., 2021)
		Mixed culture	Higher acetate production rate was obtained under batch mode compared to continuous mode, likely due to the wash out of microbes in continuous mode (Bajracharya et al., 2017)
		Mixed culture dominated by <i>Acetobacterium</i>	Higher acetate production rates, coulombic and energetic efficiencies were obtained at continuous mode compared to batch mode (Arends et al., 2017)
Cathode potential	Microbial formation, biofilm products, carbon efficiency, catalytic ability of cathode	Mixed culture	Higher acetate, butyrate, propionate yield, coulombic efficiency, and carbon recovery efficiency were obtained when the cathodic potential increased from -0.8 V to -1.2 V (vs. Ag/AgCl) (Das et al., 2020)
		Mixed culture	Higher CH <sub>4</sub> production rate and faradaic efficiency were obtained when the cathodic potential was changed from -0.95 V to -1.1 V (vs. Ag/AgCl) (Xia et al., 2023)
		Mixed culture dominated by <i>Burkholderiales</i>	The -0.68 V (vs. Ag/AgCl) resulted in the most efficient biofilm and the highest acetate yield compared to -0.55 V and -0.72 V (Ameen et al., 2020)

The cathodic pH is also an important operational parameter in MES, which affects the availability of CO<sub>2</sub> and the metabolic pathways of the microbial community. At the cathode, proton consumption due to the biological CO<sub>2</sub> reduction or hydrogen evolution can result in an increase of cathodic pH, which could inhibit microbial growth and activity. Therefore, a buffer-based catholyte is commonly used to maintain a stable condition for MES. Most of the MES studies have been running at a slightly acidic to neutral pH, as it is optimal for most acetogenic bacteria growth (Harnisch et al., 2024). However, the optimal pH range can vary depending on microbial strain. For instance, a thermoacidophilic *Knallgas* strain dominated microbial community was reported to grow at acidic pH of 3.5 in MES (Reiner et al., 2020). In addition to microbial growth, pH also affects microbial metabolism, especially the competition between acidogenesis and solventogenesis. For example, *Clostridium autoethanogenum*, *C. carboxidivorans* and *C. ljungdahlii* produced mainly acids (e.g., acetate, butyrate) when the pH was maintained between 5.0–6.0, but the metabolism shifted toward solvent production (e.g., ethanol) under more acidic conditions (pH < 5.0) (He et al., 2022; Maddipati et al., 2011). The metabolic shift is often triggered by the accumulation of undissociated acids, which lower the pH and signal the bacteria to enter solventogenic phases to detoxify their environment (Shaw et al., 2015). Moreover, the pH could also play a role in the substrate availability of MES. For example, compared to pH 6.8, low pH in the catholyte (5.8) can result in a higher proton availability and CO<sub>2</sub> concentration, consequently enhancing the abiotic hydrogen evolution and acetate production (Batlle-Vilanova et al., 2016).

Pressure is another critical parameter in MES, as it directly influences gas solubility and mass transfer. Increasing CO<sub>2</sub> or H<sub>2</sub> partial pressure improves substrate availability by enhancing their dissolution in the liquid phase. In general, microorganisms can tolerate elevated pressures in biotechnological processes, such as gas fermentation (Van Hecke et al., 2019). For example, increasing the pressure of the gases (CO<sub>2</sub>/H<sub>2</sub>) to 10 atm enhanced the product yield compared to atmospheric pressures (Roger et al., 2018; Ullrich et al., 2018), which was likely due to the improved substrate availability and mass transfer. However, microbial growth could be inhibited when the pressure increases. The balance between microbial tolerance and enhanced productivity needs to be managed. In MES, studies on pressurized MES are limited. Only a few studies in MES have increased the pressures of H<sub>2</sub>/CO<sub>2</sub>, with maximum total pressures of 3 atm, to promote ethanol and butyrate production (Romans-Casas et al., 2023, 2024).

Feeding mode is also affecting both substrate availability and microbial activity in MES. In MES systems, feeding mode can refer to CO<sub>2</sub> delivery, nutrient addition, or both. Generally, MES can be operated in batch, fed-batch, or continuous feeding modes. Continuous CO<sub>2</sub> feeding could ensure the CO<sub>2</sub> availability, while continuous catholyte feeding could ensure nutrient availability, remove products and in pH control (Izadi et al., 2021). In addition, fed-batch feeding has also been explored, in which CO<sub>2</sub> is periodically added without fully refreshing the catholyte. Several studies have compared the MES performance under different feeding strategies. For instance, Bajracharya et al. (2017) evaluated continuous versus batch catholyte feeding with continuous CO<sub>2</sub> supply. The study indicated that batch mode resulted in higher acetate production rate, likely due to stable conditions and minimal product washout. Acetate production decreased from 149 to 100 mg L<sup>-1</sup> d<sup>-1</sup> under continuous mode, potentially due to the washout of the microorganisms with continuous feeding. Similar results were also obtained by Arends et al. (2017). Additionally, a study by Izadi et al. (2021) compared continuous mode to fed-batch mode and obtained higher acetate production rate with continuous mode due to the better pH control and constant medium refreshment.

The cathode potential has been reported to play a critical role in biofilm formation, catalytic activity of the cathode, and microbial metabolism in MES. Generally, applying more negative potential supplies additional reducing equivalents for CO<sub>2</sub> bio-reduction, thereby favoring product formation. For example, Das et al., (2020) demonstrated in a mixed-culture MES study that overall yields increased progressively as the cathode potential was changed from -0.8 V to -1.2 V (vs. Ag/AgCl). However, lowering the potential also increases energy input, and the lowest energy consumption for acetate production (0.15 kWh kg<sup>-1</sup>) was achieved at -0.7 V (vs. Ag/AgCl). Furthermore, cathode potential affects biofilm development, thus affecting the overall production in MES (Vassilev et al., 2022). A study by Ameen et al. (2020) evaluating potentials between -0.55 V, -0.68 V and -0.72 V (vs. Ag/AgCl) revealed that the most efficient and conductive biofilm was formed at -0.68 V (vs. Ag/AgCl), resulting in the highest acetate yield of 2.2 g L<sup>-1</sup>. In addition, cathode potential has been shown to influence the catalytic activity of the electrode. For instance, the CH<sub>4</sub> production rate increased almost linearly when the potential was shifted from -0.95 V to -1.1 V (vs. Ag/AgCl), due to enhanced catalytic activity (Xia et al., 2023). In MES, the optimal cathode potential depends on the experimental configuration, the structure and composition of the microbial community, and the properties of the electrode material. In addition, cathode potential has been shown to influence the catalytic activity of the electrode itself. For

instance, the CH<sub>4</sub> production rate increased almost linearly when the potential was shifted from -0.95 V to -1.1 V (vs. Ag/AgCl), due to enhanced catalytic activity (Xia et al., 2023). In MES, the optimal cathode potential depends on the experimental configuration, the structure and composition of the microbial community, and the properties of the electrode material.

## 2.2.4 Product spectrum in MES

The initial MES products included both acetate and methane. The bioelectrochemical production of methane from CO<sub>2</sub> was obtained using pure methanogenic cultures such as *Methanobacterium palustre* (Cheng et al., 2009) and *Methanococcus maripaludis* (Mayer et al., 2019), as well as mixed cultures dominated by methanogens (Hengsbach et al., 2022). The highest reported methane production rate is 12.5 L L<sup>-1</sup> d<sup>-1</sup>, with a 65% current-to-methane efficiency, achieved in a galvanostatic flat cell designed to optimize surface area and flow distribution using a mixed culture from a biogas plant (Geppert et al., 2019). In mixed culture MES targeting for the production of VFAs, the production of methane is often inhibited by various methods, including the addition of 2-bromoethanesulfonate, operating MES at mildly acidic pH, and thermal/oxidative pretreatment of the inoculum (Batlle-Vilanova et al., 2016; Marshall et al., 2012; Modestra & Mohan, 2017). The product spectrum is then most often dominated by acetate. After more than a decade of research, the product spectrum in MES has expanded beyond acetate to include various value-added commodities.

Acetate production in MES is primarily driven by acetogenic bacteria through the WLP, including *Sporomusa spp.*, *Clostridium spp.*, *Acetobacterium woodii*, and *Moorella thermoacetica*. Production rates have increased significantly over the past decade—from ca. 1.3 g m<sup>-2</sup> d<sup>-1</sup> (Nevin et al., 2010) up to 790 g m<sup>-2</sup> d<sup>-1</sup>, using a 3D macroporous carbon felt electrodes, which enhanced the microbe–electrode interaction and improved mass transfer (Jourdin et al., 2016). Acetate production can be obtained with over 90% product selectivity (Jourdin & Burdyny, 2021). However, acetate has a relatively low market value (ca. 500 euro t<sup>-1</sup> (Statista, 2025)), which limits the commercial attractiveness of MES. One possible solution is to use genetically modified tools or introduce non-acetogenic microorganisms to expand product spectrum. For instance, Le et al. (2024) reported a single-step MES process which converted CO<sub>2</sub> to acetate by acetogenic bacteria and subsequent reduction to

polyhydroxybutyrate (PHB) by PHB accumulating bacteria, achieving PHB yields up to 45.3 mg L<sup>-1</sup> with the cathodic potential of -1.0 V (vs. Ag/AgCl). Other novel products include terpenes like  $\alpha$ -humulene (17 mg g<sup>-1</sup> cell dry weight) and lycopene (1.73 mg L<sup>-1</sup>), produced from CO<sub>2</sub> by engineered *Cupriavidus necator* (Krieg et al., 2018; H. Wu et al., 2022; Yadav et al., 2022). In addition to producing platform chemicals, MES generates products that serve as feedstocks for spatially separated bioprocesses. For example, feeding acetate from MES to *Acinetobacter baylyi* ADP1 led to production of long chain alkyl esters (wax esters) with the titer of 38  $\mu$ mol L<sup>-1</sup> (Lehtinen et al., 2017).

More commonly, acetate production in MES can be upgraded to alcohol or longer chain fatty acids by coupling different metabolisms in single or separate steps. Ethanol (Srikanth et al., 2018), isopropanol (Arends et al., 2017), butanol (Vassilev et al., 2018), and hexanol (Vassilev et al., 2018) production have been reported in MES (Table 2). Alcohol production in MES could promote chain elongation and result in the production of butyrate and caproate. In MES, butyrate production was reported for the first time in 2015 by Ganigüé et al. (2015), who obtained the maximum butyrate titer of 0.45 g L<sup>-1</sup> and production rate of 0.04 g L<sup>-1</sup> d<sup>-1</sup>. Caproate was firstly reported as a non-quantified trace compound in MES (Batlle-Vilanova et al., 2017). Subsequently, quantified and continuous caproate production was reported by both Jourdin et al. (2018) and Vassilev et al. (2018) with the maximum caproate titer of ca. 1 g L<sup>-1</sup> in both studies after running MES for over 300 days. In 2019, Jourdin et al. (2019) further improved caproate production by using continuous CO<sub>2</sub> and nutrient feeding with CO<sub>2</sub> loading rate of 173 L d<sup>-1</sup> and hydraulic retention time of 14 days. This approach resulted in a maximum caproate titer of 3.1 g L<sup>-1</sup> and a production rate of 0.4 g L<sup>-1</sup> d<sup>-1</sup>, which is the highest reported values in MES fed with only CO<sub>2</sub>.

**Table 2.** Products reported in MES or MES integrated processes.

Major product	Carbon source	Microbial culture	Applied/ Obtained cathodic potential (V) (vs. Ag/AgCl)	Reactor type	Cathode materials	Production rate	Titer/Yield	Feeding mode	Reference
<b>Methane</b>	CO <sub>2</sub>	Mixed culture dominated by <i>Methanobacterium palustre</i>	-1.2	H-type	Carbon cloth	656 mmol-CH <sub>4</sub> d <sup>-1</sup> m <sup>-2</sup>	n.a	Batch CO <sub>2</sub> feeding	Cheng et al., 2009
<b>Acetate</b>	CO <sub>2</sub>	<i>Sporomusa ovata</i>	-0.6	H-type	Graphite sticks	n.a.	n.a.	Continuous CO <sub>2</sub> feeding (0.1 mL min <sup>-1</sup> )	Nevin et al., 2010
<b>Ethanol</b>	CO <sub>2</sub>	Sulfate reducing bacteria and iron reducing bacteria	-1.0	H-type	Graphite plate loaded with carbon powder	n.a.	5.2 g L <sup>-1</sup>	Fed batch (daily CO <sub>2</sub> feeding)	Srikant et al., 2018
<b>Butanol</b>	CO <sub>2</sub>	Mixed culture dominated by <i>Megasphaera</i>	-0.6	Flat cell type	Carbon felt	27.0 mg L <sup>-1</sup> d <sup>-1</sup>	0.2 g L <sup>-1</sup>	Fed batch (periodically CO <sub>2</sub> feeding)	Romans-Casas et al., 2024
<b>Isopropanol</b>	CO <sub>2</sub>	Mixed culture dominated by <i>Acetobacterium</i>	-1.1	Flat cell type	Carbon felt	60.0 mg L <sup>-1</sup> d <sup>-1</sup>	0.82 g L <sup>-1</sup>	Continuous CO <sub>2</sub> feeding (9.7mL min <sup>-1</sup> )	Arrends et al., 2017
<b>Butyrate</b>	CO <sub>2</sub>	Mixed culture dominated by <i>Clostridium</i>	-1.0	H-type	Carbon cloth	0.04 g L <sup>-1</sup> d <sup>-1</sup>	0.45 g L <sup>-1</sup>	Fed batch (every 2/3 days for 5 mins CO <sub>2</sub> feeding)	Ganigüé et al., 2015
<b>Caproate</b>	CO <sub>2</sub>	Mixed culture dominated by <i>Clostridium</i>	-0.8	Bottle-type	Graphite granules	38.7 mg L <sup>-1</sup> d <sup>-1</sup>	1.2 g L <sup>-1</sup>	Fed batch (periodically CO <sub>2</sub> feeding)	Vassilev et al., 2018

<b>poly(3-hydroxybutyrate) (PHB)</b>	CO <sub>2</sub>	Mixed culture dominated by PHB-biosynthesizing bacteria	-1.0	Flat cell type	Carbon felt	n.a.	43.5 mg L <sup>-1</sup>	Fed batch (daily CO <sub>2</sub> feeding)	Le et al., 2024
<b><math>\alpha</math>-humulene</b>	CO <sub>2</sub>	Genetic modified <i>Cupriavidus necator</i>	-2.0	Bottle-type	Stainless steel foil	n.a.	17 mg $\alpha$ -humulene per g (cell dry weight)	Continuous CO <sub>2</sub> feeding (10-15 mL min <sup>-1</sup> )	Krieg et al., 2018
<b>Lycopene</b>	Exhaust gas (10–15% v/v CO <sub>2</sub> )	Genetic modified <i>Cupriavidus necator</i>	4.5 (whole cell volatge)	Bottle-type	Stainless steel mesh	n.a.	1.7 mg L <sup>-1</sup>	Fed batch (daily CO <sub>2</sub> feeding)	H. Wu et al., 2022
<b>Wax ester</b>	CO <sub>2</sub>	<i>Sporomusa ovata</i> and <i>Acinetobacter baylyi</i> ADP1	-1.0	H-type (MES) and flask	Graphite stick	n.a.	38 $\mu$ mol L <sup>-1</sup>	Continuous CO <sub>2</sub> feeding	Lehtinen et al., 2017

n.a. denotes not applicable

## 2.3 Butyrate production in MES

### 2.3.1 Usage of electron donors for butyrate production

Out of the diversified products in MES, butyrate can be a promising product. Butyrate is a C4 chemical with various applications in chemical, food, pharmaceutical and animal feed industries. For example, butyrate is widely used to enhance fruit fragrance and in perfume production (Jiang et al., 2018). Butyrate can also be used for chemical synthesis, i.e. a precursor to produced thermoplastic cellulose acetate butyrate, an important organic solvent (Dwidar et al., 2012). For the pharmaceutical industry, butyrate has shown therapeutic effects for treating diseases including stomach and intestine diseases (Huang et al., 2011). Several butyrate derivatives have been developed as antithyroid drugs and used in anesthetics (Hakalehto et al., 2022; Jiang et al., 2018).

Currently, butyrate production is mainly achieved by chemical synthesis via the oxidation of butyraldehyde which is a petrochemical feedstock (Câmara-Salim et al., 2021). The standard butyrate production can achieve over 90% yield of crude butyrate, yet this process requires high temperature and pressure conditions (e.g. over 20 MPa and 180°C) (Cascone, 2008; Pryde, 1978). Thus, producing butyrate by microbial fermentation from renewable feedstocks has gained general interest. For example, using sugarcane bagasse (Wei et al., 2013), oilseed rape straw (Huang et al., 2016), rice straw (Lee et al., 2015), and wheat straw (Liu et al., 2013) as feedstocks for butyrate production in fermentation has been reported. However, these feedstocks are food based and raise the question of competing with agricultural lands. Using CO<sub>2</sub> as the feedstock could avoid such competition and thus, make MES an alternative process for butyrate production.

Since the first reported butyrate production in MES (Ganigué et al., 2015,) optimizations have been carried out to improve the butyrate production rate/selectivity (Table 3). For instance, by controlling the pH at ca. 5 and increasing the H<sub>2</sub> partial pressure over 1 atm, Batlle-Vilanova et al. (2017) promoted in-situ ethanol production and increased the butyrate production rate to 0.16 g L<sup>-1</sup> d<sup>-1</sup>. Later in 2019, Jourdin et al. (2019) reported a continuously CO<sub>2</sub> fed MES with the loading rate of 173 L d<sup>-1</sup> and the hydraulic retention time of 14 days to obtain a butyrate production rate of 0.7 g L<sup>-1</sup> d<sup>-1</sup>, which was also achieved by ethanol assisted chain

elongation. As ethanol provides reducing power for butyrate production, MES has been further optimized to achieve the maximum ethanol production and thus to promote butyrate production. For example, the work from Romans-Casas et al. (2024) applied the optimal conditions for solventogenesis ( $H_2$  partial pressure of 1.7 atm) obtaining highly selective butyrate production (78% selectivity) with butyrate production rate of  $0.18 \text{ g L}^{-1} \text{ d}^{-1}$ . Moreover, a new reactor design has been proposed by Vassilev et al. (2019), which employed dual-cathode chamber MES reactors allowing pH control in separate cathodes—one maintaining pH at 6.9 for acetogenesis and chain elongation, while the other maintaining pH at 4.9 in a second stage to promote solventogenesis and ethanol production. Additionally, the modification of cathode materials has been shown to improve butyrate production. Tahir et al. (2021) reported a  $\text{NiFe}_2\text{O}_4$ -coated carbon felt cathode in a  $\text{CO}_2$  fed MES, improving butyrate selectivity from 37% to 95% compared to unmodified carbon felt.

Instead of optimizing solventogenesis for in-situ ethanol production, an alternative strategy is to supply external electron donors as co-substrates alongside  $\text{CO}_2$  in MES. This approach mitigates competition between ethanol production and butyrate formation, as the operational conditions favoring solventogenesis, such as low pH and high  $H_2$  partial pressure, often diverge from those required for efficient butyrate production. In MES, potential exogenous electron donors include ethanol (Izadi et al., 2021; Jiang et al., 2020), lactate (Zhang et al., 2023) and formate (Izadi et al., 2021). Adding  $5 \text{ g L}^{-1}$  ethanol to MES can obtain selective butyrate production (80% selectivity) with the production rate  $0.44 \text{ g L}^{-1} \text{ d}^{-1}$  (Zhang et al., 2023). Increasing ethanol addition likely resulted in reduction of butyrate concentration, resulting in selective caproate production (92% selectivity) in MES (Jiang et al., 2020). The addition of formate or lactate resulted in butyrate production rate of  $0.008 \text{ g L}^{-1} \text{ d}^{-1}$  (Izadi et al., 2021) and  $0.17 \text{ g L}^{-1} \text{ d}^{-1}$  (Zhang et al., 2023), respectively. The reported electron recovery in butyrate varied considerably across MES studies. An electron recovery in butyrate (54%) was obtained when external ethanol was added, and the majority of electrons in butyrate was originated from ethanol rather than from the cathode, which contributed less than 10% of the total electron input (Zhang et al., 2023). Out of the aforementioned electron donors, ethanol has resulted in the most selective and highest butyrate production rates, which is likely due to the highest reducing power of ethanol. The degree of reduction (DoR) evaluates the number of available electrons per carbon atom in a compound, indicating its thermodynamic reduction ability. Ethanol has the DoR per carbon of 6, which is higher than formate (1) and lactate (4). However, ethanol is a valuable biochemical

within industrial production competing with the food production. Moreover, the high dosage of ethanol addition in MES likely further resulted in butyrate reduction, shifting the dominant product to caproate (Jiang et al., 2020). Finding an alternative electron donor which has a high DoR, renewable sources, and capability for selective butyrate production is required.

Methanol is a promising alternative to ethanol. Compared to ethanol, methanol has the same DoR per carbon. However, the production of methanol has been implemented from non-food-based feedstocks at industrial scale. For instance, Biomethanol Chemie (Netherlands) uses glycerol or wood chips; Värmlandsmetanol (Sweden) uses forest residues; and Carbon Recycling International (Iceland) produces methanol from industrial CO<sub>2</sub> emissions and hydrogen generated via water electrolysis using renewable electricity. Although ethanol can also be produced from lignocellulosic biomass, methanol offers higher yields and requires lower capital investment than ethanol from the same feedstock (Tarud & Phillips, 2001). Moreover, methanol has been reported to reduce CO<sub>2</sub>/acetate into butyrate in both pure culture (Dietrich et al., 2021; Gentner et al., 1981) or mixed culture fermentation (Chen et al., 2016). Gentner et al. (1981) reported *Eubacterium limosum*, a methanol and H<sub>2</sub>-CO<sub>2</sub>-utilizing species, to produce acetate, butyrate and caproate, with butyrate as the predominant product. Building on this, Chen et al. (2016) demonstrated methanol can also be used in open mixed culture to drive chain elongation of acetate into butyrate and caproate. Adding methanol as a co-substrate can also help overcome key limitations often reported in MES, such as low biomass growth and inefficient CO<sub>2</sub> utilization. In particular, adding CO<sub>2</sub> with methanol has been shown to stimulate microbial growth and improve substrate utilization efficiency (H<sub>2</sub> and CO<sub>2</sub>) in gas fermentation (Kim et al., 2021). All those aforementioned characteristics make methanol a promising addition for MES to produce butyrate, yet this has never been reported.

**Table 3.** Comparison of butyrate production in mixed culture MES studies fed with CO<sub>2</sub> and with different electron donors. For each electron donor, the first reported studies and studies with the highest butyrate production rates/titers are included in the table. (Adapted from publication II (Yao, Romans-Casas, et al., 2025), licensed under CC BY-NC 4.0.).

Electron donor(s)	Running time (d)	Substrate feeding mode	Titer (g L <sup>-1</sup> )	Production rate (g L <sup>-1</sup> d <sup>-1</sup> )	Production rate (g m <sup>-2</sup> d <sup>-1</sup> )	Selectivity (%)	Dominant genus in mixed culture	Electron recovery for butyrate (%)	References
Electrode	34	Fed-batch	0.4	0.04	n.a.	< 30 <sup>a</sup>	Clostridium	n.a.	Ganigüé et al., 2015
Electrode	35	Fed-batch	1.0	0.2	15.4	95 <sup>a</sup>	Ochrobactrum	n.a.	Tahir et al., 2021
Electrode	263	Continuous	9.3	0.7	125.0	< 40 <sup>b</sup>	n.a.	27.6	Jourdin et al., 2019
Electrode+ Formate	45	Fed-batch	0.1	0.008	0.5	6 <sup>a</sup>	<i>Pullulanibacillus</i>	n.a.	Izadi et al., 2021
Electrode+ L-lactate	7	Batch	1.2	0.17	17.0	72 <sup>a</sup>	<i>Desulfovibrio</i>	Ca. 50	Zhang et al., 2023
Electrode+ Ethanol	7	Batch	1.2	0.2	29.1	< 10 <sup>a</sup>	<i>Clostridium</i>	Ca.10	Jiang et al., 2020
Electrode+ Ethanol	7	Batch	3.1	0.4	44.0	79 <sup>a</sup>	<i>Clostridium</i>	54.0	Zhang et al., 2023

a Selectivity is reported estimated based on the amount of one compound versus the total amount of products reported in the original work.

b Selectivity is defined as the ratio between the production rate of butyrate and the total production rate of organics over the same period of time.

c Selectivity is defined as the electron concentration of the butyrate divided by the electron consumption from the substrates.

n.a. denotes not applicable

### 2.3.2 Butyrate producing microbial communities in MES

The current butyrate production in MES is mostly reported with mixed cultures. Therefore, characterization of the microbial communities is important to understand the responsible microorganisms and potential biochemical pathways. Sequencing methods, including 16S ribosomal RNA (rRNA) gene sequencing and shotgun metagenomic sequencing are two commonly used methods. 16S rRNA gene sequencing is a method used to identify and compare bacteria and archaea within a sample, by focusing on the 16S ribosomal RNA gene, which is highly conserved across prokaryotes but contains variable regions that allow for taxonomic classification, often down to the genus level. This technique is widely used for microbial community profiling due to its cost-effectiveness and simplicity, though it provides limited insight into the functional potential of the microbes (Tringe & Hugenholtz, 2008). Shotgun metagenomic sequencing sequences all the genetic material in a sample, including bacteria, archaea, viruses, and eukaryotes (Quince et al., 2017). Unlike 16S rRNA gene sequencing, it does not rely on a specific marker gene and enables both taxonomic and functional profiling, which provides deeper insights into the metabolic capabilities, gene content, and potential interactions within complex microbial communities. Both 16S rRNA gene sequencing and shotgun metagenomic sequencing have been employed to characterize the microbiome in MES systems (LaBelle et al., 2019; Marshall et al., 2017).

Although direct butyrate production from CO<sub>2</sub> has been hypothesized (Ganigué et al., 2015; Raes et al., 2017), it still lacks direct scientific evidences and the biochemical pathways remain unclear. More commonly, butyrate production in MES relies on carbon chain elongation from acetate. Therefore, chain elongators are dominant in the butyrate producing communities (Table 3). For the ethanol assisted butyrate production in MES, the bacterial communities are mostly dominated by genus *Clostridium* (Ganigué et al., 2015; Jiang et al., 2020; Vassilev et al., 2018; Zhang et al., 2023). Additionally, pure culture MES study also reported butyrate production from CO<sub>2</sub> with *Clostridium scatologenes* ATCC 25775<sup>T</sup> (Liu et al., 2018). Members of the genus *Clostridium*, such as the *C. kuyveri*, are known to perform carbon chain elongation via the reverse β-oxidation (RBO) pathway (Fernández-Blanco et al., 2023; Seedorf et al., 2008). The most studied electron donor is ethanol, which acts as the carbon and energy source and provider of reducing equivalents for the process. Part of ethanol is oxidized to acetate for metabolic energy, while the remaining ethanol is converted into acetyl-CoA. Subsequently, the acetyl-CoA

condenses with acetate, resulting in a two-carbon chain elongation and the formation of butyrate or repeated such process for the formation of caproate (Fernández-Blanco et al., 2023). Additionally, Tahir et al. (2021) reported an *Ochrobacterium* dominated mixed culture (relative abundances of 61.4%) for a selective butyrate production. However, *Ochrobacterium* has not been reported in other studies facilitating chain elongation, thus the potential biochemical pathways need to be further investigated. Unfortunately, the microbial community compositions are not reported in some studies (Jourdin et al., 2019) or not reported to the genus level (Wu et al., 2022). For the lactate assisted MES, only one study was carried out by Zhang et al. (2023), in which *Desulfovibrio* was the dominant bacteria with relative abundances of over 80%. The genus *Desulfovibrio* has also been reported to facilitate lactate assisted chain elongation (Kucek et al., 2016; Qiang et al., 2025). Similar to ethanol, lactate is oxidized to acetyl-CoA, which part of the acetyl-CoA is converted to acetate for ATP generation and the remaining parts enter the RBO pathway (Wu et al., 2019). For the formate assisted MES, Izadi et al. (2021) reported the microbial community being dominated by *Pullulanibacillus*, which had the relative abundances of 63.5%. However, *Pullulanibacillus* is rarely reported for chain elongation and its potential role for butyrate production remains elucidated. Therefore, bioinformatics tools, including genomics, transcriptomics, proteomics, and metabolomics, are important to use for understanding the microbial composition and functions involved in the chain elongation process during MES.

### 3 RESEARCH METHODOLOGY

This section summarizes the microbial culture, cultivation media, experimental set-ups, analytical methods, bioinformatics, calculations and statistical analysis used in this research. More detailed information can be found in the original publications I-III.

#### 3.1 Culture and cultivation media

The original inoculum was acquired from a running MES reactors fed with CO<sub>2</sub> and aiming for carboxylates production, which was dominated by *Eubacterium*, *Proteiniphilum* and *Cellulosimicrobium* (Vassilev et al., 2024). For the cultivation of the microbiome used in this research, a phosphate buffered media was used, consisting of 18 g L<sup>-1</sup> Na<sub>2</sub>HPO<sub>4</sub> 2H<sub>2</sub>O, 3 g L<sup>-1</sup> KH<sub>2</sub>PO<sub>4</sub>, 3 g L<sup>-1</sup> NH<sub>4</sub>Cl, 15 mg L<sup>-1</sup> CaCl<sub>2</sub>, 20 mg L<sup>-1</sup> MgSO<sub>4</sub> 7H<sub>2</sub>O, 2.1 g L<sup>-1</sup> sodium 2-bromoethanesulfonate, 1 g L<sup>-1</sup> yeast extract as well as 10 mL L<sup>-1</sup> trace elements solution and 1 mL L<sup>-1</sup> vitamin solution. Detailed composition of the trace elements and vitamin solution can be found from publication I. In publication II, the concentration of Na<sub>2</sub>HPO<sub>4</sub> 2H<sub>2</sub>O and KH<sub>2</sub>PO<sub>4</sub> were adjusted aiming for different buffering pH values. After preparation, all media were filtered (0.2 µm, Fisherbrand™ Disposable PES Filter Units, USA) for sterilization and sparged with N<sub>2</sub> (ca. 60 mL min<sup>-1</sup>) to eliminate dissolved oxygen from the medium.

#### 3.2 Experimental set-up and operation

The MES reactors used in this research (publication I-III) were carried out in two-chamber electrochemical reactors connected to the recirculation bottles with details specified in the following chapters.

### 3.2.1 MES with graphite granules as the cathode

Two-chamber flat plate MES reactor (Figure 2) was used for enrichment of the culture in publication I and in experiments carried out in publication II. Each chamber had an internal volume of 124 mL (7.5 cm × 5.5 cm × 3 cm) for the cathodic chamber, and 62 mL (7.5 cm × 5.5 cm × 1.5 cm) for the anodic chamber. Two chambers were separated by a cation exchange membrane (CEM, CXM-200, membrane international, USA), with an active surface area of 41 cm<sup>2</sup>. The cathodic chamber was packed with graphite granules, and two graphite rods were used as current collectors. A reference electrode (+ 0.206 V vs. SHE, MF-2052, BASi, USA) was inserted into a cathodic chamber via a capillary glass frit (4 × 60 mm) through the side port. The anode was composed of platinum wire (0.4 mm in diameter). The cell was operated with a 3-electrode configuration, controlled by a potentiostat. In publication I, chronoamperometry method was applied to enrich the culture with cathodic potential poised at the range of -0.75 V to -0.95 V (vs. Ag/AgCl). In publication II, chronopotentiometry method (-100 mA) was used resulting in current density of 0.14 mA cm<sup>-2</sup> (calculated based on the estimation of the cathode surface area).

A similar reactor set-up (Figure 3) was used for the experiments in publication I to compare results of different feeding regimes. Differences were as follows: The anodic and cathodic chambers had an internal volume of 35 mL (7 cm × 5 cm × 1 cm) and CEM had an active surface area of 35 cm<sup>2</sup>.

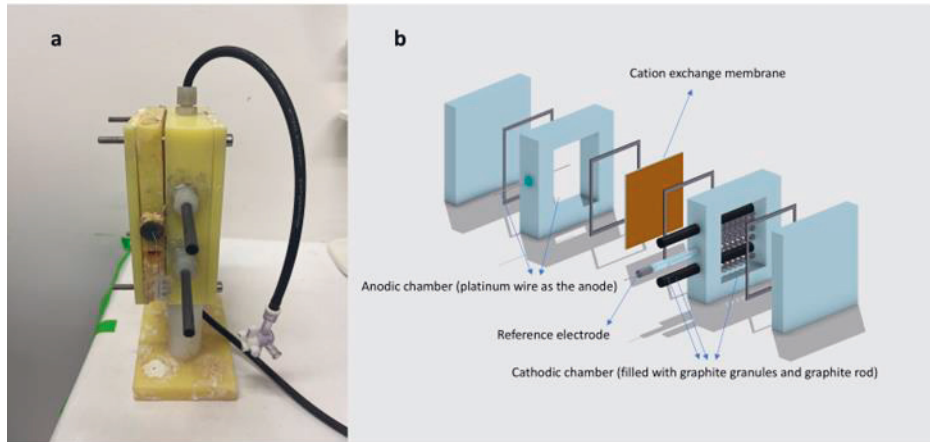


**Figure 2.** Reactor used in publication I-II, with a) photo of the granular bed reactor, and b) schematic of the reactor.

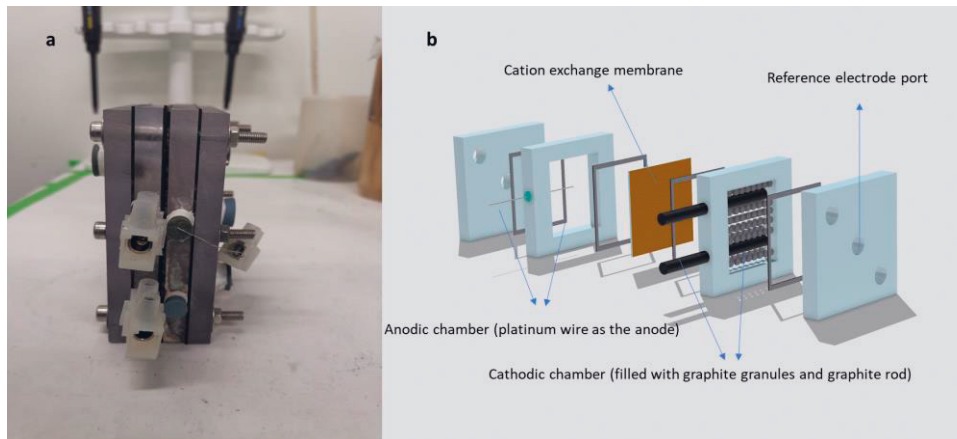


**Figure 3.** Reactor used in publication I, with a) photo of the granular bed reactor, and b) schematic of the reactor.

### 3.2.2 MES with graphite felt as the cathode

A commercial electrochemical cell (Figure 4) was used for the experiments in publication III to test operational conditions with overpressures of H<sub>2</sub> and CO<sub>2</sub>. The internal volumes of the cathode and anode chambers were 4 mL and 3 mL, respectively, separated by reinforced CEM (Nafion N324, USA). Carbon felt and a

dimensionally stable electrode (DSA-O2) with projected surface areas of 10 cm<sup>2</sup> were used as the cathode and anode, respectively. A reference electrode (+0.197 V vs. SHE) was inserted into the anodic recirculation lines. The whole cell voltage was operated with a potentiostat by using chronopotentiometry method (-15 or -30 mA), while the cathodic potential was measured once a week with a multimeter.

A customized two-chamber reactor (Figure 5) was used in publication III, testing the optimal conditions for efficient butyrate production. The cathode and anode (internal volume of 23 mL, respectively) were separated by a CEM, which had an active surface area of 20 cm<sup>2</sup>. A reference electrode (+0.197 V vs. SHE) was integrated into the cathodic recirculation line via a closed vial. A platinum wire (0.4 mm in diameter) was used as the anode. Graphite felt was used as the cathode (projected surface area of 20 cm<sup>2</sup>). The cell was operated with a 3-electrode configuration using a chronopotentiometry technique (-87 mA), controlled by a potentiostat, resulting in current density of 4.35 mA cm<sup>-2</sup>.

Reactors used in publications I and II were selected based on their stable performance in our previous MES experiments, and their ability to enhance microbial growth through the use of packed graphite granules. The reactor used in publication III (Figure 4) was employed due to its capacity to maintain overpressure conditions in MES cells. Another MES reactor presented in publication III (Figure 5) was utilized to reduce cell voltage in order to optimize methanol assisted MES with respect to energy input.

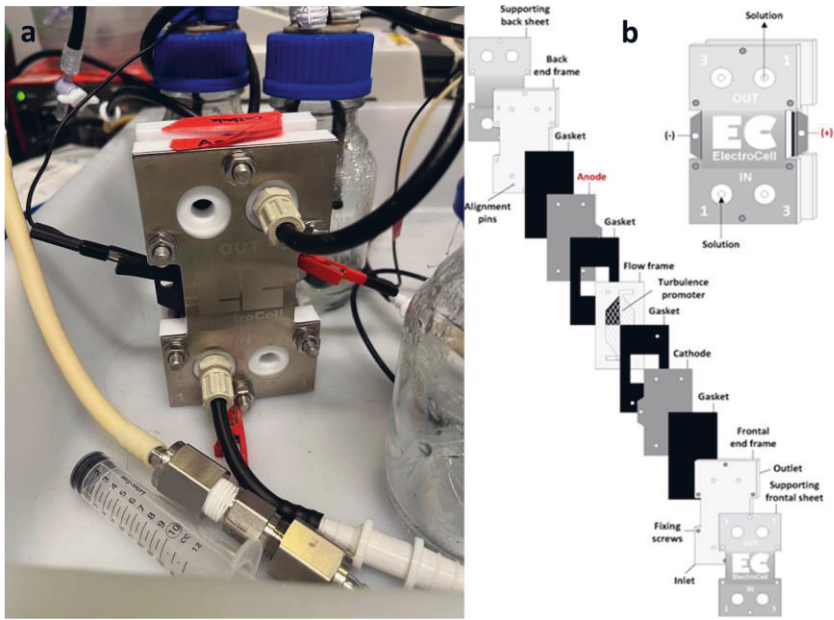


**Figure 4.** Reactor used in publication III, with a) photo of the compact reactor, and b) schematic of the reactor (reproduced from Morais et al., 2024, Chemical Engineering Journal, licensed under CC BY 4.0.).

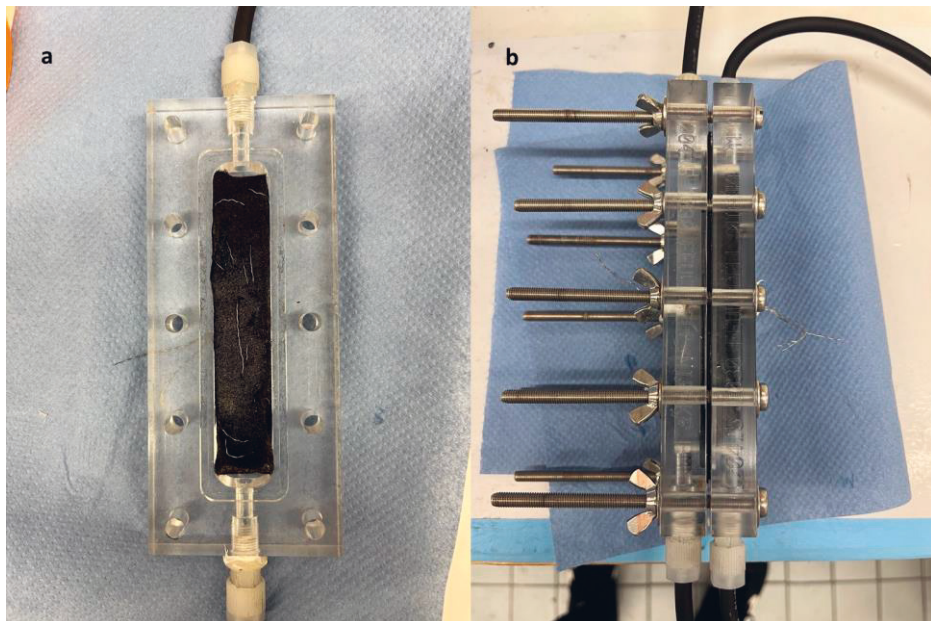


**Figure 5.** Reactor used in publication III, with a) photo of the graphite felt cathode, and b) photo of the reactor

### 3.2.3 Experimental operation

In this thesis, both MES and fermentation experiments were carried out (Table 4). For the MES experiments, Publication I aimed to validate the methanol assisted MES by comparing results between three substrate feeding regimes: methanol and CO<sub>2</sub>, only CO<sub>2</sub> and only methanol feeding. Publication II aimed to investigate the effects of cathodic pH on the methanol assisted MES, in which pH values of 5.5, 6 and 7 were tested. Publication III aimed to improve butyrate production rates by choosing the optimal running temperature, pressure and methanol/CO<sub>2</sub> ratio. For all experiments, methanol and CO<sub>2</sub> were fed to the reactors three times a week. Each batch MES experiment was operated between 28 to 32 days. Broth conductivity was monitored during each sampling to ensure sufficient ionic strength and stable electrochemical operation. Methanol was added using the prepared methanol stock solution and CO<sub>2</sub> was sparged to the recirculation bottles of the cathodic chamber controlled by a rotameter at a flow rate of 0.4 L min<sup>-1</sup> (EK-2LR, Kytola, Finland) (publication I), or mass flow controller (F-201CV, Bronkhorst, the Netherlands) at a flow rate of 50 mL min<sup>-1</sup> and collected in the gas bags (publication II and III). In publication I and II, methanol was added to the cathodic recirculation bottles to obtain a 20 mmol L<sup>-1</sup> addition every time. For publication III, a methanol/CO<sub>2</sub> ratio of 3 was maintained by the following procedure: On each substrate addition day, methanol was dosed based on the methanol concentrations obtained the same day to maintain the target methanol/CO<sub>2</sub> ratio at the beginning of each fed-batch cycle. In publication III, MES was conducted at 23°C under overpressure conditions. Overpressure was achieved by sparging CO<sub>2</sub> into the cathodic recirculation bottles and adjusting the system pressure to 1.5 atm using a differential pressure gauge (Testo 512, Spain). In addition, a continuous CO<sub>2</sub> feeding regime was tested—though the results were not published, they are included in this dissertation. During this experiment, CO<sub>2</sub> was continuously sparged through the cathodic recirculation bottles at 1 mL min<sup>-1</sup> and collected in gas bags, while methanol was added three times a week.

For the fermentation experiments, methanol and CO<sub>2</sub> were added three times a week in fed-batch mode. Two different gas compositions were supplied. In publication I, only CO<sub>2</sub> was sparged through the serum bottles (liquid volume 80 mL, total volume 120 mL) and collected in an attached gas bag (500 mL) to investigate whether the microbial community could be sustained with only CO<sub>2</sub>. In publication III, a mixture of H<sub>2</sub>/CO<sub>2</sub> (80%/20%) was provided to serum bottles (liquid volume 40 mL, total volume 120 mL) to simulate MES condition and test the effects of different operational parameter combinations, which included

methanol/CO<sub>2</sub> ratios (0.5 to 5), temperatures (23 and 35°C) and pressures (1 to 2 atm). These results were subsequently used to choose the operating conditions of the methanol assisted MES reactors for maximizing butyrate production. All the serum bottles were placed on the shaker with 120 rpm to ensure mixing.

**Table 4.** Tested operational conditions in this dissertation

Operational conditions		Purpose	Publication
Cathode materials	Graphite granules	-	I-III
	Carbon felt	Decreasing the energy consumption	III
CO <sub>2</sub> Feeding	Sparged through the recirculation bottles	-	I
	Sparged and collected in the gas bags/recirculation bottles	Obtaining fixed amount/pressure	II, III
Methanol feeding	20 mM addition each time	-	I, II
	Adjust the methanol addition to obtain certain methanol/CO <sub>2</sub> ratios	Investigating the effects of methanol/CO <sub>2</sub> ratio	III
Cathodic pH	Maintained > 6 when necessary	-	I, III
	Controlled at pH 5.5, 6 and 7	Investigating the effects of pH	II
Temperature	35°C	-	I-III
	23°C	Altering the main product to acetate	III
Pressures	Atmospheric pressure	-	I-III
	Maximum total pressure of 1.5 atm	Altering the main product to acetate	III

Symbol “-” indicates that the use of certain conditions is based on previous studies conducted in our lab.

### 3.3 Analytical methods

#### 3.3.1 Chemical analysis

Liquid samples for all publications were analyzed to check the optical density (OD<sub>600</sub>), pH and volatile fatty acids (VFAs) production (Table 5). Liquid samples were filtered through a 0.2 µm filter before the analysis. Total inorganic carbon (TIC) was analyzed by a total organic carbon analyzer with ASI-V sampler (Publication I and II). VFAs and alcohols were analyzed via gas chromatography with a flame ionization detector (GC-FID), equipped with AOC-20s autosampler and a Zebron

ZB-WAX plus column (0.25 µm diameter, 30 m length) (publication I-III) or with a GC-FID equipped with a DB-FFAP column (publication III).

Gas samples were analyzed for the composition and volume in all publications. The gas composition were analyzed by a GC with thermal conductivity detector (GC-TCD) equipped with an Agilent J&W packed GC column (1.8 m length, 2mm) (publication I-III) and a micro GC-TCD equipped with two columns: a CP-Molesieve 5A with helium as the carrier gas for CH<sub>4</sub>, CO, H<sub>2</sub>, O<sub>2</sub>, and N<sub>2</sub> analysis, and a CP-Poraplot U with argon as the carrier gas for CO<sub>2</sub> analysis. The gas volume was determined by a water replacement method (publication I-III). Additionally, for the MES reactors running with overpressure in publication III, gas amounts were calculated based on the headspace volume and pressures changes which were monitored by a pressure meter.

**Table 5.** List of analytic methods/instruments used in the study.

Analyses	Instruments/Methods	Publication
pH	Portable pH meter	I, III
	Endress-Hauser transmitter	II
Optical density	UV-vis spectrophotometer	I-III
Oxidation-reduction potential	Endress-Hauser transmitter	II
Total inorganic carbon	Total organic carbon analyzer	I, II
Volatile fatty acids	GC-FID	I-III
Gas composition	GC-TCD	I-III
Gas volume	Water replacement column	I-III
Gas pressures	Pressure meter	III
Microbial community characterization	16S rRNA sequencing	I
	Shotgun metagenomic sequencing	II
Biomass growth	qPCR	I
Biofilm observation	SEM	I

### 3.3.2 Microbiome characterization

The microbial DNA was extracted from both biofilm (i.e., growing on the surface of electrode) and planktonic samples (i.e., floating in the liquid medium) by using the DNeasy PowerSoil Pro Kit (Qiagen, Germany). Bacterial abundance was measured using the quantitative polymerase chain reaction (qPCR) analysis by a Bio-Rad CFX96 (CFX96 Touch Real-Time PCR Detection System, Bio-Rad, USA), as described in publication I. The primer pair 338F/518R was used to target the V3 region of eubacterial 16S rRNA gene. The microbial composition was characterized by 16 rRNA sequencing (publication I) using primer pairs 341F/806R and shotgun

metagenomic sequencing (publication II) using the Illumina platforms. Further details are described in publications I and II. Additionally, the biofilm growth on graphite granules was observed with the scanning electron microscopy (SEM) in publication I (see detailed protocol in publication I).

### 3.4 Calculations and statistical analysis

In publications I-III, the performance of the experiments was assessed by the mass balances. Carbon (CR) and energy (ER) recoveries were calculated according to equations (1) and (2) (publication I-III).

$$CR_i = \frac{n_i}{n_{(carbon\ dioxide)} + n_{(methanol)}} \times 100\% \quad (1)$$

Where CR<sub>i</sub> is defined as the ratio of amount of carbon recovered to product *i* and the total carbon provided, n(*i*) is the amounts of products in mol-C, n(carbon dioxide) and n(methanol) are the amounts of consumed CO<sub>2</sub> and methanol in mol-C, respectively.

$$ER_i = \frac{F \times n_i \times z_i}{\int I dt + F \times n_{(methanol)} \times z_{(methanol)}} \times 100\% \quad (2)$$

Where ER<sub>i</sub> is defined as the ratio of amount of electrons transferred to product *i* and the total electrons provided,  $z_i$  represents the number of electrons for product *i*. Specifically, the number of electrons were 2 for H<sub>2</sub>, 6 for methanol, 8 for acetate, 14 for propionate, 20 for n-butyrate and i-butyrate, and 32 for caproate. *F* is faraday's constant (96485 C mol<sup>-1</sup> electron), *n* is the amount of product *i*, and *I* is the current consumed along the considered time (in amperes, A).

Product selectivity was used to assess efficiency, with which the percentage fraction of carbon ended up in a specific product in relation to the total carbon recovered in products (publications I and III), or ratios of the production rate of product against the production rate of all organic products (publication II).

All results are reported as average values with standard deviations, unless otherwise specified. Microbiome compositions were identified using alpha diversity metrics (Shannon and Simpson indexes) (publication II), beta diversity metrics with weighted-Unifrac dissimilarity using the q2-diversity plugin in qiime2 software 2021.4 (publication I) (Bolyen et al., 2019), and with Bray-Curtis dissimilarity using

vegan package (Adonis) in R (publication I). Principal coordinate analysis (PCoA) was calculated using the q2-diversity plugin in qiime2 software 2021.4 (publication I) and vegan package in R (publication II). Further statistical analysis including permutational analysis of variance (PERMANOVA) (publication I-III), one way analysis of variance (ANOVA), repeated measure ANOVA, Tukey's honest significant difference (HSD) tests as well as two-sample t-tests conducted in R (publication I-III). Outliers in the fermentation results were also identified and excluded based on boxplot visualizations (publication III).

## 4 RESULTS AND DISCUSSION

This section summarizes the main results and provides further discussion. The research first investigated the role of methanol addition in microbial electrosynthesis, i.e., methanol assisted MES. Further results focused on the optimization of the process to obtain a selective and efficient butyrate production by investigating the effects of operational parameters including pH, CO<sub>2</sub> feeding mode, temperature, headspace pressures and methanol/CO<sub>2</sub> ratios. In addition, the responsible bacteria for methanol utilization and butyrate production and their corresponding pathways were studied by characterizing the microbiome via sequencing methods.

### 4.1 Microbial community enrichment and taxonomic characterization

#### 4.1.1 Enrichment of the microbiome utilizing methanol and CO<sub>2</sub>

Methanol has been reported to facilitate methanol assisted chain elongation (Chen et al., 2016, 2017, 2020; De Leeuw et al., 2020), providing reducing power to produce more reduced compound. The utilization of methanol in MES process has not yet been implemented. The enrichment process began with feeding with only CO<sub>2</sub> for four days (two-times feeding), which resulted in mainly acetate production, with acetate titer reaching  $3.5 \pm 0.6$  g L<sup>-1</sup>. Methanol was periodically added along with CO<sub>2</sub> starting from day five, which resulted in both acetate consumption and butyrate production. Butyrate titer steadily increased, peaking at  $5.8 \pm 0.1$  g L<sup>-1</sup> on day 22, while acetate titer stabilized at approximately 1.8 g L<sup>-1</sup>. Similar VFA production pattern was obtained across the subsequent five batches, where acetate was initially produced until it reached about 1.8 g L<sup>-1</sup>, after which butyrate production began. Additionally, caproate production was detected in all enrichment batches, with highest titers ranging from 0.22 g L<sup>-1</sup> to 0.50 g L<sup>-1</sup>. The microbial culture was maintained to utilize methanol and CO<sub>2</sub> in MES reactors for four years and was used as the inoculum for all the experiments in this dissertation. The enrichment culture was maintained in

batch mode, with each batch lasting 35–50 days. At the end of each batch, the broth in the recirculation bottle was replaced with fresh medium. Before using the inoculum for experiments, the VFA concentrations of the enrichment culture were measured to confirm microbial activity. Planktonic cells from these batches were collected and used as inoculum for all subsequent MES experiments. While this approach ensured culture consistency, potential shifts in microbial community composition over time cannot be ruled out.

#### 4.1.2 Taxonomic profiling of the enrichment culture

The enrichment culture was first characterized by 16s rRNA gene sequencing (publication I). As the biofilm samples could not be collected during the enrichments, only the planktonic samples were sequenced at the end of each enrichment batch. The original inoculum fed with only CO<sub>2</sub> composed of *Eubacterium*, *Proteiniphilum* and *Cellulosimicrobium* as the most abundant genera, and the relative abundance of *Eubacterium* was below 20% (Vassilev et al., 2024). The addition of methanol changed the microbial community composition (Figure 6). After the first enrichment batch, the relative abundance of *Eubacterium* increased to 42.2±1.0 % and maintained at the range of 42.7±1.0% to 55.0±4.5% in the following enrichment batches. In addition to *Eubacterium*, *Proteiniphilum* and *Cellulosimicrobium* were observed with relative abundances lower than 5%. Other abundant genera included *Bacteroides* and *Sporanaerobacter*, with the relative abundances ranging from 7.6±0.2% to 26.5±1.5% and 9.1±5.2% to 18.8±0.9%, respectively. In summary, an *Eubacterium* dominated mixed culture was enriched with a stable microbial composition

As the 16s rRNA gene sequencing does not support the identification of the microbial composition at the species level, shotgun metagenomic sequencing was carried out to further characterize the microbial culture, originating from publication I and used as inoculum in publication II (publication II). The predominant species was identified as *Eubacterium callanderi* (with relative abundances of over 50%). In addition, *Sporanaerobacter acetigenes* and *Proteiniphilum acetatigenes* were also present in the inoculum (with the relative abundances of below 20%). *E. callanderi* is an anaerobic acetogen which was not originally reported to grow with one-carbon substrates as the only carbon source, yet recent studies showed that *E. callanderi* was able to produce butyrate from methanol and H<sub>2</sub>/CO<sub>2</sub> (Dietrich et al., 2021). *P. acetatigenes* is an anaerobic fermentative acetogen, which was reported to grow on

amino acids or cell debris for acetate production (Chen & Dong, 2005). *S. acetigenes* is an anaerobic heterotrophic bacterium, which was reported to utilize sugars for acetate production (Hernandez-Eugenio et al., 2002), and was also suggested to facilitate electron transfer between different species (Dang et al., 2016). However, both *P. acetatigenes* and *S. acetigenes* are heterotrophic anaerobes that have not been reported to utilize methanol and CO<sub>2</sub> or produce butyrate. Their growth was likely supported by metabolites such as acetate or cell debris, suggesting that their persistence in the community is supported by cross-feeding on products released by autotrophic members.

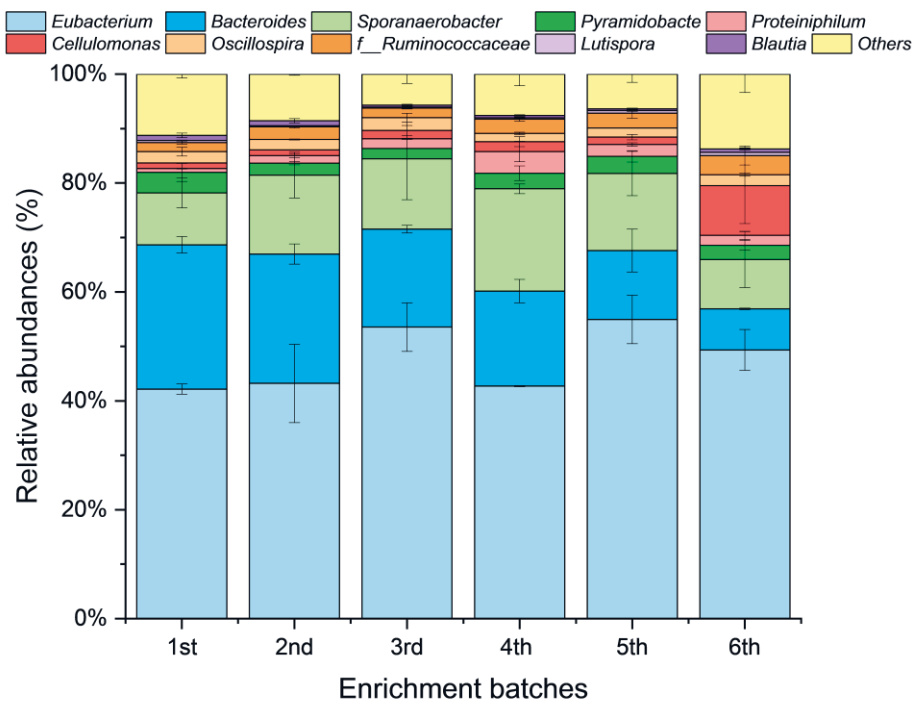


**Figure 6.** Microbial composition at the end of different enrichment batches with ten most abundant genera. Specifically, the *f\_Ruminococcaceae* stands for family level as the genus remains unidentified. The error bars indicate the standard deviations between duplicates (Adapted from publication I, licensed under CC BY 4.0.).

## 4.2 Methanol assisted MES: proof of concept and optimization

### 4.2.1 Revealing the potential roles of methanol in MES

To understand the role of methanol in MES, three feeding regimes were applied in MES reactors, including only CO<sub>2</sub> (CD), only methanol (ME), and both methanol and CO<sub>2</sub> (ME-CD) (publication I). Throughout the experiments, acetate and butyrate were the main products (Figure 7.a). In fact, no VFA production was observed in ME reactors, indicating methanol alone was not sufficient for VFA production in MES. For ME-CD and CD, similar acetate production pattern was observed, with acetate production initiating immediately from the inoculation and achieving threshold concentration (ca 1.8 g L<sup>-1</sup>) on day two (Figure 7.a). The threshold acetate concentration was likely required for *Eubacterium callanderi* to utilize acetate as the CoA acceptor in the conversion of butyryl-CoA to butyrate, while other acetogens in the community also contributed to acetate accumulation for energy conservation (detailed discussion in publication II). From day two onwards, acetate concentration fluctuated between 1.7 g L<sup>-1</sup> and 2.0 g L<sup>-1</sup> until the end of the experiments. However, different butyrate production was observed between ME-CD and CD. In CD, butyrate production initiated from day two and reached the highest butyrate titer (5.2±0.1 g L<sup>-1</sup>) on day 28, with the production rate of 0.20±0.03 g L<sup>-1</sup> d<sup>-1</sup>. However, in ME-CD, higher butyrate production rate (0.36±0.01 g L<sup>-1</sup> d<sup>-1</sup>) and butyrate titer (8.6±0.2 g L<sup>-1</sup>) were obtained. The methanol addition boosted the highest butyrate titer by 1.7-fold and butyrate production rates by 1.8-fold. Overall, MES fed with methanol and CO<sub>2</sub> resulted in a significant improvement in butyrate production ( $p < 0.05$ ), surpassing the MES fed with methanol (ME) or CO<sub>2</sub> (CD).

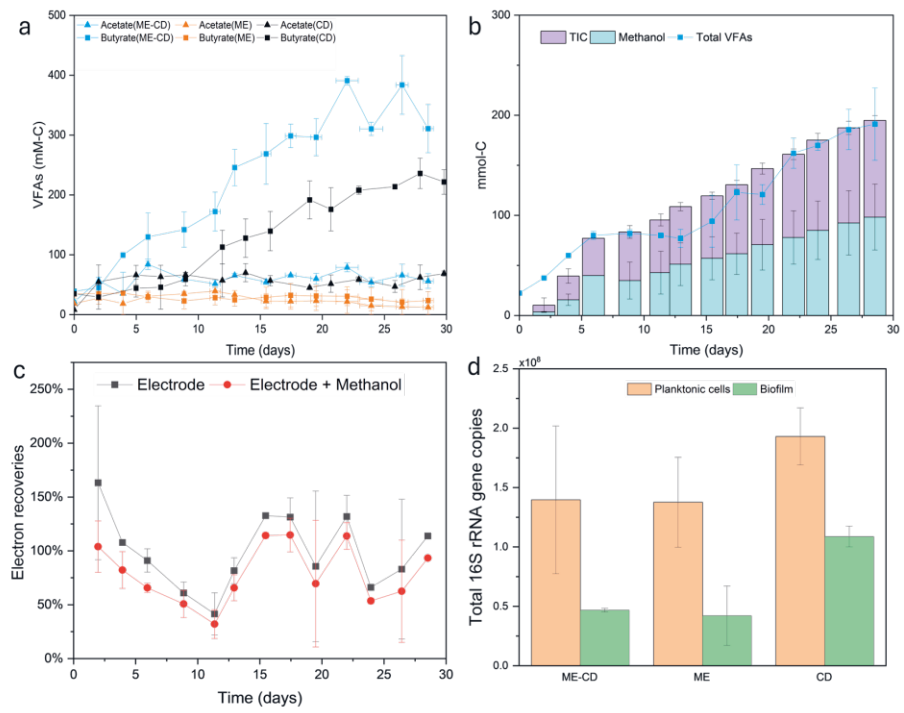


**Figure 7.** VFAs profile obtained with different feeding regimes (a), carbon source consumption and production in ME-CD (b), electron recoveries in ME-CD (c) and total 16S rRNA gene copies measures with different feeding regimes (d). The error bars present duplicate reactors (Adapted from publication I, licensed under CC BY 4.0.).

Total of  $99.4 \pm 24.1$  mmol-C TIC (equivalent to  $1.2 \pm 0.3$  g-C) as  $\text{CO}_2$  was consumed with the average rate of  $0.05 \pm 0.01$  g-C d $^{-1}$ . Methanol was consumed in a similar rate (ca.  $0.05$  g-C d $^{-1}$ ) and resulted in the overall consumption of methanol as  $98.3 \pm 32.9$  mmol-C (equivalent to  $1.2 \pm 0.4$  g-C) (Figure 7.b). After taking into account the VFA losses due to  $\text{CO}_2$  sparging,  $101.8 \pm 4.9\%$  of the carbon sources (TIC + methanol) utilized in ME-CD were recovered in VFAs, of which  $86.3 \pm 4.4\%$  was recovered in butyrate. The carbon recoveries indicated an important role of methanol as carbon source for VFA production. It is worth mentioning that TIC was always completely depleted between the sampling days, yet methanol was observed to remain available, suggesting  $\text{CO}_2$  was the limiting substrate in the process. In CD, total of  $200.7 \pm 2.1$  mmol-C TIC (equivalent to  $2.4 \pm 0.03$  g-C) was consumed with the rate of  $0.08 \pm 0.002$  g-C d $^{-1}$ , of which  $39.4 \pm 9.2\%$  of the carbon was recovered in VFAs.

The low carbon recoveries in CD compared to ME-CD can be attributed to the microbial growth which was quantified with qPCR at the end of the experiments

from the DNA extracted from biofilm and planktonic cells (Figure 7.d). In biofilm, over two-fold of total 16 rRNA gene copies were observed in CD than in ME-CD, and the highest gene copies in planktonic cells were obtained in CD, with ca. 1.4-fold increase compared to results in ME-CD. The results from biofilm and planktonic cells indicated that more carbon sources were directed to biomass growth than products in CD. A study by Claassens et al. (2019) experimentally measured microbial growth parameters and production titers to calculate energetic efficiency. They proposed that acetogens utilizing methanol as a substrate are more energetically efficient than those growing on H<sub>2</sub>, as less carbon is diverted to energy generation, allowing more carbon to be directed towards product formation for adequate ATP synthesis. This finding is in accordance with the higher carbon efficiency achieved in ME-CD than in CD in this study.

In order to investigate whether methanol was used as the electron donor in ME-CD, the electron recovery was first calculated considering electrode as the sole electron source (Figure 7.c). Specifically, for ME-CD, at maximum  $133.1 \pm 1.0$  % electron recovery was observed between three consecutive substrate-feeding timepoints (days 15, 17 and 22) (Figure 7.c), which implied the potential role of methanol as an additional electron source in ME-CD. If the electrons provided by methanol were also considered, the overall electron recoveries of  $76.9 \pm 0.6$  % were obtained in ME-CD and  $65.4 \pm 5.4$  % in CD. Additionally, electron recoveries exceeding 100% may be due to unaccounted electron donors from yeast extract, the undefined composition of which (e.g., amino acids, carbohydrates) was not included in the calculation. In summary, methanol acted as both the carbon and electron donor, which resulted in butyrate dominant production in methanol assisted MES.

#### 4.2.2 Improving the butyrate selectivity by optimizing cathodic pH

In biological processes, pH plays an important role in regulating metabolism, product spectrum as well as production rates. The effects of pH have been studied in MES (Batlle-Vilanova et al., 2016; Quintela et al., 2024) and chain elongation process (Pacaud et al., 1985; San-Valero et al., 2020). However, the effects of pH on methanol assisted MES have never been reported before. The optimal pH for most acetogens is located between 5 and 8. However, pH 5 has the potential to trigger solventogenesis (Vassilev et al., 2019), which could introduce other electron donors such as ethanol. Therefore, pH 5.5, 6 and 7 were evaluated in methanol assisted MES (publication II).

Regardless of different pH values, acetate and butyrate were the two main VFAs, with butyrate being the dominate product (Figure 8). The production of butyrate initiated on days 2 with the significantly higher butyrate production rates/titers obtained at pH 6 and 7 compared to pH 5.5 ( $p<0.05$ ). At pH 5.5, butyrate production rate of  $0.12\pm0.04$  g L<sup>-1</sup> d<sup>-1</sup> was obtained, while pH 6 and pH 7 resulted in butyrate production rate of  $0.28\pm0.04$  g L<sup>-1</sup> d<sup>-1</sup> and  $0.29\pm0.05$  g L<sup>-1</sup> d<sup>-1</sup>, respectively. Therefore, the lowest butyrate tier of  $3.4\pm1.4$  g L<sup>-1</sup> was obtained at pH 5.5, yet  $7.0\pm1.0$  g L<sup>-1</sup> and  $7.5\pm1.1$  g L<sup>-1</sup> of butyrate titers were obtained at pH 6 and pH 7, respectively. As for the acetate production, pH 7 enhanced the acetate production compared to the slightly acidic conditions (pH 5.5 and 6), obtaining the acetate titer of  $5.8\pm1.8$  g L<sup>-1</sup> and production rates of  $0.2\pm0.1$  g L<sup>-1</sup> d<sup>-1</sup>. However, the acetate titers at pH 5.5 and 6 stabilized between 1.3 to 2.1 g L<sup>-1</sup> throughout the experiments with the production rates below 0.06 g L<sup>-1</sup> d<sup>-1</sup> at both pH values. In all, pH 7 reactors resulted in the highest overall VFA production ( $307\pm20$  mmol-C), surpassing pH 6 ( $187\pm16$  mmol-C) and pH 5.5 ( $111\pm27$  mmol-C).

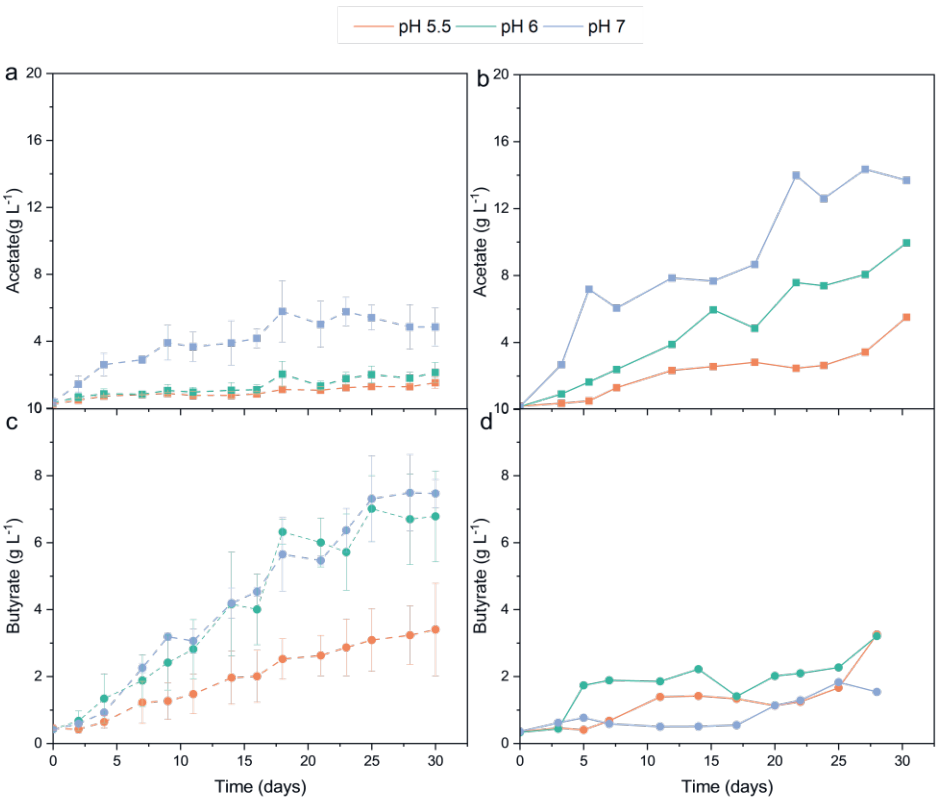


**Figure 8.** Acetate (a, b) and butyrate (c, d) concentrations at cathodic pH of 5.5, 6 and 7. The dashed lines represent the results with semi-batch  $\text{CO}_2$  feeding obtained from triplicated reactors with error bars showing the standard deviations, and solid lines represent the results with continuous  $\text{CO}_2$  feeding. The results at pH 5.5 were shown in orange, those at pH 6 in green, and those at pH 7 in blue.

Methanol and  $\text{CO}_2$  utilization were also affected by the pH. At pH 5.5, only  $70.2 \pm 13.8\%$  of the supplied methanol was utilized, whereas at pH 6 methanol consumption increased to  $91.6 \pm 3.5\%$  and at pH 7 complete methanol utilization was achieved. While methanol was efficiently consumed at pH 7, it accumulated to concentrations of  $3.7 \text{ g L}^{-1}$  and  $2.2 \text{ g L}^{-1}$  at pH 5.5 and pH 6, respectively, by the end of the experiments.  $\text{CO}_2$  consumption was similar at pH 6 ( $5.3 \pm 1.0 \text{ L}$ ) and pH 7 ( $4.6 \pm 1.0 \text{ L}$ ), both significantly higher than at pH 5.5 ( $2.4 \pm 1.0 \text{ L}$ ).

Recently, a thermodynamic model was developed by Rovira-Alsina et al. (2022) to understand the energy conversion in MES. The model provided insights into the

underlying factors driving experimental observations across different pH conditions. According to the model, butyrate production was thermodynamically more favorable than acetate production across all pH values, as it consistently obtained a more negative Gibbs free energy variations ( $\Delta G'$ ) (for details, see publication II). The  $\Delta G'$  for butyrate production ranged from -125 to -480 kJ mol<sup>-1</sup>, while the  $\Delta G'$  for acetate production was higher, in the range of -15 to -109 kJ mol<sup>-1</sup>. Acetate formation and accumulation were observed throughout the experiment at pH 7, whereas at pH 5.5 and pH 6, both the acetate production rates and final titers were significantly lower. When using methanol and CO<sub>2</sub> as substrates, acetate formation is thermodynamically more favorable than homoacetogenesis relying on CO<sub>2</sub> and H<sub>2</sub>. However, the insufficient methanol utilization at pH 5.5 and 6 likely limited acetate formation. The thermodynamic-based model highlights the importance of methanol utilization for acetate and butyrate production and can also guide the theoretical assessment of other process parameters to support future experimental design.

In addition to the productivity and titer, butyrate selectivity was also used to assess the feasibility of butyrate production in MES, considering the downstream extraction and recovery (Batlle-Vilanova et al., 2017). Among all three pH values, pH 6 resulted in the most selective butyrate production (86.9±1.5%), which was slightly higher than the butyrate selectivity at pH 5.5 (80.5±5.9%). However, due to the significant acetate production at pH 7, butyrate selectivity at pH 7 decreased to 69.8±7.7%. Additionally, trace amounts of other products (propionate, i-butyrate, valerate, and caproate) were also obtained during the experiments, with their combined concentrations accounted for less than 5% of the total production. Other aforementioned electron donors, ethanol, lactate and formate were not detected throughout the experiments, suggesting the butyrate production is only achieved by utilizing methanol as the electron donor. The increase in acetate and butyrate production observed at higher pH in this study contrasts with earlier MES study by Batlle-Vilanova et al. (2016) where elevated pH hindered the acetate formation. A possible explanation is that the use of chronopotentiometry in this thesis maintained continuous H<sub>2</sub> generation through water reduction, even under conditions of lower proton availability, thereby sustaining microbial metabolism more effectively than in systems operated with chronoamperometry. However, operation at higher pH also requires a more negative cathode potential, which increases the overall energy demand of the system. The future study could focus on the balance between the microbial activity and electrochemical efficiency when evaluating the effect of pH in methanol assisted MES.

#### 4.2.3 Continuous CO<sub>2</sub> feeding resulted in mainly acetate production (unpublished results)

As discussed in chapter 4.2.1, the semi-batch CO<sub>2</sub> feeding resulted in the TIC depletion during each fed-batch cycle and thus, CO<sub>2</sub> was continuously fed (1.44 L d<sup>-1</sup>) to recirculation bottles at pH 5.5, 6 and 7 to ensure CO<sub>2</sub> availability. Compared to the semi-batch CO<sub>2</sub> feeding used in the three publications, continuous CO<sub>2</sub> feeding (unpublished results) resulted in a product spectrum dominated by acetate at all pH values (Figure 8). Acetate production started immediately and peaked at the end of the experiments. The highest acetate titer of 14.4 g L<sup>-1</sup> was obtained at pH 7 with the production rate of 0.48 g L<sup>-1</sup> d<sup>-1</sup>. At pH 5.5 and 6, acetate titers of 5.5 g L<sup>-1</sup> and 10.0 g L<sup>-1</sup> were obtained, respectively. Similar butyrate titers of 3.2 g L<sup>-1</sup> and 3.3 g L<sup>-1</sup> were obtained at pH 5.5 and pH 6, respectively, surpassing the butyrate titer of 1.5 g L<sup>-1</sup> at pH 7. With the continuous CO<sub>2</sub> feeding, butyrate selectivity decreased to 42.7% at pH 5.5, 28.6% at pH 6 and 10.7% at pH 7. Under continuous CO<sub>2</sub> feeding, methanol accumulation was observed at pH 5.5, reaching concentration up to 2.3 g L<sup>-1</sup>, with 87% of the supplied methanol being utilized. Methanol was completely utilized at pH 6 and 7, obtaining at ca. 90 mmol-C (1.1 g-C), both higher than at pH 5.5, which with 70.7 mmol-C (0.8 g-C) of utilization.

The continuous CO<sub>2</sub> feeding ensured high availability of CO<sub>2</sub>, which reduced the thermodynamic driving force for methanol oxidation and thus potentially inhibited butyrate production. However, as methanol can be converted to acetyl-CoA for the formation of acetate, the methanol utilization rate remained similar (ca. 0.05 g-C d<sup>-1</sup>) between the continuous and semi-batch CO<sub>2</sub> feeding mode. Thus, this hypothesis needs further investigation.

#### 4.2.4 Investigating the effects of temperature, methanol/CO<sub>2</sub> ratio and pressure on butyrate production during fermentation

A total of 24 different combinations of temperature (23 °C and 35 °C), headspace pressure (1, 1.5, and 2 atm), and methanol/CO<sub>2</sub> ratios (0.5, 1, 3 and 5) were initially tested in fermentation experiments, and the results were subsequently used to design the operating conditions of the methanol assisted MES reactors for maximizing butyrate production rates.

At 23 °C, total of 2.5 to 6.0 mmol-C acetate was produced, while butyrate production was only detected in trace amounts, not exceeding 0.3 mmol-C (Figure 9). Consequently, butyrate selectivity remained below 10% under all tested conditions at 23 °C. However, at 35 °C acetate production (2.7–6.2 mmol-C) was

comparable to that at 23 °C ( $p > 0.05$ ), while butyrate production increased significantly, reaching 0.8 to 3.5 mmol-C total production, with the butyrate selectivity rising to 16.9–48.9%. A similar temperature-dependent trend has been observed in ethanol assisted chain elongation. Ren et al., (2024) compared the results of chain elongation from ethanol and acetate between 25 to 55°C, reporting the highest caproate yield and selectivity at 40 °C, while the lowest yield was obtained at 25 and 30°C. At these lower temperatures, acetate production increased, suggesting a metabolic shift (Ren et al., 2024). This behavior was attributed to variations in microbial community composition, notably the enrichment of *Clostridium kluyveri*—a key chain elongator—at 40 °C (Ren et al., 2024). *E. callanderi* also has the optimal growth temperature at 37°C (Rode et al., 1981). In this study, methanol consumption remained similar between 23 and 35 °C, with no significant differences. This suggests that the limited butyrate production at 23 °C may not be due to methanol availability and utilization, but rather due to inhibited activity of the RBO pathway responsible for butyrate production at lower temperatures. However, this hypothesis requires further validation through transcriptomic or proteomic analyses to investigate temperature effects on the activity of the key metabolic pathways.

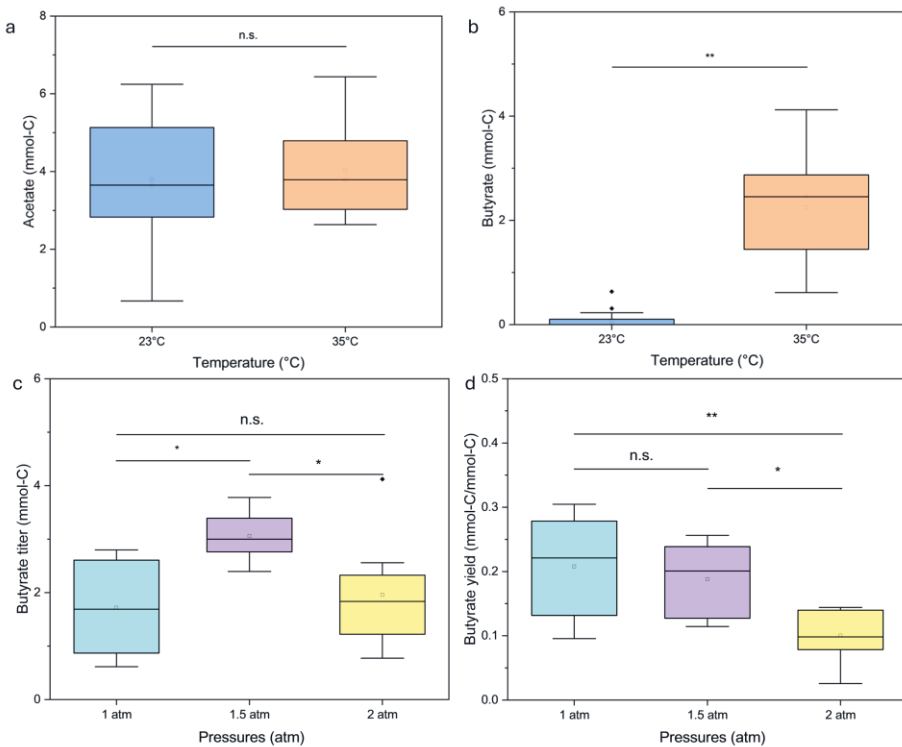


**Figure 9.** Acetate (a) and butyrate titers (b) at different temperatures, and butyrate titer (c) and butyrate yield (d) at different pressures. Significance of the results between different conditions was tested by one way ANOVA test, with Tukey HSD post-hoc analysis. The symbol \* represents  $p < 0.05$ , symbol \*\* represents  $p < 0.005$ , symbol n.s. represents not significant (Reproduced from publication III).

As the focus was on enhancing butyrate production, the remaining results are reported at temperature of 35°C. Higher butyrate titers, ranging from 2.4 to 3.8 mmol-C, were obtained at a headspace pressure of 1.5 atm (Figure 9.c). In comparison, butyrate titers at 1 atm ranged from 0.6 to 2.8 mmol-C and at 2 atm from 0.8 to 2.6 mmol-C with one exception: at a methanol/CO<sub>2</sub> ratio of 5, 4.1 mmol-C of butyrate was produced. Overall, increasing the pressure from 1 atm to 1.5 atm enhanced butyrate production. This enhancement is likely due to improved gas–liquid mass transfer and increased solubility of gaseous compounds, according to Henry’s Law, resulting in higher CO<sub>2</sub> availability. However, butyrate yields at 1.5 atm (0.12–0.25 mol-C mol-C<sup>-1</sup>) were similar to those at 1 atm (0.15–0.29 mol-C mol-C<sup>-1</sup>) indicating that the higher titers were likely due to greater carbon availability, rather than improved conversion efficiency. When the pressure increased further to 2 atm, both butyrate titers and yields (0.08–0.11 mol-C mol-C<sup>-1</sup>) declined, suggesting that

butyrate production was hindered, likely due to pressure-induced inhibition. This observation aligns with findings from Van Hecke et al. (2019), who reported that exceeding certain total or partial gas pressure thresholds can negatively impact microbial growth and metabolism. In this study, that threshold appears to lie between 1.5 and 2 atm. Although the highest butyrate titers were observed at 1.5 atm, slightly higher yields were achieved at 1 atm. Given the technical challenges of maintaining overpressure in MES systems, atmospheric pressure was selected as the optimal condition for maximizing butyrate production in MES studies.

Based on the results obtained, the effects of various methanol/CO<sub>2</sub> ratios (mol mol<sup>-1</sup>) were further evaluated at 35°C and atmospheric headspace pressure. At a methanol/CO<sub>2</sub> ratio of 0.5, a relatively low butyrate titer of 0.8±0.2 mmol-C and a yield of 0.17±0.06 mol-C mol-C<sup>-1</sup> were obtained. When the ratio was increased to 1, the butyrate titer improved to 1.0±0.3 mmol-C with the yield of 0.15±0.06 mol-C mol-C<sup>-1</sup>. The most substantial butyrate production was obtained at a methanol/CO<sub>2</sub> ratio of 3, with the titer of 2.6±0.1 mmol-C and yield of 0.29±0.02 mol-C mol-C<sup>-1</sup>. However, further increasing the ratio to 5 resulted in a titer plateau of 2.4±0.4 mol-C with a lower yield of 0.22±0.07 mol-C mol-C<sup>-1</sup>. In a study carried out by Wood et al., (2022), a higher ratio of methanol to formate (over 5) promoted butanol production, which is a more reduced product than butyrate. Therefore, increasing the ratio from 0.5 to 3 was expected to enhance butyrate production. However, a ratio of 5 led to methanol accumulation exceeding 250 mM by the end of the experiment, which likely hindered the biomass growth and production efficiency. According to a study by Gentner and Bryant (1987), over 198 mM of methanol hindered the growth of *E. limosum* by increasing the doubling time. Thus, the high methanol concentration at ratio of 5 likely hindered the biomass growth and production efficiency in this study. Therefore, according to all the results in fermentation studies, the optimal butyrate production was achieved at temperature of 35°C, atmospheric pressure, and a methanol/CO<sub>2</sub> ratio of 3.

#### 4.2.5 The optimized operation conditions for butyrate production in methanol assisted MES

Duplicated MES reactors were run to maximize the butyrate production rate with optimized operational parameters (35°C, atmospheric pressure, and a methanol/CO<sub>2</sub> ratio of 3) (Publication III). Acetate production began immediately after inoculation, with a rate of 0.2±0.1 g L<sup>-1</sup> d<sup>-1</sup>, reaching a titer of 5.6±1.0 g L<sup>-1</sup>.

Butyrate production started on day 3 at a rate of  $0.6 \pm 0.1 \text{ g L}^{-1} \text{ d}^{-1}$  ( $107.4 \pm 19.7 \text{ g m}^{-2} \text{ d}^{-1}$ ), peaking at  $9.2 \pm 1.6 \text{ g L}^{-1}$  (Figure 10). Butyrate was the dominant product, with a selectivity of  $75.2 \pm 1.1\%$ . Methanol and the electrode served as the two primary electron donors, collectively providing  $3255 \pm 38 \text{ mmol}$  electron equivalents. Of these,  $42.9 \pm 1.9\%$  of the electrons were recovered as  $\text{H}_2$ ,  $17.9 \pm 0.7\%$  were recovered in butyrate and  $6.7 \pm 1.0\%$  were recovered in acetate. The carbon recovery efficiency was  $64.0 \pm 5.8\%$ , and the overall electron recovery was  $67.6 \pm 3.5\%$ , indicating that further optimization of electron and carbon utilization remains possible. Butyrate yield was  $0.58 \pm 0.01 \text{ mol-C mol-C}^{-1}$ , representing approximately a 2-fold improvement over the best yield obtained in serum flasks ( $0.29 \pm 0.02 \text{ mol-C mol-C}^{-1}$ ).

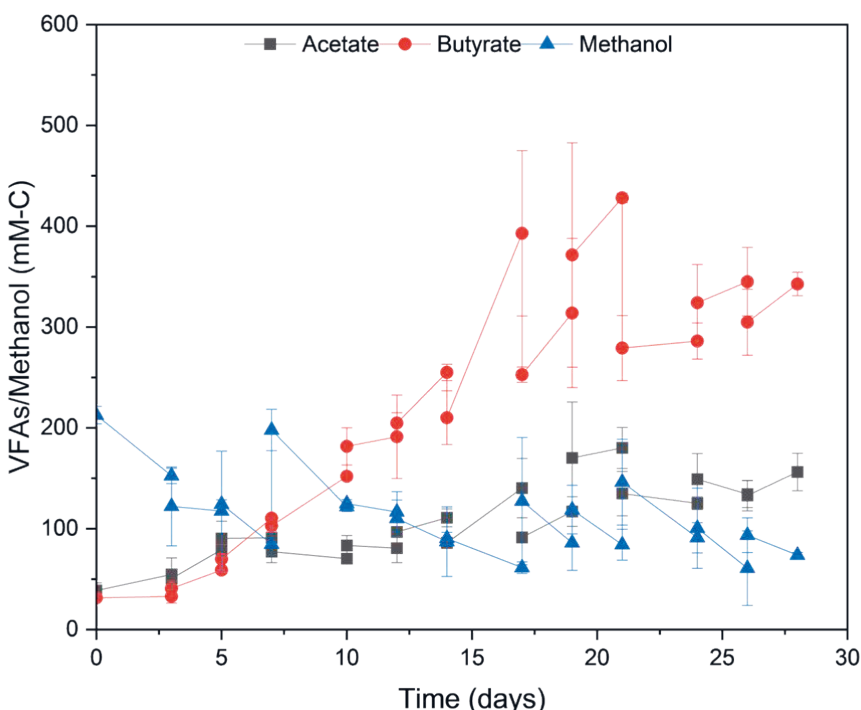


**Figure 10.** VFAs and methanol concentrations throughout the MES experiments at  $35^\circ\text{C}$ . Error bars show the duplicate results (Reproduced from publication III).

The experiments were conducted with an average methanol/ $\text{CO}_2$  ratio of  $2.9 \pm 0.3$  at the start of each fed-batch cycle. In total,  $206 \pm 6 \text{ mmol}$  ( $6.6 \pm 0.2 \text{ g}$ ) of methanol was

added, of which  $87.8 \pm 1.8\%$  ( $181 \pm 6$  mmol,  $5.8 \pm 0.2$  g) was consumed. Simultaneously,  $89 \pm 9$  mmol ( $3.9 \pm 0.4$ ) g of CO<sub>2</sub> was utilized. The average methanol consumption rate was  $0.58 \pm 0.00$  g L<sup>-1</sup> d<sup>-1</sup>, approximately 1.7-fold higher than in publication I ( $0.32$  g L<sup>-1</sup> d<sup>-1</sup>) where a lower methanol/CO<sub>2</sub> ratio (ca. 1) was used (Yao et al., 2024). This suggests that the higher methanol/CO<sub>2</sub> ratio likely promoted methanol utilization and thus enhanced the butyrate production rates ( $0.6$  g L<sup>-1</sup> d<sup>-1</sup>) compared to  $0.4$  g L<sup>-1</sup> d<sup>-1</sup> obtained in publication I and  $0.3$  g L<sup>-1</sup> d<sup>-1</sup> obtained in publication II. The butyrate selectivity was ca. 80% for publication I and III, in which the initial pH was 7.4 and maintained above 6 when it decreased during the experiments. In publication II, the pH was controlled at pH 6 throughout the experiments, which was an efficient strategy to increase the butyrate selectivity to 87%. In this thesis, the highest butyrate production rate of  $0.6$  g L<sup>-1</sup> d<sup>-1</sup> ( $107.4$  g m<sup>-2</sup> d<sup>-1</sup>) (Yao et al., 2025) was achieved with methanol assisted MES, which is comparable to the highest rates reported in MES studies, such as  $0.7$  g L<sup>-1</sup> d<sup>-1</sup> ( $125$  g m<sup>-2</sup> d<sup>-1</sup>) obtained by Jourdin et al. (2019) using high CO<sub>2</sub> loading rate and long HRT, and  $0.54$  g L<sup>-1</sup> d<sup>-1</sup> achieved by Raes et al. (2017) with acetate feeding. The butyrate selectivity of ca. 80% observed in this study is also consistent with values obtained in ethanol-assisted MES, while the highest reported selectivity of 95% was achieved employing a nickel ferrite-coated carbon felt (Tahir et al., 2021). Taken together, these comparisons indicate that methanol co-feeding enables production rates on par with state-of-the-art MES studies. In addition, the energy consumption for butyrate has also been improved, with the energy demand decreased from over 70 kWh kg<sup>-1</sup> butyrate in publication I to 53.1 kWh kg<sup>-1</sup> butyrate in publication III, which is comparable to the values of 64.3 kWh kg<sup>-1</sup> reported by Jourdin et al., 2018, but higher than values of 34.6 kWh kg<sup>-1</sup> (Romans-Casas et al., 2024), which the latter value was calculated only over the active butyrate-producing period and in a compact reactor, indicating scope for further efficiency improvements in methanol assisted MES process. Additionally, other expenses such as gas handling, pH control, nutrients, and downstream separation also need to be considered, all of which will further affect process economics.

## 4.3 Potential biochemical pathways in methanol assisted MES

In publication II, the biofilm and planktonic samples were sequenced by shotgun metagenomic sequencing methods to reveal microbial composition to species level and the potential biochemical pathways for methanol and CO<sub>2</sub> assimilation and butyrate production across different pH conditions. *E. callanderi* was the dominant species in both biofilm and planktonic communities under all tested pH values. No statistically significant differences in community structures were observed, as indicated by comparable alpha diversity metrics. More detailed pathway analyses are presented in publication II. For the purpose of maintaining a coherent storyline in this thesis, only the most relevant results are included here. Readers are referred to publication II for comprehensive genome-resolved analyses and the functional roles of the wider community.

### 4.3.1 Methanol and CO<sub>2</sub> assimilation pathways

In acetogens, methanol and CO<sub>2</sub> assimilation are both achieved by the WLP (Kremp & Müller, 2021). The methanol utilization, however, requires the methyltransferase system to transfer methyl-group to tetrahydrofolate (THF) and enter the WLP (Kremp & Müller, 2021). The common methyltransferase system includes the [methyl-Co(III) methanol-specific corrinoid protein]—coenzyme M methyltransferase (MTII, encoded by mtaA), methanol—corrinoid protein Co-methyltransferase (MTI, encoded by mtaB), and a cobalamin or cobamide-binding corrinoid protein (CoP) (encoded by mtaC) (Kremp & Müller, 2021).

In this study, however, only mtaA and mtaB were observed in the microbiome with a relative abundance of approximately 3×10<sup>-80%</sup>, with these abundances being five orders of magnitude lower than those of other detected genes, suggesting the potential presence of alternative methyltransferase systems. Instead, the methionine synthases (MetH) had relative abundance of ca. 1%, and likely were responsible for methyl group transfer (Figure 11). Majority of the gene encoding MetH was contributed by *E. callanderi* (Over 90%). The MetH-catalyzed methyltransferase has been implicated in methanol utilization in a *Sporomusa ovata* strain (Visser et al., 2016), where MetH replaced the function of mtaA. In this strain, an AcsE/MetH homolog was found downstream of mtaC and mtaB, instead of a typical methanogenic mtaA homolog. This suggests that, rather than the canonical MTII complex, MetH may transfer the methyl group bound to THF for further assimilation. Furthermore, it has been proposed that MTII in acetogens resembles the methyl-THF binding domain of the cobalamin-dependent MetH (Kremp & Müller, 2021). However, this

hypothesis has not been investigated in *Eubacterium* species, and its validation would require further studies, such as metagenomic assembly and binning of metagenome-assembled genome of *E. callanderi* (and other bacteria) in our system, coupled with transcriptomic and proteomic analyses.

Through the WLP, the methyl-THF originated from methanol and CO<sub>2</sub> were used for the generation acetyl-CoA. The methyl-THF was converted to methyl-CoFeSP, which was further reacted with CO from the carbonyl branch for the formation of acetyl-CoA, catalysed by the CO-methylating acetyl-CoA synthase (ACS/CODH). Methyl-THF was oxidized by the methylenetetrahydrofolate reductase (MTHFR), the methylenetetrahydrofolate dehydrogenase (MTHFD), methenyltetrahydrofolate cyclohydrolase (MTHFC), formate-tetrahydrofolate ligase (FTHFS), and formate dehydrogenase (FDH) (Ragsdale & Pierce, 2008).

In this study, the presence of the WLP encoding genes was found in the microbiome, with the *E. callanderi* being the major contributor (Figure 11). The only exception was the FDH, which was not originating from *E. callanderi*, which was likely due to the fact that the FDH coding genes were absent in the reference genome of the *E. callanderi* (*E. callanderi* KIST612) (Roh et al., 2011). In our metagenomic analysis, FDH-coding genes were present but were predominantly assigned as “unclassified,” indicating that they could not be linked with high confidence to any known reference genome. Suggesting either that *E. callanderi* harbors divergent FDH homologs absent from the current reference genome, or alternatively, that FDH activity is contributed by other, less-characterized taxa in the community. Further genome-resolved or transcriptomic studies will be required to clarify the precise origin of FDH activity in this system.

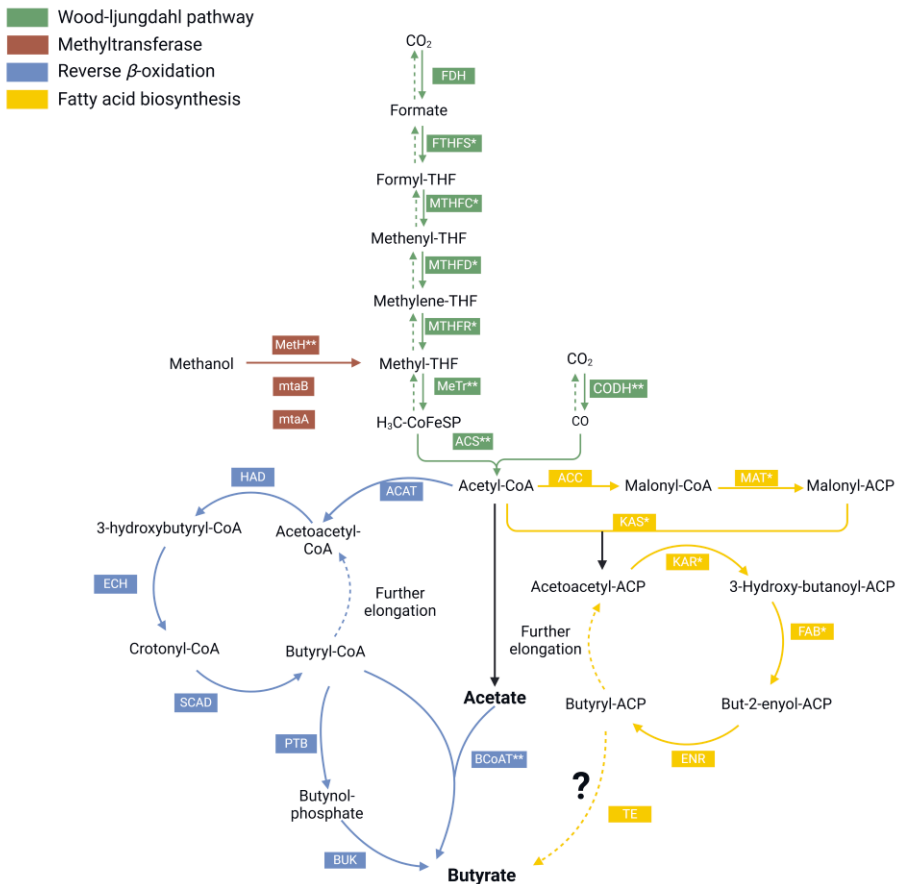


**Figure 11.** Putative metabolic pathway for butyrate production from methanol and  $\text{CO}_2$ .

Abbreviations: CODH, carbon-monoxide dehydrogenase; FDH, formate dehydrogenase; FTHFS, Formate-tetrahydrofolate ligase; MTHFC, methenyltetrahydrofolate cyclohydrolase; MTHFD, methylenetetrahydrofolate dehydrogenase; MTHFR, methylenetetrahydrofolate reductase; MeTr, 5-methyltetrahydrofolate--corrinoid/iron-sulfur protein Co-methyltransferase; ACS, CO-methylating acetyl-CoA synthase; ACAT, acetyl-CoA C-acetyltransferase; HAD, 3-hydroxyacyl-CoA dehydrogenase; ECH, enoyl-CoA hydratase; SCAD, short-chain acyl-CoA dehydrogenase BCoAT, butyryl-CoA,acetate CoA transferase; BUK, butyrate kinase; PTB, phosphate butyryltransferase; ACC, acetyl-CoA carboxylase; MAT, malonyl transferase; KAS, ketoacyl-ACP synthase; KAR, ketoacyl-ACP reductase; FAB, hydroxyacyl-ACP dehydratase; ENR, enoyl-ACP reductase; TE, thioesterase; MethH, methionine synthase; *mtaA*, [methyl-Co(III)] methanol-specific corrinoid protein--coenzyme M methyltransferase; *mtaB*, methanol--corrinoid protein Co-methyltransferase. \* and \*\* represents that *E. callanderi* contribute to over 50% and 90% of the abundances, respectively. (Adapted from publication II (Yao, Romans-Casas, et al., 2025), licensed under CC BY-NC 4.0.).

### 4.3.2 Butyrate production pathways

One of the main pathways for butyrate production from CO<sub>2</sub> is the RBO pathway. In this study, genes encoding enzymes involved in RBO were identified in the microbiome (Figure 11). RBO pathway begins with the condensation of two acetyl-CoA molecules into acetoacetyl-CoA, catalyzed by acetyl-CoA C-acetyltransferase (ACAT) (Kallscheuer et al., 2017). The resulting acetoacetyl-CoA then enters the RBO pathway to form butyryl-CoA. In this study, the major contributor to RBO activity appeared to be an unidentified species, likely due to the absence of annotated RBO-related genes in the reference genome of *E. callanderi* (Roh et al., 2011).

One route for converting butyryl-CoA to butyrate involves the use of acetate as a substrate, mediated by butyryl-CoA:acetate CoA-transferase (BCoAT). In this reaction, the CoA moiety from butyryl-CoA is transferred to acetate, resulting in acetate consumption(Yang et al., 2021). Genes encoding BCoAT were detected in the microbiome, with *E. callanderi* identified as the main contributor, with the relative abundance of ca. 0.01%.

An alternative route involves butyryl-CoA phosphorylation, where butyryl-phosphate is formed via butyryltransferase (PTB), and then converted to butyrate by butyrate kinase (BUK) (Hartmanis, 1987; Twarog & Wolfe, 1962). Unlike the BCoAT route, this pathway produces butyrate without consuming acetate. However, in this study, genes encoding PTB and BUK were present at much lower relative abundances (ca.  $1 \times 10^{-4}\%$ ), two orders of magnitude less than BCoAT. Additionally, these genes are not found in the *E. callanderi* genome, suggesting that BCoAT route is the responsible for butyrate production.

Fatty acid biosynthesis (FAB) pathway is another route for butyrate production in addition to RBO pathway (Figure 11). However, in this study, genes encoding the key enzyme (thioesterase), were not found to be present in the microbiome. Moreover, FAB is less energy efficient than RBO, as it requires extra ATP input during the initiation (Sarria et al., 2017). Given the absence of thioesterase encoding genes and the higher energetic cost of FAB, it is reasonable to conclude that RBO pathway was the primary pathway for butyrate production in methanol assisted MES.

In summary, the microbiome was dominated by *E. callanderi*, which was responsible for methanol and CO<sub>2</sub> assimilation via the WLP, and butyrate production via the RBO pathway. Specifically, MetH was likely responsible for the transfer of methanol into the WLP. Across the tested pH values (5.5, 6, and 7), the microbial community composition and the relative abundance of key functional genes remained consistent.

## 5 CONCLUSIONS AND OUTLOOK

MES has been developed for more than a decade. The competitiveness of MES lies in the usage of CO<sub>2</sub> and renewable electricity to produce platform chemicals, which is a potential route for production of chemicals in the biobased economy. This work demonstrated for the first time the usage of methanol as an additional electron donor in MES (methanol assisted MES). The process operation parameters were also optimized, including catholyte pH, CO<sub>2</sub> feeding mode, pressure, methanol/CO<sub>2</sub> ratio, and temperature, which further enhanced the butyrate production rate and selectivity. A microbiome was cultivated in MES reactors to utilize methanol and CO<sub>2</sub>, obtaining butyrate dominated product spectrum (RQ1). Adding methanol with CO<sub>2</sub> in MES resulted in butyrate titers up to 8.6 g L<sup>-1</sup> and production rates of 0.4 g L<sup>-1</sup> d<sup>-1</sup>. Compared to MES fed with only CO<sub>2</sub>, addition of methanol improved butyrate titers by 1.7-fold and production rates by 1.8-fold. In addition to the role of electron donor, methanol also served as a carbon donor, which contributed to about half of the carbon recovered in the final products.

Characterizing the microbiome provided insights into the key microbial species and metabolic pathways responsible for methanol assisted MES. The community was dominated by *Eubacterium callanderi* with the relative abundances of over 50% (RQ2). Most of the identified genes encoding metabolic pathways involved in carbon assimilation and product formation were also mapped to *E. callanderi*, revealing its role in CO<sub>2</sub> fixation via the Wood–Ljungdahl pathway and butyrate synthesis through reverse β-oxidation. Notably, a methionine synthase–driven methyl transfer system was proposed for methanol assimilation.

The effects of the operational parameters on methanol assisted MES were investigated to optimize the butyrate selectivity and productivity (RQ3). Firstly, the performance of the methanol assisted MES was compared with three cathodic pH values (5.5, 6 and 7). The most selective butyrate production (87% selectivity) was obtained at pH 6 with a production rate of 0.3 g L<sup>-1</sup> d<sup>-1</sup>. A similar butyrate production rate was observed at pH 7, however, substantial acetate formation at this pH reduced the butyrate selectivity to 70%. In contrast, pH 5.5 hindered both CO<sub>2</sub> and methanol consumption and thus resulted in the lowest butyrate production rate of 0.1 g L<sup>-1</sup> d<sup>-1</sup> yet with a butyrate selectivity of 81%.

The other operational parameters, including CO<sub>2</sub> feeding mode, temperature, pressure, and methanol/CO<sub>2</sub> ratios were evaluated to maximize the butyrate productivity. Firstly, the continuous CO<sub>2</sub> feeding resulted in mainly acetate production in methanol assisted MES. Fermentation experiments further revealed that the temperature of 23°C resulted in only acetate production. With H<sub>2</sub>/CO<sub>2</sub> (80%/20%) as the headspace gas, comparable butyrate yields were observed at 1 and 1.5 atm, but yields decreased at 2 atm. Increasing the methanol/CO<sub>2</sub> ratio from 0.5 to 3.0 (mol mol<sup>-1</sup>) enhanced butyrate yields, while a further increase to 5 reduced butyrate yields. Based on these findings, MES was operated under optimized conditions: 35°C, atmospheric pressure, a methanol/CO<sub>2</sub> ratio of 3 and a fed-batch CO<sub>2</sub> feeding mode. Under these conditions, butyrate production rate of 0.6 g L<sup>-1</sup> d<sup>-1</sup> (107.4 g m<sup>-2</sup> d<sup>-1</sup>) was obtained. In summary, this research demonstrates, for the first time, the usage of methanol for selective butyrate production in MES. By optimizing operational parameters, the methanol assisted MES achieved both butyrate selectivity and productivity among the highest values reported to date. Additionally, the pathways for methanol and CO<sub>2</sub> assimilation, as well as butyrate production, were identified.

Methanol assisted MES faces several intrinsic challenges that must be considered for future development. Industrial condensates, such as those from Kraft pulp mills, can contain methanol in concentrations ranging from 1 to 46 g L<sup>-1</sup> (31 to 1436 mM), along with other organic compounds such as sulfur-containing species and phenolics that may inhibit microbial activity. In this study, methanol concentrations above 200 mM were found to limit biomass growth, indicating concentration-dependent toxicity, while the maximum methanol consumption rate (20 mM d<sup>-1</sup>) was substantially lower than that of aerobic methylotrophs, suggesting the need for metabolic engineering to improve utilization efficiency. Furthermore, although methanol and CO<sub>2</sub> were supplied at roughly equal volumetric ratios in this work, in practical applications CO<sub>2</sub> emissions are often several orders of magnitude higher than methanol availability, which could lead to substrate imbalances if not properly managed.

Future work should focus on several key aspects to enhance the performance and scalability of methanol assisted MES. From a microbial perspective, isolating or genetically engineering strains such as *E. callanderi* to improve methanol utilization rates and reverse β-oxidation efficiency could enhance butyrate productivity. Additionally, further metatranscriptomic, proteomic, and metabolomic analyses are needed to clarify the roles of uncharacterized species and to better understand alternative methanol assimilation pathways, such as those involving methionine

synthase–driven methyl transfer. From an engineering perspective, improvements in reactor design, including the use of flow-through reactor configurations, could enhance gas–liquid mass transfer and overall system performance. The development of advanced cathode materials may not only support more robust and stable biofilm formation but also reduce electrochemical losses through improved conductivity and reduced overpotentials. To expand the product spectrum, co-feeding methanol with other electron donors like ethanol or lactate could facilitate the production of medium-chain carboxylates, such as caproate. Furthermore, the integration of in-situ product recovery/extraction technologies could help releasing the end-product inhibition and improve overall efficiency. Finally, the comprehensive techno-economic assessments and the evaluation of system integration with waste CO<sub>2</sub> streams and renewable methanol sources will be essential to assess the feasibility of scaling methanol assisted MES for industrial applications.

## 6 REFERENCES

2024 was the world's warmest year on record | National Oceanic and Atmospheric Administration. (2025, January 10). <https://www.noaa.gov/news/2024-was-worlds-warmest-year-on-record>

Abdollahi, M., Al Sbei, S., Rosenbaum, M. A., & Harnisch, F. (2022). The oxygen dilemma: The challenge of the anode reaction for microbial electrosynthesis from CO<sub>2</sub>. *Frontiers in Microbiology*, 13. <https://doi.org/10.3389/fmicb.2022.947550>

Acetic acid global market volume 2015-2030. (n.d.). Statista. Retrieved May 29, 2025, from <https://www.statista.com/statistics/1245203/acetic-acid-market-volume-worldwide/>

Ameen, F., Alshehri, W. A., & Nadhari, S. A. (2020). Effect of Electroactive Biofilm Formation on Acetic Acid Production in Anaerobic Sludge Driven Microbial Electrosynthesis. *ACS Sustainable Chemistry & Engineering*, 8(1), 311–318. <https://doi.org/10.1021/acssuschemeng.9b05420>

Arends, J. B. A., Patil, S. A., Roume, H., & Rabaey, K. (2017). Continuous long-term electricity-driven bioproduction of carboxylates and isopropanol from CO<sub>2</sub>

with a mixed microbial community. *Journal of CO<sub>2</sub> Utilization*, 20, 141–149.

<https://doi.org/10.1016/j.jcou.2017.04.014>

Bajracharya, S., Krige, A., Matsakas, L., Rova, U., & Christakopoulos, P. (2022).

Advances in cathode designs and reactor configurations of microbial electrosynthesis systems to facilitate gas electro-fermentation. *Bioresource Technology*, 354, 127178. <https://doi.org/10.1016/j.biortech.2022.127178>

Bajracharya, S., Krige, A., Matsakas, L., Rova, U., & Christakopoulos, P. (2024).

Microbial Electrosynthesis Using 3D Bioprinting of *Sporomusa ovata* on Copper, Stainless-Steel, and Titanium Cathodes for CO<sub>2</sub> Reduction. *Fermentation*, 10(1), Article 1.

<https://doi.org/10.3390/fermentation10010034>

Bajracharya, S., Vanbroekhoven, K., Buisman, C. J. N., Strik, D. P. B. T. B., & Pant, D. (2017). Bioelectrochemical conversion of CO<sub>2</sub> to chemicals: CO<sub>2</sub> as a next generation feedstock for electricity-driven bioproduction in batch and continuous modes. *Faraday Discussions*, 202, 433–449.

<https://doi.org/10.1039/C7FD00050B>

Barbosa, S. G., Peixoto, L., Alves, J. I., & Alves, M. M. (2021). Bioelectrochemical systems (BESs) towards conversion of carbon monoxide/syngas: A mini-review. *Renewable and Sustainable Energy Reviews*, 135, 110358.

<https://doi.org/10.1016/j.rser.2020.110358>

Batlle-Vilanova, P., Ganigué, R., Ramió-Pujol, S., Bañeras, L., Jiménez, G., Hidalgo, M., Balaguer, M. D., Colprim, J., & Puig, S. (2017). Microbial electrosynthesis of butyrate from carbon dioxide: Production and extraction. *Bioelectrochemistry*, 117, 57–64.  
<https://doi.org/10.1016/j.bioelechem.2017.06.004>

Batlle-Vilanova, P., Puig, S., Gonzalez-Olmos, R., Balaguer, M. D., & Colprim, J. (2016). Continuous acetate production through microbial electrosynthesis from CO<sub>2</sub> with microbial mixed culture. *Journal of Chemical Technology & Biotechnology*, 91(4), 921–927.

Berg, I. A., Kockelkorn, D., Buckel, W., & Fuchs, G. (2007). A 3-Hydroxypropionate/4-Hydroxybutyrate Autotrophic Carbon Dioxide Assimilation Pathway in Archaea. *Science*, 318(5857), 1782–1786.  
<https://doi.org/10.1126/science.1149976>

Bolyen, E., Rideout, J. R., Dillon, M. R., Bokulich, N. A., Abnet, C. C., Al-Ghalith, G. A., Alexander, H., Alm, E. J., Arumugam, M., Asnicar, F., Bai, Y., Bisanz, J. E., Bittinger, K., Brejnrod, A., Brislawn, C. J., Brown, C. T., Callahan, B. J., Caraballo-Rodríguez, A. M., Chase, J., ... Caporaso, J. G. (2019). Reproducible, interactive, scalable and extensible microbiome data science using QIIME 2. *Nature Biotechnology*, 37(8), Article 8.  
<https://doi.org/10.1038/s41587-019-0209-9>

*Butyric Acid Prices, News, Chart, Analysis and Forecast.* (n.d.). Retrieved May 29, 2025, from <https://www.imarcgroup.com/butyric-acid-pricing-report>

Calvin, K., Dasgupta, D., Krinner, G., Mukherji, A., Thorne, P. W., Trisos, C., Romero, J., Aldunce, P., Barrett, K., Blanco, G., Cheung, W. W. L., Connors, S., Denton, F., Diongue-Niang, A., Dodman, D., Garschagen, M., Geden, O., Hayward, B., Jones, C., ... Péan, C. (2023). *IPCC, 2023: Climate Change 2023: Synthesis Report. Contribution of Working Groups I, II and III to the Sixth Assessment Report of the Intergovernmental Panel on Climate Change [Core Writing Team, H. Lee and J. Romero (eds.)].* IPCC, Geneva, Switzerland. (First). Intergovernmental Panel on Climate Change (IPCC).  
<https://doi.org/10.59327/IPCC/AR6-9789291691647>

Calvin, M., & Benson, A. A. (1948). The Path of Carbon in Photosynthesis. *Science*, 107(2784), 476–480. <https://doi.org/10.1126/science.107.2784.476>

Câmara-Salim, I., González-García, S., Feijoo, G., & Moreira, M. T. (2021). Screening the environmental sustainability of microbial production of butyric acid produced from lignocellulosic waste streams. *Industrial Crops and Products*, 162, 113280. <https://doi.org/10.1016/j.indcrop.2021.113280>

Cascone, R. (2008). Biobutanol-A replacement for bioethanol? *Chem. Eng. Prog.*, 104(8), S 4.

Ceballos-Escalera, A., Pous, N., Chiluiza-Ramos, P., Korth, B., Harnisch, F., Bañeras, L., Balaguer, M. D., & Puig, S. (2021). Electro-bioremediation of nitrate and arsenite polluted groundwater. *Water Research*, 190, 116748. <https://doi.org/10.1016/j.watres.2020.116748>

Chen, S., & Dong, X. (2005). Proteiniphilum acetatigenes gen. Nov., sp. Nov., from a UASB reactor treating brewery wastewater. *International Journal of Systematic and Evolutionary Microbiology*, 55(Pt 6), 2257–2261. <https://doi.org/10.1099/ijsm.0.63807-0>

Chen, W. S., Huang, S., Plugge, C. M., Buisman, C. J. N., & Strik, D. P. B. T. B. (2020). Concurrent use of methanol and ethanol for chain-elongating short chain fatty acids into caproate and isobutyrate. *Journal of Environmental Management*, 258(December 2019), 110008. <https://doi.org/10.1016/j.jenvman.2019.110008>

Chen, W. S., Huang, S., Strik, D. P. B. T. B., & Buisman, C. J. N. (2017). Isobutyrate biosynthesis via methanol chain elongation: Converting organic wastes to platform chemicals. *Journal of Chemical Technology and Biotechnology*, 92(6), 1370–1379. <https://doi.org/10.1002/jctb.5132>

Chen, W. S., Ye, Y., Steinbusch, K. J. J., Strik, D. P. B. T. B., & Buisman, C. J. N. (2016). Methanol as an alternative electron donor in chain elongation for

butyrate and caproate formation. *Biomass and Bioenergy*, 93, 201–208.  
<https://doi.org/10.1016/j.biombioe.2016.07.008>

Cheng, S., Xing, D., Call, D. F., & Logan, B. E. (2009). Direct Biological Conversion of Electrical Current into Methane by Electromethanogenesis. *Environmental Science & Technology*, 43(10), 3953–3958. <https://doi.org/10.1021/es803531g>

Claassens, N. J., Cotton, C. A. R., Kopljar, D., & Bar-Even, A. (2019). Making quantitative sense of electromicrobial production. *Nature Catalysis*, 2(5), 437–447. <https://doi.org/10.1038/s41929-019-0272-0>

Creasey, R. C. G., Mostert, A. B., Nguyen, T. A. H., Virdis, B., Freguia, S., & Laycock, B. (2018). Microbial nanowires – Electron transport and the role of synthetic analogues. *Acta Biomaterialia*, 69, 1–30. <https://doi.org/10.1016/j.actbio.2018.01.007>

Dang, Y., Holmes, D. E., Zhao, Z., Woodard, T. L., Zhang, Y., Sun, D., Wang, L.-Y., Nevin, K. P., & Lovley, D. R. (2016). Enhancing anaerobic digestion of complex organic waste with carbon-based conductive materials. *Bioresource Technology*, 220, 516–522. <https://doi.org/10.1016/j.biortech.2016.08.114>

Das, S., Das, I., & Ghargrekar, M. M. (2020). Role of applied potential on microbial electrosynthesis of organic compounds through carbon dioxide

sequestration. *Journal of Environmental Chemical Engineering*, 8(4), 104028.  
<https://doi.org/10.1016/j.jece.2020.104028>

De Leeuw, K. D., De Smit, S. M., Van Oossanen, S., Moerland, M. J., Buisman, C. J. N., & Strik, D. P. B. T. B. (2020). Methanol-Based Chain Elongation with Acetate to n-Butyrate and Isobutyrate at Varying Selectivities Dependent on pH. *ACS Sustainable Chemistry and Engineering*, 8(22), 8184–8194.  
<https://doi.org/10.1021/acssuschemeng.0c00907>

De Tessera, S., Köpke, M., Simpson, S. D., Humphreys, C., Minton, N. P., & Dürre, P. (2019). Syngas Biorefinery and Syngas Utilization. In K. Wagemann & N. Tippkötter (Eds.), *Biorefineries* (pp. 247–280). Springer International Publishing. [https://doi.org/10.1007/10\\_2017\\_5](https://doi.org/10.1007/10_2017_5)

Deutzmann, J. S., Kracke, F., Gu, W., & Spormann, A. M. (2022). Microbial Electrosynthesis of Acetate Powered by Intermittent Electricity. *Environmental Science & Technology*, 56(22), 16073–16081.  
<https://doi.org/10.1021/acs.est.2c05085>

Dietrich, H. M., Kremp, F., Öppinger, C., Ribaric, L., & Müller, V. (2021). Biochemistry of methanol-dependent acetogenesis in *Eubacterium callanderi* KIST612. *Environmental Microbiology*, 23(8), 4505–4517.  
<https://doi.org/10.1111/1462-2920.15643>

Dinh, H. T. T., Kambara, H., Matsushita, S., Aoi, Y., Kindaichi, T., Ozaki, N., & Ohashi, A. (2022). Biological methane production coupled with sulfur oxidation in a microbial electrosynthesis system without organic substrates. *Journal of Environmental Sciences*, 116, 68–78.  
<https://doi.org/10.1016/j.jes.2021.07.027>

Dong, Z., Wang, H., Tian, S., Yang, Y., Yuan, H., Huang, Q., Song, T., & Xie, J. (2018). Fluidized granular activated carbon electrode for efficient microbial electrosynthesis of acetate from carbon dioxide. *Bioresource Technology*, 269, 203–209. <https://doi.org/10.1016/j.biortech.2018.08.103>

Dürre, P. (2016). Gas fermentation – a biotechnological solution for today's challenges. *Microbial Biotechnology*, 10(1), 14–16.  
<https://doi.org/10.1111/1751-7915.12431>

Dwidar, M., Park, J.-Y., Mitchell, R. J., & Sang, B.-I. (2012). The Future of Butyric Acid in Industry. *The Scientific World Journal*, 2012, e471417.  
<https://doi.org/10.1100/2012/471417>

Eurostat, S. (2022). *Electricity and heat statistics*.

Evans, M. C., Buchanan, B. B., & Arnon, D. I. (1966). A new ferredoxin-dependent carbon reduction cycle in a photosynthetic bacterium. *Proceedings of the*

*National Academy of Sciences*, 55(4), 928–934.  
<https://doi.org/10.1073/pnas.55.4.928>

Faraghiparapari, N., & Zengler, K. (2017). Production of organics from CO<sub>2</sub> by microbial electrosynthesis (MES) at high temperature. *Journal of Chemical Technology & Biotechnology*, 92(2), 375–381.

<https://doi.org/10.1002/jctb.5015>

Fernández-Blanco, C., Robles-Iglesias, R., Naveira-Pazos, C., Veiga, M. C., & Kennes, C. (2023). Production of biofuels from C1-gases with Clostridium and related bacteria—Recent advances. *Microbial Biotechnology*, 16(4), 726–741. <https://doi.org/10.1111/1751-7915.14220>

Flexer, V., & Jourdin, L. (2020). Purposely Designed Hierarchical Porous Electrodes for High Rate Microbial Electrosynthesis of Acetate from Carbon Dioxide. *Accounts of Chemical Research*, 53(2), 311–321.  
<https://doi.org/10.1021/acs.accounts.9b00523>

Ganigué, R., Puig, S., Batlle-Vilanova, P., Balaguer, M. D., & Colprim, J. (2015). Microbial electrosynthesis of butyrate from carbon dioxide. *Chemical Communications*, 51(15), 3235–3238. <https://doi.org/10.1039/c4cc10121a>

Genthner, B. R., Davis, C. L., & Bryant, M. P. (1981). Features of rumen and sewage sludge strains of *Eubacterium limosum*, a methanol- and H<sub>2</sub>-CO<sub>2</sub>-utilizing

species. *Applied and Environmental Microbiology*, 42(1), 12–19.

<https://doi.org/10.1128/aem.42.1.12-19.1981>

Geppert, F., Liu, D., Weidner, E., & Heijne, A. ter. (2019). Redox-flow battery design for a methane-producing bioelectrochemical system. *International Journal of Hydrogen Energy*, 44(39), 21464–21469.

<https://doi.org/10.1016/j.ijhydene.2019.06.189>

Gong, F., Zhu, H., Zhang, Y., & Li, Y. (2018). Biological carbon fixation: From natural to synthetic. *Journal of CO<sub>2</sub> Utilization*, 28, 221–227.

<https://doi.org/10.1016/j.jcou.2018.09.014>

Hakalehto, E., Adusei-Mensah, F., Heitto, A., Jääskeläinen, A., Kivelä, J., Den Boer, J., & Den Boer, E. (2022). Fermented foods and novel or upgraded raw materials for food commodities by microbial communities. *Microbiology of Food Quality: Challenges in Food Production and Distribution during and after the Pandemics*. De Gruyter, Berlin, 47–98.

Harnisch, F., Deutzmann, J. S., Boto, S. T., & Rosenbaum, M. A. (2024). Microbial electrosynthesis: Opportunities for microbial pure cultures. *Trends in Biotechnology*, 42(8), 1035–1047.

<https://doi.org/10.1016/j.tibtech.2024.02.004>

Hartmanis, M. G. (1987). Butyrate kinase from Clostridium acetobutylicum. *The Journal of Biological Chemistry*, 262(2), 617–621.

Hartshorne, R. S., Jepson, B. N., Clarke, T. A., Field, S. J., Fredrickson, J., Zachara, J., Shi, L., Butt, J. N., & Richardson, D. J. (2007). Characterization of Shewanella oneidensis MtrC: A cell-surface decaheme cytochrome involved in respiratory electron transport to extracellular electron acceptors. *JBIC Journal of Biological Inorganic Chemistry*, 12(7), 1083–1094.  
<https://doi.org/10.1007/s00775-007-0278-y>

He, Y., Kennes, C., & Lens, P. N. L. (2022). Enhanced solventogenesis in syngas bioconversion: Role of process parameters and thermodynamics. *Chemosphere*, 299, 134425.  
<https://doi.org/10.1016/j.chemosphere.2022.134425>

Hengsbach, J.-N., Sabel-Becker, B., Ulber, R., & Holtmann, D. (2022). Microbial electrosynthesis of methane and acetate—Comparison of pure and mixed cultures. *Applied Microbiology and Biotechnology*, 106(12), 4427–4443.  
<https://doi.org/10.1007/s00253-022-12031-9>

Hernandez-Eugenio, G., Fardeau, M.-L., Cayol, J.-L., Patel, B. K. C., Thomas, P., Macarie, H., Garcia, J.-L., & Ollivier, B. (2002). Sporanaerobacter acetigenes gen. Nov., sp. Nov., a novel acetogenic, facultatively sulfur-reducing

bacterium. *International Journal of Systematic and Evolutionary Microbiology*, 52(Pt 4), 1217–1223. <https://doi.org/10.1099/00207713-52-4-1217>

Hoang, T.-D., & Nghiem, N. (2021). Recent Developments and Current Status of Commercial Production of Fuel Ethanol. *Fermentation*, 7(4), Article 4. <https://doi.org/10.3390/fermentation7040314>

Huang, H., Wang, H., Huang, Q., Song, T., & Xie, J. (2021). Mo<sub>2</sub>C/N-doped 3D loofah sponge cathode promotes microbial electrosynthesis from carbon dioxide. *International Journal of Hydrogen Energy*, 46(39), 20325–20337. <https://doi.org/10.1016/j.ijhydene.2021.03.165>

Huang, J., Cai, J., Wang, J., Zhu, X., Huang, L., Yang, S.-T., & Xu, Z. (2011). Efficient production of butyric acid from Jerusalem artichoke by immobilized *Clostridium tyrobutyricum* in a fibrous-bed bioreactor. *Bioresource Technology*, 102(4), 3923–3926. <https://doi.org/10.1016/j.biortech.2010.11.112>

Huang, J., Zhu, H., Tang, W., Wang, P., & Yang, S.-T. (2016). Butyric acid production from oilseed rape straw by *Clostridium tyrobutyricum* immobilized in a fibrous bed bioreactor. *Process Biochemistry*, 51(12), 1930–1934.

Huber, H., Gallenberger, M., Jahn, U., Eylert, E., Berg, I. A., Kockelkorn, D., Eisenreich, W., & Fuchs, G. (2008). A dicarboxylate/4-hydroxybutyrate autotrophic carbon assimilation cycle in the hyperthermophilic Archaeum Ignicoccus hospitalis. *Proceedings of the National Academy of Sciences*, 105(22), 7851–7856. <https://doi.org/10.1073/pnas.0801043105>

Hui, S., Jiang, Y., Jiang, Y., Lyu, Z., Ding, S., Song, B., Zhu, W., & Zhu, J.-J. (2023). Cathode materials in microbial electrosynthesis systems for carbon dioxide reduction: Recent progress and perspectives. *Energy Materials*, 3(6), N/A-N/A. <https://doi.org/10.20517/energymater.2023.60>

IEA, I. (2023). CO<sub>2</sub> Emissions in 2022. *IEA, Paris*.

Izadi, P., Fontmorin, J. M., Virdis, B., Head, I. M., & Yu, E. H. (2021). The effect of the polarised cathode, formate and ethanol on chain elongation of acetate in microbial electrosynthesis. *Applied Energy*, 283(April 2020), 116310. <https://doi.org/10.1016/j.apenergy.2020.116310>

Izadi, P., Fontmorin, J.-M., Lim, S. S., Head, I. M., & Eileen, H. Y. (2021). Enhanced bio-production from CO<sub>2</sub> by microbial electrosynthesis (MES) with continuous operational mode. *Faraday Discussions*, 230, 344–359.

Jiang, L., Fu, H., Yang, H. K., Xu, W., Wang, J., & Yang, S.-T. (2018). Butyric acid: Applications and recent advances in its bioproduction. *Biotechnology Advances*, 36(8), 2101–2117. <https://doi.org/10.1016/j.biotechadv.2018.09.005>

Jiang, Y., Chu, N., Qian, D.-K., & Jianxiong Zeng, R. (2020). Microbial electrochemical stimulation of caproate production from ethanol and carbon dioxide. *Bioresource Technology*, 295, 122266. <https://doi.org/10.1016/j.biortech.2019.122266>

Jourdin, L., & Burdyny, T. (2021). Microbial Electrosynthesis: Where Do We Go from Here? *Trends in Biotechnology*, 39(4), 359–369. <https://doi.org/10.1016/j.tibtech.2020.10.014>

Jourdin, L., Freguia, S., Flexer, V., & Keller, J. (2016). Bringing High-Rate, CO<sub>2</sub>-Based Microbial Electrosynthesis Closer to Practical Implementation through Improved Electrode Design and Operating Conditions. *Environmental Science & Technology*, 50(4), 1982–1989. <https://doi.org/10.1021/acs.est.5b04431>

Jourdin, L., Raes, S. M. T., Buisman, C. J. N., & Strik, D. P. B. T. B. (2018). Critical Biofilm Growth throughout Unmodified Carbon Felts Allows Continuous Bioelectrochemical Chain Elongation from CO<sub>2</sub> up to Caproate at High Current Density. *Frontiers in Energy Research*, 6. <https://doi.org/10.3389/fenrg.2018.00007>

Jourdin, L., Winkelhorst, M., Rawls, B., Buisman, C. J. N., & Strik, D. P. B. T. B. (2019). Bioresource Technology Reports Enhanced selectivity to butyrate and caproate above acetate in continuous bioelectrochemical chain elongation from CO<sub>2</sub>: Steering with CO<sub>2</sub> loading rate and hydraulic retention time. *Bioresource Technology Reports*, 7(May), 100284. <https://doi.org/10.1016/j.biteb.2019.100284>

Kallscheuer, N., Polen, T., Bott, M., & Marienhagen, J. (2017). Reversal of β-oxidative pathways for the microbial production of chemicals and polymer building blocks. *Metabolic Engineering*, 42(February), 33–42. <https://doi.org/10.1016/j.ymben.2017.05.004>

Kerr, R. A. (2007). Global Warming Is Changing the World. *Science*, 316(5822), 188–190. <https://doi.org/10.1126/science.316.5822.188>

Kim, E., Kim, M., Li, S., Song, Y. E., Maile, N., Jang, M., Son, S. H., Jae, J., Kim, H., & Kim, J. R. (2024). Electrodeposited polyaniline on graphite felt (PANI/GF) improves start-up time and acetate productivity of microbial electrosynthesis cell. *Journal of Power Sources*, 612, 234776. <https://doi.org/10.1016/j.jpowsour.2024.234776>

Kim, J.-Y., Park, S., Jeong, J., Lee, M., Kang, B., Jang, S. H., Jeon, J., Jang, N., Oh, S., Park, Z.-Y., & Chang, I. S. (2021). Methanol supply speeds up synthesis gas fermentation by methylotrophic-acetogenic bacterium, *Eubacterium*

limosum KIST612. *Bioresource Technology*, 321, 124521.  
<https://doi.org/10.1016/j.biortech.2020.124521>

Köpke, M., & Simpson, S. D. (2020). Pollution to products: Recycling of 'above ground' carbon by gas fermentation. *Current Opinion in Biotechnology*, 65, 180–189. <https://doi.org/10.1016/j.copbio.2020.02.017>

Kremp, F., & Müller, V. (2021). Methanol and methyl group conversion in acetogenic bacteria: Biochemistry, physiology and application. *FEMS Microbiology Reviews*, 45(2), fuaa040.  
<https://doi.org/10.1093/femsre/fuua040>

Krieg, T., Madjarov, J., Rosa, L. F. M., Enzmann, F., Harnisch, F., Holtmann, D., & Rabaey, K. (2019). Reactors for Microbial Electrobiotherapy. In F. Harnisch & D. Holtmann (Eds.), *Bioelectrosynthesis* (pp. 231–271). Springer International Publishing. [https://doi.org/10.1007/10\\_2017\\_40](https://doi.org/10.1007/10_2017_40)

Krieg, T., Sydow, A., Faust, S., Huth, I., & Holtmann, D. (2018). CO<sub>2</sub> to Terpenes: Autotrophic and Electroautotrophic  $\alpha$ -Humulene Production with Cupriavidus necator. *Angewandte Chemie International Edition*, 57(7), 1879–1882. <https://doi.org/10.1002/anie.201711302>

Kucek, L. A., Nguyen, M., & Angenent, L. T. (2016). Conversion of l-lactate into *n*-caproate by a continuously fed reactor microbiome. *Water Research*, 93, 163–171. <https://doi.org/10.1016/j.watres.2016.02.018>

LaBelle, E. V., Marshall, C. W., Gilbert, J. A., & May, H. D. (2014). Influence of Acidic pH on Hydrogen and Acetate Production by an Electrosynthetic Microbiome. *PLoS ONE*, 9(10), e109935. <https://doi.org/10.1371/journal.pone.0109935>

LaBelle, E. V., Marshall, C. W., & May, H. D. (2019). Microbiome for the electrosynthesis of chemicals from carbon dioxide. *Accounts of Chemical Research*, 53(1), 62–71.

Le, G. T. H., Omar Mohamed, H., Kim, H., Yoo, K., Eisa, T., Jadhav, D. A., Nguyen, H. T. T., Eam, H., Myung, J., Castaño, P., & Chae, K.-J. (2024). Microbial symbiotic electrobioconversion of carbon dioxide to biopolymer (poly (3-hydroxybutyrate)) via single-step microbial electrosynthesis cell. *Chemical Engineering Journal*, 500, 156635. <https://doi.org/10.1016/j.cej.2024.156635>

Leang, C., Coppi, M. V., & Lovley, D. R. (2003). OmcB, a c-Type Polyheme Cytochrome, Involved in Fe(III) Reduction in *Geobacter sulfurreducens*. *Journal of Bacteriology*, 185(7), 2096–2103. <https://doi.org/10.1128/jb.185.7.2096-2103.2003>

Lee, K. M., Kim, K.-Y., Choi, O., Woo, H. M., Kim, Y., Han, S. O., Sang, B.-I., & Um, Y. (2015). In situ detoxification of lignocellulosic hydrolysate using a surfactant for butyric acid production by *Clostridium tyrobutyricum* ATCC 25755. *Process Biochemistry*, 50(4), 630–635.

Lee, S. Y., Oh, Y.-K., Lee, S., Fitriana, H. N., Moon, M., Kim, M.-S., Lee, J., Min, K., Park, G. W., Lee, J.-P., & Lee, J.-S. (2021). Recent developments and key barriers to microbial CO<sub>2</sub> electrobiorefinery. *Bioresource Technology*, 320, 124350. <https://doi.org/10.1016/j.biortech.2020.124350>

Lehtinen, T., Efimova, E., Tremblay, P.-L., Santala, S., Zhang, T., & Santala, V. (2017). Production of long chain alkyl esters from carbon dioxide and electricity by a two-stage bacterial process. *Bioresource Technology*, 243, 30–36. <https://doi.org/10.1016/j.biortech.2017.06.073>

Leonzio, G., & Shah, N. (2024). Recent advancements and challenges in carbon capture, utilization and storage. *Current Opinion in Green and Sustainable Chemistry*, 46, 100895. <https://doi.org/10.1016/j.cogsc.2024.100895>

Li, Y., Luo, Q., Su, J., Dong, G., Cao, M., & Wang, Y. (2023). Metabolic regulation of *Shewanella oneidensis* for microbial electrosynthesis: From extracellular to intracellular. *Metabolic Engineering*, 80, 1–11. <https://doi.org/10.1016/j.ymben.2023.08.004>

Liew, F., Martin, M. E., Tappel, R. C., Heijstra, B. D., Mihalcea, C., & Köpke, M. (2016). Gas Fermentation—A Flexible Platform for Commercial Scale Production of Low-Carbon-Fuels and Chemicals from Waste and Renewable Feedstocks. *Frontiers in Microbiology*, 7. <https://doi.org/10.3389/fmicb.2016.00694>

Litty, D. (2021). Brief Report Butyrate production in the acetogen *Eubacterium limosum* is dependent on the carbon and energy source. <https://doi.org/10.1111/1751-7915.13779>

Liu, H., Ramnarayanan, R., & Logan, B. E. (2004). Production of Electricity during Wastewater Treatment Using a Single Chamber Microbial Fuel Cell. *Environmental Science & Technology*, 38(7), 2281–2285. <https://doi.org/10.1021/es034923g>

Liu, H., Song, T., Fei, K., Wang, H., & Xie, J. (2018). Microbial electrosynthesis of organic chemicals from CO<sub>2</sub> by Clostridium scatologenes ATCC 25775T. *Bioresources and Bioprocessing*, 5(1), 7. <https://doi.org/10.1186/s40643-018-0195-7>

Liu, S., Bischoff, K. M., Leathers, T. D., Qureshi, N., Rich, J. O., & Hughes, S. R. (2013). Butyric acid from anaerobic fermentation of lignocellulosic biomass hydrolysates by Clostridium tyrobutyricum strain RPT-4213. *Bioresource Technology*, 143, 322–329.

Liu, Z., Xue, X., Cai, W., Cui, K., Patil, S. A., & Guo, K. (2023). Recent progress on microbial electrosynthesis reactor designs and strategies to enhance the reactor performance. *Biochemical Engineering Journal*, 190, 108745. <https://doi.org/10.1016/j.bej.2022.108745>

Lovley, D. R. (2017). Syntrophy Goes Electric: Direct Interspecies Electron Transfer. *Annual Review of Microbiology*, 71(Volume 71, 2017), 643–664. <https://doi.org/10.1146/annurev-micro-030117-020420>

Maddipati, P., Atiyeh, H. K., Bellmer, D. D., & Huhnke, R. L. (2011). Ethanol production from syngas by Clostridium strain P11 using corn steep liquor as a nutrient replacement to yeast extract. *Bioresource Technology*, 102(11), 6494–6501. <https://doi.org/10.1016/j.biortech.2011.03.047>

Marshall, C. W., Ross, D. E., Fichot, E. B., Norman, R. S., & May, H. D. (2012). Electrosynthesis of Commodity Chemicals by an Autotrophic Microbial Community. *Applied and Environmental Microbiology*, 78(23), 8412–8420. <https://doi.org/10.1128/AEM.02401-12>

Marshall, C. W., Ross, D. E., Fichot, E. B., Norman, R. S., & May, H. D. (2013). Long-term Operation of Microbial Electrosynthesis Systems Improves Acetate Production by Autotrophic Microbiomes. *Environmental Science & Technology*, 47(11), 6023–6029. <https://doi.org/10.1021/es400341b>

Marshall, C. W., Ross, D. E., Handley, K. M., Weisenhorn, P. B., Edirisinghe, J. N., Henry, C. S., Gilbert, J. A., May, H. D., & Norman, R. S. (2017). Metabolic Reconstruction and Modeling Microbial Electrosynthesis. *Scientific Reports*, 7(1), 8391. <https://doi.org/10.1038/s41598-017-08877-z>

Mayer, F., Enzmann, F., Lopez, A. M., & Holtmann, D. (2019). Performance of different methanogenic species for the microbial electrosynthesis of methane from carbon dioxide. *Bioresource Technology*, 289, 121706. <https://doi.org/10.1016/j.biortech.2019.121706>

Modestra, J. A., & Mohan, S. V. (2017). Microbial electrosynthesis of carboxylic acids through CO<sub>2</sub> reduction with selectively enriched biocatalyst: Microbial dynamics. *Journal of CO<sub>2</sub> Utilization*, 20, 190–199. <https://doi.org/10.1016/j.jcou.2017.05.011>

Molitor, B., Richter, H., Martin, M. E., Jensen, R. O., Juminaga, A., Mihalcea, C., & Angenent, L. T. (2016). Carbon recovery by fermentation of CO-rich off gases – Turning steel mills into biorefineries. *Bioresource Technology*, 215, 386–396. <https://doi.org/10.1016/j.biortech.2016.03.094>

Morais, D. F. S., Lopes, J. C. B., Dias, M. M., Vilar, V. J. P., & Moreira, F. C. (2024).  $\epsilon$ -NETmix: A pioneering electrochemical flow reactor with enhanced mass transfer. *Chemical Engineering Journal*, 481, 148244. <https://doi.org/10.1016/j.cej.2023.148244>

Nevin, K. P., Woodard, T. L., Franks, A. E., Summers, Z. M., & Lovley, D. R. (2010).

Microbial electrosynthesis: Feeding microbes electricity to convert carbon dioxide and water to multicarbon extracellular organic compounds. *MBio*, 1(2), e00103-10.

Pacaud, S., Loubiere, P., & Goma, G. (1985). Methanol metabolism by *Eubacterium limosum* B2: Effects of pH and carbon dioxide on growth and organic acid production. *Current Microbiology*, 12(5), 245–250.  
<https://doi.org/10.1007/BF01567972>

Phillips, J. R., Huhnke, R. L., & Atiyeh, H. K. (2017). Syngas Fermentation: A Microbial Conversion Process of Gaseous Substrates to Various Products. *Fermentation*, 3(2), Article 2. <https://doi.org/10.3390/fermentation3020028>

Pryde, E. M. (1978). Carboxylic acids (economic aspects). *Encyclopedia of Chemical Technology*, 41, 853–859.

Qiang, H., Liu, Z., Dong, Z., Li, D., He, Z., Liu, W., Yue, X., & Zhou, A. (2025). Deciphering the role and mechanism of zero-valent iron on medium-chain fatty acid production from acetate via chain elongation in microbial electro-fermentation. *Chemical Engineering Journal*, 515, 163712.  
<https://doi.org/10.1016/j.cej.2025.163712>

Quince, C., Walker, A. W., Simpson, J. T., Loman, N. J., & Segata, N. (2017).

Shotgun metagenomics, from sampling to analysis. *Nature Biotechnology*, 35(9), 833–844. <https://doi.org/10.1038/nbt.3935>

Quintela, C., Bountzis, P., Rezaei, B., Im, C., Modin, O., Nygård, Y., Olsson, L.,

Skiadas, I. V., & Gavala, H. N. (2024). Chain elongation in continuous microbial electrosynthesis cells: The effect of pH and precursors supply.

*Journal of CO2 Utilization*, 83, 102789.

<https://doi.org/10.1016/j.jcou.2024.102789>

Rabaey, K., & Rozendal, R. A. (2010). Microbial electrosynthesis—Revisiting the electrical route for microbial production. *Nature Publishing Group*, 8.  
<https://doi.org/10.1038/nrmicro2422>

Raes, S. M. T., Jourdin, L., Buisman, C. J. N., & Strik, D. P. B. T. B. (2017).

Continuous Long-Term Bioelectrochemical Chain Elongation to Butyrate. *ChemElectroChem*, 4(2), 386–395. <https://doi.org/10.1002/celc.201600587>

Ragsdale, S. W., & Pierce, E. (2008). Acetogenesis and the Wood–Ljungdahl pathway of CO<sub>2</sub> fixation. *Biochimica et Biophysica Acta (BBA) - Proteins and Proteomics*, 1784(12), 1873–1898. <https://doi.org/10.1016/j.bbapap.2008.08.012>

Reiner, J. E., Geiger, K., Hackbarth, M., Fink, M., Lapp, C. J., Jung, T., Dötsch, A., Hügler, M., Wagner, M., Hille-Reichel, A., Wilcke, W., Kerzenmacher, S.,

Horn, H., & Gescher, J. (2020). From an extremophilic community to an electroautotrophic production strain: Identifying a novel Knallgas bacterium as cathodic biofilm biocatalyst. *The ISME Journal*, 14(5), 1125–1140.  
<https://doi.org/10.1038/s41396-020-0595-5>

Ren, W., He, P., Zhang, H., & Lü, F. (2024). Temperature is an underestimated parameter to regulate the start-up of enhanced carbon chain elongation. *Renewable Energy*, 234, 121221.  
<https://doi.org/10.1016/j.renene.2024.121221>

Rode, L. M., Genthner, B. R. S., & Bryant, M. P. (1981). Syntrophic association by cocultures of the methanol- and CO<sub>2</sub>-H<sub>2</sub>-utilizing species Eubacterium limosum and pectin-fermenting Lachnospira multiparus during growth in a pectin medium. *Applied and Environmental Microbiology*, 42(1), 20–22.  
<https://doi.org/10.1128/aem.42.1.20-22.1981>

Roger, M., Brown, F., Gabrielli, W., & Sargent, F. (2018). Efficient Hydrogen-Dependent Carbon Dioxide Reduction by *Escherichia coli*. *Current Biology*, 28(1), 140-145.e2. <https://doi.org/10.1016/j.cub.2017.11.050>

Roh, H., Ko, H.-J., Kim, D., Choi, D. G., Park, S., Kim, S., Chang, I. S., & Choi, I.-G. (2011). Complete genome sequence of a carbon monoxide-utilizing acetogen, *Eubacterium limosum* KIST612. *Journal of Bacteriology*, 193(1), 307–308. <https://doi.org/10.1128/JB.01217-10>

Rohbohm, N., Sun, T., Blasco-Gómez, R., M. Byrne, J., Kappler, A., & T. Angenent, L. (2023). Carbon oxidation with sacrificial anodes to inhibit O<sub>2</sub> evolution in membrane-less bioelectrochemical systems for microbial electrosynthesis. *EES Catalysis*, 1(6), 972–986. <https://doi.org/10.1039/D3EY00141E>

Romans-Casas, M., Feliu-Paradeda, L., Tedesco, M., Hamelers, H. V., Bañeras, L., Balaguer, M. D., Puig, S., & Dessì, P. (2024). Selective butyric acid production from CO<sub>2</sub> and its upgrade to butanol in microbial electrosynthesis cells. *Environmental Science and Ecotechnology*, 17, 100303.

Romans-Casas, M., Perona-Vico, E., Dessì, P., Bañeras, L., Balaguer, M. D., & Puig, S. (2023). Boosting ethanol production rates from carbon dioxide in MES cells under optimal solventogenic conditions. *Science of The Total Environment*, 856, 159124. <https://doi.org/10.1016/j.scitotenv.2022.159124>

Rovira-Alsina, L., Romans-Casas, M., Balaguer, M. D., & Puig, S. (2022). Thermodynamic approach to foresee experimental CO<sub>2</sub> reduction to organic compounds. *Bioresource Technology*, 354, 127181. <https://doi.org/10.1016/j.biortech.2022.127181>

Sánchez-Andrea, I., Guedes, I. A., Hornung, B., Boeren, S., Lawson, C. E., Sousa, D. Z., Bar-Even, A., Claassens, N. J., & Stams, A. J. M. (2020). The reductive glycine pathway allows autotrophic growth of *Desulfovibrio desulfuricans*.

*Nature Communications*, 11(1), 5090. <https://doi.org/10.1038/s41467-020-18906-7>

San-Valero, P., Abubackar, H. N., Veiga, M. C., & Kennes, C. (2020). Effect of pH, yeast extract and inorganic carbon on chain elongation for hexanoic acid production. *Bioresource Technology*, 300, 122659.

<https://doi.org/10.1016/j.biortech.2019.122659>

Sarria, S., Kruyer, N. S., & Peralta-Yahya, P. (2017). Microbial synthesis of medium-chain chemicals from renewables. *Nature Biotechnology*, 35(12), 1158–1166. <https://doi.org/10.1038/nbt.4022>

Schlager, S., Dibenedetto, A., Aresta, M., Apaydin, D. H., Dumitru, L. M., Neugebauer, H., & Sariciftci, N. S. (2017). Biocatalytic and Bioelectrocatalytic Approaches for the Reduction of Carbon Dioxide using Enzymes. *Energy Technology*, 5(6), 812–821. <https://doi.org/10.1002/ente.201600610>

Schulman, M., Parker, D., Ljungdahl, L. G., & Wood, H. G. (1972). Total synthesis of acetate from CO<sub>2</sub> V. Determination by mass analysis of the different types of acetate formed from <sup>13</sup>CO<sub>2</sub> by heterotrophic bacteria. *Journal of Bacteriology*, 109(2), 633–644.

Seedorf, H., Fricke, W. F., Veith, B., Brüggemann, H., Liesegang, H., Strittmatter, A., Miethke, M., Buckel, W., Hinderberger, J., Li, F., Hagemeier, C., Thauer, R. K., & Gottschalk, G. (2008). The genome of *Clostridium kluyveri*, a strict anaerobe with unique metabolic features. *Proceedings of the National Academy of Sciences*, 105(6), 2128–2133. <https://doi.org/10.1073/pnas.0711093105>

Sharak Gentner, B. R., & Bryant, M. P. (1987). Additional characteristics of one-carbon-compound utilization by *Eubacterium limosum* and *Acetobacterium woodii*. *Applied and Environmental Microbiology*, 53(3), 471–476.

Shaw, A. J., Miller, B. B., Rogers, S. R., Kenealy, W. R., Meola, A., Bhandiwad, A., Sillers, W. R., Shikhare, I., Hogsett, D. A., & Herring, C. D. (2015). Anaerobic detoxification of acetic acid in a thermophilic ethanologen. *Biotechnology for Biofuels*, 8(1), 75. <https://doi.org/10.1186/s13068-015-0257-4>

Song, Y. E., Mohamed, A., Kim, C., Kim, M., Li, S., Sundstrom, E., Beyenal, H., & Kim, J. R. (2022). Biofilm matrix and artificial mediator for efficient electron transport in CO<sub>2</sub> microbial electrosynthesis. *Chemical Engineering Journal*, 427, 131885. <https://doi.org/10.1016/j.cej.2021.131885>

Soussan, L., Riess, J., Erable, B., Delia, M.-L., & Bergel, A. (2013). Electrochemical reduction of CO<sub>2</sub> catalysed by *Geobacter sulfurreducens* grown on polarized

stainless steel cathodes. *Electrochemistry Communications*, 28, 27–30.  
<https://doi.org/10.1016/j.elecom.2012.11.033>

Srikanth, S., Kumar, M., Singh, D., Singh, M. P., Puri, S. K., & Ramakumar, S. S. V. (2018). Long-term operation of electro-biocatalytic reactor for carbon dioxide transformation into organic molecules. *Bioresource Technology*, 265, 66–74. <https://doi.org/10.1016/j.biortech.2017.12.075>

Strauss, G., & Fuchs, G. (1993). Enzymes of a novel autotrophic CO<sub>2</sub> fixation pathway in the phototrophic bacterium *Chloroflexus aurantiacus*, the 3-hydroxypropionate cycle. *European Journal of Biochemistry*, 215(3), 633–643.  
<https://doi.org/10.1111/j.1432-1033.1993.tb18074.x>

Tahir, K., Miran, W., Jang, J., Woo, S. H., & Lee, D. S. (2021). Enhanced product selectivity in the microbial electrosynthesis of butyrate using a nickel ferrite-coated biocathode. *Environmental Research*, 196, 110907.  
<https://doi.org/10.1016/j.envres.2021.110907>

Tarud, J., & Phillips, S. (1 C.E.). Technoeconomic Comparison of Biofuels: Ethanol, Methanol, and Gasoline from Gasification of Woody Residues (Presentation). *Report Number: NREL/PR-5100-52636*.  
<https://www.osti.gov/biblio/1028039>

T. Boto, S., Bardl, B., Harnisch, F., & A. Rosenbaum, M. (2023). Microbial electrosynthesis with *Clostridium ljungdahlii* benefits from hydrogen electron mediation and permits a greater variety of products. *Green Chemistry*, 25(11), 4375–4386. <https://doi.org/10.1039/D3GC00471F>

Thakur, I. S., Kumar, M., Varjani, S. J., Wu, Y., Gnansounou, E., & Ravindran, S. (2018). Sequestration and utilization of carbon dioxide by chemical and biological methods for biofuels and biomaterials by chemoautotrophs: Opportunities and challenges. *Bioresource Technology*, 256, 478–490. <https://doi.org/10.1016/j.biortech.2018.02.039>

The Methanol Industry. (n.d.). *Methanol Institute*. Retrieved May 2, 2025, from <https://www.methanol.org/the-methanol-industry/>

T. Pio, D., M. Vilas-Boas, A. C., C. Rodrigues, N. F., & Mendes, A. (2022). Carbon neutral methanol from pulp mills towards full energy decarbonization: An inside perspective and critical review. *Green Chemistry*, 24(14), 5403–5428. <https://doi.org/10.1039/D2GC01528E>

Tringe, S. G., & Hugenholtz, P. (2008). A renaissance for the pioneering 16S rRNA gene. *Current Opinion in Microbiology*, 11(5), 442–446. <https://doi.org/10.1016/j.mib.2008.09.011>

Twarog, R., & Wolfe, R. S. (1962). Enzymatic phosphorylation of butyrate. *The Journal of Biological Chemistry*, 237, 2474–2477.

Ul, Z., Sulonen, M., Baeza, J. A., & Guisasola, A. (2024). Continuous high-purity bioelectrochemical nitrogen recovery from high N-loaded wastewaters. *Bioelectrochemistry*, 158, 108707.  
<https://doi.org/10.1016/j.bioelechem.2024.108707>

Ullrich, T., Lindner, J., Bär, K., Mörs, F., Graf, F., & Lemmer, A. (2018). Influence of operating pressure on the biological hydrogen methanation in trickle-bed reactors. *Bioresource Technology*, 247, 7–13.  
<https://doi.org/10.1016/j.biortech.2017.09.069>

Van Hecke, W., Bockrath, R., & De Wever, H. (2019). Effects of moderately elevated pressure on gas fermentation processes. *Bioresource Technology*, 293, 122129.  
<https://doi.org/10.1016/j.biortech.2019.122129>

Vassilev, I., Dessì, P., Puig, S., & Kokko, M. (2022). Cathodic biofilms – A prerequisite for microbial electrosynthesis. *Bioresource Technology*, 348, 126788.  
<https://doi.org/10.1016/j.biortech.2022.126788>

Vassilev, I., Hernandez, P. A., Batlle-Vilanova, P., Freguia, S., Krömer, J. O., Keller, J., Ledezma, P., & Virdis, B. (2018). Microbial Electrosynthesis of Isobutyric, Butyric, Caproic Acids, and Corresponding Alcohols from Carbon Dioxide.

*ACS Sustainable Chemistry and Engineering*, 6(7), 8485–8493.  
<https://doi.org/10.1021/acssuschemeng.8b00739>

Vassilev, I., Kracke, F., Freguia, S., Keller, J., Krömer, J. O., Ledezma, P., & Virdis, B. (2019). Microbial electrosynthesis system with dual biocathode arrangement for simultaneous acetogenesis, solventogenesis and carbon chain elongation. *Chemical Communications*.  
<https://doi.org/10.1039/c9cc00208a>

Vassilev, I., Rinta-Kanto, J. M., & Kokko, M. (2024). Comparing the performance of fluidized and fixed granular activated carbon beds as cathodes for microbial electrosynthesis of carboxylates from CO<sub>2</sub>. *Bioresource Technology*, 130896. <https://doi.org/10.1016/j.biortech.2024.130896>

Visser, M., Pieterse, M. M., Pinkse, M. W. H., Nijssse, B., Verhaert, P. D. E. M., de Vos, W. M., Schaap, P. J., & Stams, A. J. M. (2016). Unravelling the one-carbon metabolism of the acetogen *Sporomusa* strain An4 by genome and proteome analysis. *Environmental Microbiology*, 18(9), 2843–2855.  
<https://doi.org/10.1111/1462-2920.12973>

Wagner, N., Wen, L., Frazão, C. J. R., & Walther, T. (2023). Next-generation feedstocks methanol and ethylene glycol and their potential in industrial biotechnology. *Biotechnology Advances*, 69, 108276.  
<https://doi.org/10.1016/j.biotechadv.2023.108276>

Wei, D., Liu, X., & Yang, S.-T. (2013). Butyric acid production from sugarcane bagasse hydrolysate by Clostridium tyrobutyricum immobilized in a fibrous-bed bioreactor. *Bioresource Technology*, 129, 553–560.

Wood, J. C., Marcellin, E., Plan, M. R., & Virdis, B. (2022). High methanol-to-formate ratios induce butanol production in *Eubacterium limosum*. *Microbial Biotechnology*, 15(5), 1542–1549. <https://doi.org/10.1111/1751-7915.13963>

Wu, H., Pan, H., Li, Z., Liu, T., Liu, F., Xiu, S., Wang, J., Wang, H., Hou, Y., Yang, B., Lei, L., & Lian, J. (2022). Efficient production of lycopene from CO<sub>2</sub> via microbial electrosynthesis. *Chemical Engineering Journal*, 430, 132943. <https://doi.org/10.1016/j.cej.2021.132943>

Wu, Q., Bao, X., Guo, W., Wang, B., Li, Y., Luo, H., Wang, H., & Ren, N. (2019). Medium chain carboxylic acids production from waste biomass: Current advances and perspectives. *Biotechnology Advances*, 37(5), 599–615. <https://doi.org/10.1016/j.biotechadv.2019.03.003>

Wu, Y., Li, W., Wang, L., Wu, Y., Wang, Y., Wang, Y., & Meng, H. (2022). Enhancing the selective synthesis of butyrate in microbial electrosynthesis system by gas diffusion membrane composite biocathode. *Chemosphere*, 308, 136088. <https://doi.org/10.1016/j.chemosphere.2022.136088>

Xia, R., Cheng, J., Chen, Z., Zhou, X., Zhang, Z., Zhou, J., & Zhang, M. (2023).

Tailoring interfacial microbiome and charge dynamics via a rationally designed atomic-nanoparticle bridge for bio-electrochemical CO<sub>2</sub>-fixation.

*Energy & Environmental Science*, 16(3), 1176–1186.

<https://doi.org/10.1039/D2EE03886B>

Xiang, Y., Liu, G., Zhang, R., Lu, Y., & Luo, H. (2017). High-efficient acetate

production from carbon dioxide using a bioanode microbial electrosynthesis system with bipolar membrane. *Bioresource Technology*, 233, 227–235.

<https://doi.org/10.1016/j.biortech.2017.02.104>

Xie, Z., Chen, Z., Zheng, X., Liu, Y., & Jiang, Y. (2025). Recent advances in

enhancing microbial electrosynthesis performance: Innovations in cathode design and reactor engineering. *International Journal of Hydrogen Energy*, 103,

528–537. <https://doi.org/10.1016/j.ijhydene.2025.01.279>

Xu, B., Li, Z., Jiang, Y., Chen, M., Chen, B., Xin, F., Dong, W., & Jiang, M. (2022).

Recent advances in the improvement of bi-directional electron transfer between abiotic/biotic interfaces in electron-assisted biosynthesis system.

*Biotechnology Advances*, 54, 107810.

<https://doi.org/10.1016/j.biotechadv.2021.107810>

Yadav, R., Chattopadhyay, B., Kiran, R., Yadav, A., Bachhawat, A. K., & Patil, S. A.

(2022). Microbial electrosynthesis from carbon dioxide feedstock linked to

yeast growth for the production of high-value isoprenoids. *Bioresource Technology*, 363, 127906. <https://doi.org/10.1016/j.biortech.2022.127906>

Yang, H.-Y., Hou, N.-N., Wang, Y.-X., Liu, J., He, C.-S., Wang, Y.-R., Li, W.-H., & Mu, Y. (2021). Mixed-culture biocathodes for acetate production from CO<sub>2</sub> reduction in the microbial electrosynthesis: Impact of temperature. *Science of The Total Environment*, 790, 148128. <https://doi.org/10.1016/j.scitotenv.2021.148128>

Yang, Q., Guo, S., Lu, Q., Tao, Y., Zheng, D., Zhou, Q., & Liu, J. (2021). Butyryl/Caproyl-CoA:Acetate CoA-transferase: Cloning, expression and characterization of the key enzyme involved in medium-chain fatty acid biosynthesis. *Bioscience Reports*, 41(8), BSR20211135. <https://doi.org/10.1042/BSR20211135>

Yao, H., Dessì, P., Romans-Casas, M., Puig, S., & Kokko, M. (2025). Optimizing butyrate production from methanol and CO<sub>2</sub> in microbial electrosynthesis. *Bioresource Technology*, 437, 133150. <https://doi.org/10.1016/j.biortech.2025.133150>

Yao, H., Rinta-Kanto, J. M., Vassilev, I., & Kokko, M. (2024). Methanol as a co-substrate with CO<sub>2</sub> enhances butyrate production in microbial electrosynthesis. *Applied Microbiology and Biotechnology*, 108(1), 372. <https://doi.org/10.1007/s00253-024-13218-y>

Yao, H., Romans-Casas, M., Vassilev, I., Rinta-Kanto, J. M., Puig, S., Rissanen, A. J., & Kokko, M. (2025). Selective butyrate production from CO<sub>2</sub> and methanol in microbial electrosynthesis—Influence of pH. *Bioelectrochemistry*, 109000. <https://doi.org/10.1016/j.bioelechem.2025.109000>

Yu, L., Yuan, Y., Tang, J., & Zhou, S. (2017). Thermophilic *Moorella thermoautotrophica*-immobilized cathode enhanced microbial electrosynthesis of acetate and formate from CO<sub>2</sub>. *Bioelectrochemistry*, 117, 23–28. <https://doi.org/10.1016/j.bioelechem.2017.05.001>

Zhang, J., Liu, H., Zhang, Y., Fu, B., Zhang, C., Cui, M., Wu, P., & Chen, C. (2023). Enhanced CO<sub>2</sub> Reduction by Electron Shuttle Molecules via Coupling Different Electron Transport Processes in Microbial Electrosynthesis. *Fermentation*, 9(7), Article 7. <https://doi.org/10.3390/fermentation9070679>

Zhang, K., Qiu, Z., Luo, D., Song, T., & Xie, J. (2023). Hybrid electron donors of ethanol and lactate stimulation chain elongation in microbial electrosynthesis with different inoculants. *Renewable Energy*, 202, 942–951. <https://doi.org/10.1016/j.renene.2022.11.123>

Zhang, X., Rabiee, H., Frank, J., Cai, C., Stark, T., Virdis, B., Yuan, Z., & Hu, S. (2020). Enhancing methane oxidation in a bioelectrochemical membrane reactor using a soluble electron mediator. *Biotechnology for Biofuels*, 13(1), 173. <https://doi.org/10.1186/s13068-020-01808-7>

Zhao, T., Li, Y., & Zhang, Y. (2021). Biological carbon fixation: A thermodynamic perspective. *Green Chemistry*, 23(20), 7852–7864.  
<https://doi.org/10.1039/D0GC03493B>

## PUBLICATIONS

# PUBLICATION

|

**Methanol as a co-substrate with CO<sub>2</sub> enhances butyrate production in microbial electrosynthesis**

Yao, H., Rinta-Kanto, J. M., Vassilev, I., & Kokko, M.

Applied Microbiology and Biotechnology, 108(1), 372.  
<https://doi.org/10.1007/s00253-024-13218-y>

**Publication is licensed under a Creative Commons Attribution 4.0 International License CC BY**



## Methanol as a co-substrate with CO<sub>2</sub> enhances butyrate production in microbial electrosynthesis

Hui Yao<sup>1</sup> · Johanna M. Rinta-Kanto<sup>1</sup> · Igor Vassilev<sup>1</sup> · Marika Kokko<sup>1</sup> 

Received: 1 December 2023 / Revised: 28 May 2024 / Accepted: 2 June 2024 / Published online: 14 June 2024  
© The Author(s) 2024

### Abstract

Methanol is a promising feedstock for the bio-based economy as it can be derived from organic waste streams or produced electrochemically from CO<sub>2</sub>. Acetate production from CO<sub>2</sub> in microbial electrosynthesis (MES) has been widely studied, while more valuable compounds such as butyrate are currently attracting attention. In this study, methanol was used as a co-substrate with CO<sub>2</sub> to enhance butyrate production in MES. Feeding with CO<sub>2</sub> and methanol resulted in the highest butyrate production rates and titres of  $0.36 \pm 0.01 \text{ g L}^{-1} \text{ d}^{-1}$  and  $8.6 \pm 0.2 \text{ g L}^{-1}$ , respectively, outperforming reactors with only CO<sub>2</sub> feeding ( $0.20 \pm 0.03 \text{ g L}^{-1} \text{ d}^{-1}$  and  $5.2 \pm 0.1 \text{ g L}^{-1}$ , respectively). Methanol acted as electron donor and as carbon source, both of which contributed ca. 50% of the carbon in the products. *Eubacterium* was the dominant genus with  $52.6 \pm 2.5\%$  relative abundance. Thus, we demonstrate attractive route for the use of the C1 substrates, CO<sub>2</sub> and methanol, to produce mainly butyrate.

### Key points

- Butyrate was the main product from methanol and CO<sub>2</sub> in MES
- Methanol acted as both carbon and electron source in MES
- *Eubacterium* dominating microbial culture was enriched in MES

**Keywords** Methanol utilisation · CO<sub>2</sub> utilisation · Microbial electrosynthesis · Butyrate · Electron donor

## Introduction

In light of replacing fossil fuel-based chemicals with renewable chemicals and reaching the goal of a carbon neutral society, it is crucial to explore new routes for the production of renewable biochemicals. The greenhouse gas CO<sub>2</sub> is considered as the major cause of the current climate warming, while it can also be regarded as an alternative carbon feedstock for the production of organic commodities (Aresta and Dibenedetto 2007). Such CO<sub>2</sub> conversion can be realised with microbial electrosynthesis (MES) where microorganisms are employed as biocatalysts to reduce CO<sub>2</sub> to multi-carbon compounds with an external energy source. In MES, an electrochemical cell is used to provide electrons for microorganisms. In the anode, water is oxidised to

release oxygen, electrons, and protons. Electrons are transferred through external load to the cathode, and the protons migrate to the cathode via ion exchange membrane. At the cathode, the protons can be abiotically/biotically reduced to H<sub>2</sub> that can be used for CO<sub>2</sub> reduction, or alternatively, CO<sub>2</sub> reduction can be achieved by microorganisms with direct utilization of electrons from the cathode electrode (Rabaey and Rozendal 2010). Since the first proof of concept of MES (Nevin et al. 2010), various studies have been undertaken during the past decade to improve the performance of MES from different perspectives, such as improvement of electrode materials (Sharma et al. 2019), reactor configuration design (Vassilev et al. 2019), and optimisation of operation parameters (Marshall et al. 2013). At the early stage, the main product of MES was acetate, which possesses limited economic value and thus, weakens the competitiveness of MES for the synthesis of chemical commodities. In order to expand the product spectrum of MES, enriching a certain microbiome (Vassilev et al. 2018) or optimising operational parameters (Jourdin et al. 2019) have been studied resulting

✉ Marika Kokko  
marika.kokko@tuni.fi

<sup>1</sup> Faculty of Engineering and Natural Sciences, Tampere University, Korkeakoulunkatu 8, 33720 Tampere, Finland

in the production of longer chain fatty acids such as butyrate, iso-butyrate, caproate, and the corresponding alcohols.

Butyrate, as a widely used compound in industries (e.g. food, chemical, and pharmaceutical industry), possesses a higher economic value than acetate. Butyrate production in MES has been demonstrated since 2015 and has been accelerated by adding a chemical electron donor (e.g. ethanol) to reach butyrate titres of  $6.3 \text{ g L}^{-1}$  (Ganigüé et al. 2015; Izadi et al. 2021b; Li et al. 2022). However, ethanol is a widely used biofuel, and the current industrial production of ethanol mainly relies on agricultural products, e.g. sugarcane and corn (Medina and Magalhaes 2021). The competition with food production makes ethanol a less promising substrate for MES from a sustainability point of view (Aro 2016). Therefore, seeking more sustainable electron donors with sufficient reducing power could improve the production of higher-value products in MES.

Methanol is a promising feedstock for bioproduction. About 80% of the methanol used in the world is currently produced from petroleum products (synthesis gas) at elevated pressure (50–100 bar) and temperature (200 to 300 °C) (Iaquaniello et al. 2017). Besides, sustainable production processes of methanol have been developed recently, using biomass or organic waste streams as substrates, which has been implemented at the industrial level by using municipal waste, including unrecyclable plastics (Hobson and Márquez 2018). In addition to its sustainable production, methanol is also abundant in certain industrial waste streams, e.g. in pulp and paper industry (Mäki et al. 2021). The methanol-rich waste streams can be directly used as the feedstock for the bioproduction of value-added products (Eregowda et al. 2021).

Methanol can act as the carbon and energy source to support the growth of microorganisms, including acetogens (Ginige et al. 2009). Acetogens are autotrophic bacteria utilising C1 compounds through the Wood-Ljungdahl pathway (WLP) with acetate as the major product. WLP is considered as one of the most energetically efficient non-photosynthetic carbon fixation pathways, and therefore acetogens have gained attention to set a carboxylate platform for the sustainable biochemical synthesis. It has been suggested that methanol could also be utilised through the WLP (Bache and Pfennig 1981), similar to the utilisation of other C1 compounds, such as CO<sub>2</sub> (Litty et al. 2022), CO (Diender et al. 2015), and formate (Balch et al. 1977). Methanol is a promising reducing agent for microorganisms, which can facilitate the carbon chain elongation of shorter chain fatty acids (acetate or propionate) to longer chain fatty acids, including n-butyrate, i-butyrate, valerate, and caproate (Chen et al. 2017, 2020; De Leeuw et al. 2020). Although the fundamentals of methanol carbon chain elongation are not fully understood, methanol has been suggested to provide reducing power to drive the carbon

chain elongation via different pathways, one of which is the reverse beta oxidation (De Smit et al. 2019). The two-carbon acetyl-coenzyme A (acetyl-CoA) is considered as the chain elongation block molecule, extending the carbon chain by two carbons at each time, i.e. acetate (C2) to butyrate (C4) or propionate (C3) to valerate (C5) (Kallscheuer et al. 2017). In MES, an electron donor (such as ethanol) addition has been proven to provide reducing power and result in the production of more reduced products than acetate (Izadi et al. 2021b). Thus, methanol also possesses the potential to provide extra reducing power in MES, while to the authors' knowledge, it has not been reported.

In this study, the use of methanol as co-substrate in MES was investigated due to its potential role as a carbon source and reducing agent. The feasibility and role of utilising methanol as the co-substrate with CO<sub>2</sub> in MES was investigated by feeding MES with either methanol or CO<sub>2</sub> or with a combination of both compounds. MES performance was evaluated by analysing the product formation, substrate utilisation, carbon and electron balances as well as by characterising the microbiomes.

## Materials and methods

### MES reactor setup

Both abiotic and biotic experiments were performed in double chamber flat plate reactors. The reactor comprised acrylic rectangular plates to create two compartments, each with an internal volume of 35 mL (7 cm × 5 cm × 1 cm) (Fig. S1). Cation exchange membrane (CMI-7000, Membranes International, USA) with a surface area of 35 cm<sup>2</sup> was used to separate the anodic and cathodic chambers. In the cathodic chamber, graphite granules (10 ± 2 mm, EC-100, Graphite Sales Inc, USA) were used to fill the compartment, serving as the cathode electrode and carrier for microbial growth. Two graphite rods (diameter 6 mm, length 15 cm, Sigma-Aldrich, USA) were placed in the packed granular bed and connected to the external circuit as current collectors. An Ag/AgCl reference electrode (+0.206 V vs. normal hydrogen electrode, BASi, USA) was connected to a capillary glass frit (4 × 60 mm, Prosense, the Netherlands) immersed in the cathodic chamber. In the anodic chamber, a platinum wire (0.4 mm, 99.95%, Advent research materials, UK) worked as the counter electrode. Catholyte and anolyte (300 mL of 50 mmol L<sup>-1</sup> H<sub>2</sub>SO<sub>4</sub>) were recirculated through external bottles with a peristaltic pump at a flow rate of 40 mL min<sup>-1</sup>. Gases from the cathodic recirculation bottle were collected in a 5 L gas bag (Supel™-Inert Gas Sampling Bags, MERCK, Germany). The system was connected to a potentiostat (VMP3, Bio-Logic, France), and all the potentials are reported with

respect to the Ag/AgCl reference electrode. All the experiments were run at 35 °C.

### Medium composition and microbial culture enrichment

The medium used in the cathodic chamber consisted of 18 g L<sup>-1</sup> Na<sub>2</sub>HPO<sub>4</sub>·2H<sub>2</sub>O, 3 g L<sup>-1</sup> KH<sub>2</sub>PO<sub>4</sub>, 3 g L<sup>-1</sup> NH<sub>4</sub>Cl, 15 mg L<sup>-1</sup> CaCl<sub>2</sub>, 20 mg L<sup>-1</sup> MgSO<sub>4</sub>·7H<sub>2</sub>O, 2.1 g L<sup>-1</sup> sodium 2-bromoethanesulfonate, 1 g L<sup>-1</sup> yeast extract as well as 10 mL L<sup>-1</sup> trace elements solution and 1 mL L<sup>-1</sup> vitamin solution (Table S1 and S2). The medium had a pH of ca. 7.2, and it was sterilised by filtration (0.2 µm, Fisherbrand™ Disposable PES Filter Units, USA) before use. The medium was sparged with N<sub>2</sub> for 30 min to remove oxygen before starting experiments.

The original inoculum was a mixed culture originating from cow rumen and enriched for carboxylate production in an MES reactor, which was fed with CO<sub>2</sub> and current over a period of one year. Microbial cultures were further enriched in two parallel MES reactors. The reactor setup was similar to the one described above, except the internal volume of each chamber was 124 mL and the projected surface area of the membrane was 41 cm<sup>2</sup>. A total of 600 mL of medium and 80 mL of inoculum were added as the catholyte to start the enrichment. A total of 300 mL of 50 mmol L<sup>-1</sup> H<sub>2</sub>SO<sub>4</sub> (prepared in milli-Q water) was added as the anolyte and replenished every two weeks during the whole operation. In this study, both anolyte and catholyte were recirculated with the rate of 40 mL min<sup>-1</sup>. CO<sub>2</sub> was sparged to the cathodic recirculation bottle every 2 to 4 days for 15 min at the rate of 0.4 L min<sup>-1</sup> (EK-2LR rotameter, Kytola, Finland). After CO<sub>2</sub> sparging, methanol stock solution (1.2 mol L<sup>-1</sup>, prepared in medium) was added to reach a methanol concentration of 20 mmol L<sup>-1</sup> in the catholyte. The pH of the catholyte was measured after CO<sub>2</sub> and methanol addition. If necessary, 1 mol L<sup>-1</sup> NaOH was added to maintain the catholyte pH between 6.0 and 6.2. The enrichment reactors were operated in semi-batch mode, and the medium in the cathodic recirculation bottles (the bottle was emptied and 500 mL of fresh medium was added) was replaced every 35 to 50 days to provide microorganisms with fresh nutrients. In total, the enrichment of microbial culture was operated for over 240 days (five semi-batches in total), during which the cathodic potential was controlled at a range of -0.75 to -0.95 V.

### Determining the role of methanol in MES

To understand the role of methanol as a co-substrate in MES, three different substrate feedings were tested: carbon

dioxide (CD), methanol (ME), and co-feeding of carbon dioxide and methanol (ME-CD). Two replicates were operated with each substrate feeding. In the beginning, 330 mL of medium and 150 mL of H<sub>2</sub>SO<sub>4</sub> were added as catholyte and anolyte, respectively. The reactors were inoculated with 40 mL of cathodic broth from the enrichment reactors and operated for 30–32 days. The cathodic current was controlled at -100 mA, and the cathodic potential was recorded. Substrate(s) were added three times a week by following the same procedure as with the enrichment reactors. The detailed operational parameters are shown in Table 1.

The potential abiotic methanol removal, i.e. electrochemical reduction of methanol or diffusion of methanol through the membrane, was examined in abiotic conditions. The abiotic experiment was carried out for 7 days with an identical MES reactor setup and with the same operating parameters as in the co-substrate experiment. The connecting tubing and graphite granules were autoclaved before use. The reactor plates were sterilised with 70% ethanol and assembled in a laminar flow hood. Yeast extract and vitamin solution were removed from the medium to minimise the possibility of microbial growth during the abiotic experiment. CO<sub>2</sub> and methanol were added according to Table 1, and samples were taken on days 0, 2, 4, and 7 from both the anode (liquid samples) and the cathode (liquid and gas samples).

### Analytical methods and calculations

Liquid samples were taken before and after the CO<sub>2</sub> and/or methanol addition from the catholyte recirculation bottles (three times a week). Catholyte pH was immediately measured with a pH meter (WTW-330i, Germany) and optical density (OD at 600 nm) with a UV-Vis spectrophotometer (UV-1800, Shimadzu, Japan). The remaining liquid samples were filtered through a 0.2 µm filter (CHROMAFIL Xtra PET, 25 mm, 0.2 µm, MACHERREY-NAGEL, Germany) and used for analysing total inorganic carbon (TIC) via a total organic carbon analyser with ASI-V sampler (TOC-VCPh, Shimadzu, Japan). Sample pH was firstly adjusted to below 3 using 3 mol L<sup>-1</sup> HCl to volatilise the inorganic

**Table 1** Operational parameters of the enrichment and co-substrate experiments

Experiment	Codes	Substrate(s) addition
Enrichment	R	CO <sub>2</sub> (15 min, 0.4 min L <sup>-1</sup> ) Methanol (20 mmol L <sup>-1</sup> )
Co-substrate	ME-CD	CO <sub>2</sub> (15 min, 0.4 min L <sup>-1</sup> ) Methanol (20 mmol L <sup>-1</sup> )
	ME	Methanol (20 mmol L <sup>-1</sup> )
	CD	CO <sub>2</sub> (15 min, 0.4 min L <sup>-1</sup> )

carbon into  $\text{CO}_2$ , which was detected by a nondispersive infrared sensor.

Volatile fatty acids (VFAs) and alcohols (i.e. methanol, ethanol, butanol, acetate, propionate, butyrate, isobutyrate, valerate, caproate) were analysed via gas chromatography with a flame ionisation detector (GC-FID 2010 Plus, Shimadzu, Japan), equipped with AOC-20s autosampler and a Zebron ZB-WAX plus column ( $0.25\text{ }\mu\text{m}$  diameter,  $30\text{ m}$  length). Helium was used as the carrier gas at a flow rate of  $84.4\text{ mL min}^{-1}$  and pressure of  $114.6\text{ kPa}$ . The column temperature was firstly set at  $40\text{ }^\circ\text{C}$  and held for  $2\text{ min}$ , followed by the heating-up program to  $160\text{ }^\circ\text{C}$  with a rate of  $20\text{ }^\circ\text{C min}^{-1}$ , and further increase the temperature to  $220\text{ }^\circ\text{C}$  with a rate of  $40\text{ }^\circ\text{C min}^{-1}$ , then hold for  $3\text{ min}$ . The injector and detector temperatures were set at  $250\text{ }^\circ\text{C}$ . The repeated measures ANOVA was carried out to analyse the differences of VFA productions between ME-CD and CD groups.

Headspace gas composition (i.e.  $\text{H}_2$ ,  $\text{CO}_2$ ,  $\text{CH}_4$ ) was analysed via gas chromatography with a thermal conductivity detector (GC-TCD 2014, Shimadzu, Japan) equipped with an Agilent J&W packed GC column ( $1.8\text{ m}$  length,  $2\text{ mm}$  Porapak, the Netherlands).  $\text{N}_2$  was used as the carrier gas at a flow rate of  $20\text{ mL min}^{-1}$ . The temperature of the injector, column, and detector was set at  $110\text{ }^\circ\text{C}$ ,  $80\text{ }^\circ\text{C}$ , and  $110\text{ }^\circ\text{C}$ , respectively. The volume in the gas bags was measured via a water replacement method, in which the volume of the gas is equalised to the volume of the replaced water in the water pillar. The temperature and pressure were recorded to calculate the gas production at  $35\text{ }^\circ\text{C}$ .

At the end of the co-substrate experiments, ca.  $10\text{ g}$  of graphite granules with biofilm were sampled for scanning electron microscopy (SEM) imaging (JSM-IT500, Jeol, Japan). The granules were firstly rinsed with  $0.1\text{ mol L}^{-1}$  phosphate buffer solution (PBS, pH  $7.0$ , prepared with  $0.058\text{ mol L}^{-1}$   $\text{Na}_2\text{HPO}_4$  and  $0.042\text{ mol L}^{-1}$   $\text{KH}_2\text{PO}_4$ , sterilised by  $0.2\text{ }\mu\text{m}$  filtration) and then fixed in  $2.5\%$  glutaraldehyde (dissolved in PBS) for  $17\text{ h}$  at  $4\text{ }^\circ\text{C}$ . The treated samples were then rinsed with PBS and dehydrated with graded ethanol series solution ( $10\%$ ,  $30\%$ ,  $50\%$ ,  $70\%$ ,  $80\%$ ,  $90\%$ ,  $100\%$ ) for  $10\text{ min}$  at  $100\text{ rpm}$  agitation to fix the biofilm on the granules. The graphite granules were glued to an SEM specimen stub and carbon coated before imaging to increase the conductivity and avoid charging. Images were taken with a secondary electron detector at the acceleration voltage of  $15\text{ kV}$ .

Carbon conversion efficiency was used to present the percentage of soluble end-products in the catholyte compared to the consumed substrates. Microbial growth as the biomass was not taken into consideration. The exact composition of the yeast extract is not available, and therefore yeast extract is not included in the carbon conversion efficiency calculation. Furthermore, the carbon originating from

sodium 2-bromoethanesulfonate was less than  $3\%$  of the total carbon provided and, therefore, was not considered in the calculation of the carbon conversion efficiency. Carbon conversion efficiency was calculated by the following equation which followed the calculation from (Mohanakrishna et al. 2018):

$$\text{Carbon conversion efficiency} = \frac{\sum_i n_{(i,t+1)} - \sum_i n_{(i,t)}}{n_{(CD,t)} - n_{(CD,t+1)} + n_{(ME,t)} - n_{(ME,t+1)}} \times 100 \quad (1)$$

where  $n_i$  is the amount of product  $i$  at the sampling time  $t$  in moles,  $n_{CD}$  and  $n_{ME}$  are the amounts of the  $\text{CO}_2$  and methanol in moles after substrate addition at the sample time  $t$ , respectively, and  $t+1$  represents the following sampling time before the substrate addition. Two and four moles of carbons are obtained from one mole of acetate and butyrate, respectively. As  $\text{CO}_2$  could be left unused in both catholyte and/or in the gas phase,  $n_{(CD,t+1)}$  was subtracted as the lost carbon. The potential losses of VFAs were calculated by comparing the VFA concentrations from before and after the substrate(s) additions as well as the removed VFAs due to the sampling. Therefore, concentrations of the VFAs are reported in the main text, while amounts of VFAs in mmol are used for the carbon conversion efficiency and electron efficiency calculations. The amount of VFAs in mmol is separately reported in the supplementary information. The results in the text are given as the average value from duplicated reactors and with standard deviations.

Electron efficiency (EE) was calculated with Eq. 2, where  $f_{e,i}$  represent the molar conversion factor of product  $i$ . For the products, 8 electron equivalents were required for the formation of one mole of acetate, 20 electron equivalents for the formation of one mole of butyrate, and 2 electron equivalents for the formation of one mole of hydrogen gas. For the electron sources, the electrons from the electrode are derived by integrating the recorded current over time. The electrons from methanol are calculated as 6 electron equivalents per mole of methanol.  $F$  is Faraday constant ( $96,485\text{ C mol}^{-1}$  electron), and  $I$  is current (A).

$$EE = \frac{F \times (\sum_i n_{(i,t+1)} - \sum_i n_{(i,t)}) \times f_{e,i}}{\int Idt + F \times (n_{(ME,t)} - n_{(ME,t+1)}) \times f_{e,ME}} \times 100 \quad (2)$$

## Characterisation of the microbial culture

Samples of planktonic cells for the microbial community analysis were collected at the end of each batch of the enrichment and at the end of the co-substrate experiment. At the end of each batch,  $40\text{ mL}$  of the cathodic broth was collected and centrifuged ( $4000\text{ rpm}$ ,  $20\text{ min}$ ), and the resulting pellets were resuspended into  $1\text{ mL}$  PBS ( $0.1\text{ mol}$

$\text{L}^{-1}$ ) and stored at  $-80^{\circ}\text{C}$ . For the biofilm samples, ca. 15 g of graphite granules at the end of the co-substrate experiment were collected and gently washed three times with PBS to remove planktonic cells. The graphite granules were then soaked in 40 mL PBS and ultrasonicated for 3 min (USC 300 T, VWR, USA). The supernatant was collected, and the ultrasonication of the granules was repeated with fresh PBS. After three repetitions, all the collected supernatant was centrifuged, and the pellet was stored in 1 mL PBS at  $-80^{\circ}\text{C}$ . DNA was extracted by using the DNeasy kit PowerSoil Pro Kit (Qiagen, Germany) as per the manufacturer's instructions and quantified using a NanoDrop spectrophotometer (NanoDrop<sup>TM</sup> 1000, Thermo Fisher Scientific, USA).

The eubacterial 16S rRNA gene copies were quantified by quantitative polymerase chain reaction (qPCR) analysis of the cathodic biofilm and planktonic samples from the end of the co-substrate experiment. The amplification was conducted by Bio-Rad CFX96 (CFX96 Touch Real-Time PCR Detection System, Bio-Rad, USA). The qPCR conditions were 95 °C for 10 min, 34 cycles of 95 °C for 15 s, and 62 °C for 60 s. Primer pairs 338F/518R were used targeting the V3-V4 region of eubacterial 16S rRNA gene (Fierer et al. 2005). SYBR Green master mix (Maxima SYBR Green/ROX qPCR Master Mix, Thermo Fisher Scientific, USA) was used for all qPCR reactions. A volume of 25  $\mu\text{L}$  was prepared for the amplification, containing 0.5  $\mu\text{M}$  of each primer, diluted sample DNA, and RNase-free sterile water. A tenfold dilution series of the plasmid DNA standard (Rinta-Kanto et al. 2016) was used to plot a standard curve with concentrations ranging from  $3 \times 10^6$  to 3000 copies per reaction to the threshold cycle ( $\text{C}_t$ ).

Both the planktonic and biofilm samples were sequenced by the Illumina Novaseq 6000 platform at a depth of 100 K (Novogene, UK). The V3-V4 region of the 16S rRNA genes was PCR amplified with the primer pair 341F/806R (5'-3' sequence: CCTAYGGGRBGCASCAG/GGACTACNNNGG TATCTAAAT). The sequenced results were processed using the DADA2 pipeline with the qiime2 software 2021.4 (Bolyen et al. 2019). The taxonomic analysis was conducted by referring to the pre-trained classifier Greengenes 13\_8 99% OTUs full-length sequences (Bokulich et al. 2018).

The data obtained during this study was deposited at the European Nucleotide Archive under project accession number PRJEB61945. The abundant OTUs were used for Megablast to search within the NCBI nucleotide database to provide extended interpretation beyond the genus level. Subsequently, beta diversity metrics (weighted-Unifrac dissimilarity) and principal coordinate analysis (PCoA) were calculated using the q2-diversity plugin. Microbial communities were statistically compared using permutational analysis of variance (PERMANOVA) (Anderson 2008).

## Results

### Enrichment of microbial culture utilising methanol and $\text{CO}_2$

A mixed microbial culture was selectively enriched for butyrate production from methanol and  $\text{CO}_2$  in MES (Fig. 1, Fig. S2). The enrichment started with solely  $\text{CO}_2$  feeding for 4 days (30 min feeding for two times), which resulted in an immediate VFA production reaching acetate and butyrate concentrations (in this study, only n-butyrate was detected, hereinafter referred to as butyrate) of  $3.5 \pm 0.6 \text{ g L}^{-1}$  and  $0.36 \pm 0.05 \text{ g L}^{-1}$ , respectively (Fig. S3). From day 5 onwards, methanol was periodically added together with  $\text{CO}_2$ . Acetate was stabilised at a concentration of ca.  $1.8 \text{ g L}^{-1}$  throughout the first batch, while butyrate concentration continuously increased and reached the maximum titre of  $5.8 \pm 0.1 \text{ g L}^{-1}$  on day 22. Afterwards, a decrease in the butyrate concentration was observed, and  $4.4 \pm 0.1 \text{ g L}^{-1}$  of butyrate was obtained at the end of the first batch (Fig. S3). Similar VFA production pattern was observed during the following four batches. Namely, acetate was first produced until the concentration reached ca.  $1.8 \text{ g L}^{-1}$ , after which a sequential butyrate production was initiated. A maximum butyrate titre observed in the second batch was  $8.0 \pm 0.2 \text{ g L}^{-1}$ , and further increases in the maximum butyrate titres were achieved in the batches three to five, varying between  $9.8 \pm 0.4$  and  $10.6 \pm 0.1 \text{ g L}^{-1}$ . The average butyrate production rate in the last three batches was  $0.17 \pm 0.05 \text{ g L}^{-1} \text{ d}^{-1}$ . In addition to acetate and butyrate, a longer chain VFA, caproate, was also observed in all enrichment batches with the maximum titres ranging between 0.22 and  $0.50 \text{ g L}^{-1}$  (Table S3).

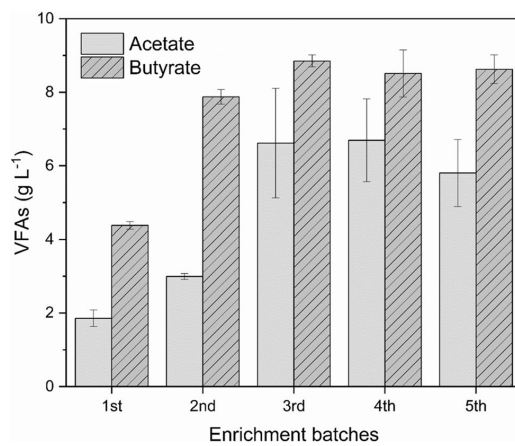


**Fig. 1** Production of VFAs at the end of each enrichment batch. Error bars indicate the standard deviations in duplicate reactors

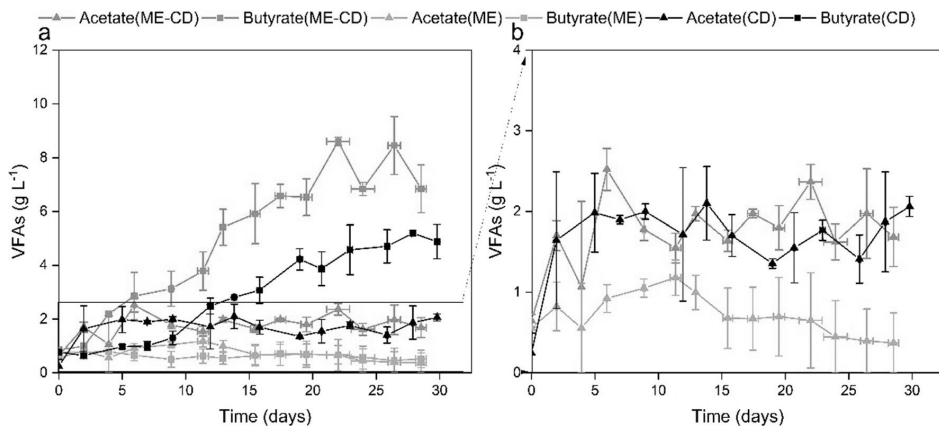


**Fig. 2** Concentrations of VFAs in the co-substrate addition experiments with **a** the overview of all detected VFAs (acetate and butyrate) and **b** the acetate production. ME-CD (fed with methanol and  $\text{CO}_2$ ); ME (fed with only methanol); CD (fed with only  $\text{CO}_2$ ). Error bars are the standard deviations in duplicate reactors

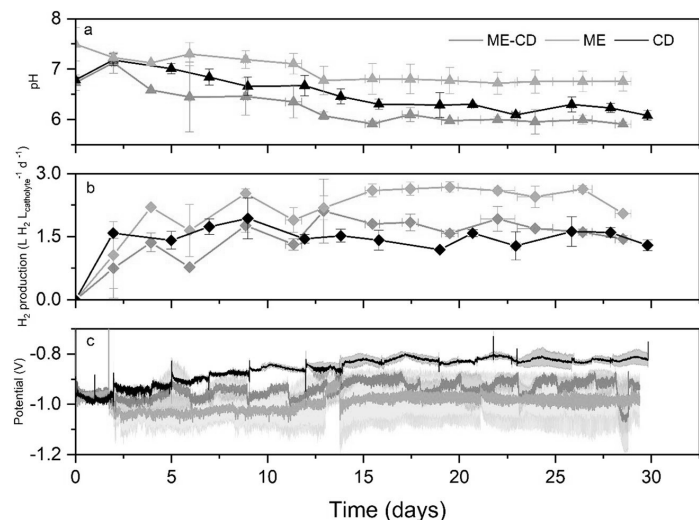
## MES performance with different substrate feedings

### VFA production

Acetate and butyrate were the observed VFAs in the co-substrate addition experiments (Fig. 2a, Fig. S4). MES fed with methanol and  $\text{CO}_2$  (ME-CD) resulted in a significant enhancement in butyrate production (ANOVA,  $p < 0.05$ , Table S4), outperforming the MES fed with methanol (ME) and  $\text{CO}_2$  (CD). In ME, a slight increase of acetate concentrations was observed from day 0 to day 9, with the

concentration increasing from  $0.56 \pm 0.02$  to  $1.05 \pm 0.11$  g L<sup>-1</sup>. However, the butyrate concentration dropped from  $0.77 \pm 0.15$  g L<sup>-1</sup> (day 0) to  $0.50 \pm 0.29$  g L<sup>-1</sup> (day 9). No VFA production was observed after day 12 although methanol was consumed (Fig. 4b). Methanol, as the sole substrate, was not utilised for the VFA production in MES, and thus, the results are not further included in the following discussion. When comparing ME-CD to CD, similar acetate production pattern was observed in both groups, where acetate production initiated immediately from the beginning of the run and reached the threshold concentration

**Fig. 3** Cathodic pH (a),  $\text{H}_2$  production rates (b), and cathodic potential (c) during the co-substrate addition experiments. ME-CD (fed with methanol and  $\text{CO}_2$ ); ME (fed with only methanol); CD (fed with only  $\text{CO}_2$ ). Error bars indicate the standard deviations in duplicate reactors



(ca.  $1.8 \text{ g L}^{-1}$ ) on day 2 (Fig. 2b). Acetate concentration then fluctuated between  $1.7$  and  $2.0 \text{ g L}^{-1}$  throughout the operation. The main difference between ME-CD and CD was in butyrate production. In CD, butyrate production initiated from day 2 and reached the maximum butyrate titre ( $5.2 \pm 0.1 \text{ g L}^{-1}$ ) on day 28 with the production rate of  $0.20 \pm 0.03 \text{ g L}^{-1} \text{ d}^{-1}$ . From day 2 onwards, VFA production in ME-CD was dominated by butyrate with a notable production rate of  $0.36 \pm 0.01 \text{ g L}^{-1} \text{ d}^{-1}$  until the maximum butyrate titre of  $8.6 \pm 0.2 \text{ g L}^{-1}$  was reached on day 22. A decrease in the VFA concentration in ME-CD was observed after day 22 due to the  $\text{CO}_2$  sparging (the concentration of VFAs decreased after sparging), which resulted in the final acetate and butyrate titres of  $1.7 \pm 0.4 \text{ g L}^{-1}$  and  $6.9 \pm 0.9 \text{ g L}^{-1}$ , respectively. However, no notable loss of VFAs was observed in CD. Overall, the addition of methanol as a co-substrate with  $\text{CO}_2$  boosted the maximum butyrate titre by 1.7-fold and the butyrate production rate by 1.8-fold.

#### $\text{H}_2$ production and pH

The role of methanol in MES was further revealed through the co-substrate addition experiment. Gradual decrease in pH was observed in both ME-CD and CD (Fig. 3a) due to the  $\text{CO}_2$  sparging and accumulation of VFAs, from which ME-CD resulted in the lowest pH values during the operation reaching value of 6.0 on day 14, after which it was manually maintained between 6.0 and 6.2 until the end of the operation. In CD, the pH also gradually decreased and ranged from 6.2 to 6.5, while in ME, no notable decrease of pH was observed (Fig. 3a). The cathodic potentials showed different profiles among the three experimental groups with the set current of  $-100 \text{ mA}$  (Fig. 3c). In the beginning of the experiments, similar cathodic potential (ca.  $-0.95 \text{ V}$ ) was recorded. The cathodic potential of CD gradually increased to between  $-0.8$  and  $-0.85 \text{ V}$ . However, lower cathodic potentials were recorded in ME-CD (between  $-0.90$  and  $-1.0 \text{ V}$ ) and ME (between  $-1.0$  and  $-1.1 \text{ V}$ ).  $\text{H}_2$  production was a crucial step in MES, which assisted the  $\text{CO}_2$  reduction. During the operation,  $\text{H}_2$  was continuously produced and accumulated in the cathodic headspace as well as the gas bags (Fig. 3b). CD resulted in the lowest  $\text{H}_2$  accumulation with an average rate of  $1.5 \pm 0.1 \text{ L H}_2 \text{ L}_{\text{catholyte}}^{-1} \text{ d}^{-1}$ , while  $\text{H}_2$  accumulated in ME-CD and ME at higher rates,  $1.6 \pm 0.1 \text{ L H}_2 \text{ L}_{\text{catholyte}}^{-1} \text{ d}^{-1}$  and  $2.1 \pm 0.3 \text{ L H}_2 \text{ L}_{\text{catholyte}}^{-1} \text{ d}^{-1}$ , respectively.

#### Carbon and electron conversion efficiencies

The total carbon that was consumed as the main carbon sources, i.e. methanol and  $\text{CO}_2$  ( $\text{CO}_2$  is referred to as total inorganic carbon (TIC) in this section), was compared to the total carbon present in the produced VFAs (Fig. 4).

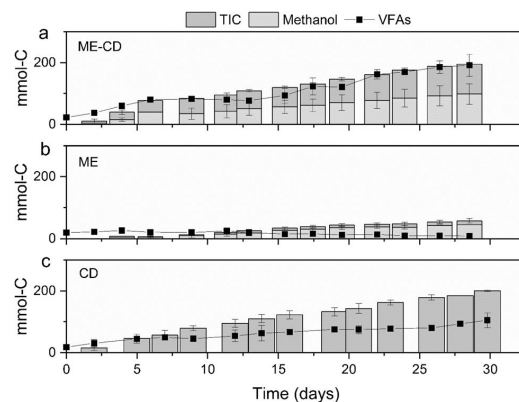


**Fig. 4** Substrate consumption and VFA production with different carbon sources. Figures a, b, and c represent the reactors fed with  $\text{CO}_2 +$  methanol (ME-CD), methanol (ME), and  $\text{CO}_2$  (CD), respectively. Error bars indicate the standard deviations in duplicate reactors

In CD, altogether  $200.7 \pm 2.1 \text{ mmol-C TIC}$  (equivalent to  $2.4 \pm 0.03 \text{ g-C}$ ) was utilised with the rate of  $0.08 \pm 0.002 \text{ g-C d}^{-1}$ , of which  $39.4 \pm 9.2\%$  of the carbon was recovered in VFAs. In ME-CD, a total of  $99.4 \pm 24.1 \text{ mmol-C TIC}$  (equivalent to  $1.2 \pm 0.3 \text{ g-C}$ ) as  $\text{CO}_2$  was utilised with the average rate of  $0.05 \pm 0.01 \text{ g-C d}^{-1}$ , while methanol was also utilised in the similar rate (ca.  $0.05 \text{ g-C d}^{-1}$ ) and resulted in the overall consumption of methanol as  $98.3 \pm 32.9 \text{ mmol-C}$  (equivalent to  $1.2 \pm 0.4 \text{ g-C}$ ). After compensating the losses of VFAs due to substrate addition and sampling,  $101.8 \pm 4.9\%$  of the carbon sources (TIC + methanol) in ME-CD were recovered in VFAs, of which  $86.3 \pm 4.4\%$  was recovered in butyrate. Although no accumulation of methanol and TIC was obtained at the end of the operation, methanol was observed to remain available between some of the two consecutive feeding timepoints (e.g. days 5 to 7 in ME-CD1, Table S5 and S6) while TIC was always completely depleted.

In ME, methanol was consumed at a rate of  $0.018 \pm 0.0009 \text{ g-C d}^{-1}$ , which resulted in a  $42.5 \pm 2.3 \text{ mmol-C}$  consumption until day 29 (Fig. 4b). As smaller methanol consumption was observed in the abiotic experiment ( $0.005 \text{ g-C d}^{-1}$  during 7 days, Table S7), the methanol consumption in ME was likely related to the microbial activity, as the biofilm growth was observed by qPCR (Fig. S5). In addition, trace amounts of TIC were observed in ME, with an overall consumption of  $12.7 \pm 7.4 \text{ mmol-C}$  (equivalent to  $0.15 \pm 0.09 \text{ g-C}$ ) (Table S5). Although methanol was the sole added carbon source in ME, the TIC present in the catholyte could originate from the oxidation of the VFAs (originating from the inoculum) or methanol oxidation to support the microbial growth in ME (Fig. S5).

The distributions of electrons and carbon in the electron sources (methanol and electrode) and in the products (acetate, butyrate, and H<sub>2</sub>) were plotted to have an insight on the electron flow and the role of methanol, respectively, in the co-substrate addition experiment (Fig. 5). Thus, the overall efficiency of the process can be assessed. The overall electron efficiency for ME, CD, and ME-CD were 61.5 ± 6.4%, 65.4 ± 5.4%, and 76.9 ± 0.6%, respectively. The majority of the electrons were recovered in H<sub>2</sub> in all three experimental groups. Overall, 62.5 ± 4.9%, 49.0 ± 3.0%, and 46.2 ± 5.0% of the electrons were recovered in H<sub>2</sub> in ME, CD, and ME-CD, respectively. Butyrate production contributed to 14.8 ± 3.3% and 26.8 ± 4.0% of the electron recovery in CD and ME-CD, respectively.

### Cathodic microbial cultures

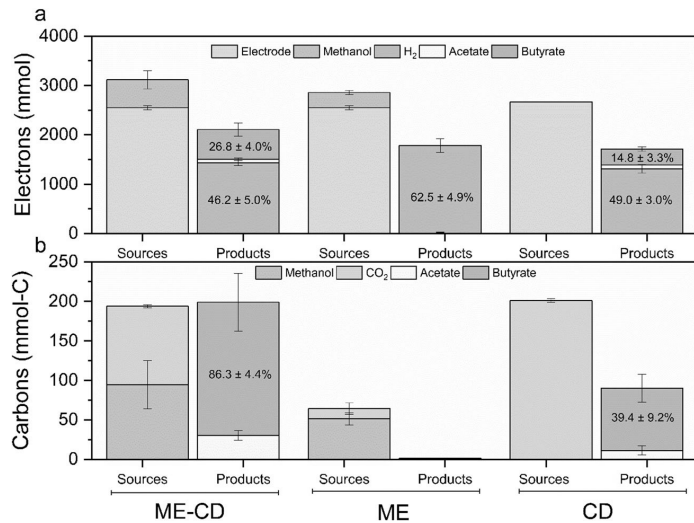
Planktonic cells and biofilms were analysed to gain knowledge of the microbial communities in MES. The microbial culture during the enrichment was adapted in five batches. *Eubacterium* was always the most dominant genus and its relative abundance increased from 42.2 ± 1.0% (first batch) to 55.0 ± 4.5% (fifth batch), while for the second most enriched genus, i.e. *Bacteroides*, the relative abundance decreased from 26.5 ± 1.5% (first batch) to 12.6 ± 4.0% (fifth batch).

In the co-substrate experiments, higher microbial growth was observed in CD compared to ME-CD and ME (Fig. S5). A total of 942 OTUs were observed. Relative abundances of the ten most abundant genera are shown in the heatmap (Fig. 6). The most enriched genus was *Eubacterium*. *Eubacterium* was predominantly enriched in the VFA-producing

cultures with the relative abundance of 50.6 ± 2.5% (CD) and 52.6 ± 2.5% (ME-CD) and was less present in the ME with the relative abundance of 30.5 ± 13.0%. In CD, the relative abundance of *Eubacterium* between biofilm and planktonic cells remained similar (50.4 ± 1.4% and 50.8 ± 3.3%, respectively). However, in the methanol-fed cultures (ME and ME-CD), *Eubacterium* was more enriched in the biofilm (ME-CD: 63.5 ± 6.7% and ME: 35.5 ± 16.4%) than in the planktonic cells (ME-CD: 42.1 ± 9.6% and ME: 25.5 ± 4.1%), respectively. Generally, smaller variations in the parallel microbial culture compositions were observed in the biofilm cells in ME-CD and CD. The presence of the biofilm on the graphite granules from all experimental groups was confirmed with SEM (Fig. S6). Genus *Bacteroides* was also present in all experimental groups with a relative abundance of 20.5 ± 4.4% (ME-CD), 24.1 ± 4.4% (CD), and 14.2 ± 2.9% (ME). Unlike *Eubacterium*, the relative abundance of *Bacteroides* between biofilm and planktonic cells remained similar in ME, but showed differences in the CO<sub>2</sub>-fed cultures (ME-CD and CD) where *Bacteroides* was more enriched in the planktonic cells (ME-CD: 30.6 ± 9.4% and CD: 27.2 ± 4.4%) than the biofilm (ME-CD: 10.5 ± 3.9% and CD: 21.1 ± 1.1%).

There was no statistical difference in terms of the richness and evenness among the three experimental groups. However, microbial communities that were plotted in PCoA indicated that ME was distinct from CD and ME-CD (Fig. S7) and the difference was further validated by the PERMANOVA ( $p < 0.05$ ). ME-CD and CD were identified to have similar microbial communities, in which *Eubacterium* and *Bacteroides* are well-known microorganisms for VFA production. The most dominant OTU was further

**Fig. 5** Electrons (a) and carbons (b) present in the inputs and in the products. Green blocks represent the electrons/carbon provided by overall consumption of methanol, grey blocks the carbon provided by consumed CO<sub>2</sub>, and orange blocks the electrons provided by electrode. ME-CD (fed with methanol and CO<sub>2</sub>); ME (fed with only methanol); CD (fed with only CO<sub>2</sub>). The percentages of carbon or electron recovery in H<sub>2</sub> or butyrate are shown the figures. The electron recoveries (a) in acetate were 3.8 ± 0.5% (ME-CD) and 1.7 ± 0.9% (CD). The carbon recoveries (b) in acetate were 15.5 ± 0.5% (ME-CD) and 5.5 ± 2.8% (CD). Error bars indicate the standard deviations in duplicate reactors



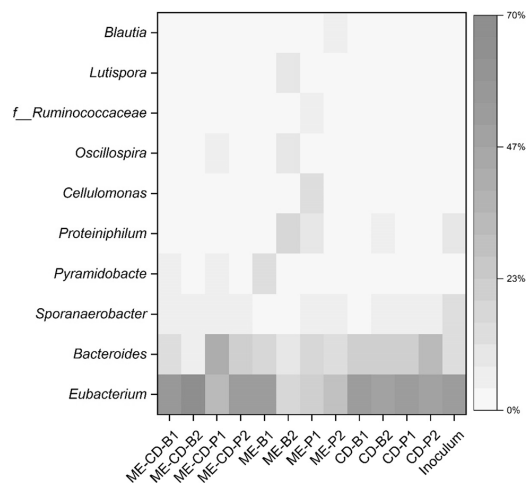


**Fig. 6** Heat map and the relative abundance of the ten most dominant genera fed with  $\text{CO}_2$  (CD), methanol (ME), and  $\text{CO}_2 + \text{methanol}$  (ME-CD) in the co-substrate experiment (B, biofilms; P, planktonic cells, 1 and 2 represent the microbial culture from each duplicate). *f\_Ruminococcaceae* is an unknown genus belonging in the family *Ruminococcaceae*. Inoculum represent the average of five enrichment batches (samples were taken from the planktonic cells at the end of each enrichment culture, error bars are not shown in the heatmap)

queried by the NCBI megablast in the 16S rRNA sequences database, and the results revealed a high similarity to *Eubacterium limosum* (100% similarity, 100% query cover) and *Eubacterium callanderi* (100% similarity, 100% query cover) (Table S8).

## Discussion

### Role of methanol as a co-substrate in MES

Adding methanol enhanced the butyrate production in MES, increasing the butyrate production rate by 1.7-fold (production rate of  $0.3 \pm 0.01 \text{ g L}^{-1}\text{d}^{-1}$ ) and maximum titres by 1.8-fold ( $8.6 \pm 0.2 \text{ g L}^{-1}$ ), while the acetate titres remained similar compared with only  $\text{CO}_2$  feeding. The overall carbon conversion efficiency for the VFA production was also enhanced to  $101.8 \pm 4.9\%$  with methanol addition (compared to  $39.4 \pm 9.2\%$  with  $\text{CO}_2$  feeding) of which methanol and  $\text{CO}_2$  contributed equally, ca. 50% of carbon (Fig. 5b). The high carbon conversion efficiency (over 100%) could be explained by the following aspects: The amount of carbon from yeast extract cannot be quantified due to its unknown chemical composition which could serve as extra carbon source. Moreover, the migration of methanol and VFAs to

the anode cannot be quantified accurately as the anode was an open system, and the evaporation of methanol and VFAs could introduce experimental errors.

For those acetogens which can utilise methanol as the carbon and energy source, it is commonly recognised that part of the methanol is utilised to reverse the WLP to provide reducing equivalents for the reduction of  $\text{CO}_2$  (Kremp and Müller 2021). The overall stoichiometric equation for methanol utilisation is shown in Eq. 3. First, every one out of four moles of methanol is completely oxidised to  $\text{CO}_2$  to provide six moles of electrons, which are utilised for the reduction of three moles of  $\text{CO}_2$  to CO. The three moles of CO are coupled with the three moles of remaining methanol and produce acetyl-CoA in WLP (Kremp and Müller 2021), which can be converted to acetate through phosphorylation resulting in ATP generation (May et al. 2016). For *E. limosum*, butyrate production has also been reported from methanol and  $\text{CO}_2$ . Another mole of methanol needs to be oxidised to provide extra reducing equivalents to convert three moles of acetyl-CoA to butyryl-CoA via the reverse  $\beta$ -oxidation. The CoA of butyryl-CoA is transferred to an acetate via the butyryl-CoA:acetate CoA transferase for the synthesis of butyrate (Kremp and Müller 2021) with reaction shown in Eq. 4.



Methanol has been reported to improve the  $\text{H}_2/\text{CO}_2$  utilisation in *Eubacterium limosum*, resulting in a higher growth rate and  $\text{H}_2$  consumption rate (Kim et al. 2021). In addition, the energy efficiency for the bioproduction of acetate from methanol under anaerobic conditions is higher compared to the gaseous substrates, e.g.  $\text{H}_2$  (Claassens et al. 2019). When utilising methanol as a substrate, more electrons are directed to products for the generation of sufficient cellular energy in the form of ATP (Claassens et al. 2019) and result in higher product yields, which is in accordance with the higher carbon efficiency achieved in ME-CD than CD in this study.

Methanol metabolism in MES could involve both methanol oxidation (releasing six electrons) and/or transfer of the electrons to acetyl-CoA without extracellular electron transfer as discussed above. In order to investigate whether methanol was used as the electron donor in ME-CD, the electron recovery was first calculated considering electrode as the sole electron source. The electron recoveries in butyrate, acetate, and  $\text{H}_2$  were  $93.8 \pm 4.6\%$ ,  $65.4 \pm 5.4\%$ , and  $68.8 \pm 5.9\%$  for ME-CD, CD, and ME, respectively. Specifically for ME-CD, at a maximum  $133.1 \pm 1.0\%$  electron recovery was observed between two consecutive substrate-feeding timepoints (days 15 to 17), which implied the potential role of methanol as another electron source in ME-CD

(Fig. S8). If the electrons provided by methanol are also considered, the electron recoveries decrease to  $76.9 \pm 0.6\%$  in ME-CD and  $61.5 \pm 6.4\%$  in ME. Methanol oxidation in acetogens can be a series of reversed WLP reactions (from methanol to  $\text{CO}_2$ ) (Kremp and Müller 2021). In this study,  $\text{CO}_2$  and reducing equivalents (e.g.  $\text{H}_2$ ) were both supplied. Thus, the methanol oxidation in MES was likely regulated by the availability of the reducing equivalents (such as the  $\text{H}_2$  partial pressure) and  $\text{CO}_2$  (Pacaud et al. 1985), as well as the characteristics of the microorganism (such as the intracellular NADH/NAD<sup>+</sup> pool) (Jeong et al. 2015). In this research, the role of methanol can be concluded as both the carbon and electron donor. However, the metabolism of methanol in MES could be affected by several factors and needs to be further investigated.

### Butyrate production in MES

Butyrate is a value-added product (market price of ca. 1500 USD/ton), with diverse applications, for example, in food and pharmaceutical industries. The current butyrate synthesis is mainly via chemical synthesis which requires the use of crude oil. In addition, butyrate can be synthesised via fermentation from sugars (Dwidar et al. 2012). In this work, the production of butyrate from methanol and  $\text{CO}_2$  is considered beneficial as methanol is a bulk chemical with the market price of ca. 300 USD/ton and it can be synthesised from renewable sources or utilised from industrial side streams.

Butyrate production in MES is often accompanied with the consumption of acetate. In this study, an acetate threshold concentration (ca.  $1.8 \text{ g L}^{-1}$ ) was necessary to promote butyrate production, which has also been reported with a slightly higher acetate threshold concentration ( $2.0$  to  $4.0 \text{ g L}^{-1}$ ) (Jourdin et al. 2019). The acetate threshold concentration was observed in both ME-CD and CD and is likely determined by the enriched microbial communities (*E. limosum* dominating mixed culture), as the certain amount of acetate is suggested to be needed for the butyrate production with *E. limosum* (Kremp and Müller 2021).

The first reported butyrate production in MES was rather low, with the maximum butyrate concentration of  $0.44 \text{ g L}^{-1}$  and a production rate of  $0.04 \text{ g L}^{-1} \text{ d}^{-1}$  (Ganigué et al. 2015). The maximum butyrate titre and production rate were further increased to  $1.9 \text{ g L}^{-1}$  and  $0.16 \text{ g L}^{-1} \text{ d}^{-1}$ , respectively, by adjusting the feeding strategy of  $\text{CO}_2$  to maintain a high  $\text{H}_2$  partial pressure (Batlle-Vilanova et al. 2017). In addition, through the continuous feeding of  $\text{CO}_2$ , butyrate production was reinforced and resulted in the butyrate production rate of  $3.2 \pm 0.1 \text{ g L}^{-1} \text{ d}^{-1}$  and butyrate titre of  $9.3 \text{ g L}^{-1}$  (Jourdin et al. 2019). In addition to  $\text{CO}_2$  as the sole carbon source, butyrate production in MES has been enhanced by adding other electron donors, such as formate, ethanol, or

lactate (Izadi et al. 2021b; Li et al. 2022; Zhang et al. 2023). Formate addition increased the maximum butyrate titre in MES by 3.8-fold (to  $0.14 \pm 0.02 \text{ g L}^{-1}$ ), while ethanol addition increased the product diversity (i.e. the production of butanol and hexanol) but not the butyrate production rates and titres (Izadi et al. 2021b). Concurrent addition of lactate and ethanol ( $5 \text{ g L}^{-1}$  each) resulted in a high butyrate production rate ( $0.9 \text{ g L}^{-1} \text{ d}^{-1}$ ) and a maximum butyrate titre of  $6.3 \text{ g L}^{-1}$  (Zhang et al. 2023). In this study, methanol addition resulted in a selective production of butyrate in MES with the maximum titre of  $8.6 \pm 0.2 \text{ g L}^{-1}$  (one of the highest values reported in MES), and production rate of  $0.36 \pm 0.01 \text{ g L}^{-1} \text{ d}^{-1}$ , which likely remained rather low due to the insufficient carbon source (further discussed in the next section).

### Limiting factors of MES fed with methanol

Although both  $\text{CO}_2$  (TIC) and methanol in the liquid phase were completely consumed by the end of the experiments in ME-CD (total consumption of both substrates was ca. 99 mmol-C), there was occasionally accumulation of methanol between the substrate feedings. In this study,  $\text{CO}_2$  was fed in semi-batch mode (ca. 6 L  $\text{CO}_2$  was purged through the medium each time). Most of the  $\text{CO}_2$  was sparged through the system, and only ca. 5% of the  $\text{CO}_2$  remained in the liquid phase as the carbon source (Table S5). TIC, as the main electron acceptor in catholyte, was completely consumed between each substrate feeding, while the electron donors (methanol and  $\text{H}_2$ ) remained available indicating that  $\text{CO}_2$  was the limiting substrate in ME-CD, CD, and ME. Continuous feeding of  $\text{CO}_2$  would provide sufficient carbon source/electron acceptor in MES, and it has been reported as an efficient strategy to increase the production rate of both acetate and the longer chain fatty acids, such as butyrate and caproate, in MES (Batlle-Vilanova et al. 2016; Jourdin et al. 2019; Izadi et al. 2021a). In this study, however, the optimisation of  $\text{CO}_2$  utilisation was not the main aim and should be improved in future studies.

The VFA production was also affected by the pH, which, in this study, had the most direct influence on the dissolution of TIC. The lower pH in ME-CD (pH 6.0 to 6.2) than in CD (pH 6.2 to 6.4) resulted in lower TIC values in ME-CD after  $\text{CO}_2$  sparging (ca.  $4.3 \text{ mM-C}$  in ME-CD vs. ca.  $7.5 \text{ mM-C}$  in CD) and subsequently limited the VFA production from  $\text{CO}_2$  in ME-CD as discussed earlier. The slightly acidic pH (5.8) has been reported to increase the acetate production rate with a mixed microbial culture (Batlle-Vilanova et al. 2016). However, the optimal pH for the growth of *E. limosum* is close to neutral, and thus, slightly acidic conditions may limit the growth of *E. limosum* (Pacaud et al. 1985), which could explain the lower microbial growth in ME-CD compared to CD (Fig. S5). On the other hand, microbial chain elongation

is also affected by pH. For example, in methanol-based chain elongation, the reactor pH facilitated the changes in product selectivity, where pH 6.75 resulted in n-butyrate production while i-butyrate production was favoured at pH 5.25 (De Leeuw et al. 2020). In this study, the pH was maintained at above 6 to avoid the potential toxicity due to the VFA accumulation, while under a more acidic pH, the product spectrum could likely be expanded (e.g. i-butyrate production). However, if the pH is elevated, the dissolution of TIC will be higher which also affects the VFA production (Pacaud et al. 1985). Thus, both the CO<sub>2</sub> feeding and pH should be optimised to enhance the production rates and titres and to alter the product spectrum in MES fed with methanol.

### **Microbial culture for butyrate production in MES**

Butyrate was the main product in both ME-CD and CD, which is attributed to the microbiome with *Eubacterium* as the dominant genus. Especially, the enrichment of *Eubacterium* in the biofilm samples (relative abundance in biofilm was 63.5 ± 6.7% in ME-CD and 50.4 ± 1.4% in CD) suggests that the biofilm played a more important role than planktonic cells in the production of VFAs. *E. limosum* and *E. callanderi* are the two species that shared the highest similarity compared to the most abundant OTUs in this study. *E. limosum* is a well-known acetogen that grows on methanol and/or CO<sub>2</sub> with acetate and butyrate as the main metabolites (Pacaud et al. 1986). *E. callanderi* was originally reported unable to utilise one-carbon compounds (e.g. methanol and CO<sub>2</sub>) (Mountfort et al. 1988). However, the *E. callanderi* KIST612 strain, formerly known as *E. limosum* KIST612, is reported to utilise methanol as well as other C1 compounds (Dietrich et al. 2021).

The inoculum for the experiments was cultivated with methanol and CO<sub>2</sub> over a period of one year before the co-substrate experiments. When comparing the inoculum used in the co-substrate experiments after the enrichment period to the original culture fed with only CO<sub>2</sub>, the relative abundance of *E. limosum* increased from 11.2% (Vassilev et al. 2024) to 52.2%, likely due to the methanol addition. In this study, feeding with only CO<sub>2</sub> resulted in similar microbial culture with the similar *E. limosum* relative abundances than reactors fed with both CO<sub>2</sub> and methanol, which is likely due to the fact that the inoculum was fed with methanol and CO<sub>2</sub> for a long time period. However, when methanol accumulated in the cathode in the reactors fed with methanol only, the high concentration of methanol likely hindered the growth of *E. limosum* as the relative abundances decreased compared to ME-CD and CD reactors.

For *E. limosum*, it is reported that the butyrate production is dependent on the carbon and energy sources (Litty and Müller 2021). Feeding with H<sub>2</sub> and CO<sub>2</sub> only in

batch bottles resulted in the production of acetate, while butyrate production was achieved with methanol and CO<sub>2</sub> feeding. However, acetate has usually been the main product with acetate: butyrate ratio of 1:0.33 growing with C1 feedstocks and their mixtures reported with *E. limosum* (Litty and Müller 2021). In this study, the product spectrum was dominated by butyrate, which could be due to the dual role of the supplied current, which not only provides electrons for the bacterial metabolism, but may also affect the extracellular oxidation-reduction potential and thus, may alter the product spectrum (Liu et al. 2013). Short batch bottle experiments done in this study (described in supplementary information and fed with methanol and CO<sub>2</sub>, without electricity) indicated that acetate would be the main product, reaching 1.7 ± 0.02 g L<sup>-1</sup> on day 6 accompanied with butyrate production (0.59 ± 0.01 g L<sup>-1</sup>) (Fig. S9). From days 6 to 8, methanol addition led to the microbial growth (OD<sub>600</sub> increased from 0.62 ± 0.08 to 0.97 ± 0.05), while acetate concentration remained at 1.7 ± 0.3 g L<sup>-1</sup> and butyrate concentration slightly increased to 0.66 ± 0.10 g L<sup>-1</sup>.

*Eubacterium* dominating cultures are widely reported in methanol-based chain elongation reactors, where it is suggested to be the responsible genus for butyrate production from acetate and methanol (Chen et al. 2016, 2020; De Leeuw et al. 2020). However, in MES *Eubacterium*-dominating cultures are rarely reported (Blasco-Gómez et al. 2019; Zhao et al. 2023). This study showed for the first time the potential of *Eubacterium* as the core microorganism in MES, which would result in the production of mainly butyrate from only CO<sub>2</sub> or a mixture of CO<sub>2</sub> and methanol.

In conclusion, methanol was employed for the first time as a co-substrate with CO<sub>2</sub> in MES resulting in an increase of butyrate production rates by 1.7-fold (up to 0.36 ± 0.01 g L<sup>-1</sup> d<sup>-1</sup>) and titres by 1.8-fold (up to 8.6 ± 0.2 g L<sup>-1</sup>) compared to CO<sub>2</sub> as the sole substrate. Methanol acted both as carbon and electron source for VFA production. *Eubacterium* was the dominant genus, known to produce butyrate from CO<sub>2</sub> as well as from CO<sub>2</sub> and methanol. Overall, this study introduces a promising strategy to enhance the bioproduction of butyrate.

**Supplementary information** The online version contains supplementary material available at <https://doi.org/10.1007/s00253-024-13218-y>.

**Acknowledgements** Tampere Microscopy Centre facilities at Tampere University is gratefully acknowledged for supporting with the SEM imaging. Antti Nuottajärvi and Mika Karttunen are also acknowledged for the support in the laboratory.

**Author contribution** HY, IV, and MK conceived and designed research. HY conducted experiments. HY and JR analysed data. HY wrote the first version of the manuscript, and all authors commented on the

manuscript and reviewed it. All authors read and approved the final manuscript.

**Funding** Open access funding provided by Tampere University (including Tampere University Hospital).

**Data availability** The datasets generated during and/or analysed during the current study are available from the corresponding author on reasonable request. The sequence data generated during the current study is available in the European Nucleotide Archive under project accession number PRJEB61945.

**Declarations** This study was funded by the Research Council of Finland (grant number 329227). Furthermore, the Research Council of Finland (Bio and Circular Economy Research Infrastructure (decision no. 353658)) is gratefully acknowledged. Authors declare that they have no competing interests that are relevant to the content of this article. This article does not contain any studies with human participants or animals performed by any of the authors.

**Open Access** This article is licensed under a Creative Commons Attribution 4.0 International License, which permits use, sharing, adaptation, distribution and reproduction in any medium or format, as long as you give appropriate credit to the original author(s) and the source, provide a link to the Creative Commons licence, and indicate if changes were made. The images or other third party material in this article are included in the article's Creative Commons licence, unless indicated otherwise in a credit line to the material. If material is not included in the article's Creative Commons licence and your intended use is not permitted by statutory regulation or exceeds the permitted use, you will need to obtain permission directly from the copyright holder. To view a copy of this licence, visit <http://creativecommons.org/licenses/by/4.0/>.

## References

- Anderson MJ (2008) A new method for non-parametric multivariate analysis of variance. *Austral Ecol* 26:32–46. <https://doi.org/10.1111/j.1442-9993.2001.01070.pp.x>
- Aresta M, Dibenedetto A (2007) Utilisation of CO<sub>2</sub> as a chemical feedstock: opportunities and challenges. *Dalton Trans* 2975–2992. <https://doi.org/10.1039/B700658F>
- Aro E-M (2016) From first generation biofuels to advanced solar biofuels. *Ambio* 45:24–31. <https://doi.org/10.1007/s13280-015-0730-0>
- Bache R, Pfennig N (1981) Selective isolation of *Acetobacterium woodii* on methoxylated aromatic acids and determination of growth yields. *Arch Microbiol* 130:255–261. <https://doi.org/10.1007/BF00459530>
- Balch WE, Schobert S, Tanner RS, Wolfe RS (1977) *Acetobacterium*, a new genus of hydrogen-oxidizing, carbon dioxide-reducing, anaerobic bacteria. *Int J Syst Bacteriol* 27:355–361. <https://doi.org/10.1099/00207713-27-4-355>
- Batlle-Vilanova P, Puig S, Gonzalez-Olmos R, Balaguer MD, Colprim J (2016) Continuous acetate production through microbial electrosynthesis from CO<sub>2</sub> with microbial mixed culture. *J Chem Technol Biotechnol* 91:921–927. <https://doi.org/10.1002/jctb.4657>
- Batlle-Vilanova P, Ganigué R, Ramió-Pujol S, Bañeras L, Jiménez G, Hidalgo M, Balaguer MD, Colprim J, Puig S (2017) Microbial electrosynthesis of butyrate from carbon dioxide: production and extraction. *Bioelectrochem* 117:57–64. <https://doi.org/10.1016/j.bioelechem.2017.06.004>
- Blasco-Gómez R, Ramió-Pujol S, Bañeras L, Colprim J, Balaguer MD, Puig S (2019) Unravelling the factors that influence the bio-electrocycling of carbon dioxide towards biofuels. *Green Chem* 21:684–691. <https://doi.org/10.1039/C8GC03417F>
- Bokulich NA, Kaehler BD, Rideout JR, Dillon M, Bolyen E, Knight R, Huttley GA (2018) Optimizing taxonomic classification of marker-gene amplicon sequences with QIIME 2's q2-feature-classifier plugin. *Microbiome* 6:90. <https://doi.org/10.1186/s40168-018-0470-z>
- Bolyen E, Rideout JR, Dillon MR, Bokulich NA, Abnet CC, Al-Ghalith GA, Alexander H, Alm EJ, Arumugam M, Asnicar F, Bai Y, Bisanz JE, Bittinger K, Brejnrod A, Brislawn CJ, Brown CT, Calahan BJ, Caraballo-Rodríguez AM, Chase J, Cope EK, Da Silva R, Diener C, Dorrestein PC, Douglas GM, Durall DM, Duvall C, Edwards CF, Ernst M, Estaki M, Fouquier J, Gauglitz JM, Gibbons SM, Gibson DL, Gonzalez A, Gorlick K, Guo J, Hillmann B, Holmes S, Holste H, Huttenhower C, Huttley GA, Janssen S, Jarmusch AK, Jiang L, Kaehler BD, Kang KB, Keefe CR, Keim P, Kelley ST, Knights D, Koester I, Koscielak T, Kreps J, Langille MGI, Lee J, Ley R, Liu Y-X, Loftfield E, Lozupone C, Maher M, Marotz C, Martin BD, McDonald D, McEvoy LJ, Melnik AV, Metcalf JL, Morgan SC, Morton JT, Naimey AT, Navas-Molina JA, Nothias LF, Orchaniuk SB, Pearson T, Peoples SL, Petras D, Preuss ML, Pruesse E, Rasmussen LB, Rivers A, Robeson MS, Rosenthal P, Segata N, Shaffer M, Shiffer A, Sinha R, Song SJ, Spear JR, Swafford AD, Thompson LR, Torres PJ, Trinh P, Tripathi A, Turnbaugh PJ, Ul-Hasan S, van der Hooft JJ, Vargas F, Vázquez-Baeza Y, Vogtmann E, von Hippel M, Walters W, Wan Y, Wang M, Warren J, Weber KC, Williamson CHD, Willis AD, Xu ZZ, Zaneveld JR, Zhang Y, Zhu Q, Knight R, Caporaso JG (2019) Reproducible, interactive, scalable and extensible microbiome data science using QIIME 2. *Nat Biotechnol* 37:852–857. <https://doi.org/10.1038/s41587-019-0209-9>
- Chen WS, Ye Y, Steinbusch KJJ, Strik DPBTB, Buisman CJN (2016) Methanol as an alternative electron donor in chain elongation for butyrate and caproate formation. *Biomass Bioenergy* 93:201–208. <https://doi.org/10.1016/j.biombioe.2016.07.008>
- Chen WS, Huang S, Strik DPBTB, Buisman CJN (2017) Isobutyrate biosynthesis via methanol chain elongation: converting organic wastes to platform chemicals. *J Chem Technol Biotechnol* 92:1370–1379. <https://doi.org/10.1002/jctb.5132>
- Chen WS, Huang S, Plugge CM, Buisman CJN, Strik DPBTB (2020) Concurrent use of methanol and ethanol for chain-elongating short chain fatty acids into caproate and isobutyrate. *J Environ Manage* 258:110008. <https://doi.org/10.1016/j.jenvman.2019.110008>
- Claassens NJ, Cotton CAR, Kopljar D, Bar-Even A (2019) Making quantitative sense of electromicrobial production. *Nat Catal* 2:437–447. <https://doi.org/10.1038/s41929-019-0272-0>
- De Leeuw KD, De Smit SM, Van Oossanen S, Moerland MJ, Buisman CJN, Strik DPBTB (2020) Methanol-based chain elongation with acetate to n-butyrate and isobutyrate at varying selectivities dependent on pH. *ACS Sustain Chem Eng* 8:8184–8194. <https://doi.org/10.1021/acssuschemeng.0c00907>
- De Smit SM, De Leeuw KD, Buisman CJN, Strik DPBTB (2019) Continuous n-valerate formation from propionate and methanol in an anaerobic chain elongation open-culture bioreactor. *Biotechnol Biofuels* 12:1–16. <https://doi.org/10.1186/s13068-019-1468-x>
- Diender M, Stams AJM, Sousa DZ (2015) Pathways and bioenergetics of anaerobic carbon monoxide fermentation. *Front Microbiol* 6:1–18. <https://doi.org/10.3389/fmicb.2015.01275>
- Dietrich HM, Kremp F, Öppinger C, Ribaric L, Müller V (2021) Biochemistry of methanol-dependent acetogenesis in *Eubacterium callanderi* KIST612. *Environ Microbiol* 23:4505–4517. <https://doi.org/10.1111/1462-2920.15643>
- Dwidar M, Park J-Y, Mitchell RJ, Sang B-I (2012) The future of butyric acid in industry. *Sci World J* 2012:e471417. <https://doi.org/10.1100/2012/471417>

- Eregowda T, Kokko ME, Rene ER, Rintala J, Lens PNL (2021) Volatile fatty acid production from Kraft mill foul condensate in upflow anaerobic sludge blanket reactors. Environ Technol 42:2447–2460. <https://doi.org/10.1080/09593330.2019.1703823>
- Fierer N, Jackson JA, Vilgalys R, Jackson RB (2005) Assessment of soil microbial community structure by use of taxon-specific quantitative PCR assays. Appl Environ Microbiol 71:4117–4120. <https://doi.org/10.1128/AEM.71.7.4117-4120.2005>
- Ganigüé R, Puig S, Batlle-Vilanova P, Balaguer MD, Colprim J (2015) Microbial electrosynthesis of butyrate from carbon dioxide. Chem Commun 51:3235–3238. <https://doi.org/10.1039/c4cc10121a>
- GINIGE MP, Bowyer JC, Foley L, Keller J, Yuan Z (2009) A comparative study of methanol as a supplementary carbon source for enhancing denitrification in primary and secondary anoxic zones. Biodegradation 20:221–234. <https://doi.org/10.1007/s10532-008-9215-1>
- Hobson C, Márquez C (2018) Renewable methanol report. Methanol Institute, Singapore <https://www.methanol.org/wp-content/uploads/2019/01/MethanolReport.pdf>. Accessed 24 May 2024
- Iaquaniello G, Centi G, Salladini A, Palo E, Perathoner S, Spadaccini L (2017) Waste-to-methanol: process and economics assessment. Bioresour Technol 243:611–619. <https://doi.org/10.1016/j.biortech.2017.06.172>
- Izadi P, Fontmorin JM, Lim SS, Head IM, Eileen HY (2021a) Enhanced bio-production from CO<sub>2</sub> by microbial electrosynthesis (MES) with continuous operational mode. Faraday Discuss 230:344–359. <https://doi.org/10.1039/D0FD00132E>
- Izadi P, Fontmorin JM, Virdis B, Head IM, Yu EH (2021b) The effect of the polarised cathode, formate and ethanol on chain elongation of acetate in microbial electrosynthesis. Appl Energy 283:116310. <https://doi.org/10.1016/j.apenergy.2020.116310>
- Jeong J, Bertsch J, Hess V, Choi S, Choi I-G, Chang IS, Müller V (2015) Energy conservation model based on genomic and experimental analyses of a carbon monoxide-utilizing, butyrate-forming acetogen, *Eubacterium limosum* KIST612. Appl Environ Microbiol 81:4782–4790. <https://doi.org/10.1128/AEM.00675-15>
- Jourdin L, Winkelhorst M, Rawls B, Busman CJN, Strik DPBTB (2019) Enhanced selectivity to butyrate and caproate above acetate in continuous bioelectrochemical chain elongation from CO<sub>2</sub>: steering with CO<sub>2</sub> loading rate and hydraulic retention time. Bioresour Technol Reports 7:100284. <https://doi.org/10.1016/j.biortech.2019.100284>
- Kallscheuer N, Polen T, Bott M, Marienhagen J (2017) Reversal of β-oxidative pathways for the microbial production of chemicals and polymer building blocks. Metab Eng 42:33–42. <https://doi.org/10.1016/j.ymben.2017.05.004>
- Kim J-Y, Park S, Jeong J, Lee M, Kang B, Jang SH, Jeon J, Jang N, Oh S, Park Z-Y, Chang IS (2021) Methanol supply speeds up synthesis gas fermentation by methylotrophic-acetogenic bacterium, *Eubacterium limosum* KIST612. Bioresour Technol 321:124521. <https://doi.org/10.1016/j.biortech.2020.124521>
- Kremp F, Müller V (2021) Methanol and methyl group conversion in acetogenic bacteria: biochemistry, physiology and application. FEMS Microbiol Rev 45:fuaa040. <https://doi.org/10.1093/femsre/fuaa040>
- Li Z, Cai J, Gao Y, Zhang L, Liang Q, Hao W, Jiang Y, Jianxiong Zeng R (2022) Efficient production of medium chain fatty acids in microbial electrosynthesis with simultaneous bio-utilization of carbon dioxide and ethanol. Bioresour Technol 352:127101. <https://doi.org/10.1016/j.biortech.2022.127101>
- Litty D, Müller V (2021) Butyrate production in the acetogen *Eubacterium limosum* is dependent on the carbon and energy source. Microb Biotechnol 14:2686–2692. <https://doi.org/10.1111/1751-7915.13779>
- Litty D, Kremp F, Müller V (2022) One substrate, many fates: different ways of methanol utilization in the acetogen *Acetobacterium woodii*. Environ Microbiol 24:3124–3133. <https://doi.org/10.1111/1462-2920.16011>
- Liu C-G, Xue C, Lin Y-H, Bai F-W (2013) Redox potential control and applications in microaerobic and anaerobic fermentations. Biotechnol Adv 31:257–265. <https://doi.org/10.1016/j.biotechadv.2012.11.005>
- Mäki E, Saastamoinen H, Melin K, Matschegg D, Piikola H (2021) Drivers and barriers in retrofitting pulp and paper industry with bioenergy for more efficient production of liquid, solid and gaseous biofuels: a review. Biomass Bioenergy 148:106036. <https://doi.org/10.1016/j.biombioe.2021.106036>
- Marshall CW, Ross DE, Fichot EB, Norman RS, May HD (2013) Long-term operation of microbial electrosynthesis systems improves acetate production by autotrophic microbiomes. Environ Sci Technol 47:6023–6029. <https://doi.org/10.1021/es400341b>
- May HD, Evans PJ, LaBelle EV (2016) The bioelectrosynthesis of acetate. Curr Opin Biotechnol 42:225–233. <https://doi.org/10.1016/j.copbio.2016.09.004>
- Medina JDC, Magalhaes Jr AI (2021) Ethanol production, current facts, future scenarios, and techno-economic assessment of different biorefinery configurations. In: Bioethanol Technologies, Inambao FL (ed.), IntechOpen. <https://doi.org/10.5772/intechopen.95081>
- Mohanakrishna G, Vanbroekhoven K, Pant D (2018) Impact of dissolved carbon dioxide concentration on the process parameters during its conversion to acetate through microbial electrosynthesis. React Chem Eng 3:371–378. <https://doi.org/10.1039/C7RE00220C>
- Mountfort DO, Grant WD, Clarke R, Asher RA (1988) *Eubacterium callanderi* sp. nov. that demethoxylates O-methoxylated aromatic acids to volatile fatty acids. Int J Syst Evol Microbiol 38:254–258. <https://doi.org/10.1099/00207713-38-3-254>
- Nevin KP, Woodard TL, Franks AE, Summers ZM, Lovley DR (2010) Microbial electrosynthesis: feeding microbes electricity to convert carbon dioxide and water to multicarbon extracellular organic compounds. Mbio 1:e00103-e110. <https://doi.org/10.1128/mbio.00103-10>
- Pacaud S, Loubiere P, Goma G (1985) Methanol metabolism by *Eubacterium limosum* B2: effects of pH and carbon dioxide on growth and organic acid production. Curr Microbiol 12:245–250. <https://doi.org/10.1007/BF01567972>
- Pacaud S, Loubiere P, Goma G, Lindley ND (1986) Effects of various organic acid supplements on growth rates of *Eubacterium limosum* B2 on methanol. Appl Microbiol Biotechnol 24:75–78. <https://doi.org/10.1007/BF00266289>
- Rabaey K, Rozendal RA (2010) Microbial electrosynthesis — revisiting the electrical route for microbial production. Nat Rev Microbiol 8(10):706–16. <https://doi.org/10.1038/nrmicro2422>
- Rinta-Kanto JM, Sinkko H, Rajala T, Al-Soud WA, Sørensen SJ, Tamminen MV, Timonen S (2016) Natural decay process affects the abundance and community structure of Bacteria and Archaea in *Picea abies* logs. FEMS Microbiol Ecol 92:fiw087. <https://doi.org/10.1093/femsec/fiw087>
- Sharma M, Alvarez-gallego Y, Achouak W, Pant D, Sarma PM, Dominguez-Benetton X (2019) Electrode material properties for designing effective microbial electrosynthesis systems. J Mater Chem A 7:24420–24436. <https://doi.org/10.1039/c9ta04886c>
- Vassilev I, Hernandez PA, Batlle-Vilanova P, Freguia S, Krömer JO, Keller J, Ledezma P, Virdis B (2018) Microbial electrosynthesis of isobutyric, butyric, caproic acids, and corresponding alcohols from carbon dioxide. ACS Sustain Chem Eng 6:8485–8493. <https://doi.org/10.1021/acssuschemeng.8b00739>
- Vassilev I, Kracke F, Freguia S, Keller J, Krömer JO, Ledezma P, Virdis B (2019) Microbial electrosynthesis system with dual biocathode arrangement for simultaneous acetogenesis, solventogenesis and carbon chain elongation. Chem Commun 55(30):4351–4. <https://doi.org/10.1039/c9cc00208a>

- Vassilev I, Rinta-Kanto JM, Kokko M (2024) Comparing the performance of fluidized and fixed granular activated carbon beds as cathodes for microbial electrosynthesis of carboxylates from CO<sub>2</sub>. *Bioresour Technol* 130896. <https://doi.org/10.1016/j.biortech.2024.130896>
- Zhang K, Qiu Z, Luo D, Song T, Xie J (2023) Hybrid electron donors of ethanol and lactate stimulation chain elongation in microbial electrosynthesis with different inoculants. *Renew Energy* 202:942–951. <https://doi.org/10.1016/j.renene.2022.11.123>
- Zhao J, Ma H, Wu W, Ali Bacar M, Wang Q, Gao M, Wu C, Xia C, Qian D (2023) Conversion of liquor brewing wastewater into medium chain fatty acids by microbial electrosynthesis: effect of cathode potential and CO<sub>2</sub> supply. *Fuel* 332:126046. <https://doi.org/10.1016/j.fuel.2022.126046>

**Publisher's Note** Springer Nature remains neutral with regard to jurisdictional claims in published maps and institutional affiliations.

**Supporting Information for the article in journal of Applied Microbiology  
and Biotechnology**

**Methanol as a co-substrate with CO<sub>2</sub> enhances butyrate  
production in microbial electrosynthesis**

Hui Yao<sup>a</sup>; Johanna Rinta-Kanto<sup>a</sup>; Igor Vassilev<sup>a</sup>; Marika Kokko<sup>a\*</sup>

<sup>a</sup> Faculty of Engineering and Natural Sciences, Tampere University, Korkeakoulunkatu 8, 33720

Tampere, Finland

\* Corresponding author: Tel.: +358 50 4478 751, e-mail: [marika.kokko@tuni.fi](mailto:marika.kokko@tuni.fi)

## Materials and Methods

Two control serum bottle experiments (duplicates) were done to understand the role of supplied electricity/hydrogen in methanol assisted microbial electrosynthesis. 90 mL of the cathodic medium was added to a serum bottle and sparged with N<sub>2</sub> for 30 mins to eliminate oxygen, following by adding 10 mL enriched culture as the inoculum before starting the experiment. Same CO<sub>2</sub> and methanol addition strategies were used in the experiment, i.e., CO<sub>2</sub> was sparged through the serum bottle every two or three days for 15 mins with the flow rate of 0.4 mL min<sup>-1</sup> and methanol containing medium was added after the CO<sub>2</sub> sparging to reach the methanol concentration of 20 mmol L<sup>-1</sup> in the serum bottle. Gas bags were connected to the serum bottle to collect any possible gas production. Analysis of the gas and liquid samples was carried out by following the methods in the main text. In total, the experiments were conducted under 35 °C for eight days.

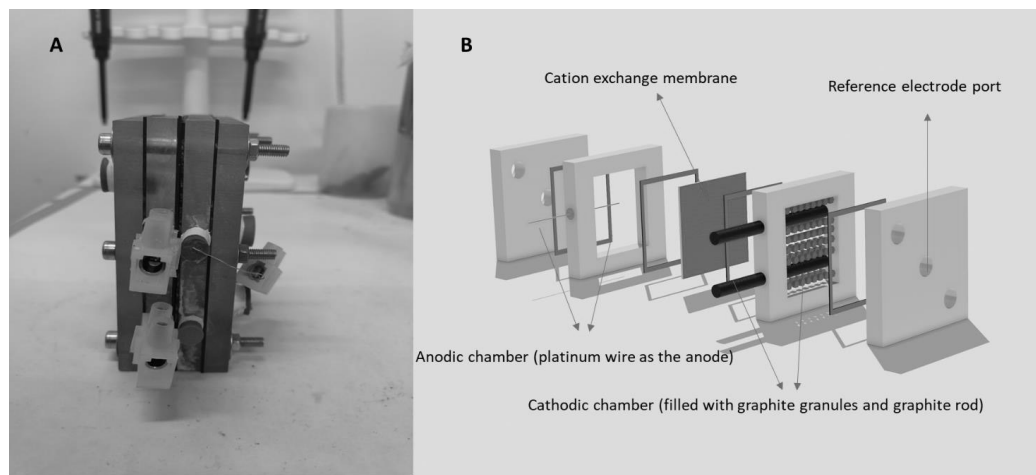


Figure S1 Reactor set-up used in this study. A: Picture of the reactor. B: Schematic illustration of the reactor. The chamber dimensions are 7 cm x 5 cm x 1 cm (internal volume of 35 cm<sup>3</sup>). Platinum wire was used as the anode, which was connected through a rubber stopper. Cathodic chamber was filled with graphite granules, where two graphite rods were used as the current collector for cathode. An Ag/AgCl reference electrode was inserted via a glass capillary frit in the reference electrode port. Cation exchange membrane was placed between cathode and anode. Catholyte and anolyte were recirculated by a peristaltic pump through the ports on the end plates.

## Results

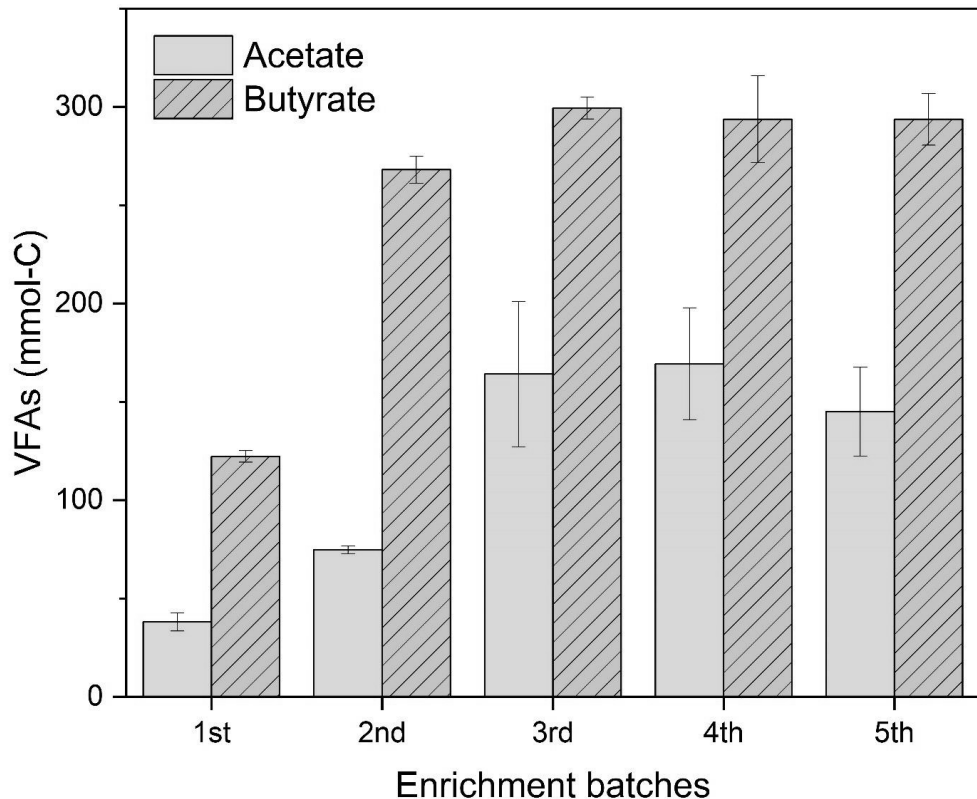


Figure S2. Production of VFAs at the end of each enrichment batch (in g L<sup>-1</sup>). Error bars indicate the standard deviation in duplicate reactors.

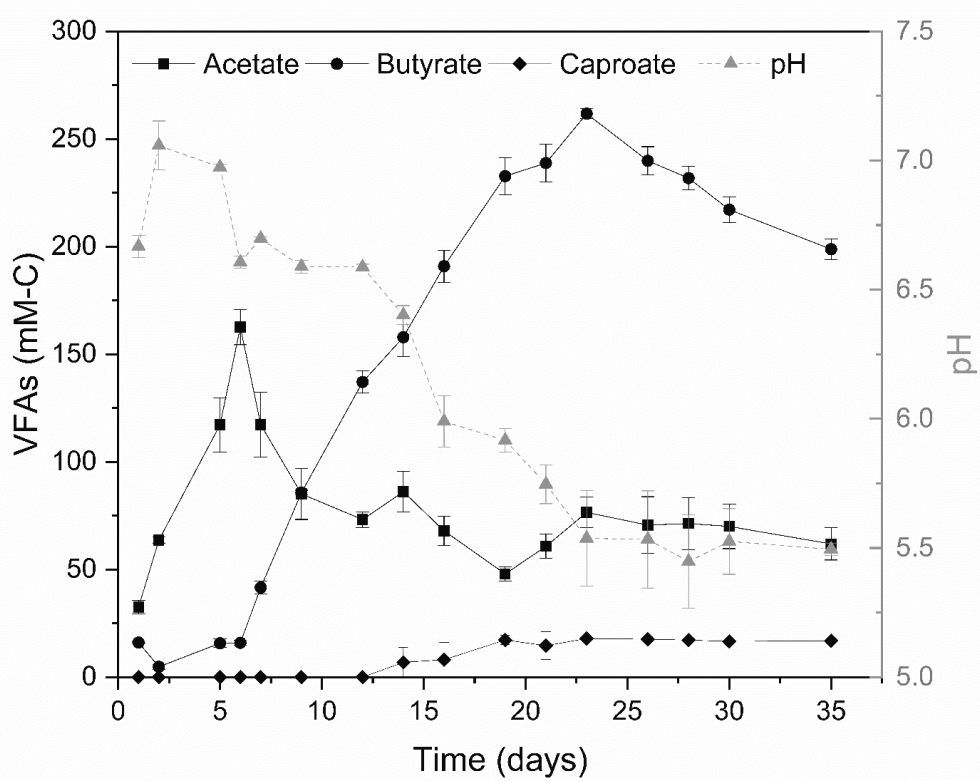


Figure S3. VFA production and pH value of the catholyte from the first enrichment batch. Error bars are the standard deviations between duplicate reactors.

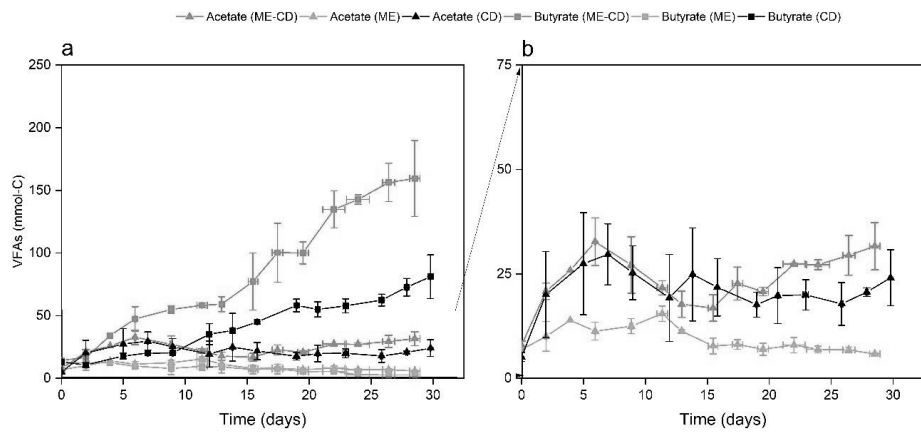


Figure S4. Amounts of VFAs in the co-substrate addition experiments, with a) the overview of all detected VFAs (acetate and butyrate), and b) the acetate production. ME-CD (fed with methanol and CO<sub>2</sub>); ME (fed with only methanol); CD (fed with only CO<sub>2</sub>). Error bars are the standard deviations in duplicate reactors.

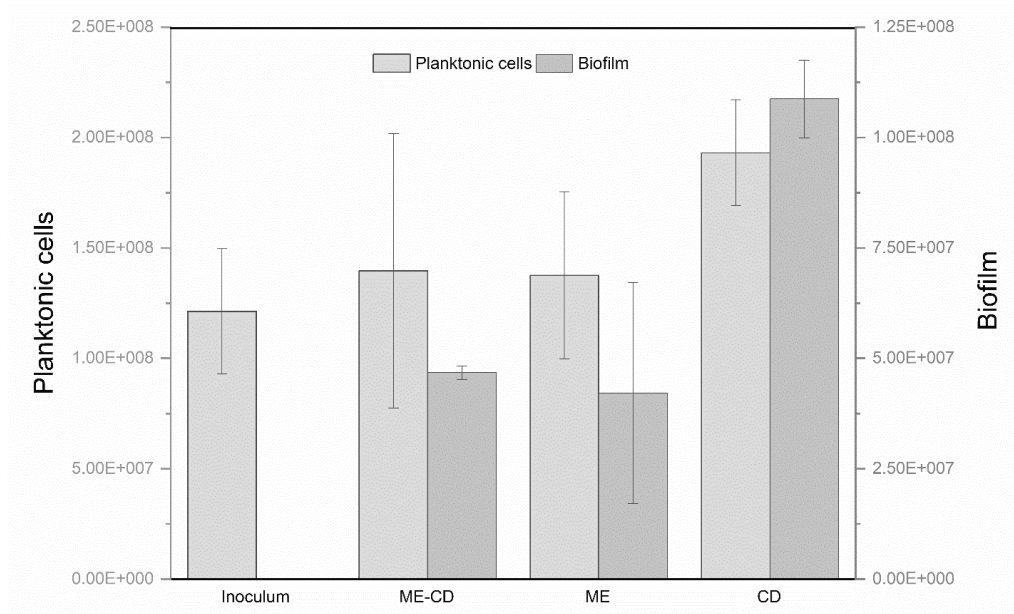


Figure S5. Total 16S rRNA gene copies obtained from the co-substrate addition experiments both for biofilm and planktonic cells from each experimental group. ME-CD (fed with methanol and CO<sub>2</sub>); ME (fed with only methanol); CD (fed with only CO<sub>2</sub>). Error bars are the standard deviations between duplicate reactors.

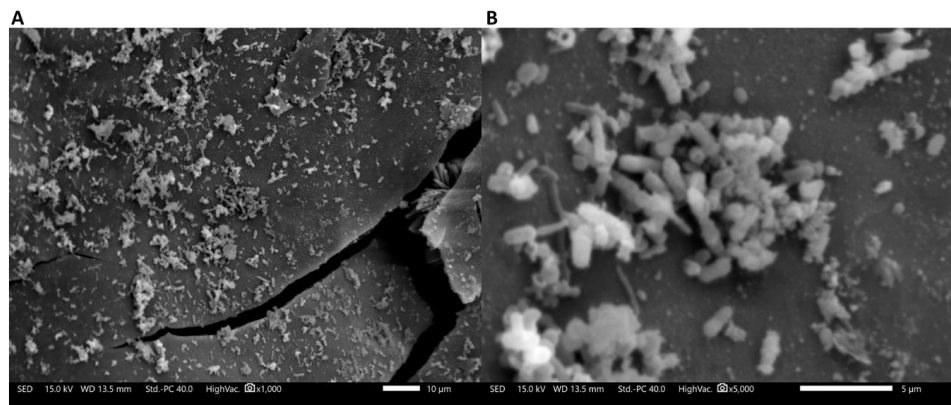


Figure S6. SEM images of the biofilms on the graphite granules from ME-CD reactors. Figure A shows the overview of the surface (1000x). Figure B shows a detailed image of the biofilm (5000x).

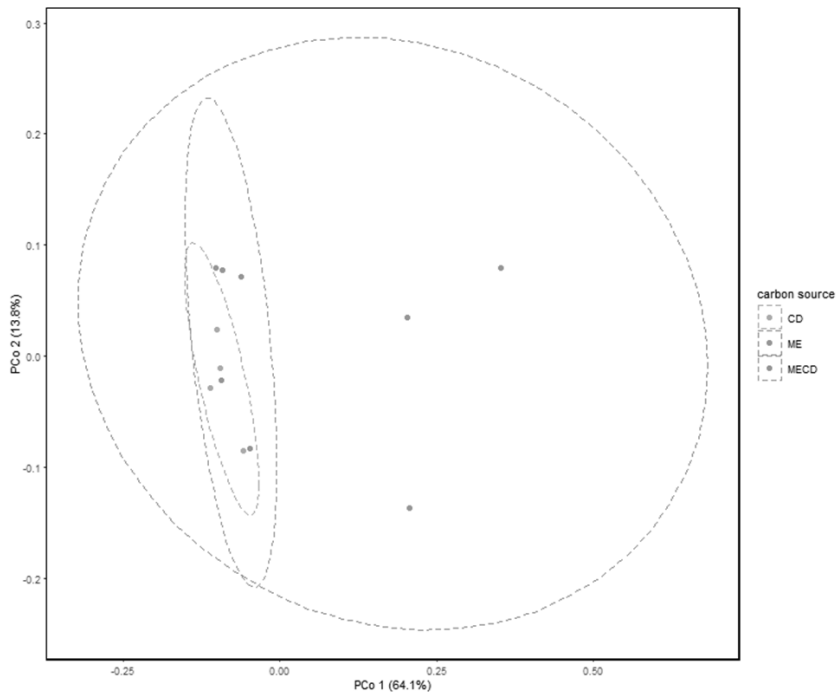


Figure S7. PCoA illustrating the differences in the microbial cultures in three different experimental groups (ME-CD, ME, and CD). Circles indicate the 90% confidential interval. The beta diversity was calculated based on the weighted-UniFrac distance.

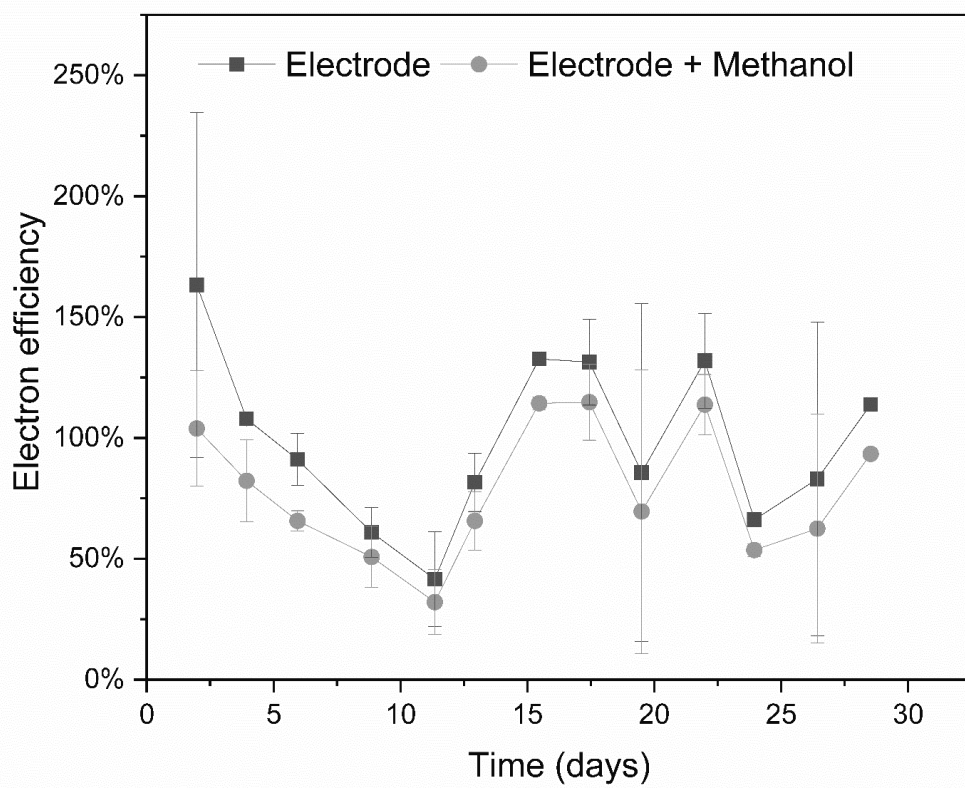


Figure S8. Electron efficiencies between two consecutive sampling timepoints for ME-CD reactors. The electron efficiency was calculated both considering only electrode as the electron source (Electrode) or considering both electrode and methanol as electron sources (Electrode + Methanol). The figure shows that the electron efficiency decreases when considering methanol as an electron source. Most of the electron efficiencies decrease to below 100% indicating the potential role of methanol as an electron source.

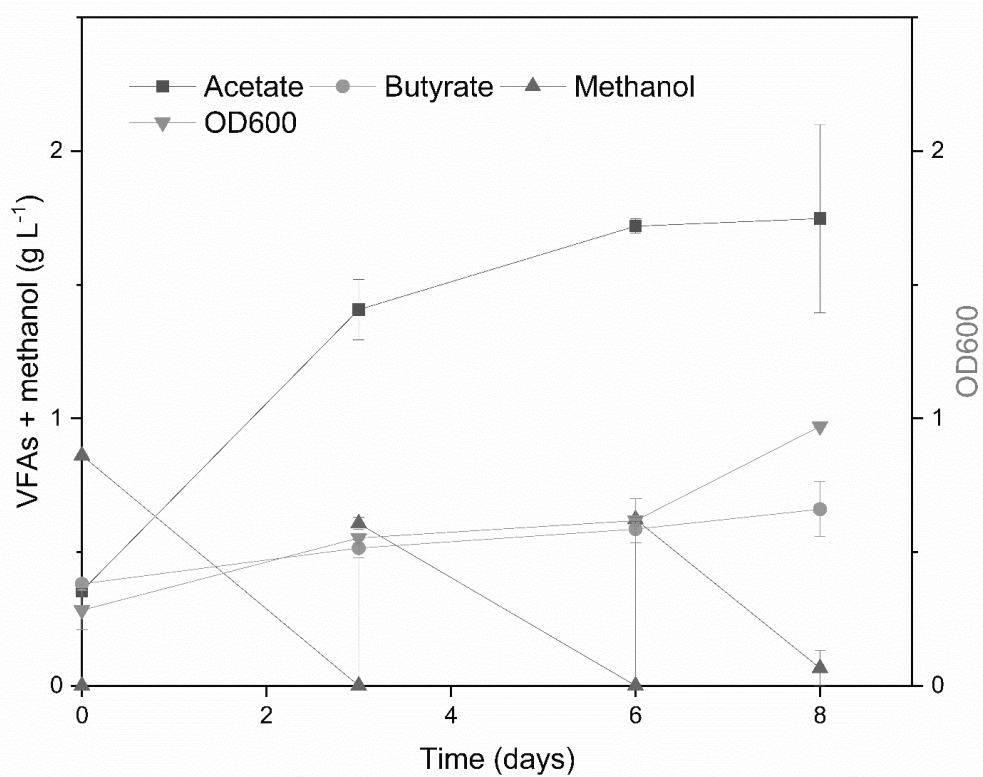


Figure S9. VFAs, methanol concentrations, and OD600 during the control experiments done in batch bottles without electricity and by feeding with CO<sub>2</sub> and methanol. Error bars are the standard deviations between duplicate reactors.

Table S1. Composition of the trace elements solution.

<b>Compound</b>	<b>Concentration (g L<sup>-1</sup>)</b>
EDTA	10.00
FeCl <sub>3</sub> ·6H <sub>2</sub> O	1.50
KI	0.18
CoCl <sub>2</sub> ·6H <sub>2</sub> O	0.15
H <sub>3</sub> BO <sub>3</sub>	0.15
MnCl <sub>2</sub> ·4H <sub>2</sub> O	0.12
ZnSO <sub>4</sub> ·7H <sub>2</sub> O	0.12
Na <sub>2</sub> MoO <sub>4</sub> ·7H <sub>2</sub> O	0.06
CuSO <sub>4</sub> ·5H <sub>2</sub> O	0.03
NiCl <sub>2</sub> ·7H <sub>2</sub> O	0.023

Table S2. Composition of the vitamin solution.

<b>Compound</b>	<b>Concentration (mg L<sup>-1</sup>)</b>
Biotin	2.0
Folic acid	2.0
Pyridoxine-HCl	10.0
Thiamine-HCl	5.0
Riboflavin	5.0
Nicotinic acid	5.0
D-Ca-pantothenate	5.0
Vitamin B12	0.1
p-Aminobenzoic acid	5.0
Lipoic acid	5.0

Table S3. Caproate concentrations at the end of the five enrichment batches of the microbial culture. Standard deviations are obtained from duplicate reactors.

Enrichment batches	Caproate (mM-C)
1 <sup>st</sup>	7.4 ± 4.1
2 <sup>nd</sup>	21.0 ± 5.0
3 <sup>rd</sup>	21.6 ± 1.8
4 <sup>th</sup>	16.9 ± 1.1
5 <sup>th</sup>	28.2 ± 0.8

Table S4. Repeated measures ANOVA for acetate and butyrate concentrations between ME-CD and CD

ANOVA					
Source of Variation	SS	DF	MS	F	P-VALUE
Acetate	51.6964443	1	51.69644431	1.058934	<b>0.312937</b>
Butyrate	9457.65089	1	9457.650886	104.2338	<b>1.37E-10</b>

Table S5. The total inorganic carbon present in the catholyte between feeding timepoints in the co-substrate addition experiment.

Days	Total inorganic carbon (mmol)											
	ME-CD1*		ME-CD2*		ME1*		ME2*		CD1*		CD2*	
	A**	B**	A**	B**	A**	B**	A**	B**	A**	B**	A**	B**
0	0.0	16.6	0.0	20.7	0.0	0.5	0.0	1.5	0.0	20.7	0.0	23.5
2	6.2	22.5	0.5	17.0	0.8	3.1	3.3	5.4	0.2	31.2	0.0	29.8
5	0.0	21.8	0.0	11.3	0.0	0.0	0.0	3.9	0.0	20.0	0.4	19.8
7	1.0	18.5	0.0	4.5	0.0	0.0	1.2	4.7	17.8	30.1	0.7	16.1
9	0.8	12.7	0.0	6.6	0.0	0.0	0.0	0.8	0.0	12.5	0.7	21.6
12	0.0	10.8	0.0	5.5	0.0	0.0	2.0	2.8	1.3	14.3	1.0	15.9
14	0.0	4.6	0.0	5.7	0.0	0.2	0.0	1.2	0.5	12.2	0.1	12.8
16	0.2	7.3	0.0	6.3	0.0	0.0	0.4	1.5	0.0	10.0	0.0	10.8
19	0.0	8.2	0.3	7.4	0.1	0.9	2.1	3.0	0.0	10.3	0.8	13.3
21	0.0	6.9	0.2	6.0	0.1	1.6	0.0	0.2	1.8	27.5	0.8	11.5
23	0.0	8.4	0.4	5.0	0.1	0.2	0.0	4.0	0.9	16.5	0.0	16.8
26	0.0	4.6	0.1	8.2	0.3	0.0	0.0	0.0	0.0	14.8	0.0	4.0
28	0.0	N/A	0.0	N/A	0.0	0.1	0.0	0.0	0.8	14.2	6.4	18.4

\*: 1 and 2 represent the duplicate reactors from each substrate feeding strategy.

\*\*: A represents the results before substrate feeding, while B represents the results after substrate feeding.

Table S6. Methanol in the catholyte between feeding timepoints in the co-substrate addition experiment.

Days	Methanol (mmol-C)			
	ME-CD1*		ME-CD2*	
	A**	B**	A**	B**
0	0.0	21.6	0.0	6.6
2	18.3	30.1	2.7	6.1
5	12.0	28.8	0.0	6.5
7	10.3	25.1	0.0	5.0
9	11.7	23.6	0.0	8.5
12	12.9	16.7	0.0	5.8
14	8.2	12.9	0.0	5.4
16	7.0	9.7	0.0	4.3
19	6.0	21.7	0.0	6.0
21	8.0	12.3	0.0	4.6
23	3.7	9.7	0.0	4.5
26	0.0	10.3	0.0	5.0
28	0.0	N/A	0.0	N/A

\*: 1 and 2 represent the duplicate reactors from each substrate feeding strategy.

\*\*: A represents the results before substrate feeding, while B represents the results after substrate feeding.

Table S7. Methanol concentration during the abiotic experiments

days	g L <sup>-1</sup>		mM	
	A*	B*	A*	B*
0	0.0	0.62	0.0	19.4
2	0.61	1.3	19.1	39.6
4	1.1	1.7	33.2	52.6
7	1.5	N/A	47.0	N/A

\*: A represents the results before substrate feeding, while B represents the results after substrate feeding.

Table S8. Result of searching the most abundant OTU in the NCBI 16s ribosomal RNA sequence (Bacteria and Archaea type strains) database using Megablast (September 2022).

NCBI Reference SEQUENCE:	Description	Score (Bits)	Query cover	E Value	Max Identify
NR_026330.1	<i>Eubacterium callanderi</i> strain DSM 3662 16S ribosomal RNA, partial sequence	750	100%	0.0	100%
NR_113248.1	<i>Eubacterium limosum</i> strain JCM 6421 16S ribosomal RNA, partial sequence	737	100%	0.0	100%



# PUBLICATION

||

**Selective butyrate production from CO<sub>2</sub> and methanol in microbial electrosynthesis—Influence of pH**

Yao, H., Romans-Casas, M., Vassilev, I., Rinta-Kanto, J. M., Puig, S., Rissanen, A. J., & Kokko, M.

Bioelectrochemistry, Volume 165, 109000  
<https://doi.org/10.1016/j.bioelechem.2025.109000>

**Publication is licensed under a Creative Commons Attribution 4.0 International License CC BY-NC**





## Selective butyrate production from CO<sub>2</sub> and methanol in microbial electrosynthesis - influence of pH

Hui Yao<sup>a</sup>, Meritxell Romans-Casas<sup>b</sup>, Igor Vassilev<sup>a</sup>, Johanna M. Rinta-Kanto<sup>a</sup>, Sebastià Puig<sup>b</sup>, Antti J. Rissanen<sup>a</sup>, Marika Kokko<sup>a,\*</sup>

<sup>a</sup> Faculty of Engineering and Natural Sciences, Tampere University, Korkeakoulunkatu 8, 33720 Tampere, Finland

<sup>b</sup> LEQUiA, Institute of the Environment, University of Girona, Campus Montilivi, C/Maria Aurelia Capmany, 69, Girona E-17003, Spain

### ARTICLE INFO

**Keywords:**  
Microbial electrosynthesis  
Butyrate  
Methanol utilization  
CO<sub>2</sub> utilization  
Redox potential  
Thermodynamic approach  
*Eubacterium*

### ABSTRACT

Methanol assisted microbial electrosynthesis (MES) enables butyrate production from carbon dioxide and methanol using external electricity. However, the effects of operational parameters on butyrate formation remain unclear. By running three flat plate MES reactors with fed-batch mode at three controlled pH values (5.5, 6 and 7), the present study investigated the influence of pH on methanol assisted MES by comparing the process performance, microbial community structure, and genetic potential. The highest butyrate selectivity (87 % on carbon basis) and the highest butyrate production rate of 0.3 g L<sup>-1</sup> d<sup>-1</sup> were obtained at pH 6. At pH 7, a comparable butyrate production rate was achieved, yet with a lower selectivity (70 %) accompanied with acetate production. Butyrate production rate was considerably hindered at pH 5.5, reaching 0.1 g L<sup>-1</sup> d<sup>-1</sup>, while the selectivity reached was up to 81 %. Methanol and CO<sub>2</sub> consumption increased with pH, along with more negative cathodic potential and more negative redox potential. Furthermore, pH affected the thermodynamical feasibility of involved reactions. The results of metagenomic analyses suggest that *Eubacterium callanderi* dominated the microbial communities at all pH values, which was responsible for methanol and CO<sub>2</sub> assimilation via the Wood-Ljungdahl pathway and was likely the main butyrate producer via the reverse β-oxidation pathway.

### 1. Introduction

Carbon dioxide (CO<sub>2</sub>) holds great promise in circular economy, as a non-conventional resource that could be recovered from various waste streams. Large amount of CO<sub>2</sub> is emitted as waste streams due to anthropogenic activities, with 36.8 Gt energy-related CO<sub>2</sub> released globally in 2022 [1]. The atmospheric CO<sub>2</sub> is restored through various biological CO<sub>2</sub> fixation pathways to maintain the global carbon cycle [2]. Among diverse carbon fixation pathways, Wood-Ljungdahl pathway (WLP) requires the least amount of ATP and thus has gained interest [2]. The WLP is widely reported to be performed by anaerobic microorganisms (including acetogens and methanogens) for the autotrophic growth on CO<sub>2</sub> and H<sub>2</sub>. CO<sub>2</sub> is reduced via the WLP by utilizing the reducing power provided by H<sub>2</sub> resulting in the production of acetyl-CoA, which is the precursor used for the formation of various valuable compounds and biomass, among others [3].

In addition to H<sub>2</sub>, certain microorganisms can uptake reducing power in the form of electrons. For example, microbial electrosynthesis

(MES) can provide reducing power either directly via the electrodes or in-situ produced H<sub>2</sub>, and can use renewable electricity for the conversion of CO<sub>2</sub> to chemicals [4]. MES consists of the use of anaerobic microbes as catalysts, capable of reducing CO<sub>2</sub> into organic compounds and cultivated in the cathode chamber of an electrochemical cell. Up to date, the most often reported product of MES has been acetate, with production rates up to 18.2 g L<sup>-1</sup> d<sup>-1</sup> (normalized to the entire catholyte volume) that has been reported in an MES reactor continuously fed with CO<sub>2</sub> [5]. In addition, 69.1 g L<sup>-1</sup> d<sup>-1</sup> acetate production rate was achieved in MES, yet it was based on the assumption that the porous electrode in that work could be used to fill the whole cathodic compartment which requires further experimental validation [6]. Although acetate is a promising building block in the chemical industry, the limited market value of acetate (ca. 500 € t<sup>-1</sup>) limits the industrialization of MES. One possibility is to upgrade acetate to more valuable products in MES, such as butyrate [7,8] that is a high-value (ca. 1500 € t<sup>-1</sup>) compound with versatile applications in pharmaceutical and chemical industries [9,10]. Currently, industrial butyrate production occurs mainly through chemical

\* Corresponding author.

E-mail address: marika.kokko@tuni.fi (M. Kokko).

synthesis. However, food and pharmaceutical industries typically favor biologically derived products and thus, require the sustainable bio-production of butyrate from renewable sources [11]. In addition to MES, microbial production of volatile fatty acids could also be combined with electrocatalysis, where  $\text{CO}_2$  is selectively reduced to formate or  $\text{CO}$ , which are further utilized as the energy source for fermentation [12–14]. For example, the tandem usage of  $\text{CO}_2$  electrolysis with syngas fermentation enabled caproate formation (ca.  $3300 \text{ g t}^{-1}$ ) [15] through syngas production from  $\text{CO}_2$  electrolysis [13].

Few studies have reported butyrate production from only  $\text{CO}_2$  in MES [8,16,17], obtaining production rates up to  $0.7 \text{ g L}^{-1} \text{ d}^{-1}$  ( $125.0 \text{ g m}^{-2} \text{ d}^{-1}$ , normalized to projected surface area of the electrode unless otherwise mentioned) [8]. The main butyrate production pathway reported in MES occurs through chain elongation of acetate, which requires utilization of reducing equivalents from electron donors, such as ethanol and lactate, which either can be natively produced in MES [18,19] or externally supplied [20]. The highest butyrate production rate of  $0.90 \text{ g L}^{-1} \text{ d}^{-1}$  ( $90 \text{ g m}^{-2} \text{ d}^{-1}$ ) in MES was obtained through chain elongation with the external addition of both lactate and ethanol that provided ca. 90 % of the electrons in products [21]. The most selective production of butyrate in MES (78 % of carbon selectivity) was obtained via ethanol-based chain elongation, in which ethanol was in-situ produced and resulted in butyrate production rate of  $0.18 \text{ g L}^{-1} \text{ d}^{-1}$  ( $14.5 \text{ g m}^{-2} \text{ d}^{-1}$ ) [19]. However, ethanol is a valuable chemical, current production of which relies on agricultural products [22]. Thus, finding a suitable compound that provides reducing power but does not compete with agricultural lands is more favorable for MES [23].

Methanol has been reported as potential electron donor in MES [24], which could provide the same amount of reducing power as ethanol (degree of reduction: 6) and higher than lactate (degree of reduction: 4) on a carbon basis. The cytotoxicity of methanol for the microbes may hinder its utilization in MES [25]. However, methanol can be naturally assimilated by some acetogens and methylotrophs, which brings up the potential of methanol utilization as substrate for biochemical production [26]. Methanol can be recovered from several biomass sources [26] or from waste streams, such as from pulp mill [27]. In addition, methanol can be produced from  $\text{CO}_2$  and  $\text{H}_2$  via hydrogenation which has been implemented on pilot scale process [26]. Our previous study illustrated for the first time that the addition of methanol in MES resulted in butyrate production with production rate of  $0.4 \text{ g L}^{-1} \text{ d}^{-1}$ , titer up to  $8.6 \text{ g L}^{-1}$ , and butyrate selectivity of 82 % (carbon based), which is one of the highest in MES studies [24]. Although a relatively high selective butyrate production was achieved in methanol assisted MES, previous studies in both MES and chain elongation processes showed that operational variables exert a considerable influence on the product spectrum, selectivity and microbial growth [8,28–30]. Reactor pH has been demonstrated to be one of the main parameters that alters the product spectrum and production rates. For acetogens, the optimal pH for growth is in the range of 5 to 8 [31–33]. Thus, slightly acidic to neutral pH values have been commonly used in MES and chain elongation studies. For example, in MES reactors fed exclusively with  $\text{CO}_2$ , a slightly acidic pH of 5.8 increased the availability of  $\text{CO}_2$  and thus resulted in ca. 3-fold increase in acetate production rates when compared to neutral pH of 6.8 [34]. However, the chain elongation process is usually inhibited at acidic pH [29,35], although the activity range highly depends on the microbial culture. In biological systems, kinetics and operational conditions play a crucial role and need to be carefully considered. Thermodynamic analysis can provide valuable information on energy conversion, offering predictive values for the products of the process [36]. Moreover, mathematical approaches are useful to understand the roles of different operational parameters and their interconnections in MES [37,38]. The effect of pH on fermentation studies has been widely reported. For example, a fermentation study carried by San-Valero et al. [35] showed a higher caproate yield at pH 6.8 compared to pH 6.4 when feeding acetate and ethanol to *Clostridium kluyveri*. In mixed culture studies, reactor pH can affect the composition

of the microbial community and thus lead to different dominant products [28,39]. For example, when methanol and acetate were fed to a mixed microbial community, pH 6.8 enhanced the growth of *Eubacterium* and increased the proportion of n-butyrate, while at pH 5.2 *Clostridium* was enriched which shifted the product spectrum to i-butyrate [28]. Despite the importance of pH on the MES performance, studies to assess the effect of pH on chain elongation in MES have been lacking and only been recently reported by Quintela et al. [40]. However, the effect of pH on methanol assisted MES has never been reported before and needs to be investigated.

The objective of this study was to evaluate the effects of cathodic pH on methanol assisted MES, specially on the selectivity towards butyrate production. Three reactors were operated in triplicate controlling the cathodic pH at 5.5, 6.0 and 7.0. Production rates and volatile fatty acid (VFAs) titers, total inorganic carbon, gas composition and volume were analyzed and used for the calculation of carbon and electron recoveries at each pH value. Biofilm and suspended samples from the end of each run were characterized by shotgun metagenomics for analyzing the community composition and functional profiling. In addition, the experimental data was integrated into an adapted thermodynamic model previously developed for MES [36] to determine the prediction potential of this model for further similar studies.

## 2. Materials and methods

### 2.1. Inoculum and experimental set-up

The culture employed as inoculum in the present work consists of a mixed culture dominated by *Eubacterium limosum* previously used by Yao et al. [24]. The inoculum was cultured with methanol and  $\text{CO}_2$  for over three years in the same MES reactor as used in this study with consistent performance. The reactor set-up consisted of a two-chamber flat-plate reactor (Fig. 1), connected to buffer tanks. Each chamber was made of ketamide with internal volumes of 124 mL ( $7.5 \text{ cm} \times 5.5 \text{ cm} \times 3 \text{ cm}$ ) for the cathodic chamber and 62 mL ( $7.5 \text{ cm} \times 5.5 \text{ cm} \times 1.5 \text{ cm}$ ) for the anodic chamber. Chambers were separated by a cation exchange membrane (CXM-200, membrane international, USA), which had an active surface area of  $41 \text{ cm}^2$ . The cathodic chamber was packed with graphite granules (ca.  $113 \text{ g}$ ,  $10 \pm 2 \text{ mm}$  of diameter, EC-100, Graphite Sales Inc., USA) and two graphite rods (diameter 6 mm, length 15 cm, Sigma-Aldrich, USA) were embedded in the granular bed serving as the current collectors. A reference electrode (+0.206 V vs. normal hydrogen electrode, MF-2052, BASi, USA) was inserted into cathodic chamber via the side port. Platinum wire (0.4 mm, 99.95 %, Advent research materials, UK) was used as the anode. The cell was operated with a 3-electrode configuration with a chronopotentiometry technique (100 mA), controlled by a potentiostat (VMP3 Multichannel Potentiostat, BioLogic, France), resulting in current density of  $0.13 \text{ mA cm}^{-2}$  calculated based on the estimation of the cathode surface area. The surface area of the granules was estimated by considering the granules as sphere particles with an average diameter of 10 mm, yielding approximately 236 granules in one chamber when considering the chamber volume. The surface area of each granule was calculated to be  $314 \text{ mm}^2$ , resulting in a total surface area of approximately  $741 \text{ cm}^2$  for all granules.

Catholyte consisted of synthetic medium containing different concentrations of phosphate buffers to obtain the pH levels of 5.5, 6 and 7 (detailed composition in Table S1). As the pKa values of acetic and butyric acid are ca. 4.8, lowering the pH to around 5 likely would trigger solventogenesis for ethanol or butanol production as previously reported in MES [18,41]. As this study focused on methanol assisted MES, pH 5.5 was chosen as the lowest pH to avoid the formation of extra electron donors other than methanol. The catholyte (350 mL) was sparged with  $\text{N}_2$  for 30 mins to remove oxygen and added to the cathodic buffer tanks. The cathodic broth (30 mL, ca. 10 % v/v) from the enrichment reactor was added to the cathodic buffer tanks to start the

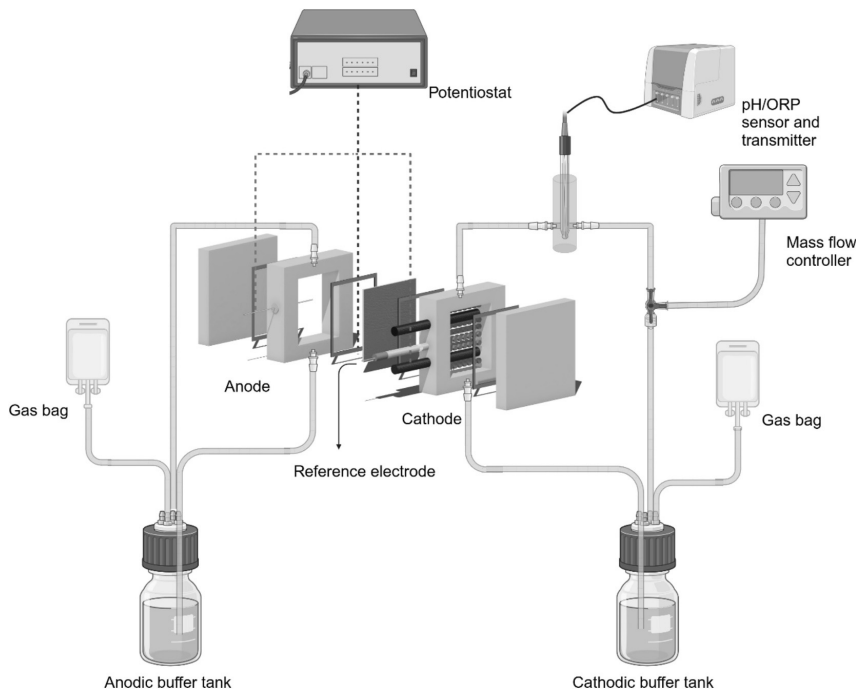


**Fig. 1.** Microbial electrosynthesis reactor (schematic illustration).

experiments, which resulted in a total volume of 380 mL and a headspace volume of ca. 800 mL in the buffer tanks. Around 250 mL of 50 mmol L<sup>-1</sup> H<sub>2</sub>SO<sub>4</sub> was used as anolyte. The liquid of both chambers was recirculated at a flow rate of 40 mL min<sup>-1</sup> with peristaltic pumps (MasterFlex L/S, Cole-Parmer, USA). Online sensors measuring oxidation-reduction potential (ORP) and pH (CPS16D, Endress+Hauser, Switzerland) were placed in the cathodic recirculation lines. Each probe was connected to an Endress+Hauser pH transmitter (CM444, Endress+Hauser, Switzerland) to monitor the pH and ORP values every five minutes. The pH was maintained manually by adding HCl (3 M) or NaOH (3 M) when required. Over the 30-day experiment, a total of 22 ± 10 mL, 36 ± 20 mL, and 93 ± 28 mL of chemicals was used at pH 5.5, 6.0, and 7.0, respectively. 10 L gas bags (Supel™-Inert Gas Sampling Bags, MERCK, Germany) were connected to the buffer tanks of both chambers, to collect the produced gas from each chamber. The cathodic gas bags were used to collect and analyze the catholyte gas composition and volume. The cathodic chamber and buffer tanks were operated under anaerobic conditions. The system was operated at 35 °C.

## 2.2. Reactor operation and analytical methods

Three reactors were simultaneously operated for 30 days at different cathodic pH values (5.5, 6 and 7). The experiments at each pH value were performed in triplicate, in a three-month window. CO<sub>2</sub> and methanol were fed to the cathode three times a week after sampling. For each feeding, CO<sub>2</sub> was sparged through the cathodic buffer tanks for 30 min at a flow rate of 50 mL min<sup>-1</sup> (a total of 1.5 L), which was controlled by mass flow controllers (F-201CV, Bronkhorst, the Netherlands), and collected in the gas bags. A methanol stock solution (0.76 mol L<sup>-1</sup>) was prepared by using the same synthetic medium as for each pH value experiment. 10 mL of methanol stock solution was added to the cathodic buffer tanks after CO<sub>2</sub> sparging to reach a methanol concentration of 0.4

g L<sup>-1</sup> (20 mM) in the cathode. Samples were taken before and after feeding. After each feeding, the pH was adjusted if required. In addition, a series of intensive samplings were conducted in the second experimental run between days 16 and 18. During the intensive sampling, six samples were collected within two days 0, 5.5, 20, 26, 31 and 46 h after feeding.

For anodic samples, 2 mL of the anolyte was taken and filtered (CHROMAFIL Xtra PET, 25 mm, 0.2 µm, MACHERREY-NAGEL, Germany) to analyze the VFAs and methanol. For cathodic samples, 4 mL of catholyte was taken. The optical density (OD<sub>600</sub>) was measured with a UV-Vis spectrophotometer (UV-1800, Shimadzu, Japan). The remaining sample was filtered (CHROMAFIL Xtra PET, 25 mm, 0.2 µm, MACHERREY-NAGEL, Germany) to analyze total inorganic carbon (TIC), alcohols and VFAs. TIC was analyzed via a total organic carbon analyzer with ASI-V sampler (TOC-VCPI, Shimadzu, Japan). VFAs and alcohols were quantified with a gas chromatography equipped with flame ionization detector (GC-FID 2010, Shimadzu, Japan). The cathodic headspace composition was analyzed by a gas chromatograph with thermal conductivity detector (GC-TCD 2014, Shimadzu, Japan) and the gas volume accumulated in the gas bag was quantified via water replacement column. The detailed parameters of TOC, GC-FID, and GC-TCD were as described in Yao et al. [24].

## 2.3. Analysis of the microbial culture

At the end of each run, suspended and biofilm samples were taken for shotgun metagenomic analysis. The detailed sample preparations and DNA extractions were done as described by Yao et al. [24]. Shortly, it was implemented as follows: the microbial samples were taken from the cathodic broth (40 mL) and graphite granules (15 g), from which the graphite granules were sonicated for three min (USC 300 T, VWR, USA) with freshly added phosphate buffer solution (40 mL, pH 7.4) to detach

the biofilm. The cathodic broth and the detached biofilm samples were centrifuged, and the resulting pellets were stored at  $-80^{\circ}\text{C}$  freezer up to six months until extraction. The pellets were then used to extract genomic DNA by using the DNeasy PowerSoil Pro Kits (QIAGEN, the Netherlands). The genomic DNA was shipped to BMKgene, Germany for library preparation and 150 bp pair-ended shotgun metagenomic analysis in NovaSeq X Plus (PE150) platform.

The reads of each sample were preprocessed to obtain the clean reads using the Multi-Domain Genome Recovery (Mudoger v1.0.1) [42]. The clean reads were fed to metagenomic phylogenetic analysis MetaPhiAn (v4.0.6) pipeline [43] to predict the taxonomic profiling at the species level, and HMP Unified Metabolic Analysis Network (HUMAN 3.0) pipeline [44] to profile the presence/absence and abundance of microbial pathways. The gene families were inferred to the UniRef90 protein clusters and then mapped to the Level 4 enzyme commission (EC) categories to acquire the function annotation of each gene. The alpha and beta diversity analyses were carried out with Vegan package in R (v4.3.2). Alpha diversity includes the Shannon and Simpson indices. Beta diversity was obtained using the Principal Coordinate Analysis (PCoA) with the Bray-Curtis dissimilarity matrix. The differences in alpha diversity and beta diversity between pH treatments were tested using *t*-test and permutational analysis of variance (PERMANOVA), respectively [45]. For PERMANOVA, the assumption of homogeneity of multivariate dispersion was assessed using the *betadisper()* function from the vegan package, followed by *permutes()* to evaluate statistical significance and *p* value  $< 0.05$  was considered statistically significant for all tests. The obtained raw reads were uploaded to the European Nucleotide Archive (ENA) under the project accession number PRJEB78858.

#### 2.4. Thermodynamic analysis

A previously developed thermodynamic model by Rovira-Alsina et al. [36] that considers the main MES parameters was adapted to fit the putative reactions investigated in the present study. Stoichiometric reactions and standard Gibbs free energy ( $\Delta G^\circ$ ) were collected from the literature (Table S2), while the formation enthalpies were calculated following the same methodology as Rovira-Alsina and co-workers [36]. Experimental results obtained during the operation were introduced as inputs of the model in order to obtain corrected Gibbs free energy at each condition. To assess the significance of the differences between the results obtained under the different tested conditions in the model, statistical analyses were performed applying one way analysis of variance (ANOVA) and Tukey's Honest Significant Difference (HSD) tests. Specifically, assumptions for ANOVA were tested prior to analysis. The normality of residuals was assessed using the Shapiro-Wilk test and visual inspection of Q-Q plots. Homogeneity of variances across groups was evaluated using Levene's test from the car package.

#### 2.5. Calculations

Unless otherwise specified, production rates reported in this study represent the average rates calculated from day 2 to day 25.

The product selectivity was calculated with eq. (1) following the principles suggested by Jourdin et al. [8]:

$$\text{Selectivity}_i = \frac{r_i}{r_{\text{sum}}} \times 100 \quad (1)$$

where selectivity of compound *i* is defined as the ratio of the production rate of compound  $r_i$  and the total production rate of organics  $r_{\text{sum}}$  in  $\text{g C L}^{-1} \text{ d}^{-1}$ .

Electron recovery (ER) was calculated according to the following equation:

$$\text{ER}_i = \frac{F \times n_i \times z_i}{\int I dt + F \times n_{\text{Me}} \times z_{\text{Me}}} \times 100 \quad (2)$$

where  $\text{ER}_i$  is defined as the ratio of amount of electrons transferred to product *i* and the total electrons provided,  $z_i$  represents the number of electrons for product *i*. Specifically, the number of electrons were 2 for  $\text{H}_2$ , 6 for methanol, 8 for acetate, 14 for propionate, 20 for butyrate, and 32 for caproate.  $F$  is faraday's constant ( $96,485 \text{ C mol}^{-1}$  electron),  $n$  is the amount of product *i*, and  $I$  is the current consumed along the considered time (A).

Carbon recovery (CR) was calculated according to the following equation:

$$\text{CR} = \frac{n_{(\text{VFAs})}}{n_{(\text{carbon dioxide})} + n_{(\text{methanol})}} \times 100 \quad (3)$$

where  $n_{(\text{VFAs})}$  is the sum of amounts of produced VFAs in mol-C,  $n_{(\text{carbon dioxide})}$  and  $n_{(\text{methanol})}$  are the amounts of consumed  $\text{CO}_2$  and methanol in mol-C, respectively.

The ANOVA and PERMANOVA were carried out in R (4.3.2) to assess differences in the VFA production among reactors operated at pH 5.5, 6, and 7, as previously described.

### 3. Results and discussion

#### 3.1. Effect of pH on VFA production

##### 3.1.1. Production rates and titers

MES reactors were operated at three different pH values ( $5.5 \pm 0.2$ ,  $6.0 \pm 0.3$  or  $7.1 \pm 0.4$ ) to test the effect of pH on the product spectrum. The VFA production, pH, and  $\text{H}_2$  accumulation rates throughout the study were as illustrated in Fig. 2.

The predominant product, n-butyrate (hereafter butyrate, referred to n-butyrate unless otherwise specified), was the same at all pH values. Acetate production initiated immediately after the startup at all pH values. At pH 5.5 and 6, acetate concentration was ranging from 1.3 to  $2.1 \text{ g L}^{-1}$  along the experiments, with production rates of  $0.03 \pm 0.01 \text{ g L}^{-1} \text{ d}^{-1}$  in case of pH 5.5 and  $0.06 \pm 0.02 \text{ g L}^{-1} \text{ d}^{-1}$  at pH 6. The highest acetate production was achieved at pH 7, reaching a titer up to  $5.8 \pm 1.8 \text{ g L}^{-1}$  with a production rate more than 3-fold higher,  $0.2 \pm 0.1 \text{ g L}^{-1} \text{ d}^{-1}$ . Butyrate production started on day 2 under all the conditions tested. At pH 5.5, butyrate production rate was considerably lower than under the rest of the tests and reached  $0.12 \pm 0.04 \text{ g L}^{-1} \text{ d}^{-1}$  with a final titer of  $3.4 \pm 1.4 \text{ g L}^{-1}$ . At higher pH values, butyrate production rates achieved were similar and up to  $0.28 \pm 0.04 \text{ g L}^{-1} \text{ d}^{-1}$  at pH 6 and  $0.29 \pm 0.05 \text{ g L}^{-1} \text{ d}^{-1}$  at pH 7 with final titers of  $7.0 \pm 1.0 \text{ g L}^{-1}$  and  $7.5 \pm 1.1 \text{ g L}^{-1}$ , respectively. Overall, the butyrate titers and production rates across all pH values were significantly different ( $p < 0.05$ , Table S3).

As both acetate and butyrate titers were enhanced at pH 7, considerably higher overall VFA production of  $307 \pm 20 \text{ mmol-C}$  was achieved at pH 7 compared to pH 6 and 5 reactors where  $187 \pm 16 \text{ mmol-C}$  and  $111 \pm 27 \text{ mmol-C}$  VFAs were reached, respectively. Butyrate selectivity is one of the key parameters to assess MES performance. Separation of butyrate from mixed carboxylates requires energy input and thus, boosting butyrate selectivity could be beneficial for the enhancement of the downstream extraction [46]. Although the highest VFA production was obtained at pH 7, the highest butyrate selectivity was obtained at pH 6 ( $86.9 \pm 1.5 \%$ ). At pH 5.5 a similar selectivity ( $80.5 \pm 5.9 \%$ ) was displayed, while the butyrate selectivity at pH 7 was significantly lower,  $69.8 \pm 7.7 \%$  ( $p < 0.05$ , Table S3). In addition to acetate and butyrate, trace amounts of propionate, i-butyrate, valerate, and caproate were detected, however, their concentrations were always below 5 mM (Table S4). It has been reported that at low pH conditions, especially below pH 5, solventogenesis is generally favored which promotes the alcohol formation from fatty acids [7]. Moreover, alcohols could be immediately consumed for longer chain fatty acids production [7,46]. Alcohols other than methanol were not detected in this study.

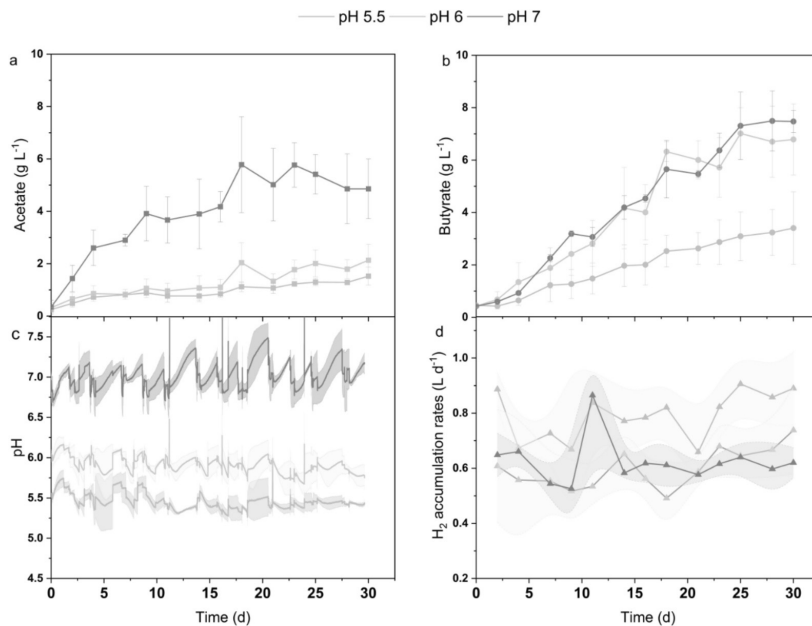


**Fig. 2.** Acetate concentration (a), butyrate concentration (b), cathodic pH (c) and  $H_2$  accumulation rate (d) over time at different pH values. Error bars in figures a and b and shadows in figures c and d indicate the standard deviations in triplicate reactors.

### 3.1.2. Carbon and electron recoveries

Methanol and  $CO_2$  utilization was also affected by the pH. The carbon recovery (i.e., the production of VFAs versus the overall utilization of methanol and  $CO_2$ ) and the electron recovery were as shown in Fig. S1. Methanol was efficiently consumed at pH 7, while it accumulated up to  $3.7\text{ g L}^{-1}$  and  $2.2\text{ g L}^{-1}$  at pH 5.5 and pH 6, respectively, resulting in a high methanol migration to the anode (Table S4), from where it likely evaporated. As the evaporation of methanol could not be quantified, methanol utilization was calculated solely based on methanol concentrations at the cathode. Methanol utilizations were in line with the VFA productions at different pH values, with total methanol consumptions of  $111 \pm 18\text{ mmol-C}$  at pH 5.5,  $129 \pm 17\text{ mmol-C}$  at pH 6, and  $139 \pm 6\text{ mmol-C}$  at pH 7 in 30 days. At pH 5.5, only  $70.2 \pm 13.8\%$  of the provided methanol was utilized, while at pH 6 the majority of provided methanol was utilized, while at pH 7 all the provided methanol was utilized ( $91.6 \pm 3.5\%$ ) and at pH 7, all the provided methanol was consumed. The consumption of  $CO_2$  at pH 6 and pH 7 remained similar,  $238 \pm 43\text{ mmol-C}$  at pH 6 and  $206 \pm 44\text{ mmol-C}$  at pH 7, which were significantly higher than at pH 5.5 ( $109 \pm 43\text{ mmol-C}$ ) ( $p < 0.05$ ). The supply of  $CO_2$  was excessive at all pH values to ensure  $CO_2$  was not the limiting carbon source in the process and thus, unused  $CO_2$  was observed in the gas bags between the sampling days. Only  $11.6 \pm 4.6\%$ ,  $25.4 \pm 4.3\%$ , and  $22.0 \pm 4.6\%$  of  $CO_2$  was utilized at pH 5.5, 6 and 7 reactors, respectively. Additionally, it is worth mentioning that the headspace pressure was maintained at atmospheric pressure throughout the experiments, as the gas bags did not become full during any of the fed-batch cycles.

In this study, both methanol and  $CO_2$  utilizations were hindered at pH 5.5, resulting in the lowest VFA production. Most likely, the lower results at pH 5.5 correspond to a lower  $HCO_3^-$  concentrations in the catholyte due to pH effect, according to the Henderson - Hasselbach equation. The TIC results showed that lower pH resulted in lower overall TIC concentrations. Before  $CO_2$  sparging, the total inorganic carbon concentrations ranged from  $144$  to  $314\text{ mg/L}$  at pH 5.5, from  $109$  to  $302\text{ mg/L}$  at pH 6, and from  $206$  to  $379\text{ mg/L}$  at pH 7. After sparging with

$CO_2$ , the concentrations increased, reaching  $467$ – $738\text{ mg/L}$  at pH 5.5,  $534$ – $723\text{ mg/L}$  at pH 6, and  $685$ – $933\text{ mg/L}$  at pH 7. This observation is consistent with a pure culture study conducted by Pacaud et al. [30] who observed that when feeding *Eubacterium* with methanol and  $CO_2$ , more methanol was consumed at higher pH and the methanol consumption was determined by the  $HCO_3^-$  concentrations within the pH range of 6.8 to 8.0. The lower utilization of methanol could therefore have been expected at lower pH in this study. In summary, carbon recoveries of  $50.5 \pm 8.0\%$ ,  $53.0 \pm 13.9\%$ , and  $87.7 \pm 12.2\%$  were obtained at pH 5.5, 6 and 7, respectively. More specifically,  $57.5 \pm 5.4\%$  of the utilized carbon was converted to butyrate at pH 7, while at pH 5.5 and 6 the carbon recoveries for butyrate dropped to  $34.4 \pm 6.5\%$  and  $39.6 \pm 10.9\%$ , respectively. Although the most selective butyrate production was obtained at pH 6, the low carbon and electron recoveries suggested further optimization is required. The loss of  $CO_2$  could be a major factor. During each fed-batch cycle, the high availability of  $CO_2$  may have facilitated its migration across the membrane, followed by evaporation, as the crossover of  $CO_2/HCO_3^-$  through the ion exchange membrane has been widely reported [47,48]. Additionally, as the biofilm could not be quantified, the carbon recovered as biomass growth was not included in the carbon recovery calculation. The pH 7 not only enhanced the carbon conversion to butyrate but also acetate production, therefore decreasing the butyrate selectivity in the final product spectrum.

Despite the same current of  $100\text{ mA}$  ( $0.13\text{ mA cm}^{-2}$ ) applied to all the reactors, different  $H_2$  accumulation rates were obtained. The highest  $H_2$  accumulation rate of  $0.76 \pm 0.08\text{ g L}^{-1}\text{ d}^{-1}$  was obtained at pH 5.5, while at pH 6 and pH 7  $H_2$  was accumulated at lower and similar rates of  $0.63 \pm 0.07\text{ g L}^{-1}\text{ d}^{-1}$  and  $0.64 \pm 0.04\text{ g L}^{-1}\text{ d}^{-1}$ , respectively. Compared to higher pH values of this study, the lower  $H_2$  accumulation rates at pH 5 was likely due to the lower consumption of  $H_2$  for the formation of organic compounds, which also implied that at pH 5.5 the bioconversion of  $H_2$  in methanol assisted MES could be hindered, although the exact mechanisms hindering the bioconversion remained unclear. Considering solely VFAs as products, electron recoveries at pH

5.5, pH 6 and pH 7 were  $15.9 \pm 4.1\%$ ,  $26.5 \pm 3.2\%$  and  $41.1 \pm 2.8\%$ , respectively. However, when taking the H<sub>2</sub> into account, the electron recoveries increased to  $78.5 \pm 2.0\%$  (pH 5.5),  $77.2 \pm 10.0\%$  (pH 6) and  $91.3 \pm 4.8\%$  (pH 7) (Fig. S1). H<sub>2</sub> was the main electron sink in this study. It has been reported that the partial pressure of H<sub>2</sub> (pH<sub>2</sub>) can affect the chain elongation process [49]. For instance, the increase of pH<sub>2</sub> reduced excessive ethanol oxidation to acetate and thus increased the availability of ethanol for chain elongation [49]. The electrons not accounted in VFAs or H<sub>2</sub> production can be lost through various means. Firstly, the migration of methanol to anode (Table S4) diverts electrons from end products, and the methanol accumulation at pH 5.5 and 6 likely resulted in a higher concentration differences across membrane compared to pH 7. Secondly, losses due to the internal resistance of the electrochemical cell, including the cathodic overpotential, the resistance between anode and cathode chamber, and oxygen intrusion by the diffusion from anodic to cathodic chamber could also consume electrons, which cannot be quantified [50]. Lastly, the biomass growth acts as an electron sink. However, as the biofilm could not be quantified, the amount of electrons utilized for biomass growth was not calculated or estimated.

Altering reactor pH has previously been an effective method to modify the product spectrum in studies focusing on chain elongation with mixed cultures [28,35,39]. For example, mildly acidic pH (below 6) favored the growth of chain elongators and kinetically favored lactate-based chain elongation process over propionate fermentation [39]. The effect of pH was also evaluated in methanol-based chain elongation with acetate and methanol as the feedstocks, in which study the low reactor pH of 5.2 resulted in the production of mainly i-butyrat e, while at pH 6.75 the production shifted to n-butyrat e [28]. In addition, the microbial community characterization in this study revealed a high relative abundance of *Eubacterium* (see chapter 3.3), which is a well-known butyrate-producer. The production of more reduced compounds than butyrate from *Eubacterium* has been achieved by providing more methanol than the co-substrates. For example, Wood et al. [57] stated that higher ratios of methanol/co-substrate (5:1 compared to 1:1) shifted the production towards butanol and caproate, as more methanol provided more reducing power. In this work, CO<sub>2</sub> was provided excessively and resulted in the accumulation of CO<sub>2</sub> in the gas bags between feedings. The methanol/co-substrate ratio in this study was ca. 0.16. Supplying more methanol compared to CO<sub>2</sub> could potentially stimulate the production of caproate, yet it needs to be further investigated.

Butyrate production from CO<sub>2</sub> in MES has often relied on the supply of extra reducing power, either by external addition [20] or in-situ production [7] of an electron donor. The comparison of butyrate production in MES studies is concluded in Table 1. For example, ethanol has

a degree of reduction of 12 (mol electrons/mol ethanol) and has been reported to promote selective butyrate production in MES [19]. Up to 78 % of butyrate (carbon based) was produced in MES where ethanol was produced in-situ and acted as electron donor [19]. Similarly, the present study used methanol as reducing power and showed an increase of butyrate selectivity up to 86.9 %, one of the highest reported up to date in MES studies. The butyrate production rate of  $0.3\text{ g L}^{-1}\text{ d}^{-1}$  obtained in this study is also among one of the highest in MES studies and comparable to the highest butyrate production rates in MES (Table 1) [19–21]. As the cathode electrode in this study consisted of graphite granules, a high projected surface area resulted in butyrate production rate of  $32\text{ g m}^{-2}\text{ d}^{-1}$ . In MES when the electrode was the sole electron donor, the highest butyrate production rate of  $0.7\text{ g L}^{-1}\text{ d}^{-1}$  ( $125\text{ g m}^{-2}\text{ d}^{-1}$ ) was obtained by continuous CO<sub>2</sub> feeding with a loading rate of  $173\text{ L d}^{-1}$  and current density of  $126\text{ A m}^{-2}$ , yet with a rather low butyrate selectivity (< 40 %) [8]. A fed batch reactor study conducted by Raes et al. [16] reported butyrate production rate of  $0.54\text{ g L}^{-1}\text{ d}^{-1}$ , however, achieved by externally adding acetate and operating the reactor at a high current density  $9.3\text{ A m}^{-2}$ . In addition, Zhang et al. [21] added  $5\text{ g L}^{-1}$  of ethanol or  $5\text{ g L}^{-1}$  of lactate to an MES reactor which resulted in butyrate production rates of  $0.4\text{ g L}^{-1}\text{ d}^{-1}$  ( $40.0\text{ g m}^{-2}\text{ d}^{-1}$ ) from ethanol and  $0.2\text{ g L}^{-1}\text{ d}^{-1}$  ( $20.0\text{ g m}^{-2}\text{ d}^{-1}$ ) from lactate. However, the addition of ethanol and lactate in the study of Zhang et al. was over two-fold higher compared to the present study (methanol addition of  $1.92\text{ g L}^{-1}$ ) and thus, it is reasonable to assume that supplying more electron donor would promote the production of more reduced products. As reported by Jiang et al. [51], adding  $10\text{ g L}^{-1}$  ethanol promoted the caproate dominant production with the production rate of  $2.4\text{ g L}^{-1}\text{ d}^{-1}$  in MES [51]. With methanol as the electron donor, a slightly higher butyrate production rate of  $0.4\text{ g L}^{-1}\text{ d}^{-1}$  was obtained from our previous study [24], where CO<sub>2</sub> was sparged through the buffer tanks, but not collected in the gas bags, and the pH was only adjusted when it dropped below 6.

In summary, methanol as the extra electron donor in MES achieved comparable butyrate titers, production rates and selectivity to those obtained with other electron donors in MES. Currently, methanol is not used in food or beverages industries and its production does not rely on the agricultural lands, avoiding the competition with food production. In addition, methanol can be recovered from wastewaters or potentially utilized directly from wastewaters [27], or methanol could be produced from renewable sources such as CO<sub>2</sub> and H<sub>2</sub>. This renewable production has been implemented at pilot scale, utilizing CO<sub>2</sub> from industrial waste streams, and H<sub>2</sub> from water electrolysis powered by renewable electricity [52]. Moreover, using methanol helps to avoid contamination during bio-production, as natural methanol assimilation is not widely

**Table 1**

Comparison of butyrate/caproate production in mixed culture MES studies fed with CO<sub>2</sub> and with different electron donors. For each electron donor, the first reported studies and studies with the highest butyrate production rates/titers are included in the table.

Electron donor(s)	Running time (d)	Substrate feeding mode	Main products	Titer (g L <sup>-1</sup> )	Production rate (g L <sup>-1</sup> d <sup>-1</sup> )	Butyrate selectivity % (carbon basis)
Electrode [17]	34	Fed-batch	Butyrate	0.4	0.04	< 30 <sup>a</sup>
Electrode [19]	35	Fed-batch	Butyrate	3.2	0.2	78 <sup>b</sup>
Electrode [8]	263	Continuous	Butyrate/ Caproate	9.3/ 3.1	0.7/0.2	< 40 <sup>b</sup>
Electrode + Formate [20]	45	Fed-batch	Butyrate/ Caproate	0.1	0.008	6 <sup>a</sup>
Electrode + ethanol [51]	7	Batch	Butyrate/ Caproate	1.2/ 7.7	0.2/2.4	n.a./92 <sup>c</sup>
Electrode + ethanol [21]	7	Batch	Butyrate/ Caproate	3.1/ 0.4	0.4/0.1	79 <sup>b</sup>
Electrode + lactate [21]	7	Batch	Butyrate	1.2	0.2	72 <sup>b</sup>
Electrode + methanol [24]	28	Fed batch	Butyrate	8.6	0.4	82 <sup>b</sup>
This study (pH 6)	28	Fed batch	Butyrate	7.0	0.3	87 <sup>b</sup>

<sup>a</sup> Selectivity is estimated based on the amounts of one compound versus the total amounts of products reported in the original work.

<sup>b</sup> Selectivity is defined as the ratio between the production rate of one compound and the total production rate of organics over the same period of time.

<sup>c</sup> Selectivity is defined as the electron concentration of the products divided by the electron consumption from the substrates.

reported. Recent studies have shown selective CO<sub>2</sub> electro-reduction to methanol with novel catalysts [53,54], which further highlights the potential of methanol as a sustainable feedstock. As the aforementioned renewable methanol synthesis routes rely on electricity, anticipated decrease in electricity costs [55] could make the integration of methanol production and methanol-assisted MES competitive with traditional large-scale chemical processes. As previously stated, both CO<sub>2</sub> and methanol can be originated from waste streams. Future studies in methanol assisted MES could focus on exploring the usage of different microbial species, utilizing metabolic engineering tools [56,57], or optimization of the process parameters (e.g. operational mode, temperature, reactor design) to achieve the more diverse/selective bio-production.

### 3.1.3. Intensive sampling and ORP

During the second run, an intensive sampling was conducted between days 18 and 20 when butyrate was actively produced, to further understand the substrate utilization and VFA production during one feeding. Before the substrate addition on day 18, over 3.2 g L<sup>-1</sup> of methanol was accumulated at pH 5.5, ca. 0.6 g L<sup>-1</sup> at pH 6, and no methanol accumulation was observed at pH 7. The intensive sampling started right after the feeding of CO<sub>2</sub> and methanol, and the changes of substrates and products were as shown in Fig. 3 (exact concentrations can be found in Table S5). During the 46 h sampling period, 0.6 g L<sup>-1</sup> of methanol were added at pH 5.5, 6 and 7 (Fig. 3b, c, d). As the consumption of CO<sub>2</sub> in the gas phase could not be quantified without

emptying the gas bags, CO<sub>2</sub> consumption was not included in the results. Butyrate was the sole VFA produced (0.4 g L<sup>-1</sup>) at pH 5.5 (Fig. 3b). At pH 6, acetate was produced (0.6 g L<sup>-1</sup>) followed by a steady increase in butyrate production (up to ca. 1.5 g L<sup>-1</sup>) and concomitant methanol consumption (Fig. 3c). In contrast, at pH 7 acetate was produced in the first 18 h (1.5 g L<sup>-1</sup>) accompanied with complete methanol utilization, after which acetate was completely consumed with simultaneous butyrate production (up to 1.9 g L<sup>-1</sup>) (Fig. 3d).

Although high butyrate production was observed both at pH 6 and pH 7, the differences in the acetate production and consumption patterns indicated that butyrate production pathways may be different. At pH 7, the formation of butyrate occurred simultaneously with the consumption of acetate, which has been reported in previous MES studies [7,24]. Acetate was first likely produced via the phosphorylation of acetyl-CoA to gain ATP and released to the medium. However, at mildly acidic pH (5.5 and 6), butyrate seemed to be produced without using acetate as an intermediate, implying that a different butyrate formation pathway could be favored.

In biological process, the extracellular ORP represents the activity of electrons in the broth, and is determined by the dissolved H<sub>2</sub>, dissolved O<sub>2</sub>, temperature, pH and the concentrations of other oxidative/reductive compounds [58]. In addition to the aforementioned conditions in biological process, ORP in bioelectrochemical system is also affected by the electrode potential. ORP has been widely used as a tool to regulate the fermentation process in bioelectrochemical systems (BES) [59]. Given the complexity of BES, the exact mechanism on how ORP was

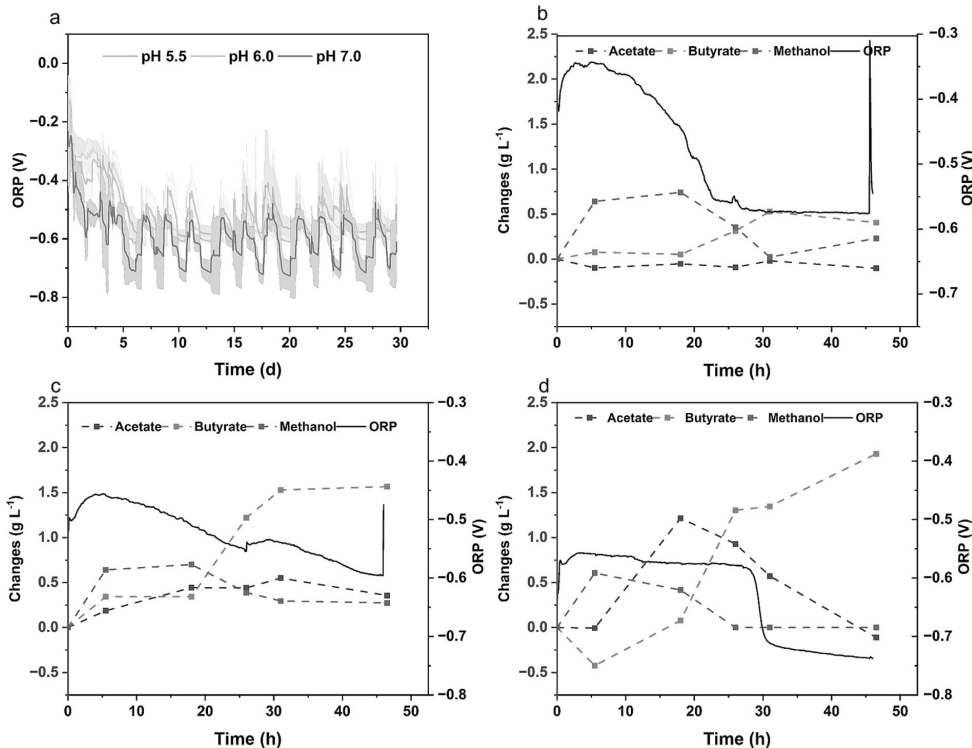


**Fig. 3.** (a) Cathodic online ORP values for all reactors for the whole experimental duration with standard deviations (triplicates) plotted in lighter shadow. Consumption of methanol and production of VFAs during intensive sampling from days 18 to 20 in the 2<sup>nd</sup> run are shown in figures b (pH 5.5), c (pH 6) and d (pH 7). The concentrations shown are the relative changes based on the concentrations of day 18 after feeding (considered as 0 g L<sup>-1</sup> in the beginning of the intensive sampling). The actual concentrations of methanol and VFAs at the beginning and end of the intensive sampling period are given in Table S5.

affected by the electrode potential remained unclear. It has been reported in several studies that the microbial metabolism/product spectrum can be regulated by changing the ORP with different working electrode potentials [59–62]. For example, the yield of 1,3-propanediol with *Clostridium pasteurianum* was improved by 57 % by increasing the extracellular ORP from –462 mV to –250 mV [62]. Although ORP has an important role in biological processes, discussion on ORP is rarely reported in MES studies. In MES, cathode is an energy source, providing electrons for H<sub>2</sub> evolution and other reduction reactions. Thus, ORP is not only affected by the cathodic potential but also affected by the produced H<sub>2</sub>, which further increases complexity.

In this study, the initial ORP of all reactors was ca. -0.2 V on day 0 (Fig. 3.a). In the first two days, a smooth ORP decrease was observed at pH 5.5 reaching –0.3 V, while at pH 6 and 7 it decreased to approximately –0.4 V and –0.55 V, respectively. A cyclic variation in ORP was observed for each fed batch cycle. Upon feeding, ORP consistently increased, likely due to the H<sub>2</sub> removal and introduction of small amounts of oxygen upon substrate feeding and pH adjustment and then decreased until stabilizing at specific plateau values before the next feeding. The plateau values were ca. –0.56 V for pH 5.5, –0.6 V for pH 6, and –0.7 V for pH 7. The decreasing of ORP after feeding can be attributed to several factors, including reduction of oxygen, the accumulation of H<sub>2</sub>, and decreasing pH due to VFA production. A theoretical model was developed by LeBaron and Sharpe [63], indicating that ORP was more sensitive to the changes in pH than dissolved H<sub>2</sub> and temperature, and a higher pH corresponded to a more negative ORP value. Yet, in this study the pH differences cannot solely explain the dissimilarities in the ORP as the theoretical ORP difference between pH 5.5 and

7 was 88.8 mV, while around 150 mV difference was observed experimentally. The ORP could also be affected by the cathodic potential, which also differed among different pH values (Fig. S2). The most negative ORP was observed at pH 7, which was in line with the most negative cathode potential observed at pH 7 (average –1.1 V), compared to pH 5.5 (–0.9 V) and pH 6 (–1.0 V) (Fig. S2). As mentioned, the electrode potential is reported to be employed aiming to control the catholyte ORP and therefore to affect the microbial metabolism in electrofermentation [59]. Enzymes can detect the changes in the extracellular ORP and thus, affect the intracellular ORP by adjusting the redox pairs ratios [64]. Furthermore, the metabolism of *E. limosum*, a close relative to *E. callanderi*, can be regulated via the ORP [65]. By adding several reducing agents, the ORP was decreased to a more reduced condition enhancing CO<sub>2</sub> consumption and affecting the balance of reduced coenzymes and the relative impact of proton ( $\Delta\text{pH}$ ) and ionic ( $\Delta\Psi$ ) gradients on the proton motive force, thus stimulating butyrate production [66]. However, the mechanisms of how electrode potential affect the solution ORP remains to be elucidated [58].

### 3.2. Evaluation of the alignment between experimental results and thermodynamics

In order to elucidate the reactions driving the observed production of VFAs and to evaluate the alignment between experimental results and theoretical predictions, a thermodynamic model was assessed. The model was adapted with the most likely reactions occurring in this study (Table S2). Moreover, only butyrate formation from methanol and acetate was considered for the calculations as there is no agreement in the

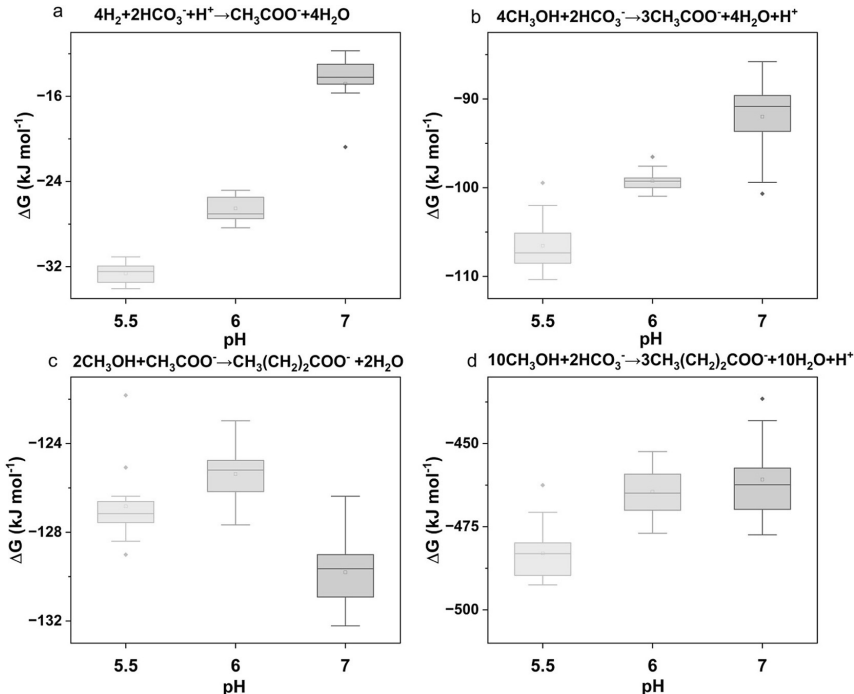


**Fig. 4.** Gibbs free energy variations ( $\Delta G$ ) of acetate and butyrate formation at all pH values tested. Graph a describes the results of homoacetogenesis reaction, b represents the results of acetate production from methanol and CO<sub>2</sub>, c represents the results of butyrate production from methanol and acetate, and d represents the results of butyrate production from methanol and CO<sub>2</sub>. The ranges of Y axis for the four inspected reactions are different for better illustration. Each box plots graph is plotted based on 14 experimental results. Box plots graphs represent the interquartile range (IQR), with whiskers representing range within 1.5 IQR. Outliers are displayed as small circles outside the box and whisker area. The line inside the box indicates the median, while the hollow cube represents the mean.

scientific community about direct formation of butyrate from H<sub>2</sub> and CO<sub>2</sub>.

As acetate and butyrate are the two main VFAs produced in this study, experimental results collected were used to feed the model and calculate the ΔG' of acetate and butyrate formation considering also the operational conditions in this study (Fig. 4). Butyrate production was thermodynamically more favorable than acetate at all pH values, as butyrate formation had the most negative ΔG' regardless of the pH. Notably, the direct synthesis of butyrate from methanol and CO<sub>2</sub> obtained the most negative ΔG', ranging from -436 to -504 kJ mol<sup>-1</sup>. However, the direct butyrate synthesis from methanol and CO<sub>2</sub> is often accompanied by acetate formation and consumption [30,67]. The metabolic applicability of direct synthesis of butyrate from methanol and CO<sub>2</sub> remains to be elucidated. Butyrate formation from methanol and acetate, however, has been extensively studied, in which methanol provide the reducing power for the acetate elongation [68]. For acetate production, using methanol compared to H<sub>2</sub> was thermodynamically more favorable, with the ΔG' of methanol driven acetate formation ranging from -85 to -112 kJ mol<sup>-1</sup> and for the homoacetogenesis from -12 to -34 kJ mol<sup>-1</sup>. Yet, it is worth mentioning that methanol was completely consumed between feeding days, especially at pH 6 and 7. Thus, the availability of methanol could limit acetate production from methanol. For all the reactions, the differences of ΔG' obtained at three pH values present significant differences ( $p < 0.05$ , ANOVA and Tukey HSD Test, Fig. S3), except for the reaction of butyrate formation from acetate and methanol between pH 5.5 and 6 ( $p > 0.05$ , ANOVA and Tukey HSD Test, Fig. S3).

Experimental outputs matched with thermodynamically obtained values regarding butyrate formation. However, at pH 7 acetate formation and accumulation was also recorded throughout the run, while at pH 5.5 and pH 6, much lower acetate production rates and titers were observed experimentally. Considering only thermodynamics, acetate is more likely to be produced using methanol and HCO<sub>3</sub><sup>-</sup> as substrates, although for the reaction employing H<sub>2</sub> as the electron donor the ΔG' was below -20 kJ mol<sup>-1</sup> (more positive), which is the minimal energy required to consider a reaction as spontaneous in natural systems [69]. Therefore, both acetate and butyrate productions in this study possibly occurred through a reaction that required methanol as substrate. At pH 7, methanol was completely utilized, while at pH 5.5 and pH 6, methanol utilization was obstructed, which likely hindered acetate formation from methanol and HCO<sub>3</sub><sup>-</sup>. In this study, methanol was likely utilized for the production of both acetate and butyrate, while electrons from the electrode were also utilized for VFA production as shown by the electron recoveries (Fig. S1).

Even though thermodynamics is a powerful tool that can provide important information, the thermodynamic-based model has certain limitations. First, thermodynamic calculations are based on the assumption of an equilibrium in the system, and considers the product formation as a one-step reaction, while the enzymatic reactions can occur far from equilibrium and often involve series of intermediate reactions. The model can be used to theoretically evaluate the process parameters in the methanol assisted MES (e.g., substrate feeding ratios, gas pressures and temperature) in addition to anticipating the results and to excluding unfavorable conditions for butyrate production. For a deeper understanding of the process, other main features have to be considered, such as kinetics, microbial culture composition and activities of the microorganisms [36].

### 3.3. Microbial cultures

#### 3.3.1. Metagenomic analysis of biofilm and suspended cells

The species present in the mixed culture were analyzed for all the reactors under different pH conditions (Fig. S4). Different microbial community results were obtained at different pH values. In addition, differences were also observed between biofilm and suspended samples (Fig. S5, Table S7). The Shannon and Simpson indices revealed that

there were no significant differences in alpha diversity across different pH values (Table S6). However, a statistically significant (Fig. S5) difference in both indices was observed between biofilm and suspended samples at pH 6. Yet, at pH 5.5 and pH 7 both indices were also lower in biofilm than in suspended samples, although not statistically significantly, indicating lower richness and evenness of the biofilm samples. Therefore, biofilm samples were dominated by fewer species compared to suspended communities, which is further discussed in the following chapter. Biofilm and suspended samples were also clustered separately in PCoA plot to characterize the beta diversity of the microbial communities (Fig. 5). The differences of β-diversity were further validated by two-way PERMANOVA, which revealed that both the sample type (biofilm/suspended) and pH resulted in significant differences on the microbial compositions (both  $p < 0.05$ , Table S7).

*Eubacterium callanderi* was the predominant species at all pH values, with relative abundances ranging from 52.2 to 63.1 % (Fig. S6). The relative abundance presented refers to the percentage of all reads, and the average values are calculated for both biofilm and suspended samples for each pH values unless otherwise specified. The presence of *E. callanderi* was enhanced under elevated pH conditions and the relative abundance was higher in biofilm than suspended samples under the same cathodic pH. Namely, the relative abundance of *E. callanderi* in biofilm samples increased from 66.7 ± 13.0 % at pH 5.5 to 76.1 ± 6.3 % at pH 6 and to 73.0 ± 12.9 % at pH 7, while in suspended samples the relative abundances were 37.8 ± 11.0 % at pH 5.5, 45.3 ± 11.3 % at pH 6, and 53.1 ± 16.3 % at pH 7. The inoculum already showed a high relative abundance of *E. callanderi* of 54.8 ± 8.3 %, as the culture was cultivated for 2.5 years with CO<sub>2</sub> and methanol [24]. The relative abundances of *E. callanderi* in suspended samples decreased compared to the inoculum samples, while in biofilm *E. callanderi* was more abundant. *E. callanderi* was not originally reported to grow with one-carbon substrates as the only carbon sources, yet recent studies have indicated that CO<sub>2</sub> and methanol could be utilized by *E. callanderi* for the production of butyrate when H<sub>2</sub> is provided as reducing power [67,70]. The differences in the abundances of *E. callanderi* were in line with the differences in butyrate production in this study suggesting that *E. callanderi* was potentially contributing to butyrate production in methanol assisted MES. Compared to the work from de Leeuw et al. [28], in which the mixed culture was fed with acetate and methanol in an anaerobic fermenter, *Clostridium litoricellari* was associated with i-butyrate production at pH 5.2, while *Eubacterium* genus was responsible for n-butyrate production at 6.75 [28]. Although similar pH range was investigated in this study, n-butyrate production was dominant under all pH values. Only trace amounts of i-butyrate were observed at pH 6 and pH 7 (Table S4). The production of i-butyrate has been suggested to occur via the isomerization of n-butyrate [28], which could be inhibited

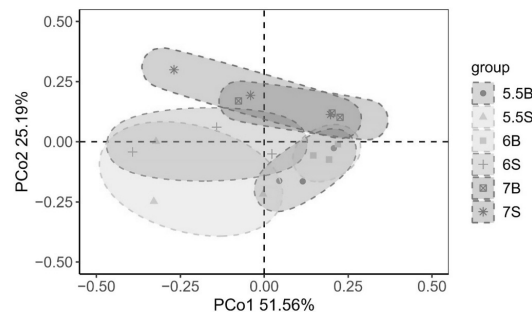
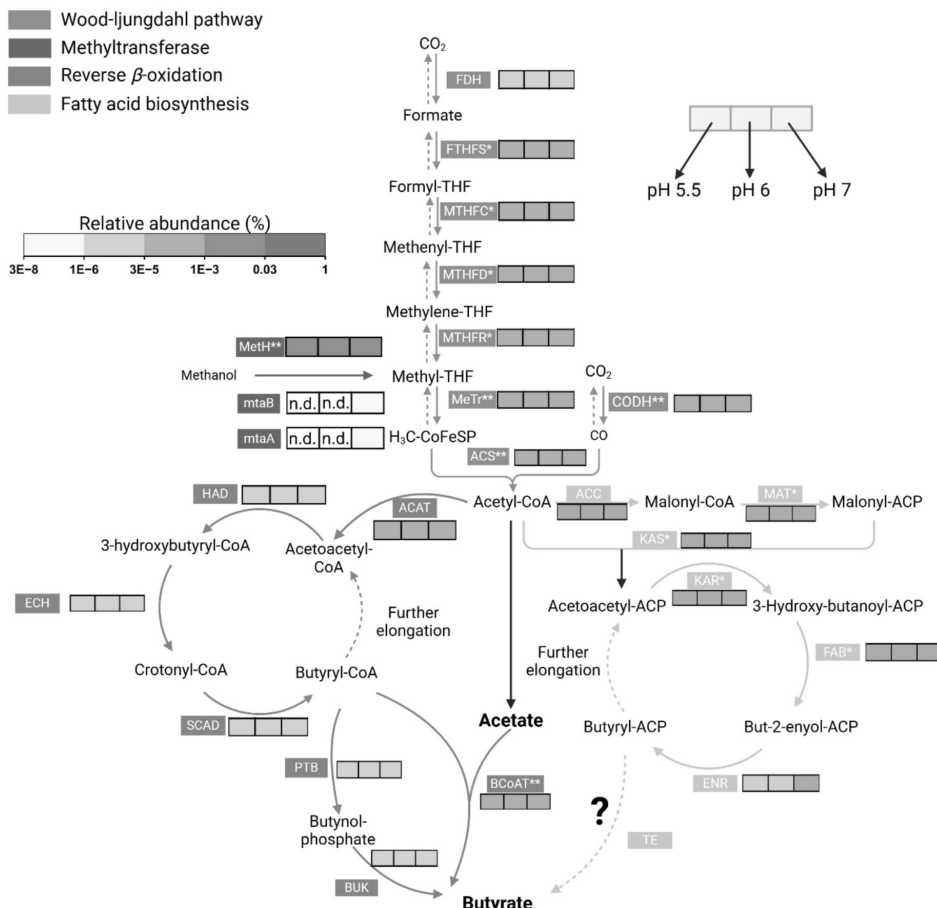


Fig. 5. Beta diversity of the microbial compositions at different pH values (species level). PCoA is based on Bray-Curtis dissimilarity matrix. Three pH groups are described as 5.5 (pH 5.5), 6 (pH 6) and 7 (pH 7). B and S represent biofilm and suspended samples, respectively.

with the addition of 2-bromoethanesulfonate [71] that was used in this study to inhibit methanogenesis.

Besides, *Proteiniphilum acetatigenes* was present specifically at pH 7 with relative abundances of  $11.9 \pm 6.1\%$  (suspended) and  $5.7 \pm 1.0\%$  (biofilm) as well as in inoculum, while it was almost absent at pH 5.5 and pH 6 (relative abundance <1%) (Fig. S6). *P. acetatigenes* is an autotrophic acetogen, capable of utilizing H<sub>2</sub> and CO<sub>2</sub> for the production of acetate [72]. The increment of *P. acetatigenes* at pH 7 might be the explanation for the high acetate yield, while its growth was hindered at pH 5.5 and 6, where low acetate titers (<2 g L<sup>-1</sup>) were obtained.

Although *P. acetatigenes* is able to grow at pH 6 [72], methanol-based methylotrophic growth has not been reported and the accumulation of methanol (up to 0.1 mol L<sup>-1</sup>) in this study could have been inhibitory for its growth. *Cellulomonas citrea* had higher relative abundances in suspended samples, i.e.,  $18.9 \pm 15.8\%$  at pH 5.5,  $26.6 \pm 15.0\%$  at pH 6, and  $12.4 \pm 7.5\%$  at pH 7 compared to the relative abundances in the biofilms (<2.0%) as well as in inoculum ( $3.0 \pm 1.7\%$ ) (Fig. S6). *C. citrea* is a facultative anaerobe, growing on lactate and cellulose [73]. Yet, *C. citrea* has not been reported to grow autotrophically up to date, and the role of *C. citrea* in the mixed culture remained unclear.



**Fig. 6.** Putative metabolic pathway for butyrate production from methanol and CO<sub>2</sub>. The relative abundances were average values of six samples. The error bars are not shown. Abbreviations: CODH, carbon-monoxide dehydrogenase; FDH, formate dehydrogenase; FTHFS, Formate-tetrahydrofolate ligase; MTHFC, methenyltetrahydrofolate cyclohydrolase; MTHFD, methylenetetrahydrofolate dehydrogenase; MTHFR, methylenetetrahydrofolate reductase; MeTr, 5-methyltetrahydrofolate—corrinooid/iron-sulfur protein Co-methyltransferase; ACS, CO-methylating acetyl-CoA synthase; ACAT, acetyl-CoA C-acetyltransferase; HAD, 3-hydroxyacyl-CoA dehydrogenase; ECH, enoyl-CoA hydratase; SCAD, short-chain acyl-CoA dehydrogenase BCoAT, butyryl-CoA,acetate CoA transferase; BUK, butyrate kinase; PTB, phosphate butyryltransferase; ACC, acetyl-CoA carboxylase; MAT, malonyl transferase; KAS, ketoacyl-ACP synthase; KAR, ketoacyl-ACP reductase; FAB, hydroxyacyl-ACP dehydratase; ENR, enoyl-ACP reductase; TE, thioesterase; MetH, methionine synthase; mtaA, [methyl-Co(II)] methanol-specific corrinooid protein—coenzyme M methyltransferase; mtaB, methanol—corrinoid protein Co-methyltransferase. \* and \*\* represents that *E. callanderi* contribute to over 50% and 90% of the abundances, respectively.

### 3.3.2. Putative butyrate synthesis pathway from methanol and CO<sub>2</sub>

The analyzed metagenome was cross-referenced to the Uniref-90 database and then annotated to the Enzyme Nomenclature (EC number system) to validate the presence of putative enzymatic-driven reactions in this study (Fig. 6). Both methanol and CO<sub>2</sub> can be potentially assimilated through the Wood-Ljungdahl pathway (WLP), where two moles of CO<sub>2</sub> are condensed to one mole of acetyl-CoA as shown in green blocks in Fig. 6 [74]. All genes coding for enzymes of the WLP were found to be present and the main contributor was *E. callanderi* (Fig. 6). The only exception was formate dehydrogenase (FDH), which was not originating from *E. callanderi*, as the FDH coding genes were absent in the reference genome of the *E. callanderi* (*E. callanderi* KIST612) [75].

The methyl group of methanol could enter WLP via the methanol:THF methyltransferase system [68]. Generally, the methyltransferase system in acetogenic bacteria includes the [methyl-Co (III)] methanol-specific corrinoid protein] —coenzyme M methyltransferase (MTII, encoded by mtaA), methanol—corrinoid protein Co-methyltransferase (MTI, encoded by mtaB) and a cobalamin or cobamide binding corrinoid protein (CoP) [68]. However, the presence of such a system was only found in the microbiome at pH 7, with a relative abundance of ca.  $3 \times 10^{-8}\%$  of mtaA and mtaB respectively. Yet, the relative abundances were five orders of magnitude lower compared to other present genes, suggesting the utilization of other methyltransferase systems. It is proposed that the methyl group of methanol was transferred by the methionine synthase (MetH) by *E. callanderi* (with the relative abundance of ca. 1 % at all pH values, and over 90 % was contributed by *E. callanderi*). The MetH catalyzed methyltransferase has been reported for methanol utilization in a *Sporomusa ovata* strain [76], in which MetH replaced the function of MTII, although MTI was still required. The mechanism of the methyltransferase system still needs to be investigated.

Butyrate was the dominant product in this study and is commonly known to be synthesized via the reverse β-oxidation pathway (RBO) in chain elongation process [77] (blue blocks and lines in Fig. 6), in which two acetyl-CoA molecules are first converted to one acetoacetyl-CoA molecule catalyzed by acetyl-CoA C-acetyltransferase (ACAT) [78]. The formed acetoacetyl-CoA then enters the RBO to produce butyryl-CoA, which can be converted to butyrate via two enzymatic reactions. The enzymes encoding genes for RBO were found at all pH values, however, they did not originate from *E. callanderi*, as most of the genes related to the reverse β-oxidation are not characterized in the genome of *E. callanderi* to date [75]. The synthesis of butyrate from butyryl-CoA can be catalyzed by butyryl-CoA:acetate CoA-transferase (BCoAT), which transfers the CoA moiety from butyryl-CoA to acetate and thus results in the consumption of acetate [68,79]. The presence of the gene encoding BCoAT was confirmed in the microbial communities, with the relative abundance of ca. 0.01 % at all pH values. The majority of the genes encoding BCoAT were mapped to *E. callanderi*, indicating that *E. callanderi* was one of the main butyrate producers in the culture. In addition, the other possible route from butyryl-CoA to butyrate is via the butyrate kinase (BUK) and phosphate butyryltransferase (PTB) [80,81], which does not require the participation of acetate as the CoA server, and could partly explain the butyrate production pattern at pH 5.5 and 6, which showed the sole butyrate production during the intensive sampling period (Fig. 3). Compared to BCoAT, lower abundances of genes encoding BUK and PTB were observed, with the relative abundances ranging from  $1.2 \times 10^{-4}\%$  to  $2.3 \times 10^{-4}\%$  (BUK) and from  $1.6 \times 10^{-4}\%$  to  $1.2 \times 10^{-3}\%$  (PTB). The genes encoding BUK and PTB are not present in the *E. callanderi* genome, which implies the cooperation of other species for butyrate production. Another evidence for the presence of another species was that for the abundances of genes encoding BUK, most of the contribution was from an unidentified species, which should be further investigated.

In addition to RBO, the fatty acid biosynthesis pathway (FAB) is an alternative route for butyrate production through chain elongation (yellow blocks and lines in Fig. 6). FAB and RBO both initiate from the

acetyl-CoA, yet in FAB, the acetyl-CoA is firstly converted to malonyl-CoA by adding CO<sub>2</sub>, which is driven by acetyl-CoA carboxylase (ACC) and requires ATP input. The malonyl-CoA is further converted to malonyl-acyl carrier protein (malonyl-ACP) by exchanging the CoA moiety which is catalyzed by malonyl transferase (MAT) [82]. The malonyl-ACP is then combined with the acyl-CoA (e.g. acetyl-CoA) to form the β-ketoacyl-ACP (e.g. acetoacetyl-ACP), driven by the ketoacyl synthase (KAS). For the butyrate production, the acetoacetyl-ACP is further converted to butyryl-ACP by the following enzymes: ketoacyl-ACP reductase (KAR), hydroxyacyl-ACP dehydratase (FAB), enoyl-ACP reductase (ENR), subsequently. The presence of genes encoding for all the mentioned enzymes of FAB was confirmed in the microbiome at all pH values, with *E. callanderi* contributing the most abundances for ACC, MAT, KAR and FAB [83]. However, the formation of butyrate from butyryl-ACP remained unclear in this study, as the genes encoding thioesterase (TE) responsible for the carboxylic acid formation from acyl-ACP [84] were not found in the microbiome in any of the pH values. Unlike BCoAT, the carboxylic acid formation from acyl-ACP does not require acetate as the CoA server, which could be another explanation for the butyrate production at pH 5.5 and 6. However, further studies need to be performed to identify the corresponding enzymes to confirm the butyrate production through FAB pathway. It is worth mentioning that FAB is less energy efficient compared to RBO as it requires extra ATP input for the initiation (acetyl-CoA to malonyl-CoA) [85].

The metagenomic data suggests that *E. callanderi* dominated methanol and CO<sub>2</sub> assimilation via the WLP and was likely the main butyrate producer via the RBO pathway. Similar relative abundances of all genes were obtained among different pH values, indicating that the differences in the VFA production could be attributed to differences in gene expression, enzymatic activity, or the fact that pH could affect the competitiveness of competing reactions between acetate and butyrate formation, which requires further validation.

## 4. Conclusions

In methanol assisted MES, a highly selective butyrate production was obtained at pH 6 ( $86.9 \pm 1.5\%$  selectivity), which was higher than at pH 5.5 ( $80.5 \pm 5.9\%$ ) and pH 7 ( $69.8 \pm 7.7\%$ ). The highest butyrate production rate of  $0.3 \text{ g L}^{-1} \text{ d}^{-1}$  was obtained at both pH 6 and 7. Compared to pH 5.5, higher methanol and CO<sub>2</sub> utilization efficiency and more reduced redox potentials were obtained at pH 6 and pH 7. The evaluation of the alignment between experimental results and thermodynamics showed that a thermodynamic model can predict part of the obtained results. However, other factors such as kinetics and microbial metabolism should be considered. Shotgun metagenomic sequencing unraveled that *E. callanderi* was the predominant bacterial species (52.2 to 63.1 % of relative abundance) at all pH levels. It was potentially responsible for the methanol and CO<sub>2</sub> assimilation likely via Wood-Ljungdahl pathway, wherein methanol was likely transferred via the MetH catalyzed methyltransferase to enter the Wood-Ljungdahl pathway. Differences in cathodic pH did not result in significant differences in the relative abundances of genes related to the pathways, suggesting the differences of butyrate selectivity could be due to the enzyme activities or gene expressions.

## CRediT authorship contribution statement

**Hui Yao:** Writing – original draft, Visualization, Methodology, Investigation, Funding acquisition, Formal analysis, Data curation, Conceptualization. **Meritxell Romans-Casas:** Writing – review & editing, Methodology, Investigation, Formal analysis. **Igor Vassilev:** Writing – review & editing. **Johanna M. Rinta-Kanto:** Writing – review & editing, Methodology. **Sebastià Puig:** Writing – review & editing, Supervision, Funding acquisition. **Antti J. Rissanen:** Writing – review & editing, Methodology, Investigation, Formal analysis. **Marika Kokko:** Writing – review & editing, Supervision, Funding acquisition,





- [83] J.P. Torella, T.J. Ford, S.N. Kim, A.M. Chen, J.C. Way, P.A. Silver, Tailored fatty acid synthesis via dynamic control of fatty acid elongation, *Proc. Natl. Acad. Sci.* 110 (2013) 11290–11295, <https://doi.org/10.1073/pnas.1307129110>.
- [84] D.I. Chan, H.J. Vogel, Current understanding of fatty acid biosynthesis and the acyl carrier protein, *Biochem. J.* 430 (2010) 1–19, <https://doi.org/10.1042/BJ20100462>.
- [85] S. Sarria, N.S. Kruyer, P. Peralta-Yahya, Microbial synthesis of medium-chain chemicals from renewables, *Nat. Biotechnol.* 35 (2017) 1158–1166, <https://doi.org/10.1038/nbt.4022>.

1                   **Supplementary Information for the article in Bioelectrochemistry**  
2

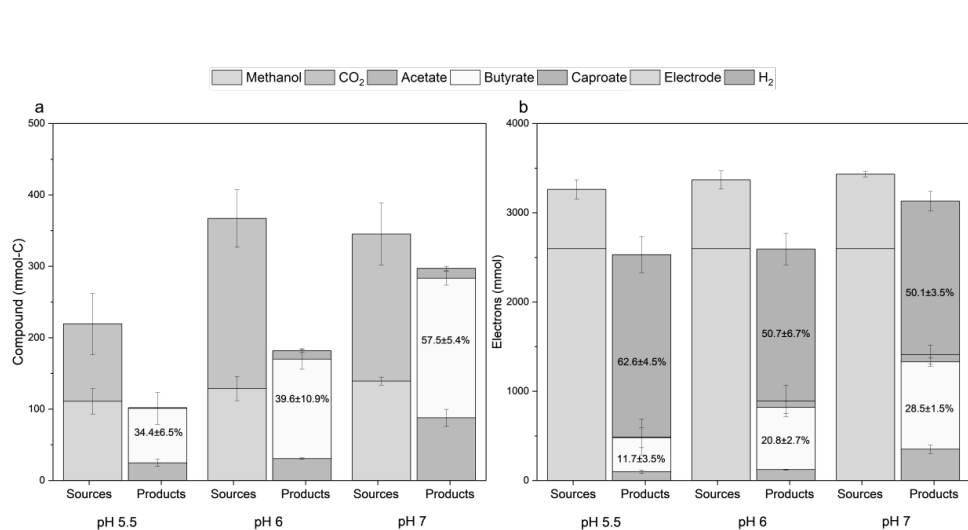
3                   **Selective butyrate production from CO<sub>2</sub> and methanol in  
4 microbial electrosynthesis - influence of pH**

5                   Yao, Hui<sup>1</sup>; Romans-Casas, Meritxell<sup>2</sup>; Vassilev, Igor<sup>1</sup>; Rinta-Kanto, Johanna M<sup>1</sup>; Puig, Sebastià<sup>2</sup>; Rissanen,  
6                   Antti J<sup>1</sup>; Kokko, Marika<sup>1\*</sup>

7                   <sup>1</sup> Faculty of Engineering and Natural Sciences, Tampere University, Korkeakoulunkatu 8, 33720 Tampere, Finland

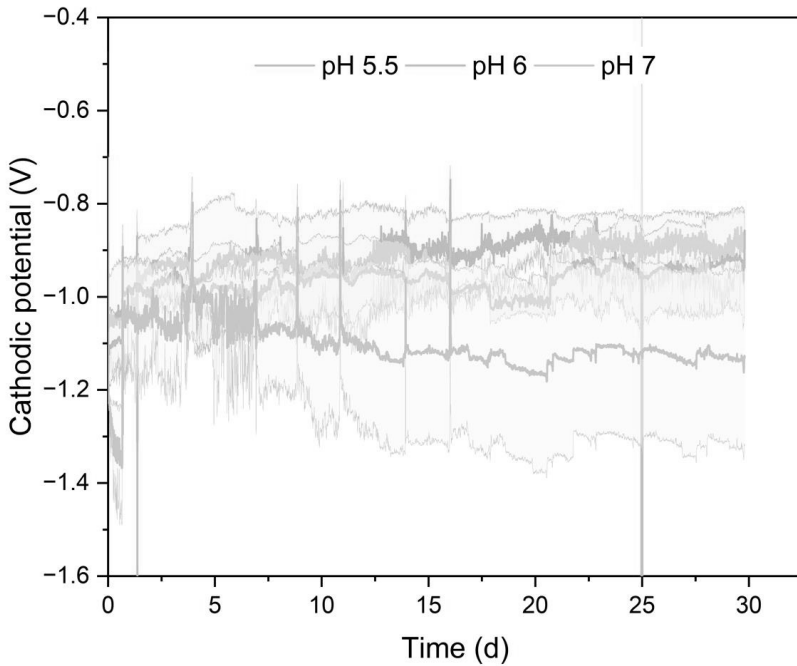
8                   <sup>2</sup> LEQUiA, Institute of the Environment, University of Girona, Campus Montilivi, C/Maria Aurèlia Capmany, 69,  
9                   Girona, E-17003, Spain

10                  \*Corresponding author: [marika.kokko@tuni.fi](mailto:marika.kokko@tuni.fi)

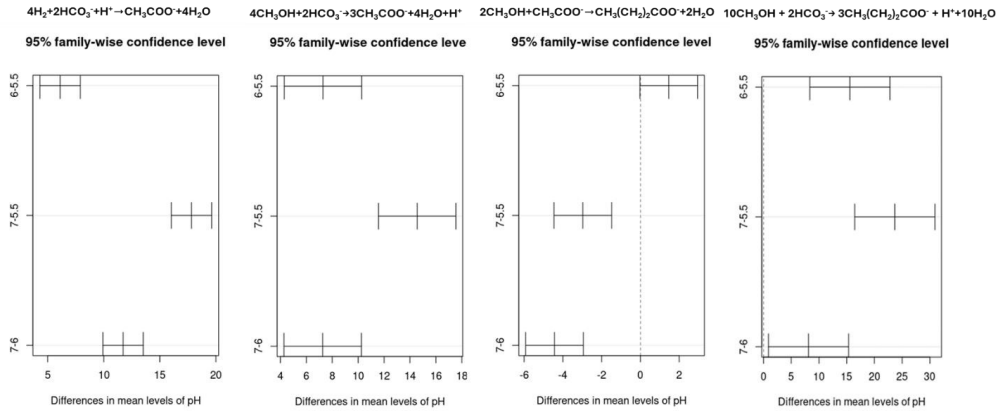


14

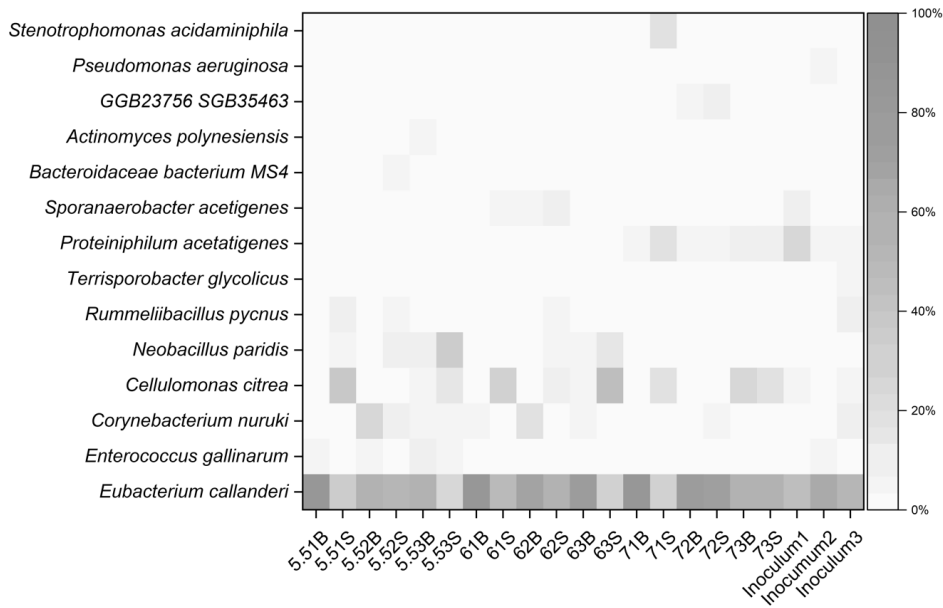
15                  Figure S1. Carbon (a) and electrons (b) present in the feedstocks (sources) and in the products. Error bars indicate the results  
16                  from triplicate MES runs. Specifically, the percentage of butyrate recovered from the sources were added to figures a and b, and  
17                  the percentage of H<sub>2</sub> recovered from the electron sources were added to the figure b.



18  
19 *Figure S2.* Cathodic potential within 30 days. The standard deviations of triplicate MES runs are shown in shades with the  
20 corresponding colors.



21  
22 *Figure S3.* Statistical analysis (Tukey HSD post HOC) for the thermodynamic results by using the  $\Delta G'$  based on experimental  
23 results for all pH values.

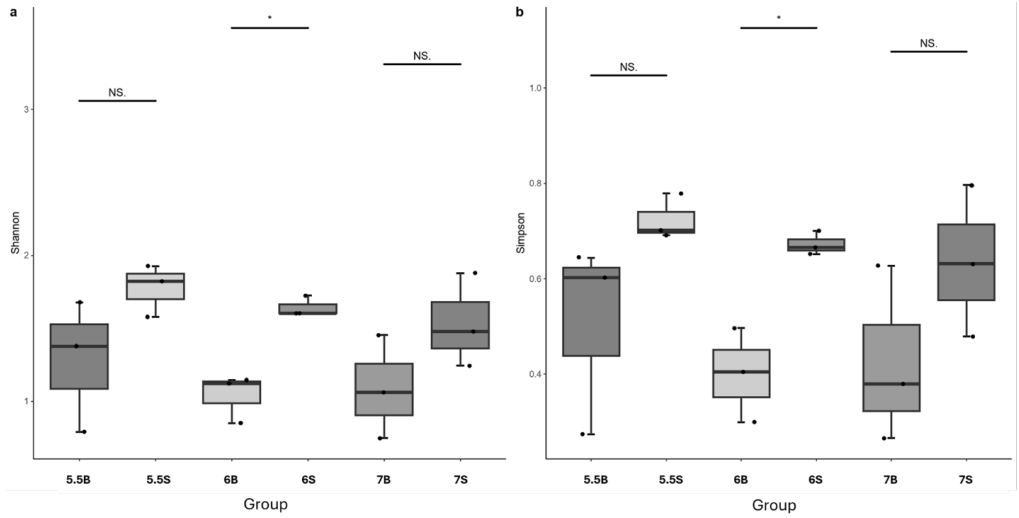


24

25 *Figure S4. Heatmap of the microbial composition including biofilm (B), suspended (S) and inoculum (Inoculum) samples at*  
 26 *species level. The results with relative abundance below 1% were left out. The initials on x-axis were named as: the pH value,*  
 27 *batch number, and sample type. For example, 5.51B represented the result from the first batch of biofilm samples at pH 5.5.*

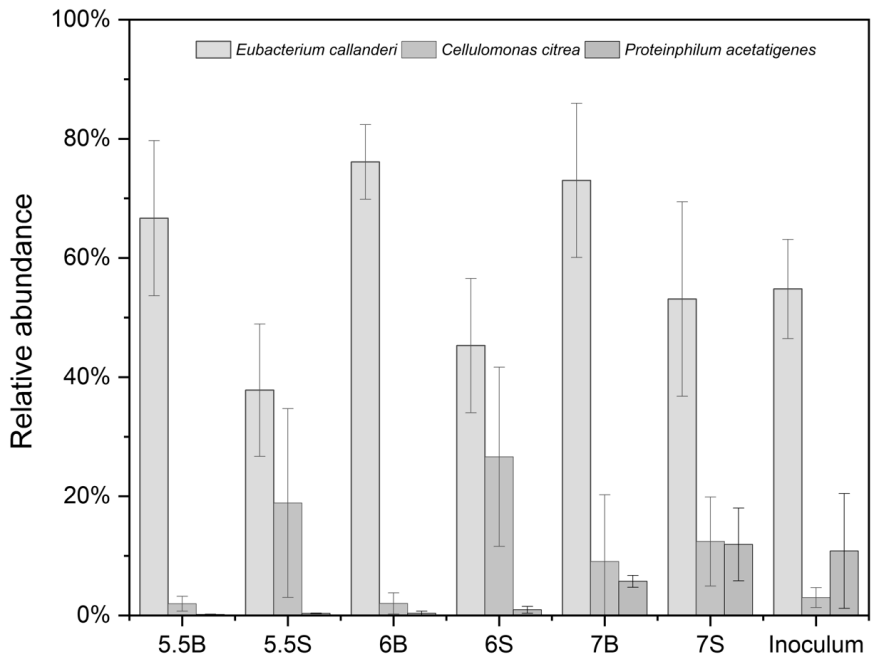
28

29



30

31 *Figure S5. Alpha diversities of the microbiome at the different pH values. Shannon (a) and Simpson (b) indices are plotted, in*  
 32 *which 5.5, 6 and 7 represent the samples from pH 5.5, 6 and 7, respectively. B stands for the biofilm samples and S stands for the*  
 33 *suspended samples. Symbol \* represents the significant difference ( $p<0.05$ , and NS. is the abbreviation for not significant*  
 34 *( $p>0.05$ ).*



35

36 *Figure S6. The relative abundance of *Eubacterium callanderi*, *Cellulomonas citrea* and *Proteiniphilum acetatigenes* from biofilm*  
 37 *(B), suspended (S) and inoculum (Inoculum) samples. Relative abundance was calculated based on the reads of each species*  
 38 *versus the whole reads. Error bars indicate the results from triplicate MES runs.*

39

40

41

Table S1. Composition of the biological medium.

Compound	Concentration (g/L)		
	pH 5.5	pH 6	pH 7
Na <sub>2</sub> HPO <sub>4</sub>	0.70	2.18	14.45
KH <sub>2</sub> PO <sub>4</sub>	16.06	14.64	2.89
NH <sub>4</sub> Cl		3.0	
CaCl <sub>2</sub>		0.015	
MgSO <sub>4</sub> ·7H <sub>2</sub> O		0.02	
sodium 2-bromoethanesulfonate		2.1	
yeast extract		1.0	
trace elements *		10 mL/L	
vitamin solution *		1 mL/L	

42 \*: The composition of trace elements solution and vitamin solution can be found at Yao *et al.*<sup>1</sup>

43

44 Table 2. Gibbs free energy of the reactions described in this study.

Reactions	KJ/mol	KJ/reaction
	ΔH-TS	ΔG 35°C
2CH <sub>3</sub> OH + CH <sub>3</sub> COO <sup>-</sup> → CH <sub>3</sub> (CH <sub>2</sub> ) <sub>2</sub> COO <sup>-</sup> + 2H <sub>2</sub> O	-129	-108.0 <sup>2</sup>
4CH <sub>3</sub> OH + 2HCO <sub>3</sub> <sup>-</sup> → 3CH <sub>3</sub> COO <sup>-</sup> + 4H <sub>2</sub> O + H <sup>+</sup>	-233	-180.2 <sup>3</sup>
4H <sub>2</sub> + 2HCO <sub>3</sub> <sup>-</sup> + H <sup>+</sup> → CH <sub>3</sub> COO <sup>-</sup> + 4H <sub>2</sub> O	-245	-140.6 <sup>4</sup>
10CH <sub>3</sub> OH + 2HCO <sub>3</sub> <sup>-</sup> → 3CH <sub>3</sub> (CH <sub>2</sub> ) <sub>2</sub> COO <sup>-</sup> + H <sup>+</sup> + 10H <sub>2</sub> O	-472	-544.2 <sup>5</sup>

45

46

47

48

49

*Table 3. Repeated measures ANOVA test for production rates and concentrations among pH 5.5, 6 and 7 results.*

<b>Concentrations</b>	<b>SS</b>	<b>df</b>	<b>MS</b>	<b>F</b>	<b>P-value</b>	<b>F crit</b>
Acetate	75578.03	2	37789.01	129.4539	3.3E-27	3.0976980
Butyrate	25107.24	2	12553.62	48.63805	4.78E-15	3.0976980
Total products	55948.37	2	27974.18	47.28949	0.001646	6.944272
<b>Production rates</b>	<b>SS</b>	<b>df</b>	<b>MS</b>	<b>F</b>	<b>P-value</b>	<b>F crit</b>
Acetate	0.032579	2	0.01629	9.211619	0.031822	6.944272
Butyrate	0.059509	2	0.029755	11.01554	0.023612	6.944272
Butyrate selectivity	0.044914	2	0.022457	7.070986	0.048613	6.944272

50

51

52

*Table 4. Final concentrations of all detected products at all pH (mM).*

<b>pH</b>	<b>Catholyte (mM)</b>						<b>Anolyte (mM)</b>		
	<b>Acetate</b>	<b>Propionate</b>	<b>i-butyrate</b>	<b>n-butyrate</b>	<b>Valerate</b>	<b>Caproate</b>	<b>Acetate</b>	<b>n-butyrate</b>	<b>Methanol</b>
5.5	32.95	0.48	0.35	44.71	1.11	2.41	17.96	2.19	15.04
6	39.12	0.87	0.69	76.02	1.47	4.13	13.83	1.52	1.56
7	75.45	1.62	0.70	89.24	2.15	4.09	12.69	1.18	0

53

54

55

56

57

58

59

60

61

62

63

64

65

66

67

*Table 5. Concentrations of VFAs and methanol during the intensive sampling period (mM).*

	Hours	Acetate	Butyrate	Caproate	Methanol
pH 5.5	0	20.9	28.7	1.4	113.4
	6	19.3	29.6	1.5	116.6
	20	20.0	29.3	1.5	104.4
	26	19.4	32.3	1.6	94.1
	31	20.6	34.7	1.6	100.6
	48	19.2	33.3	1.7	94.6
pH 6	0	27.5	53.5	2.4	37.1
	6	30.6	57.4	2.6	38.9
	20	34.9	57.4	2.7	29.2
	26	34.8	67.3	2.7	26.3
	31	36.6	70.8	2.7	25.6
	48	33.4	71.2	3.0	22.9
pH 7	0	75.4	67.4	2.4	18.9
	6	75.4	62.6	2.3	13.0
	20	95.7	68.2	2.6	0
	26	90.9	82.2	2.7	0
	31	85.0	82.6	2.7	0
	48	73.6	89.3	2.9	0

68

69

70

*Table 6. Two-way PERMANOVA test for the alpha diversity of the microbiome at all pH values.*

Factors	df	SumOfSqs	R2	statistic	p.value
pH	2	0.1945141	0.067736768	0.9586838	0.420
Type(biofilm/ planktonic)	1	1.4369909	0.500411572	14.1647280	0.004
pH : Type	2	0.0227306	0.007915607	0.1120302	0.897
Residual	12	1.2173825	0.423936053	NA	NA
Total	17	2.8716181	1.000000000	NA	NA

71

72

73

74

75

*Table 7. Two-way PERMANOVA test for the beta diversity of the microbiome at all pH values.*

76

<b>Factors</b>	<b>df</b>	<b>SumOfSqs</b>	<b>R2</b>	<b>statistic</b>	<b>p.value</b>
pH	2	0.305	0.269	4.39	0.008
Type (biofilm/planktonic)	1	0.365	0.322	10.5	0.002
pH : Type	2	0.0471	0.0414	0.676	0.633
Residual	12	0.417	0.368	NA	NA
Total	17	1.14	1	NA	NA

77

78 **References:**

- 79 1 H. Yao, J. M. Rinta-Kanto, I. Vassilev and M. Kokko, *Appl Microbiol Biotechnol*, 2024, **108**, 372.  
 80 2 M. T. Agler, B. A. Wrenn, S. H. Zinder and L. T. Angenent, *Trends in biotechnology*, 2011, **29**, 70–78.  
 81 3 S. Pacaud, P. Loubiere and G. Goma, *Current Microbiology*, 1985, **12**, 245–250.  
 82 4 J. A. Breznak and M. D. Kane, *FEMS microbiology reviews*, 1990, **7**, 309–313.  
 83 5 S. Huang, R. Kleerebezem, K. Rabaey and R. Ganigué, *Appl Microbiol Biotechnol*, 2020, **104**, 5119–5131.  
 84



# PUBLICATION

|||

**Optimizing butyrate production from methanol and CO<sub>2</sub> in microbial electrosynthesis**

Yao, H., Dessì, P., Romans-Casas, M., Puig, S., Kokko, M.

Bioresource Technology 437, 133150  
<https://doi.org/10.1016/j.biortech.2025.133150>

**Publication is licensed under a Creative Commons Attribution 4.0 International License CC BY**





## Optimizing butyrate production from methanol and CO<sub>2</sub> in microbial electrosynthesis

Hui Yao<sup>a</sup> , Paolo Dessì<sup>c</sup> , Meritxell Romans-Casas<sup>b</sup> , Sebastià Puig<sup>b</sup> , Marika Kokko<sup>a,\*</sup>

<sup>a</sup> Faculty of Engineering and Natural Sciences, Tampere University, Korkeakoulunkatu 8, 33720 Tampere, Finland

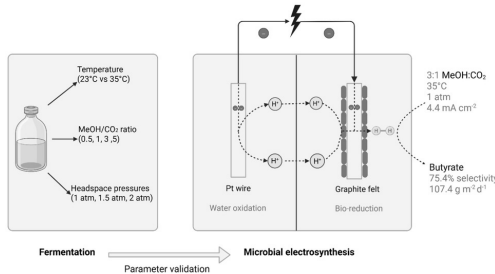
<sup>b</sup> LEQUiA, Institute of the Environment, University of Girona, Campus Montilivi, C/Maria Aurèlia Capmany, 69, Girona 17003, Spain

<sup>c</sup> Department of Agricultural Sciences, University of Naples Federico II, Piazza Carlo di Borbone 1, 80055 Portici, Italy

### HIGHLIGHTS

- MeOH/CO<sub>2</sub> ratios, temperatures and gas pressures were optimized in gas fermentation.
- Butyrate production was ceased at 23 °C.
- Optimal butyrate production obtained at 35 °C, 3:1 MeOH/CO<sub>2</sub> ratio, and 1 atm.
- Optimal scenario was validated in MES: butyrate production rate of 107 g m<sup>-2</sup> d<sup>-1</sup>.
- 3:1 MeOH/CO<sub>2</sub> ratio enhanced the methanol utilization rate.

### GRAPHICAL ABSTRACT



### ARTICLE INFO

**Keywords:**  
Microbial electrosynthesis  
Butyrate  
Methanol  
Carbon dioxide  
Process optimization

### ABSTRACT

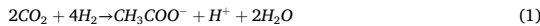
Microbial electrosynthesis (MES) enables the conversion of carbon dioxide (CO<sub>2</sub>) into valuable chemicals utilizing renewable electricity. Acetate is often the main product but supplying a soluble electron donor facilitates upgrading acetate to butyrate via chain elongation. Compared to ethanol as the electron donor, methanol is a promising alternative as its production avoids the competition with food production. However, the optimal operation conditions for maximizing butyrate production rates in methanol assisted MES have not yet been determined. In this study, methanol assisted chain elongation process was first evaluated in batch bottles to set up the optimal scenario for butyrate production. The highest butyrate production rates and titers were achieved at 35 °C temperature, 1 atm headspace pressure, and a methanol/CO<sub>2</sub> ratio of 3 (on a carbon basis). These operational conditions were subsequently applied to a MES cell operated in fed-batch mode, obtaining a remarkable average butyrate production rate of  $107.4 \pm 19.7 \text{ g m}^{-2} \text{ d}^{-1}$  and a selectivity of  $75.2 \pm 1.1 \%$ . In particular, temperature was a pivotal factor determining butyrate productivity. At 23 °C, regardless of changes in pressure or methanol/CO<sub>2</sub> ratio, acetate remained the main product (with selectivity over 80 %) in both fermentation batch bottles and in MES. In conclusion, this study not only provided a comprehensive multi-variable analysis to optimize key operational parameters for methanol assisted chain elongation but also demonstrated an effective strategy for butyrate production from CO<sub>2</sub> and methanol in MES.

\* Corresponding author.

E-mail address: marika.kokko@tuni.fi (M. Kokko).

## 1. Introduction

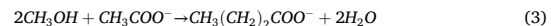
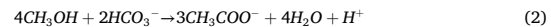
Carbon dioxide ( $\text{CO}_2$ ) can be seen as a critical feedstock for producing a plethora of commodities, such as biofuels and platform chemicals offering a pathway towards carbon neutrality (Appel et al., 2013). Among the existing  $\text{CO}_2$  conversion routes, the Wood-Ljungdahl pathway (WLP) is the most ancient and energetically favorable, considering the net adenosine triphosphate (ATP) input (Zhao et al., 2021). In WLP, acetogenic bacteria reduce  $\text{CO}_2$  into biochemicals using hydrogen ( $\text{H}_2$ ) as an electron donor (Ragsdale and Pierce, 2008), and resulting in the formation of acetyl-CoA, which can be further converted to acetate (Eq. (1)) or reduced to valuable compounds (Ragsdale and Pierce, 2008).



Several biological processes have employed acetogenic bacteria for the biochemical production from  $\text{CO}_2$ . For example, gas fermentation is a process where microorganisms convert gaseous substrates (carbon monoxide ( $\text{CO}$ ),  $\text{CO}_2$  and  $\text{H}_2$ ) into biochemicals. However, the gas fermentation kinetics are limited by mass transfer of gases to the liquid phase (Ale Enríquez and Ahring, 2023). An alternative biological  $\text{CO}_2$  fixation method is microbial electrosynthesis (MES). In MES, acetogens are cultivated in an electrochemical cell by utilizing electrons from a cathode electrode as reducing power (Nevin et al., 2010). In situ produced  $\text{H}_2$  at the cathode serves as the electron donor for acetogens to reduce  $\text{CO}_2$  via the WLP, with acetate being often the primary product (Jourdin and Burdyny, 2021).

MES, additional electron donors could facilitate the chain elongation process and yielding spectrum of products including short to medium-chain carboxylic acids (Izadi et al., 2021; Romans-Casas et al., 2024; Vassilev et al., 2018). The most common electron donor in MES is ethanol, which shifts the production from acetate to butyrate (Vassilev et al., 2019), butanol (Romans-Casas et al., 2024), and caproate (Jiang et al., 2020). However, the current ethanol production is mainly crop-based and raises concerns between food and fuels competition (Joyia et al., 2024). Methanol can be a great substitute for ethanol as electron donor for chain elongation. Currently, methanol is primarily produced from natural gas-derived syngas, with an annual global production of approximately 110 million metric tons, making it a low-cost and well established feedstock chemical (Tabibian and Sharifzadeh, 2023). Moreover, methanol can potentially be synthesized from biomass-derived gases (Varela et al., 2024) or directly from  $\text{CO}_2$  via electrochemical routes (Lee et al., 2024), though the electrochemical methanol synthesis from  $\text{CO}_2$  is still in the early stages of development and primarily limited to laboratory-scale applications (Li et al., 2024a). In bioproduction processes, the utilization of methanol has been extensively explored since the 1970 s (Taylor and Senior, 1978), and anaerobic methylotrophic archaea and acetogenic bacteria have been widely reported for natural methanol assimilation (Kremp and Müller, 2021). For example, *Eubacterium limosum* is a well-known bacteria for methanol assimilation, starting by transferring the methyl group of methanol to tetrahydrofolate (THF), which is further reduced via the WLP, releasing reducing equivalents that not only promote the production of acetate (Eq. (2)), but also the production of butyrate (Eq. (3)), butanol and caproate (Kremp and Müller, 2021; Wood et al., 2022). Therefore, methanol was used by mixed cultures to conduct the chain elongation process from acetate for butyrate, isobutyrate and caproate production by utilizing the reducing power of methanol (Chen et al., 2017, 2016; De Leeuw et al., 2020). Moreover, the addition of methanol has been shown to enhance performance of both gas fermentation and MES processes (Kim et al., 2021; Yao et al., 2024). In gas fermentation, adding methanol along with  $\text{H}_2/\text{CO}_2$  boosted the microbial growth rates by four-fold and the  $\text{H}_2$  consumption rate by 2.7-fold (Yasin et al., 2015). The addition of methanol along with  $\text{CO}_2$  in MES shifted the product spectrum from acetate towards butyrate (82 % selectivity), resulting in

1.8-fold higher production rates and 1.7-fold higher titer than using  $\text{CO}_2$  as the sole substrate (Yao et al., 2024).



In this study, methanol was chosen as the electron donor not only for its metabolic compatibility with *E. limosum*, but also due to its lower cost and the non-competition with food resources. The *Eubacterium*-dominated microbiome was not selected, but has been continuously enriched in over three-years cultivations when fed only with methanol and  $\text{CO}_2$ . Although methanol has shown potential to enhance the performance of MES, operational parameters remain underexplored in methanol assisted MES. So far, only the cathodic pH has been optimized, obtaining a selective butyrate production (87 % selectivity) at pH 6 (Yao et al., 2025). Other operational parameters including temperature, headspace pressure, and methanol/ $\text{CO}_2$  ratio could also potentially affect the methanol assisted MES. Acetogenic bacteria are generally grown in mesophilic conditions and thus most of the MES studies have been conducted between 20 °C to 37 °C (Yang et al., 2018). Within this range, temperature can also affect the MES performance. For example, a mixed culture study carried out by Yang et al. (2021) compared the performance of  $\text{CO}_2$ -fed MES from 10 °C to 70 °C, which showed a slightly higher acetate titer of  $525.8 \pm 1.5 \text{ mg L}^{-1}$  at 25 °C compared to the titer of  $468.5 \pm 7.1 \text{ mg L}^{-1}$  at 35 °C, yet a higher acetate production rate at 35 °C ( $49.2 \pm 0.5 \text{ mg L}^{-1}\text{d}^{-1}$ ) compared to 25 °C ( $25.3 \pm 1.5 \text{ mg L}^{-1}\text{d}^{-1}$ ) (Yang et al., 2021). Specifically, the experimental temperatures of 23 °C and 35 °C were interesting based on prior studies and practical considerations. While 37 °C is reported as the optimal growth temperature for *E. limosum*, 35 °C has been widely used in both pure culture studies (Flaiz et al., 2024; Shin et al., 2023) and mixed-culture methanol-based chain elongation and MES systems (Chen et al., 2017; De Smit et al., 2019; Rode et al., 1981). On the other hand, 23 °C was chosen to evaluate system performance under room temperature conditions, offering insights relevant to scale-up and environmental variability. The partial pressures of  $\text{H}_2$  ( $P_{\text{H}_2}$ ) and  $\text{CO}_2$  ( $P_{\text{CO}_2}$ ) are other key parameters that affect microbial metabolism and bioproduction in both gas fermentation and MES (Romans-Casas et al., 2024; Skidmore et al., 2013; Yerushalmi et al., 1985). For instance, increasing the headspace pressure in gas fermentation has been shown to improve the gas to liquid mass transfer and thus improve the overall production and biomass growth (Oswald et al., 2018; Van Hecke et al., 2019). In MES, sustaining a  $P_{\text{CO}_2}$  of 1.5 atm by daily replenishment was an efficient strategy to promote selective butyrate production (bringing to a 78 % selectivity on a carbon basis) with  $\text{CO}_2$  as the only carbon source (Romans-Casas et al., 2024). Lastly, the methanol/ $\text{CO}_2$  ratios could also potentially affect the product spectrum. High ratios could promote production of more reduced products over acetate. As reported in a fermentation study by Wood et al., (2022) increasing the methanol to formate ratio above five (mol/mol) induced the production of butanol by *E. limosum*. Although the influence of the aforementioned process parameters could offer valuable insights into the role of methanol and its potential to enhance butyrate production, these factors have, to the best of our knowledge, not been extensively explored within the context of methanol-assisted gas fermentation and microbial electrosynthesis (MES) processes.

Therefore, this study investigated the effects of key operational parameters — temperature, methanol/ $\text{CO}_2$  ratios, and headspace partial pressures — on methanol assisted MES as a basis for process optimization in terms of production rates, titers and selectivity. Various combinations of these operational parameters were first tested under gas fermentation conditions in serum flasks fed with methanol and  $\text{H}_2/\text{CO}_2$ . The obtained results were subsequently validated in MES reactors operating in fed-batch mode and fed with methanol and  $\text{CO}_2$  providing insights for further steps in process intensification.

## 2. Materials and methods

### 2.1. Inoculum and medium

An *Eubacterium* sp. dominated mixed culture was obtained from the cathodic chamber of a MES reactor (Yao et al., 2024) and used as the inoculum in this study. The catholyte from the inoculum reactor was added to the fresh biological medium with a 1:10 (v/v) ratio to start the experiments. The medium was a phosphate buffered biological medium prepared by following the recipe in the supplementary information. Before the inoculation, N<sub>2</sub> was sparged through the medium to eliminate dissolved oxygen.

### 2.2. Fermentation in serum flasks

The working volume of the serum flask was 40 mL with an 80 mL headspace volume. The effect of operational parameters on fermentative carboxylate production from methanol, CO<sub>2</sub> and H<sub>2</sub> were tested in serum flasks in duplicate for seven days (Table 1). Parameters of interest included temperature, methanol/CO<sub>2</sub> feeding ratios, P<sub>H2</sub> and P<sub>CO2</sub>. The initial pH of the fermentation broth was set at 7.2 for all conditions. The flasks were sealed and placed under agitation at 120 rpm at either room temperature (23 °C) or in a temperature-controlled incubator (35 °C). Different initial methanol/CO<sub>2</sub> ratios (from 0.5 to 5) were set by supplementing methanol from a stock solution (0.2 to 2.3 mol L<sup>-1</sup>), every two to three days for a total of three additions. A gas mixture of 80 % H<sub>2</sub> and 20 % CO<sub>2</sub> was used to sparge the flasks and then to apply pressures of either 1, 1.5 or 2 atm. Both liquid and gas samples were collected daily, accompanied with sparging the serum flasks for three minutes and regulating the headspace pressures via a gas manometer (Leo1 Keller, Switzerland).

### 2.3. MES reactor set-up and operation

Based on fermentation experiment results, two different operational parameter combinations were evaluated with the aim of achieving selective production of butyrate or acetate in methanol-assisted MES. One

combination (35 °C, atmospheric pressure, and methanol/CO<sub>2</sub> ratio of 3) was aiming for optimal butyrate production (MES-35). Another combination (23 °C, maximum overpressure of 1.5 atm and ratios ranging from 0.3 to 1) was aiming to achieve selective acetate production (MES-23). As proposed by Yao et al. (2025), the pH in the MES experiments was manually adjusted to above 6 using 3 mol L<sup>-1</sup> NaOH when it fell below 6 to prevent potential inhibition of methanol utilization.

To maintain overpressure requirements, two commercial, pressurizable electrochemical cells (MicroFlowCell, ElectroCell, Denmark) were employed to conduct MES-23 experiments. Carbon felt (99 %, Fisher scientific, Spain) and a dimensionally stable electrode (DSA-O2) with projected surface areas of 10 cm<sup>2</sup> each were used as the cathode and anode, respectively. The working volumes of the cathode and anode chambers were 4 and 3 mL, respectively, separated by a reinforced cation exchange membrane (CEM, Nafion N324, USA) (Romans-Casas et al., 2024). Both the cathode and anode were connected to their respective recirculation bottles through recirculation lines using a peristaltic pump (Watson Marlow 205U, UK) with a flow rate of 5.2 mL min<sup>-1</sup>. Anodic recirculation bottles were open to the ambient atmosphere, while the cathodic recirculation bottles were sealed to prevent gas leakage (headspace volume of 76 mL). The total volume of both catholyte and anolyte was 80 mL. A reference electrode (Ag/AgCl, +0.197 V vs. SHE, RE-5B, BASI, USA) was inserted into the anodic recirculation line.

The MES-23 experiments lasted for 70 days, during which CO<sub>2</sub> was sparged through the cathodic recirculation bottles for three minutes every two to three days, after which an initial P<sub>CO2</sub> of 1.5 atm was set by closing the gas outlet. The cells were operated in two-electrode configuration and in galvanostatic mode by using a potentiostat (VSP, Bio-Logic, France). The applied current density was set to 1.5 mA cm<sup>-2</sup> from days 0 to day 43, and 3.0 mA cm<sup>-2</sup> from day 43 to day 70, while cell voltage was continuously monitored. The methanol addition ranged from 12 mmol per week to 2 mmol per week to maintain methanol/CO<sub>2</sub> ratios between 0.3 and 1.

As the MES-35 experiments did not require overpressure condition, a two-chamber flat-plate reactor was used, with a working volume of 23

**Table 1**

Operational parameters tested as fermentation process in shake flasks, and the results obtained for biomass growth (as OD<sub>600</sub>), net production of acetate and butyrate, butyrate selectivity (S<sub>B</sub>) and carbon conversion efficiency (CCE). All the runs were run as duplicates for seven days.

Operation conditions			Results				
T (°C)	p (atm)	Methanol/ CO <sub>2</sub> ratio	OD <sub>600</sub> (nm)	Acetate produced (mmol·G)	Butyrate produced (mmol·G)	S <sub>B</sub> (%)	CCE (%)
23	1	0.5	2.1 ± 0.2	3.09 ± 0.77	0.32 ± 0.32*	7.1 ± 7.1*	77.6 ± 4.3
		1	2.2 ± 0.4	2.66 ± 0.24	0.15 ± 0.15*	4.8 ± 4.8*	52.1 ± 3.9
		3	1.9 ± 0.2	3.99 ± 0.60	0.11 ± 0.11*	2.4 ± 2.4*	63.6 ± 7.8
	1.5	5	1.3 ± 0.2	2.45 ± 0.91	—	—	23.2 ± 11.3
		0.5	1.3 ± 0.1	3.93 ± 0.05	—	—	67.7 ± 4.4
		1	1.4 ± 0.2	2.87 ± 2.20	—	—	33.0 ± 22.5
	2	3	1.2 ± 0.2	3.76 ± 0.31	0.02 ± 0.02*	0.6 ± 0.6*	23.8 ± 4.6
		5	1.0 ± 0.3	3.03 ± 0.27	—	—	22.4 ± 5.2
		0.5	2.2 ± 0.1	5.42 ± 0.24	0.10 ± 0.03	1.8 ± 0.6	61.6 ± 0.8
35	1	1	0.8 ± 0.0	2.69 ± 0.53	—	—	40.8 ± 2.3
		3	2.3 ± 0.1	5.75 ± 0.12	0.08 ± 0.06	1.5 ± 1	27.7 ± 1.9
		5	2.4 ± 0.0	5.95 ± 0.30	0.12 ± 0.04	2.0 ± 0.6	18.2 ± 1.7
	1.5	0.5	2.3 ± 0.4	3.79 ± 0.03	0.81 ± 0.20	17.5 ± 3.5	96.1 ± 13.1
		1	3.4 ± 0.5	2.94 ± 1.03	1.03 ± 0.31	25.5 ± 6.1	58.3 ± 9.2
		3	3.0 ± 0.4	3.11 ± 2.61	2.61 ± 0.09	45.7 ± 3.7	62.5 ± 0.8
		5	2.4 ± 0.3	2.82 ± 2.42	2.42 ± 0.38	46.0 ± 5.5	46.3 ± 10.1
		0.5	2.6 ± 0.3	3.30 ± 0.27	2.53 ± 0.13	43.4 ± 0.7	56.5 ± 3.5
	2	1	3.0 ± 0.0	3.88 ± 0.86	3.10 ± 0.22	45.0 ± 3.8	52.1 ± 2.2
		3	2.7 ± 0.3	3.61 ± 0.33	3.45 ± 0.33	48.9 ± 0.1	32.3 ± 4.1
		5	2.8 ± 0.1	4.31 ± 0.20	3.16 ± 0.30	42.2 ± 1.2	27.4 ± 1.1
		0.5	2.0 ± 0.1	6.23 ± 0.21	1.29 ± 0.52	16.9 ± 6.2	61.9 ± 0.4
		1	2.6 ± 0.0	5.48 ± 0.24	1.82 ± 0.27	25.0 ± 3.6	45.3 ± 2.7
	3	3	3.5 ± 0.1	5.17 ± 0.34	2.21 ± 0.35	29.7 ± 2.0	33.1 ± 0.6
		5	2.9 ± 0.03	3.93 ± 0.59	2.51 ± 1.62	35.8 ± 19.4	20.7 ± 5.1

Symbol \* denotes only one of the duplicates produced butyrate.

mL in each chamber. The chambers were separated by a cation exchange membrane (CXM-200, Membrane International, USA), with an active surface area of 20 cm<sup>2</sup>. The cell was operated under galvanostatic mode, controlled by a potentiostat (VMP3, BioLogic, France). A platinum wire (0.4 mm, 99.95 %, Advent Research Materials, UK) was used as the anode electrode. Graphite felt (99.9 %, Thermo Scientific, USA) was pierced by stainless steel wire (current collector) and placed in the center of the cathodic chamber as the cathode (projected surface area of 20 cm<sup>2</sup>). The electrodes and membrane were placed tightly to reduce energy losses due to internal resistance. A reference electrode (SE11NSK7, Sensorschrein Meinsberg, Germany) was integrated into the cathodic recirculation line close to the outlet (ca. 10 cm) of the cathode chamber via a sealed glass vial. The total volume of catholyte and anolyte were 360 mL and 200 mL, respectively. Each chamber was connected to a recirculation bottle, and the electrolytes were circulated at a flow rate of 40 mL min<sup>-1</sup> (Masterflex L/S Digital Drive pump). The cathodic recirculation bottle was connected to a gas bag to prevent overpressures and collect gases, while the anodic recirculation bottles were open to ambient conditions.

The MES-35 experiments lasted for 30 days, with gas sparging, methanol addition, and sampling occurring three times a week. In order to obtain the 80 % H<sub>2</sub> and 20 % CO<sub>2</sub> headspace gas composition during each fed-batch cycle, the cell was operated at a current of -87 mA (4.4 mA cm<sup>-2</sup>), and CO<sub>2</sub> was sparged through the cathodic recirculation bottles and collected in the gas bags for ten minutes at a flow rate of 50 mL min<sup>-1</sup> (F-201CV, Bronkhorst, the Netherlands). The experiments were initiated by adding 180 mM methanol to the cell, and methanol concentration was maintained at 120 mM for two days and 180 mM for the following three days to achieve a target dosing rate of 60 mM d<sup>-1</sup>, thereby sustaining a 3:1 methanol/CO<sub>2</sub> ratio (carbon basis) in each fed-batch cycle. Residual methanol concentration in the catholyte was measured before CO<sub>2</sub> sparging, and the required amount was manually added to adjust the concentration accordingly. Both liquid and gas samples were collected every two to three days.

#### 2.4. Analyses and calculations

Gas and liquid samples were taken two to three days per week. Gas pressure was measured with a pressure meter (differential pressure gauge, Testo 512, Spain). Gas composition was analyzed by a gas chromatograph equipped with a thermal conductivity detector (GC-TCD, Shimadzu, Japan) and Agilent J&W packed GC column (2.00 mm internal diameter, 1.8 m length) or another GC-TCD (Micro GC 490, Agilent Technologies, USA) with two columns: a CP-Molesieve 5A column, and a CP-Poraplot U column. When using gas bags, the gas amount was quantified by the water displacement method to measure the gas volume inside the bags. The headspace pressure and volume were used for calculating gas volumes in fermentation and MES-23 experiments. Liquid samples (3 mL) were taken from both cathodic and anodic recirculation bottles in MES three times a week or daily for fermentation experiments, and analyzed for pH, optical density (OD), and the organics. The pH and OD<sub>600</sub> were measured with a pH meter (Basic 20+, Crison Instruments, Spain or pH 3320, WTW, Germany) and a spectrophotometer (DR3900, Hach, Germany or UV-1800, Shimadzu, Japan), respectively. The remaining samples were filtered (0.2 µm) and analyzed by GC equipped with a flame ionization detector (GC-FID, GC 7890 A, Agilent Technologies, USA) using a DB-FFAP column or a GC-FID (GC-2010, Shimadzu, Japan) with a Zebron column (ZB-WAX plus, 0.25 µm diameter, 30 m length). Further details can be found in Romans-Casas et al., (2024) and in Yao et al., (2024), respectively.

The selectivity of the compound *i* was calculated according to Eq. (4):

$$\text{Selectivity}_i = \frac{n_i}{n_{\text{sum}}} \times 100 \quad (4)$$

where selectivity of compound *i* is defined as the ratio of amount of

compound *n<sub>i</sub>* and the total amount of organic products *n<sub>sum</sub>* in mol-C.

The yield of the compound *i* was calculated with Eq. (5):

$$\text{Yield}_i = \frac{n_i}{n_{(\text{carbon dioxide})} + n_{(\text{methanol})}} \quad (5)$$

where *n<sub>i</sub>* is the amount of compound *i* in mol-C, *n<sub>(carbon dioxide)</sub>* and *n<sub>(methanol)</sub>* are the amounts of consumed CO<sub>2</sub> and methanol in mol-C, respectively.

The faradaic efficiency (FE) of the compound *i* was calculated according to Eq. (6):

$$FE_i = \frac{F \times n_i \times z_i}{\int Idt + F \times n_{Me} \times z_{ME}} \times 100 \quad (6)$$

where *FE<sub>i</sub>* is defined as the ratio of electrons transferred to product *i* and the total electrons provided, *z<sub>i</sub>* represent the number of electrons transferred to each molecule of the product *i*. *F* is faradaic constant (96485 C mol<sup>-1</sup> electron), *n* is the amount of product *i* (mol), and *Idt* is the current consumed along the considered time (Ah).

The total carbon conversion efficiency (CCE) was calculated according to the following Eq. (7):

$$CCE = \frac{n_{(VFAs)}}{n_{(\text{carbon dioxide})} + n_{(\text{methanol.t1})}} \times 100 \quad (7)$$

where *n<sub>(VFAs)</sub>* is the sum of amounts of produced VFAs in mol-C, *n<sub>(carbon dioxide)</sub>* and *n<sub>(methanol)</sub>* are the amounts of consumed CO<sub>2</sub> and methanol in mol-C, respectively.

Obtained results were compared to test the significance of the differences obtained from different conditions. was assessed by using *t*-test or one-way analysis of variance (ANOVA) Post Hoc test, where the *p* < 0.05 was recognized as significant. The data was analyzed using ANOVA without the exclusion of outliers. Outliers were identified visually via box plots. The robustness of ANOVA ensured that the analysis remains valid even in the presence of these extreme values. The analyses were carried out in Origin 2024b.

## 3. Results and discussions

### 3.1. Methanol and H<sub>2</sub>/CO<sub>2</sub> fermentation with different combinations of operational parameters

The fermentation experiments tested 24 different scenarios including different combinations of temperature (23 °C and 35 °C), headspace pressure (1, 1.5, and 2 atm), and methanol/CO<sub>2</sub> ratios (0.5, 1, 3 and 5). A summary of the operational parameters and results is shown in Table 1.

#### 3.1.1. VFA production at different temperatures

Acetate and butyrate were the two main products obtained in all fermentation experiments. Values represented correspond to net productions, calculated considering the concentrations measured at the end of each fermentation experiment. At room temperature, acetate was the dominant product, with amounts ranging between 2.5 and 6.0 mmol-C (Fig. 1.a). Meanwhile, only trace amounts of butyrate were produced with a titer not exceeding 0.32 mmol-C (Fig. 1.b). Thus, butyrate selectivity (*S<sub>B</sub>*) under room temperature was below 10 % for every scenario (Table 1). At 35 °C, acetate production was in the same range as at 23 °C (2.7–6.2 mmol-C) and no statistically significant difference was observed (*p* > 0.05). This range reflects the values observed across different methanol/CO<sub>2</sub> ratios and pressure conditions tested at 35 °C, while the corresponding average values for each condition are listed in Table 1. However, butyrate production was significantly higher at 35 °C than at 23 °C. Butyrate accumulated to a titer of 0.8–3.5 mmol-C with selectivity ranging between 16.9 and 48.9 % (Table 1).

A similar trend has been observed with ethanol assisted chain elongation. A study carried out by Ren et al., (2024) compared chain

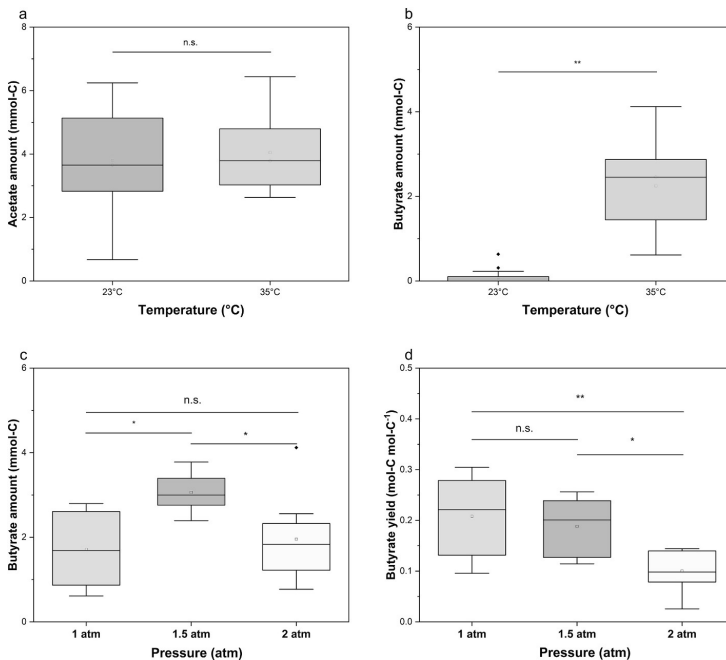


**Fig. 1.** Acetate (a) and butyrate production (b) at different temperatures, including results obtained at different pressure (1, 1.5 and 2 atm) and methanol/CO<sub>2</sub> ratio (0.5, 1, 3, and 5). Significance of results was tested by ANOVA and t-test. Butyrate amounts (c) and butyrate yields (d) at different pressures in fermentation experiments at 35 °C. The symbol \* represents  $p < 0.05$ , symbol \*\* represents  $p < 0.005$ , symbol n.s. represents not significant.

elongation from ethanol and acetate between 25 and 55 °C, obtaining the highest caproate yield and selectivity at 40 °C. In contrast, the lowest caproate yield was obtained at 25 and 30 °C, where acetate production was stimulated (Ren et al., 2024). A reason for such difference was the composition of the microbial communities, as the key chain elongator, *Clostridium kluveri*, was mostly enriched at 40 °C (Ren et al., 2024). Similarly, the dominant species in the inoculum used in this study, *E. limosum*, likely responsible for methanol utilization and butyrate production (Yao et al., 2025), has the optimal growth temperature at 37 °C (Rode et al., 1981).

### 3.1.2. VFA production at different pressures

As butyrate production mainly occurred at 35 °C, the effects of headspace pressures on butyrate production are discussed at that temperature (Fig. 1.c). As different substrate ratios (0.5, 1, 3, and 5) were used, a total of eight results were obtained for each pressure. Higher butyrate amounts, in the range of 2.4–3.8 mmol-C, were obtained at a headspace pressure of 1.5 atm. At 1 atm, butyrate amounts were in the range 0.6–2.8 mmol-C, while at 2 atm they were at 0.8–2.6 mmol-C, except at a methanol/CO<sub>2</sub> ratio of 5 where 4.1 mmol-C butyrate was obtained. In summary, butyrate productions were enhanced when the pressure was increased from 1 atm to 1.5 atm. Increasing the pressure enhances gas-to-liquid mass transfer and results in a higher solubility of gaseous compounds (according to Henry's law). Thus, the higher the P<sub>CO<sub>2</sub></sub>, the higher is the availability of soluble carbon sources. The butyrate yields (Fig. 1.d) were similar at 1 and 1.5 atm (0.15–0.29 and 0.12–0.25 mol-C mol-C<sup>-1</sup>, respectively), both higher than the 0.08–0.11 mol-C mol-C<sup>-1</sup> observed at 2 atm. Therefore, the higher butyrate amounts at 1.5 atm were likely due to the higher carbon availability compared to 1 atm, rather than a butyrate yield increase. Further increasing pressure (from 1.5 atm to 2 atm) resulted in higher biomass

formation, as indicated by the increase in average OD<sub>600</sub> from 2.0 to 2.4 (Table 1). However, both butyrate amount and yield decreased, suggesting that butyrate production was hindered.

On the other side, pressure increases also affected acetate production (see supplementary information). The highest acetate amount of 2.2–6.2 mmol-C was obtained at 2 atm. At pressures of 1 and 1.5 atm, acetate amounts decreased to 1.5–4.6 mmol-C and 0.7–5.1 mmol-C, respectively. The differences in acetate and butyrate production between 1.5 and 2 atm suggests elevated pressure may affect metabolism, potentially altering carbon fluxes. In addition to altering the product spectrum, microbial growth was also affected by the elevated pressures. Many studies have shown that the increased pressure resulted in higher biomass production (Gaddy, 1997; von Canstein et al., 2008; Wendlandt et al., 1993). However, the opposite effect has been observed as well, especially with higher pressure compared to values studied in this work. For instance, increasing the total pressure from 1 to 7 atm during cultivation with H<sub>2</sub>/CO<sub>2</sub> gas mixtures led to a gradual decline in *C. ljungdahlii* biomass formation, likely resulting from the inhibitory effects of high P<sub>H<sub>2</sub></sub> (Oswald et al., 2018).

### 3.1.3. Butyrate production with different methanol/CO<sub>2</sub> ratios

Based on the results obtained, 35 °C and atmospheric headspace pressure were selected as the optimal conditions for evaluating butyrate production under various methanol/CO<sub>2</sub> ratios. Under such conditions, increasing the methanol/CO<sub>2</sub> ratio in the range 0.5 to 3 resulted in higher butyrate amounts (Table 1) and yields (Fig. 2). At a methanol/CO<sub>2</sub> ratio of 0.5, a relatively low butyrate amount of  $0.8 \pm 0.2$  mmol-C and a yield of  $0.17 \pm 0.06$  mol-C mol-C<sup>-1</sup> were obtained. When the ratio was increased to 1, the butyrate amount increased to  $1.0 \pm 0.3$  mmol-C with a yield of  $0.15 \pm 0.06$  mol-C mol-C<sup>-1</sup>. The highest butyrate production was obtained at a methanol/CO<sub>2</sub> ratio of 3, with the amount of

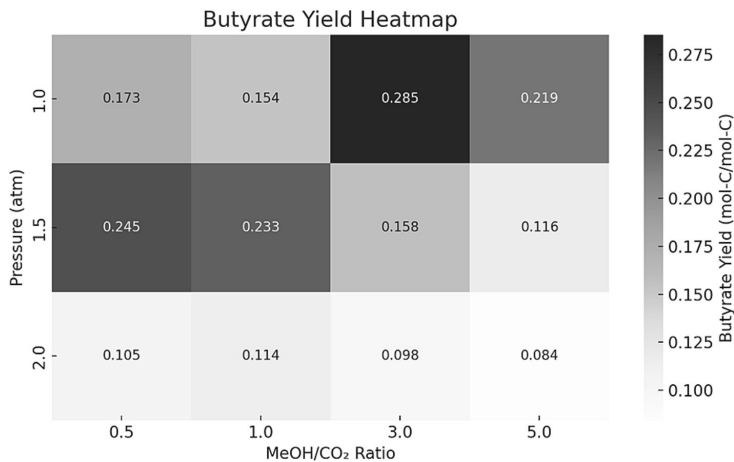


Fig. 2. Butyrate yield ( $\text{mol-C mol-C}^{-1}$ ) at 35 °C at different pressure and methanol/CO<sub>2</sub> ratios.

$2.6 \pm 0.1 \text{ mmol-C}$  and yield of  $0.29 \pm 0.02 \text{ mol-C mol-C}^{-1}$ . However, increasing the ratio to 5 did not further increase the butyrate amount ( $2.4 \pm 0.4 \text{ mmol-C}$ ) and resulted in a slightly lower yield of  $0.22 \pm 0.07 \text{ mol-C mol-C}^{-1}$ . As Wood et al., (2022) suggested, a higher ratio of electron donor to electron acceptor promotes the synthesis of more reduced compounds in methanol assisted chain elongation. Therefore, increasing the ratio from 0.5 to 3 was expected to enhance butyrate production. However, a ratio of 5 led to methanol accumulation exceeding 250 mM, which could hinder the biomass growth and production efficiency (Kremp and Müller, 2021). According to Sharak Gentner and Bryant, (1987), methanol concentrations above 198 mM negatively affect *E. limosum* growth by increasing the doubling time and resulting in a lag phase of 79 h. To summarize, the optimal butyrate production was achieved at a temperature of 35 °C, atmospheric pressure, and a methanol/CO<sub>2</sub> ratio of 3.

### 3.2. Process validation in MES reactors

#### 3.2.1. Acetate as the main product with pressurized conditions at 23 °C

The first experiment in MES reactors aimed at testing methanol assisted MES under pressurized condition to target acetate production. Thus, based on the batch experiment results, room temperature (23 °C) was selected. As CO<sub>2</sub> was provided in overpressure, thereby increasing the solubilized CO<sub>2</sub> concentration, maintaining a high methanol/CO<sub>2</sub> ratio could lead to excessive methanol accumulation that could hinder microbial growth (Kremp and Müller, 2021). Thus, since no clear beneficial effect of high methanol/CO<sub>2</sub> ratios on the acetate productivity was observed in the incubation at 23 °C (Table 1), low methanol/CO<sub>2</sub> ratios (below 1) were used in this test. The two pressurized cells (MES-23-R1 and -R2) were initially operated at a constant current density of

1.5 mA cm<sup>-2</sup> and an addition of 4 mmol methanol three times per week. The OD<sub>600</sub> sharply increased from 0.04 to 0.17 on day 7 and remained between 0.15 and 0.2 until day 42 (see supplementary information). To maintain a methanol/CO<sub>2</sub> ratio below 1, only 2 mmol of methanol were added three time a week from day 7 to 26, resulting in a methanol/CO<sub>2</sub> ratio of ca.  $0.9 \pm 0.1$  which enabled acetate production at rates up to  $0.40 \pm 0.04 \text{ g L}^{-1} \text{ d}^{-1}$  ( $37.5 \pm 4.0 \text{ g m}^{-2} \text{ d}^{-1}$ ) (Table 2). From day 26 onwards, methanol dosage was further decreased to 2 mmol per week, thus decreasing methanol/CO<sub>2</sub> ratio to  $0.5 \pm 0.3$ . The highest acetate titer of  $5.8 \pm 0.8 \text{ g L}^{-1}$  was achieved on day 33 with a production rate of  $0.47 \pm 0.2 \text{ g L}^{-1} \text{ d}^{-1}$  ( $46.8 \pm 18.3 \text{ g m}^{-2} \text{ d}^{-1}$ ) in MES-23-R1. In MES-23-R2, 80 % of the catholyte was replaced with fresh medium on both days 26 and 35, which resulted in the highest acetate production rate of  $0.7 \text{ g L}^{-1} \text{ d}^{-1}$  ( $69.4 \text{ g m}^{-2} \text{ d}^{-1}$ ) between days 35 to 42 (see supplementary information).

From day 42 onwards, the current density for both MES cells was increased to 3.0 mA cm<sup>-2</sup>, resulting in higher H<sub>2</sub> accumulation at the end of each batch cycle (pressure increased from ca. 0.8 atm to 1.2 atm). This led to a higher microbial growth resulting in an OD<sub>600</sub> increase from 0.15 to 0.26 (Table 2). This observation was in line with the results from gas fermentation experiments, in which higher microbial growth was obtained when applying higher overpressures. The acetate titer increased to  $8.5 \pm 1.1 \text{ g L}^{-1}$  while the acetate production rates remained at  $0.41 \pm 0.04 \text{ g L}^{-1} \text{ d}^{-1}$  ( $41.2 \pm 3.5 \text{ g m}^{-2} \text{ d}^{-1}$ ). In addition to acetate, butyrate production was observed throughout the experiments, yet with a low production rate (below  $0.01 \text{ g L}^{-1} \text{ d}^{-1}$ ) resulting in a titer of only  $0.6 \pm 0.1 \text{ g L}^{-1}$ . Butyrate production was not affected by changes in either the applied current or methanol/CO<sub>2</sub> ratio.

One of the putative causes for the hindered butyrate production was the insufficient methanol utilization. In the MES experiments, methanol

Table 2  
Operational conditions and key performance results for MES-23 reactors.

Main Product	Production period (days)	Current density (mA cm <sup>-2</sup> )	Methanol addition (mmol/week)	MeOH/CO <sub>2</sub> ratio	Final OD <sub>600</sub> (nm)	Production rate		Titer (g L <sup>-1</sup> )
						mg L <sup>-1</sup> d <sup>-1</sup>	g m <sup>-2</sup> d <sup>-1</sup>	
Acetate	9–19 (R1) 14–21(R2)	1.5	6.0	0.9 ± 0.1	0.15 ± 0.01	374.8 ± 39.7	37.5 ± 4.0	5.0 ± 0.3
	26–33 (R1,R2)	1.5	2.0	0.5 ± 0.3	0.18 ± 0.01	467.6 ± 182.7	46.8 ± 18.3	5.6 ± 0.8
	35–42 (R2)							
	44–51 (R1)	3.0	2.0	0.3 ± 0.1	0.26 ± 0.01	412.7 ± 35.8	41.3 ± 3.6	8.5 ± 1.1
	42–47 (R2)							

was utilized at an average rate of  $0.17 \text{ g L}^{-1} \text{ d}^{-1}$ , while a methanol utilization rate of  $0.32 \text{ g L}^{-1} \text{ d}^{-1}$  was obtained in previous experiments in MES at  $35^\circ\text{C}$  (Yao et al., 2024). A carbon conversion efficiency (CCE) of  $17.9 \pm 1.7\%$  was obtained throughout the MES-23 runs, indicating that most of the carbon was not recovered in the products. Several factors likely resulted in the low CCE. For example, although the reactor itself was designed to handle pressurized condition, the membrane was not optimized for pressurized conditions, which likely resulted in the leakage of  $\text{CO}_2$  and methanol (Fang et al., 2024; Koskue et al., 2021).

### 3.2.2. MES optimization for efficient butyrate production

Based on the results from gas fermentation (section 3.1), complementary MES experiments (MES-35) were conducted at  $35^\circ\text{C}$  and atmospheric pressure setting methanol/ $\text{CO}_2$  ratio of 3 aiming for selective butyrate production (Fig. 3). Acetate production initiated immediately after inoculating the reactors, with a production rate of  $0.2 \pm 0.1 \text{ g L}^{-1} \text{ d}^{-1}$  reaching a highest acetate titer of  $5.6 \pm 1.0 \text{ g L}^{-1}$ . Butyrate production initiated from day 3 at a production rate of  $0.6 \pm 0.1 \text{ g L}^{-1} \text{ d}^{-1}$  ( $107.4 \pm 19.7 \text{ g m}^{-2} \text{ d}^{-1}$ ), obtaining a titer of  $9.2 \pm 1.6 \text{ g L}^{-1}$  on day 17 before plateauing (Fig. 3). Overall, butyrate was the dominant product with  $75.2 \pm 1.1\%$  selectivity. One of the possible reasons for rather stable butyrate concentrations after day 17 of operation was product losses by volatilization during  $\text{CO}_2$  sparging, which was reported in our previous work (Yao et al., 2024). The losses became noticeable when the VFAs started to accumulate and reached a certain concentration (ca.  $8.8 \text{ g L}^{-1}$ ). Additionally, trace amounts of caproate were obtained at the end of the experiments, although the final titer remained below  $0.3 \text{ g L}^{-1}$ .

Each batch cycle was conducted with an average initial methanol/ $\text{CO}_2$  ratio of  $2.9 \pm 0.3$ . In total,  $206.5 \pm 6.4 \text{ mmol-C}$  ( $6.6 \pm 0.2 \text{ g}$ ) of methanol were supplied to the MES cell,  $87.8 \pm 1.8\%$  of which ( $181.3 \pm 6.4 \text{ mmol-C}$  ( $5.8 \pm 0.2 \text{ g}$ )) was consumed. In addition, a total of  $88.4 \pm 8.4 \text{ mmol-C}$  ( $3.9 \pm 0.4 \text{ g}$ ) of  $\text{CO}_2$  was utilized throughout the experiments. The average methanol consumption rate was  $18.0 \pm 0.6 \text{ mM d}^{-1}$  ( $0.58 \pm 0.02 \text{ g L}^{-1} \text{ d}^{-1}$ ), which was 1.7-fold higher than our previous study ( $0.32 \text{ g L}^{-1} \text{ d}^{-1}$ ) (Yao et al., 2024). Compared to the previous study, where methanol/ $\text{CO}_2$  ratio averaged 0.33, this study assessed a ratio of 3, which promoted butyrate production and resulted in the due to the higher availability of reducing equivalents.

Methanol and the cathode electrode were the two electron donors, which collectively provided  $3254.5 \pm 37.8 \text{ mmol}$  equivalents of

electrons. Out of these,  $42.9 \pm 1.9\%$  were recovered as  $\text{H}_2$ ,  $17.9 \pm 0.7\%$  were recovered as butyrate and  $6.7 \pm 1.0\%$  were recovered as acetate. In summary, a carbon conversion efficiency of  $64.0 \pm 5.8\%$  and a faradaic efficiency of  $67.6 \pm 3.5\%$  were obtained (see supplementary information), suggesting further optimization of electron utilization should be done. For example, addition of exogenous electron mediators to improve the electron transfer (Yu et al., 2025), cathode development to enhance the  $\text{H}_2$  utilization and thus the biofilm formation (Li et al., 2024b), and reactor design development (Cabau-Peinado et al., 2024) have the potential to improve the faradaic efficiency in MES studies. It is worth mentioning that product losses due to volatilization during gas sparging were not included in the carbon and faradaic efficiency calculations. The  $\text{OD}_{600}$  of the catholyte at the end of the experiments was only 0.2 (see supplementary information), suggesting that carbon sources were directed to the products, rather than biomass. The butyrate yield obtained was  $0.58 \pm 0.01 \text{ mol-C mol-C}^{-1}$ , indicating a ca. 2-fold enhancement compared to the highest results obtained in serum flasks ( $0.29 \pm 0.02 \text{ mol-C mol-C}^{-1}$ ).

The highest butyrate production rate obtained in this study,  $0.6 \text{ g L}^{-1} \text{ d}^{-1}$  ( $107.4 \text{ g m}^{-2} \text{ d}^{-1}$ ) is close to the highest butyrate production reported from  $\text{CO}_2$  in MES studies (Fig. 4.a). Several studies have demonstrated the production of butyrate with only  $\text{CO}_2$  supply, although direct elongation of  $\text{CO}_2$  to butyrate has not been proven. For example, Jourdin and his co-workers (Jourdin et al., 2019) achieved a high butyrate production rate of  $0.7 \pm 0.2 \text{ g L}^{-1} \text{ d}^{-1}$  ( $125 \pm 44.9 \text{ g m}^{-2} \text{ d}^{-1}$ ) by increasing the  $\text{CO}_2$  loading rate ( $173 \text{ L d}^{-1}$ ) and high hydraulic retention time (14 d) in continuous feeding mode, which is the highest butyrate production rate reported so far in MES. The high  $\text{CO}_2$  loading rate provided excessive amount of carbon for carboxylates production (less than 1 % of the provided carbon was utilized), while the long HRT enabled sufficient time for elongating acetate to butyrate (Jourdin et al., 2019). Raes et al., (2017) added acetate as a co-substrate with  $\text{CO}_2$  to facilitate butyrate formation in MES, obtaining a butyrate production rate of  $0.54 \text{ g L}^{-1} \text{ d}^{-1}$ . Both studies stated that the most-likely chain elongation route was through ethanol formation, although ethanol was not observed as it was simultaneously produced and consumed.

As suggested by Izadi et al. (2021), butyrate production in MES often requires an additional electron donor apart from  $\text{H}_2$ . One effective strategy to enhance butyrate production is to promote solventogenesis, thereby increasing the ethanol production in MES. Generally, low pH (below 5) and high  $P_{\text{H}_2}$  (over 1 atm) are favorable for solventogenesis (Romans-Casas et al., 2023). These strategies have been applied in MES to enhance the in-situ ethanol production (Romans-Casas et al., 2024; Vassilev et al., 2019), achieving butyrate production rates of  $0.18 \text{ g L}^{-1} \text{ d}^{-1}$  ( $14.4 \text{ g m}^{-2} \text{ d}^{-1}$ ) (Romans-Casas et al., 2024). Other approaches were based on supplying exogenous electron donors, such as ethanol (Izadi et al., 2021; Jiang et al., 2020), formate (Izadi et al., 2021), lactate (Zhang et al., 2023) or methanol (Yao et al., 2024) to support butyrate production in MES. Out of them, ethanol and methanol possess the highest reducing power (degree of reduction 6) compared to formate (1) and lactate (4). Ethanol driven butyrate production in MES was obtained by Zhang et al., (2023), with a butyrate production rate of  $0.44 \text{ g L}^{-1} \text{ d}^{-1}$  ( $44.0 \text{ g m}^{-2} \text{ d}^{-1}$ ) by adding  $5 \text{ g L}^{-1}$  of ethanol at the beginning of the experiment. In the same study, butyrate production rate further increased to  $0.9 \text{ g L}^{-1} \text{ d}^{-1}$  ( $90.0 \text{ g m}^{-2} \text{ d}^{-1}$ ) with the addition of both ethanol and lactate ( $5 \text{ g L}^{-1}$  each). Compared to Zhang et al. (2023), similar butyrate production rate of  $0.6 \text{ g L}^{-1} \text{ d}^{-1}$  ( $107.4 \text{ g m}^{-2} \text{ d}^{-1}$ ) was obtained in this study by adding similar amounts of methanol ( $4.6 \text{ g L}^{-1}$  of methanol). Compared to our previous study, in which methanol/ $\text{CO}_2$  ratios of around 1 were utilized, the butyrate production rate improved by 1.5-fold (a volumetric production rate) or 3.4-fold (normalized to the electrode surface) (Yao et al., 2024). Methanol/ $\text{CO}_2$  ratio of 3, pH of 6 (Yao et al., 2025), atmospheric pressure, and  $35^\circ\text{C}$  temperature should be set to enhance butyrate production rate in methanol-assisted MES.

The butyrate selectivity of ca. 80 % achieved in this study with methanol assisted MES is in line with the selectivity obtained in ethanol

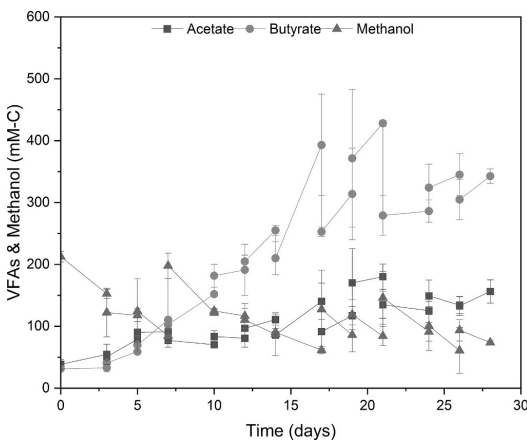


**Fig. 3.** VFAs and methanol concentrations throughout the MES-35 experiments. Error bars show the standard deviation of duplicate results. Two data points per day represent measurements taken before and after  $\text{CO}_2$  sparging. Differences between the two may result from partial loss of volatile fatty acids during sparging, particularly at higher butyrate concentrations.

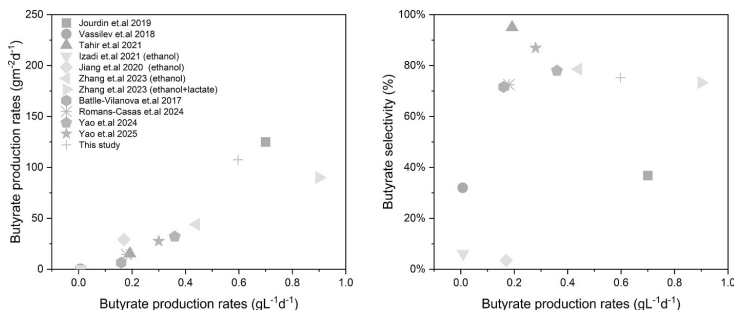


**Fig. 4.** Comparison of butyrate production rates per projected electrode surface area (a); and butyrate selectivity (b) reported in this study and in other published MES studies (Battile-Vilanova et al., 2017; Izadi et al., 2021; Jiang et al., 2020; Jourdin et al., 2019; Romans-Casas et al., 2024; Tahir et al., 2021; Vassilev et al., 2018; Yao et al., 2024, 2025; Zhang et al., 2023). Both figures use butyrate production rates normalized to catholyte volume on the x-axis. The figures are split to provide a clearer comparison of the different parameters. Color coding: Orange denotes MES studies without observing ethanol production/consumption. Yellow denotes MES studies with exogenous electron donor addition. Grey denotes MES studies with in-situ ethanol production. Blue denotes methanol assisted MES studies. (For interpretation of the references to color in this figure legend, the reader is referred to the web version of this article.)

assisted MES (Fig. 4, b). However, the highest reported butyrate selectivity in MES (95 %) was obtained with only  $\text{CO}_2$  feeding (Tahir et al., 2021). The butyrate selectivity increased from 37 % with unmodified carbon felt to 95 % with the nickel ferrite-coated carbon felt, which suggests that integrating advanced electrode designs with methanol-assisted MES has the potential to further enhance butyrate selectivity while maintaining high production rates.

The two MES validations demonstrated different product spectra in methanol assisted MES. Future studies should focus on microbial community profiling and employ bioinformatics tools, including transcriptomics, metabolomics, and proteomics to better understand the metabolic changes driving these shifts in product distribution.

#### 4. Conclusions

In this study, the effects of different operational parameter combinations on methanol assisted butyrate production via gas fermentation and MES were studied. In gas fermentation experiments, a maximum butyrate yield of  $0.29 \text{ mol-C mol-C}^{-1}$  was obtained at  $35^\circ\text{C}$ , 1 atm headspace pressure and a methanol/ $\text{CO}_2$  ratio of 3. This combination was further validated in fed-batch MES system, obtaining a butyrate production rate of  $107.4 \pm 19.7 \text{ g m}^{-2} \text{ d}^{-1}$ , with  $75.2 \pm 1.1 \%$  selectivity. The high methanol/ $\text{CO}_2$  ratio enabled efficient methanol utilization at a rate of  $0.58 \pm 0.02 \text{ g L}^{-1} \text{ d}^{-1}$  and achieved a carbon conversion efficiency of  $64.0 \pm 5.8 \%$  and faradaic efficiency of  $67.6 \pm 3.5 \%$ . In summary, a high-rate butyrate production in methanol assisted MES while maintaining high butyrate selectivity was obtained by increasing the methanol/ $\text{CO}_2$  ratio. However, excessive methanol concentration in the catholyte (above 250 mM) may hinder the butyrate producing microbial community.

#### CRediT authorship contribution statement

**Hui Yao:** Writing – review & editing, Visualization, Methodology, Investigation, Formal analysis, Conceptualization. **Paolo Densi:** Writing – review & editing, Supervision, Methodology, Funding acquisition. **Meritxell Romans-Casas:** Writing – review & editing, Methodology, Investigation. **Sebastià Puig:** Writing – review & editing, Supervision, Funding acquisition, Conceptualization. **Marika Kokko:** Writing – review & editing, Supervision, Funding acquisition, Conceptualization.

#### Declaration of competing interest

The authors declare that they have no known competing financial

interests or personal relationships that could have appeared to influence the work reported in this paper.

#### Acknowledgements

The authors acknowledge the funding from Research Council of Finland (grant no. 329227), the Bio and Circular Economy Research Infrastructure (decision no. 353658), and the Finnish cultural foundation (grant no. 241237) and Spanish Ministry of Innovation and Science (ref. PID2021-126240OB-I00). The authors also acknowledge the technical support of Serveis Tècnics de Recerca-Universitat de Girona. S.P. is a Serra Hunter Fellow (UdG-AG-575) and acknowledges the funding from the AGAUR-ICREA Acadèmia Programme, supported by the Department of Research and Universities of the Government of Catalonia. LEQUiA has been recognized as “consolidated research group” (Ref. 2021 SGR01352) by the Catalan Agency of Research and Universities. P.D. acknowledges the support from the project RESTART, funded through the “Dipartimenti di Eccellenza 2023-2027” initiative of the Italian Ministry of University and Research.

#### Appendix A. Supplementary data

Supplementary data to this article can be found online at <https://doi.org/10.1016/j.biortech.2025.133150>.

#### Data availability

Data will be made available on request.

#### References

- Joyia, A.K., M., Ahmad, M., Chen, Y.-F., Mustaqueem, M., Ali, A., Abbas, A., Ashraf Gondal, M., 2024. Trends and advances in sustainable bioethanol production technologies from first to fourth generation: a critical review. *Energ. Convers. Manage.* 321, 119037. <https://doi.org/10.1016/j.enconman.2024.119037>.
- Alvarez-Enriquez, F., Ahring, B.K., 2023. Strategies to overcome mass transfer limitations of hydrogen during anaerobic gaseous fermentations: a comprehensive review. *Bioresour. Technol.* 377, 128948. <https://doi.org/10.1016/j.biortech.2023.128948>.
- Appel, A.M., Bercaw, J.E., Bocarsly, A.B., Dobbek, H., DuBois, D.L., Dupuis, M., Ferry, J. G., Fujita, E., Hille, R., Kenis, P.J.A., Kerfeld, C.A., Morris, R.H., Peden, C.H.F., Portis, A.R., Ragsdale, S.W., Rauchfuss, T.B., Reek, J.N.H., Seefeldt, L.C., Thauer, R. K., Waldrop, G.L., 2013. Frontiers, Opportunities, and challenges in Biochemical and Chemical Catalysis of  $\text{CO}_2$  Fixation. *Chem. Rev.* 113, 6621–6658. <https://doi.org/10.1021/cr300463y>.
- Battile-Vilanova, P., Ganigüé, R., Ramió-Pujol, S., Bañeras, L., Jiménez, G., Hidalgo, M., Balaguer, M.D., Colprin, J., Puig, S., 2017. Microbial electrosynthesis of butyrate from carbon dioxide: Production and extraction. *Bioelectrochemistry* 117, 57–64. <https://doi.org/10.1016/j.bioelechem.2017.06.004>.



Supplementary information for:

Optimizing butyrate production from methanol and CO<sub>2</sub> in  
microbial electrosynthesis

## Biological medium composition

The biological medium used in this study consisted of  $18 \text{ g L}^{-1}$   $\text{Na}_2\text{HPO}_4 \cdot 2\text{H}_2\text{O}$ ,  $3 \text{ g L}^{-1}$   $\text{KH}_2\text{PO}_4$ ,  $3 \text{ g L}^{-1}$   $\text{NH}_4\text{Cl}$ ,  $15 \text{ mg L}^{-1}$   $\text{CaCl}_2$ ,  $20 \text{ mg L}^{-1}$   $\text{MgSO}_4 \cdot 7\text{H}_2\text{O}$ ,  $2.1 \text{ g L}^{-1}$  sodium 2-bromoethanesulfonate,  $1 \text{ g L}^{-1}$  yeast extract as well as  $10 \text{ mL L}^{-1}$  trace elements solution and  $1 \text{ mL L}^{-1}$  vitamin solution, which the detailed composition for trace elements and vitamin solution can be found at (Yao et al., 2024).

**Table A.1** Summary of the performance from both MES-23 and MES-35 reactors, with standard deviations calculated between duplicates.

	MES-23	MES-35
Supplied CO <sub>2</sub> (mmol-C)	390.0±0.6	250
Utilized CO <sub>2</sub> (mmol-C)	262.0±4.7	117.6±9.5
Supplied methanol (mmol-C)	43.5±0.9	206.5±3.1
Utilized methanol (mmol-C)	42.0±0.7	181.3±6.4
Acetate production rate (g L <sup>-1</sup> d <sup>-1</sup> )	0.4±0.1	0.2±0.1
Butyrate production rate (g L <sup>-1</sup> d <sup>-1</sup> )	-	0.6±0.1
Carbon recovery (%)	17.9±1.7	64.0±5.8
Electron recovery (%)	44.8±2.1	67.6±3.5

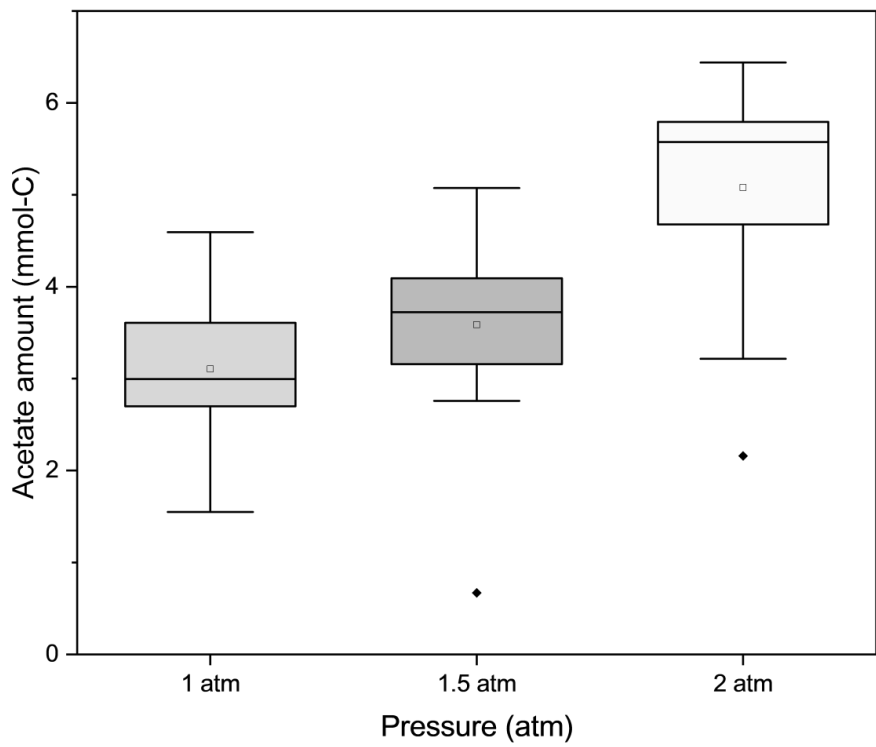


**Figure A.1** Acetate amount with different headspace pressures in fermentation experiments.

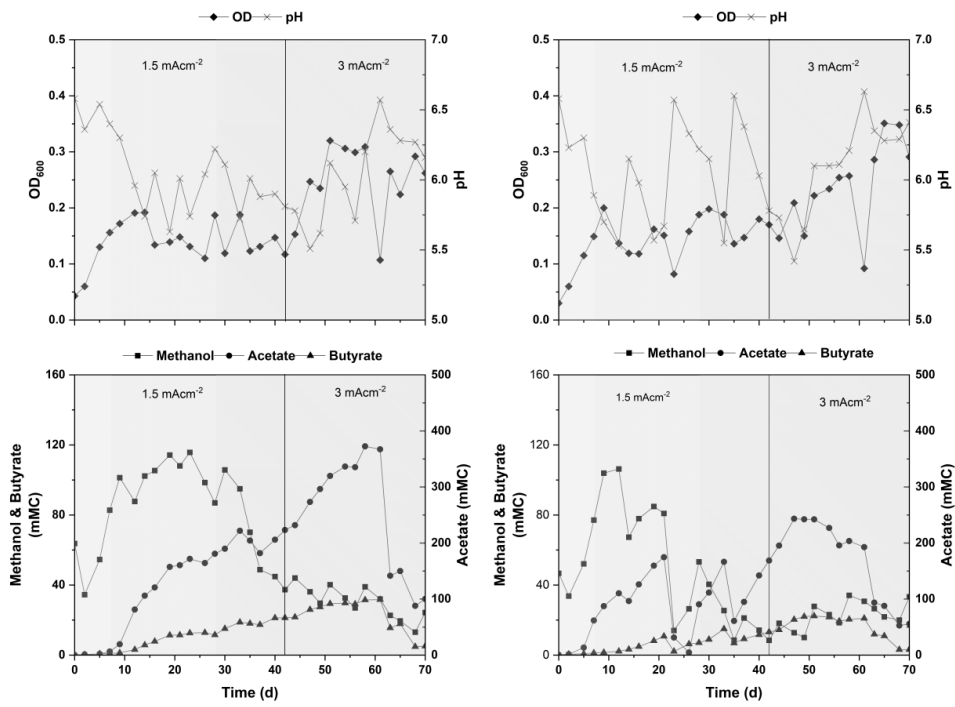


**Figure A.2** OD<sub>600</sub>, pH, methanol and VFA production for MES-23-1 (a, c) and MES-23-2 (b,d). Methanol feeding regime was changed from 40 mM addition each time (yellow), 20 mM each time (green), and 20 mM every seven days (purple).

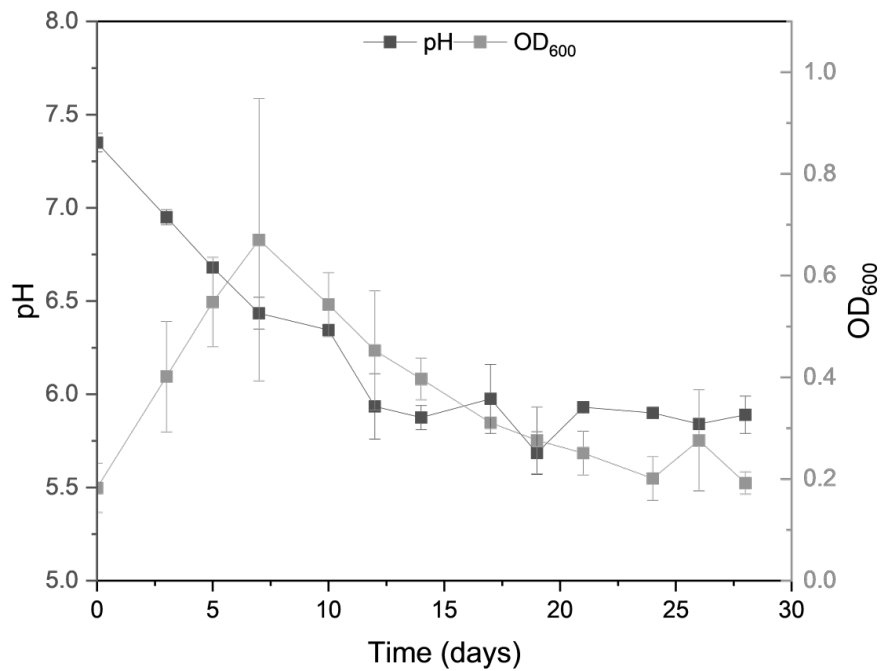


**Figure A.3** Catholyte pH and OD<sub>600</sub> from MES-35 reactors.

## References

Yao, H., Rinta-Kanto, J.M., Vassilev, I., Kokko, M., 2024. Methanol as a co-substrate with CO<sub>2</sub> enhances butyrate production in microbial electrosynthesis. *Appl Microbiol Biotechnol* 108, 372. <https://doi.org/10.1007/s00253-024-13218-y>



